Protein Interactomes of Alzheimer's Disease Risk Genes *Abi3* and *Trem2* in Microglia-like Cells

A thesis submitted for the degree of Doctor of Philosophy

At

Cardiff University

School of Medicine

Catherine Widnall

2022

Thesis Summary

Alzheimer's disease (AD) is a progressive neurodegenerative disorder and the most prevalent form of dementia. Over 50 genetic susceptibility loci have been identified for late onset AD, including coding variants in the *ABI3* and *TREM2* genes. The ABI3 protein is known to interact with the WAVE regulatory complex (WRC) which regulates actin cytoskeletal dynamics. By contrast, TREM2 is a membrane receptor, expressed by myeloid cells including microglia, that regulates many cellular functions including inflammatory responses and cytoskeletal remodelling. While genetic variants of *ABI3* and *TREM2* contribute to the genetic risk of AD, little is known about the function of these genes in microglia. Elucidating the interactome of these proteins provides a mechanistic insight into their role in microglia and can be used to explore the functional consequences of AD-associated genetic coding variants on molecular interactions.

The proximity labelling technique BioID was used to determine the protein-protein interactions of Abi3, Abi3-S212F (mouse equivalent of the human risk variant p.S209F) and Trem2 in mouse BV2 microglia-like cells. Abi3 was found to interact with the WRC components Wasf2 and Cyfip1, demonstrating the efficacy of BioID for detecting interacting proteins. Several novel interactors, including the centrosomal protein Cep170, were also identified as components of the Abi3 interactome. Abi3-S212F interacted with several proteins found in the Abi3 interactome in addition to several unique interactors that were not associated with wild type Abi3. Quantitative differences were observed between shared components of the Abi3 and Abi3-S212F interactomes, potentially suggesting that Abi3-S212F may be more tightly associated with the WRC. Trem2 interactors mostly consisted of secretory and endosomal pathway proteins suggesting the life cycle of Trem2 from the endoplasmic reticulum/Golgi to the plasma membrane and receptor internalisation and recycling was captured. The data presented herein define the first protein interactomes for Abi3, Abi3-S212F, and Trem2 in disease-relevant cells, contributing to our understanding of the molecular mechanism of AD risk.

Acknowledgements

Firstly, I would like to thank my supervisors. To Dr. Matt Hill for initial conception of the project, bringing me on board, and supervision throughout the first year of my PhD. To Professor Derek Blake for continued technical assistance, imparting of knowledge and experience and supervision throughout the final years of my PhD. To Professor Phil Taylor for adopting me into your lab group and allowing me to contribute to your ongoing research. And finally, to Professor Nick Bray for your invaluable guidance and advice in the writing of this thesis. I would also like to thank the Wellcome Trust for their support and funding of this PhD.

Within the lab I would like to thank Chris Smith for giving up his valuable time to impart his excellent and comprehensive technical knowledge and skills. Your contribution of generating the initial stable cell lines for this project underpins all the experiments that make up this thesis. None of the data presented here would be possible without you.

For keeping me going throughout the last 3 years I would like to thank Cerys Ballard, Lauren Thorburn, Dina Fathalla, Laura Heraty, and Marieta Vassileva. You've all stuck with me through (sometimes literal) blood, sweat, tears, and COVID with much needed, sometimes socially distanced, tea breaks and advice. To Cerys, a special thank you for technical assistance and training at the start of my PhD and still answering my questions even when you'd completed your PhD and moved on to new heights! To Lauren, every single story, picture, and video of Biscuit, Bandit, and Ellie have kept me going, particularly when things got tough. I've missed you both since you've left but I'm so proud of all the things you've achieved in the last year. To Dina, Laura, and Marieta, you guys have been my rock throughout the final year of my PhD. There is no way I could have got this far without you. I will always remember the tea breaks where we could vent, cry, laugh, and put the world to rights. Laura and Marieta, I wish you both the best of luck in the final months of your PhDs and Dina, I wish you all the best in your new role! I'll miss seeing you all every day. I would also like to thank all the DRI students who have made my time at Cardiff fun, interesting, and worthwhile. Good luck to you all and I wish you all the best.

A massive thank you to my family for your support over the last few years. To Stephen, Pip, and Alex (and Lexi!), thank you for your wonderful hospitality and

allowing me to join your COVID bubble! To Mum, Dad, and Chris, thank you for your constant support and love. Without you I wouldn't have had such a comfortable home to escape to or the resilience to keep going when things got tough.

An extra special thanks to Ashley Attwood. I will never understand how you could possibly have fallen in love with me during the final year of a PhD but I will forever be grateful. You've kept me going at the lowest moments and made the best ones even better. I love you.

And finally, a massive thank you to the (unintentional) co-author of this thesis, Holly. Even with your midnight sprints, 6 am wakeup calls, and your love of the laptop keyboard, your nightly snuggles, daily cuddles, and lockdown companionship have kept me sane and allowed me to relax when I needed to. All typos are dedicated to you.

Abbreviations

4EHP – eIF4E homologous protein

AA – Arachidonic acids

ABHD12 – Alpha/beta-hydrolase domain containing 12

ABI – Abl interacting protein

ABL2 – Abelson 2

ACh – Acetylcholine

AChE – Acetylcholinesterase

AD – Alzheimer's Disease

ADAM10 - Disintegrin and metalloproteinase domain-containing protein 10

AICD – APP intracellular domain

AP – Affinity purification

APBA – Aβ A4 precursor protein-binding family A

APH-1 – Anterior pharynx defective 1

ApoE4 - ε4 allele of apolipoprotein E

APOJ – Apolipoprotein J

APP – Amyloid precursor protein

APPsα - α-secretase-generated APP ectodomain fragment

APPsβ – β-secretase-generated APP ectodomain fragment

APS - Ammonium persulphate

ARFGAP2 - ADP ribosylation factor GTPase activating protein 2

ARFGEF2 - ADP Ribosylation Factor Guanine Nucleotide Exchange Factor 2

ARP – Actin related protein

Arp2/3 – Actin related proteins 2/3

ATP – Adenosine triphosphate

AU – Airy unit

Aβ – Amyloid β

BACE – β-site APP cleaving enzyme

BFDR – Bayesian false discovery rate

BioAMP – biotinoyl-5'-adenosine monophosphate

BioGRID – Biological General Repository for Interaction Datasets

BSA – Bovine serum albumin

Abbreviations

BSG – Basigin

CAT – Choline acetyltransferase

CCC – COMMD/CCDC22/CCDC93

CCDC22 – Coiled-coil domain containing protein 2

CD – Cluster of differentiation

CDK-5 – Cyclin-dependent-like kinase 5

CEP170 – Centrosomal protein of 170 kDa

CEP170P1 – CEP170-like protein

CF – Cystic fibrosis

CFTR – Cystic fibrosis transmembrane conductance regulator

CHO – Chinese hamster ovary

CLU – Clusterin

CMV – Cytomegalovirus

CNS – Central nervous system

COMMD – Copper metabolism gene MURR1 domain containing protein

CR1 – Complement receptor 1

CSF – Cerebral spinal fluid

CTFα – C-terminal fragment

CYFIP – Cytoplasmic fragile X messenger ribonucleoprotein 1 interacting protein

DAM – Disease associated microglia

DAP12 – DNAX-activating protein

DMEM – Dulbecco’s modified eagle medium

DNA – Deoxyribose nucleic acid

DOK3 – Docking protein 3

DUB – Deubiquitinase

DYRK1A – Dual specificity tyrosine-phosphorylation-regulated kinase 1A

ECM – Extracellular Matrix

EDTA - Ethylenediaminetetraacetic acid

EGTA – Egtazic acid

eIF – Eukaryotic translation initiation factor

EM – Electron Microscopy

EMMPRIN – Extracellular matrix metalloproteinase inducer

EOAD – Early onset AD

Abbreviations

ER – Endoplasmic reticulum

FAM – Family with sequence similarity

FBS – Foetal bovine serum

FDA – Food and Drug Administration

FLRT2 – Fibronectin leucine-rich repeat transmembrane protein

FPKM – Fragments per kilobase of transcript her million fragments mapped

fvAD – Frontal variant of AD

GABA – γ-aminobutyric acid

GalC – Galactocerebroside

GFAP – Glial fibrillary acidic protein

GFP -Green fluorescent protein

GIGYF2 – Growth factor receptor-bound protein interacting glycine-tyrosine phenylalanine domain protein 2

GLMN – Glomulin

GO – Gene ontology

GRB – Growth factor receptor-bound protein

GSK-3β – Glycogen synthase kinase 3β

GTP – Guanosine triphosphate

GWAS – Genome wide association studies

HD – Huntington's disease

HEK – Human embryonic kidney

HEM – Hematopoietic proteins

HGP – Human Genome Project

HRP – Horse radish peroxidase

HRPD – Human Protein Reference Database

HSCP300 – Haematopoietic stem/progenitor cell protein 300

Ig-SF – Immunoglobulin superfamily

IL – Interleukin

IP – Immunoprecipitation

IRES – Internal ribosome entry site

ITAF – IRES trans-acting factor

ITAM – Immunoreceptor tyrosine-based activation motif

IκB – Inhibitor of NF-κB

Abbreviations

JNK – c-Jun N-terminal kinases

KARAP – Killer cell activating receptor-associated protein

LC – Liquid chromatography

LD – Linkage disequilibrium

LOAD – Late onset AD

LPS – Lipopolysaccharide

LRP – Low-density lipoprotein receptor-related protein

LTP – Long-term potentiation

LTR – Long terminal repeat

MAC1 – Macrophage-1 antigen

MAC2 – Macrophage-2 antigen

MAF – Minor allele frequency

MAGMA – Multi-marker Analysis of Genomic Annotation

MAPK – Mitogen-activated protein kinase

MAPT – Microtubule-associated protein tau

MEG3 – Maternally expressed gene 3

MENA – Mammalian-enabled

Mint – Munc-18-interacting

mPGK – Mouse phosphoglycerate kinase

MRI – Magnetic resonance imaging

mRNA – Messenger RNA

MS – Mass spectrometry

MS/MS – Tandem MS

MTSS1 – Metastasis suppressor protein 1

NAP1 – Nucelosome assembly protein 1

NCBI – National Center for Biotechnology Information

NCT – Nicastrin

NESH – New molecule encoding Src homology 3

NFT – Neurofibrillary tangles

NF-κB – Nuclear factor kappa-light-chain-enhancer of activated B cells

NGS – Next generation sequencing

NMDA – N-methyl-D-aspartate

NO – Nitric oxide

Abbreviations

PAGE – Polyacrylamide gel electrophoresis

PAK – p21-activated kinase

PBS – Phosphate-buffered saline

PCA – Protein-fragment complementation assay

PCR – Polymerase chain reaction

PD – Parkinson's disease

PET – Positron emission tomography

PEN2 – PSEN enhancer 2

PFA – Paraformaldehyde

PI3K - Phosphatidylinositol 3-kinase

PICALM – Phosphatidylinositol-binding clathrin assembly protein

PIK3AP1 - Phosphoinositide-3-Kinase adaptor protein 1

PIP2 – Phosphatidylinositol-4,5-biphosphate

PIP3 – Phosphatidylinositol-3,4,5-triphosphate

PKB – Protein kinase B

PLC – Phospholipase C

PLOSL – Polycystic lipomembraneous osteodysplasia with sclerosing leukoencephalopathy

PP2A – Protein phosphatase 2A

PPI – Protein-protein interaction

PSEN – Presenilin

RIPA – Radioimmunoprecipitation assay

RIPK3 – Receptor-interacting serine/threonine-protein kinase 3

RNA – Ribose nucleic acid

RPMI – Roswell Park memorial institute

SAINT – Significant analysis of interactome

SDS – Sodium dodecyl sulphate

SH3 – Src homology 3

SNAP – Synaptosome-associated protein

SNP – Single nucleotide polymorphism

SSRI – Selective serotonin reuptake inhibitor

STAT3 – Signal transducer and activator of transcription 3

sTREM2 – Soluble TREM2

STRING – Search Tool for the Retrieval of Interacting Genes/Proteins

Abbreviations

SYK – Spleen tyrosine kinase

SZ – Schizophrenia

TANC1 – Tetratricopeptide Repeat, Ankyrin Repeat and Coiled-Coil Containing 1

TCEP - tris(2-carboxyethyl)phosphine

TEMED - N,N,N',N-Tetramethylethylenediamine

TESPA - 3-triethoxysilylpropylamine

TGN – Trans-Golgi network

TLR – Toll-like receptor

TNF-α – Tumour necrosis factor α

TREM2 – Triggering receptor expressed on myeloid cells 2

TYROBP – Tyrosine kinases binding protein

Vsp – Vacuolar protein sorting

v/v – Volume/volume

w/v – Weight/volume

WASF – WASP-family member

WASH – WASP and scar homolog

WASP – Wiskott-Aldrich syndrome protein

WAVE - WASP-family verprolin-homologous protein

WDR62 – WD repeat-containing protein 62

WRC – WAVE regulatory complex

Y2H – Yeast two-hybrid

ZAP70 – Zeta-chain-associated protein kinase 70

Table of Contents

Thesis Summary ..... **ii**

Acknowledgements ..... **iii**

Abbreviations ..... **v**

Chapter 1 – General Introduction **1**

1.1 Alzheimer's Disease *1*

1.1.1 Symptoms and Diagnosis 1

1.1.2 Pathology 3

1.1.3 Current Treatments 12

1.2 Microglia *14*

1.2.1 Microglial Biology 14

1.2.2 Microglia in Neurodegeneration 16

1.2.3 In Vitro Microglia Models 17

1.3 Genetics *19*

1.3.1 Introduction to Genetics 19

1.3.2 Genetics of Alzheimer's Disease 22

1.3.3 ABI3 27

1.3.4 TREM2 30

1.3.5 Indirect interactions between ABI3 and TREM2 37

1.4 Protein Networks *38*

1.4.1 Protein Interactomes 38

1.4.2 Techniques to Study PPIs 38

1.4.3 Application of Protein Interaction Analyses to Cell Biology and Disease 41

1.5 Thesis Aims and Structure *43*

Chapter 2 – Methods **44**

2.1 Cell Biology *44*

2.1.1 Cell Culture 44

2.2 Protein Analysis *45*

2.2.1 Sample Preparation for Protein Analysis 45

2.2.2 Sodium Dodecyl Sulphate-Polyacrylamide Gel Electrophoresis 47

2.2.3 Western Blot 47

2.2.4 Coomassie Staining 48

2.2.5 Immunocytochemistry 49

2.3 Plasmid Preparation *52*
2.3.1 Plasmid Vectors 52
2.3.2 Plasmid Construction 53
2.3.3 Plasmid DNA Isolation 53

2.4 Proteomics *56*
2.4.1 Biotin-Affinity Capture 56
2.4.2 Mass Spectrometry 56
2.4.3 Immunoprecipitation 56

2.5 Bioinformatics *57*
2.5.1 General 57
2.5.2 Mass Spectrometry Data Analysis 57

Chapter 3 – Investigation of the Abi3 Protein Interactome 61

3.1 Introduction *61*
3.1.1 Abi3 61
3.1.2 Aims 63

3.2 Results *63*
3.2.1 Generation and Validation of BV2 Cells Stably Expressing HA-BirA* and HA-BirA*-Abi3 63
3.2.2 Biotin-Affinity Capture of the Abi3 Interactome in BV2 Stable Cell Line 68
3.2.3 Proteomic Analysis of Protein Interactome 69
3.2.4 Functional Annotation of Interactors 78
3.2.5 Proteins of Interest 79
3.2.6 Validating Putative Interactors 80

3.3 Discussion *82*
3.3.1 Confirmed and Novel Protein Interactors of Abi3 82
3.3.2 Strengths and Limitations of BioID 88
3.3.3 Conclusions 90

Chapter 4 – Investigation of the Protein Interactome of the AD Risk Variant Abi3-S212F 91

4.1 Introduction *91*
4.1.1 ABI3 AD-Associated Risk Variants 91
4.1.2 Aims 93

4.2 Results *93*
4.2.1 Generation and Validation of BV2 Cells Stably Expressing HA-BirA*-Abi3-S212F 93
4.2.2 Biotin-Affinity Capture of the Abi3-S212F Interactome in BV2 Stable Cell Line 95
4.2.3 Proteomic Analysis of Protein Interactome 96
4.2.4 Functional Annotation of Interactors 105
4.2.5 Proteins of Interest 107

Table of Contents

4.3 Discussion *107*
4.3.1 Abi3-S212F Exists in Similar Pathways to Abi3 107
4.3.2 p.S212F Results in Gain of Interactions 115
4.3.3 p.S212F Results in Loss of Interactions 116
4.3.3 Limitations 116
4.3.4 Conclusions 117

Chapter 5 – Investigation of the Trem2 Protein Interactome 119

5.1 Introduction *119*
5.1.1 Trem2 119
5.1.2 Aims 121

5.2 Results *122*
5.2.1 Generation and Validation of BV2 Cells Stably Expressing Trem2-BirA*-HA 122
5.2.2 Biotin-Affinity Capture of the Trem2 Interactome in BV2 Stable Cell Line 125
5.2.3 Proteomic Analysis of Trem2 Interactome 126
5.2.4 Functional Annotation of Interactors 135
5.2.5 Proteins of Interest 136
5.2.6 Validation of Interaction 136

5.3 Discussion *142*
5.3.1 Trem2-BirA*-HA is Located in the Endosomal and Secretory Pathways 142
5.3.2 Trem2-BirA*-HA May Interact with Other Proteins Implicated in AD Pathology 146
5.3.3 Limitations 151
5.3.4 Conclusions 151

Chapter 6 – General Discussion 153

6.1 Abi3 and Abi3-S212F Interactomes Give Insights into Mechanisms in Physiology and Disease *154*

6.2 Trem2 Interactome Highlights the Importance of the Secretory Pathway and Receptor Recycling *156*

6.3 Abi3 may Influence the Life Cycle of Trem2 via the Endocytic Pathway *156*

6.4 Future Directions *158*

6.5 Final Conclusions *160*

Appendix 1 198

Appendix 2 237

Appendix 3 274

Chapter 1 – General Introduction

1.1 Alzheimer's Disease

In 1906, Alois Alzheimer presented the case of a 50-year-old woman with symptoms which included memory disturbances, paranoia, aggression, and confusion to the 37th meeting of South-West German Psychiatrists. He reported "A peculiar severe disease process of the cerebral cortex" which was later named 'Alzheimer's Disease' (AD) (Hippius and Neundörfer, 2003). Today, AD is the most common form of dementia and affects 850,000 people in the UK, including 1 in 14 people over the age of 65. By 2050, this figure is expected to rise to 2 million (Prince et al., 2014). Globally, 50 million people are estimated to be living with AD, including 5.2% of the population over 60. This is estimated to increase by 204% to 152 million by 2050, with low income countries most affected (an estimated increase of 264%) (World Health Organisation, 2019, Prince et al., 2015). In 2017, AD was the leading cause of death for women in the UK, and the second leading cause for men. As a percentage of total deaths in the UK, deaths due to AD have been increasing since 2005, whereas deaths due to ischemic heart diseases and cerebrovascular diseases have decreased. In 2016, there were almost 2 million deaths globally due to AD and this is expected to rise by almost 65% by 2030 (World Health Organisation, 2018). In 2014, the cost of caring for AD patients in the UK was £23.6 billion and, without intervention, is projected to increase to almost £60 billion by 2050. It is estimated that potential treatments delaying the onset of AD by 2 years could reduce this projection to £46.5 billion and a 5-year delayed onset could reduce it to £38.2 billion (Lewis et al., 2014). Currently, AD is the only condition in the top 10 causes of death in the UK without preventative, curative, or effective progression-delaying treatments (Alzheimer's Research UK, 2017).

1.1.1 Symptoms and Diagnosis

The most prominent symptom of AD is episodic memory loss. Recent memories are affected in the early/mild stages followed by a loss of more distant memories as the disease progresses to middle/moderate and late/severe stages. AD also presents with other cognitive symptoms, including executive dysfunction, aphasia, and changes in personality. Executive dysfunction starts in the predementia stage and

worsens as the disease progresses along with a loss of visuospatial skills and aphasia. Patients also experience neuropsychiatric symptoms such as apathy, anxiety, anosognosia, and irritability. These symptoms commonly present in mild AD, with the addition of disinhibition, hallucinations, delusions, and appetite and sleep disturbances in moderate and severe stages. In these later stages neurological symptoms also occur, such as incontinence, dysphasia, and pathologic reflexes. At this stage patients often become bedridden, and death is most commonly caused by complications such as risk of asphyxiation, malnutrition, and immobility (Apostolova, 2016).

Diagnostic criteria for AD have been produced by the National Institute on Aging and the Alzheimer's Association (McKhann et al., 2011). For diagnosis of a dementia syndrome, patients must show decline in at least two signs of the following cognitive or behavioural functions: memory, reasoning and complex task handling, visuospatial ability, language, and personality. There must also be a decline from previously recorded levels of functioning. Probable AD can be diagnosed when the following criteria are met: the onset is insidious, there is gradual progression of the decline, no other disorders are present which interfere with cognition, and identification of positive biomarkers. These include amyloid β (Aβ) in the cerebral spinal fluid (CSF) or via position emission tomography (PET) scan and hippocampal atrophy measured by magnetic resonance imaging (MRI) (McKhann et al., 2011, Apostolova, 2016). There are also atypical variants of AD, complicating clinical diagnosis. These are less common and present differently, including the frontal variant of AD (fvAD) where neuropsychiatric symptoms present most strongly as the frontal cortex is affected before the hippocampus. AD patients can also present with posterior cortical atrophy resulting in early environmental disorientation and apraxia when episodic memories are relatively unaffected. Language disturbances can also present at earlier stages than typically seen in AD (Apostolova, 2016, Johnson et al., 1999). AD can only be confirmed post-mortem when cellular hallmarks of the disease such as amyloid plaques and neurofibrillary tangles are seen. It is the presence of these pathological markers that differentiate atypical forms like fvAD from other dementias, such as frontotemporal dementia (Johnson et al., 1999).

1.1.2 Pathology

One of the clearest pathological signs of AD is gross atrophy of the hippocampus and cortex caused by neural degeneration (Fox et al., 1996a, Fox et al., 1996b, Niikura et al., 2006). The volume of the hippocampus begins to decline before the onset of clinical symptoms and correlates with a decline in verbal and visual memory (Fox et al., 1996b). This degeneration spreads to temporal and parietal regions as the disease progresses, with atrophy of the frontal lobe occurring in the late stages of AD (Scahill et al., 2002). The exact cause of this is currently unknown, but disruptions to various cellular mechanisms have been linked with AD, to which current treatments are targeted.

1.1.2.1 Neurodegeneration

The degeneration of neurons in AD is the primary pathology underlying cognitive decline and clinical symptoms. The excitotoxicity hypothesis was first proposed by Olney et al. (1997) who suggested that, counterintuitively, the hypoactivity of N-methyl-D-aspartate (NMDA) receptors observed in aging leads to chronic excitotoxicity. This was suggested to be due to disinhibition, where decreased activation of excitatory neurons leads to reduced activation of GABAergic (GABA: γ-aminobutyric acid) inhibitory neurons, the overall consequence of which is heightened glutamatergic and cholinergic excitation. NMDA receptors are known to play a pivotal role in memory and synaptic plasticity, underlying the mechanism of long-term potentiation (LTP) (Lau et al., 2009). The increase in intracellular calcium that occurs during over-activation of excitatory mechanisms is also proposed to contribute to neurodegeneration by inducing oxidative stress (Sharma et al., 2019).

Neurons are particularly susceptible to oxidative stress as neuronal activity is adenosine triphosphate (ATP)-intensive, requiring a high oxygen consumption (around 20% of the oxygen taken in by the human body goes to the brain). Redox reactions are also critical for neuronal functions such as synaptic plasticity (Cobley et al., 2018). Neurons also contain relatively low levels of antioxidants and rely on support from release of glutathione from surrounding astrocytes (Bell, 2013). Further increases in susceptibility of neurons to oxidative stress are found in neurodegenerative diseases, including AD (Nguyen et al., 2011, Porta et al., 2007). This damage correlates with areas abundant in Aβ, suggesting a link between amyloid pathology and oxidative stress (Butterfield et al., 2001). Both amyloid

precursor protein (APP) and Aβ has also been shown to localise to mitochondrial membranes early in the pathology of AD, resulting in increased levels of oxygen radicals and oxidative stress (Reddy and Beal, 2008). Localisation and cleavage of APP at the ER, Golgi apparatus, mitochondria, and endosomes, in addition to the plasma membrane, has been shown (Anandatheerthavarada et al., 2003, Sambamurti et al., 1992). Mitochondrial $A\beta_{42}$ is thought to be a key component of AD pathogenesis and associated with neuronal mitochondria in energy-rich regions with high synaptic activity, such as the hippocampus (Pickett et al., 2018, Ashleigh et al., 2023). This may explain the link between mitochondrial dysfunction and synaptic disruption which could underlie the cognitive defects seen in AD patients (Gillardon et al., 2007, Mungarro-Menchaca et al., 2002).

These reactions are not themselves considered to be the cause of AD, but the mechanisms triggered by the underlying cause which result in the characteristic degeneration and atrophy in the brains of patients resulting in the observable symptoms and cognitive decline. Targeting these areas may therefore provide symptomatic relief but is unlikely to halt the progression of AD and eventual cognitive decline.

1.1.2.2 Amyloid Hypothesis of Alzheimer's Disease

One of the major hallmarks of AD is the presence of a large number of extracellular Aβ plaques (Selkoe, 1991). The amyloid hypothesis of AD was first put forward by Hardy and Allsop (1991) who argued that Aβ protein was the cause of AD pathology by triggering a cascade of neurotoxic effects. The theory initially came from studies of the neuropathology of Down's syndrome as there is a higher incidence of early onset AD (EOAD) in these patients compared to the general population (Hartley et al., 2015). The disorder is caused by a trisomy of chromosome 21 which carries the *APP* gene.

The proposed mechanism of pathology in AD involves abnormal processing of APP leading to increased deposition of Aβ. Proteolytic fragments of APP have been shown to mediate diverse cellular functions including nervous system development and dendritic spine density(Müller et al., 2017). At the plasma membrane, APP can be cleaved by two different pathways: non-amyloidogenic and amyloidogenic. In the non-amyloidogenic pathway α-secretase enzymes (Disintegrin and metalloproteinase domain-containing protein 10 (ADAM10) being the most prominent

(Kuhn et al., 2010)) cleaves APP within the Aβ sequence, releasing the α-secretase-generated APP ectodomain fragment (APPsα) and leaving the α C-terminal fragment (CTFα) in the plasma membrane. The γ-secretase complex (consisting of presenilin 1 and 2 (PSEN1/2), nicastrin (NCT), anterior pharynx defective 1 (APH-1), and PSEN enhancer 2 (PEN2) (Zhang et al., 2014a)) then cleaves the CTFα to release the peptide p3 into the extracellular matrix (ECM) and the APP intracellular domain (AICD) into the cytoplasm (Müller et al., 2017). In the amyloidogenic pathway, APP is cleaved by β-site APP cleaving enzymes 1 and 2 (BACE1 and BACE2) at the N-terminus of the Aβ sequence, producing the β-secretase-generated APP ectodomain fragment (APPsβ) and the CTFβ. The γ-secretase complex then cleaves the CTFβ to generate AICD and Aβ monomers (Figure 1.1) (Müller et al., 2017, Kuhn et al., 2010). Aβ is cleared from the CNS via several pathways. Non-enzymatic pathways include drainage via the interstitial fluid, uptake by microglial or astrocytic phagocytosis, and transport across the blood-brain barrier. Aβ can also be cleared by enzymes including neprilysin, insulin-degrading enzyme, and matrix metalloproteinase-9 (Yoon and Jo, 2012). In AD, an imbalance between Aβ production and clearance has been suggested, leading to aggregates of Aβ monomers forming Aβ oligomers. These can aggregate to form Aβ fibrils which eventually lead to formation of Aβ plaques (Nie et al., 2011, Mawuenyega et al., 2010).

Aβ peptides vary in length from 36 to 43 amino acids. The solubility and aggregation of Aβ peptides is dependent on the amino acid length, with $Aβ_{42}$ being the most likely to form plaques. An increased ratio of $Aβ_{42}$:$Aβ_{40}$ is associated with AD (Burdick et al., 1992, Iwatsubo et al., 1996, Selkoe and Hardy, 2016). These plaques are thought to induce neurotoxicity through multiple mechanisms: initiation of oxidative stress via binding with redox active metal ions (copper, zinc, etc.) catalysing the production of reactive oxygen species resulting in both DNA damage and modifications of Tau protein which favour formation of neurofibrillary tangles (NFTs; see section 1.1.2.3); activating inflammatory mechanisms by accumulation in parenchyma and blood vessels inducing production of pro-inflammatory cytokines, promoting microglial activation and phagocytosis; and alteration of plasma membrane conductance due to interactions between Aβ and cell membrane lipids (Wiatrak et al., 2021, Meraz-Ríos et al., 2013, Cheignon et al., 2018). Aβ oligomers have also been shown to exert

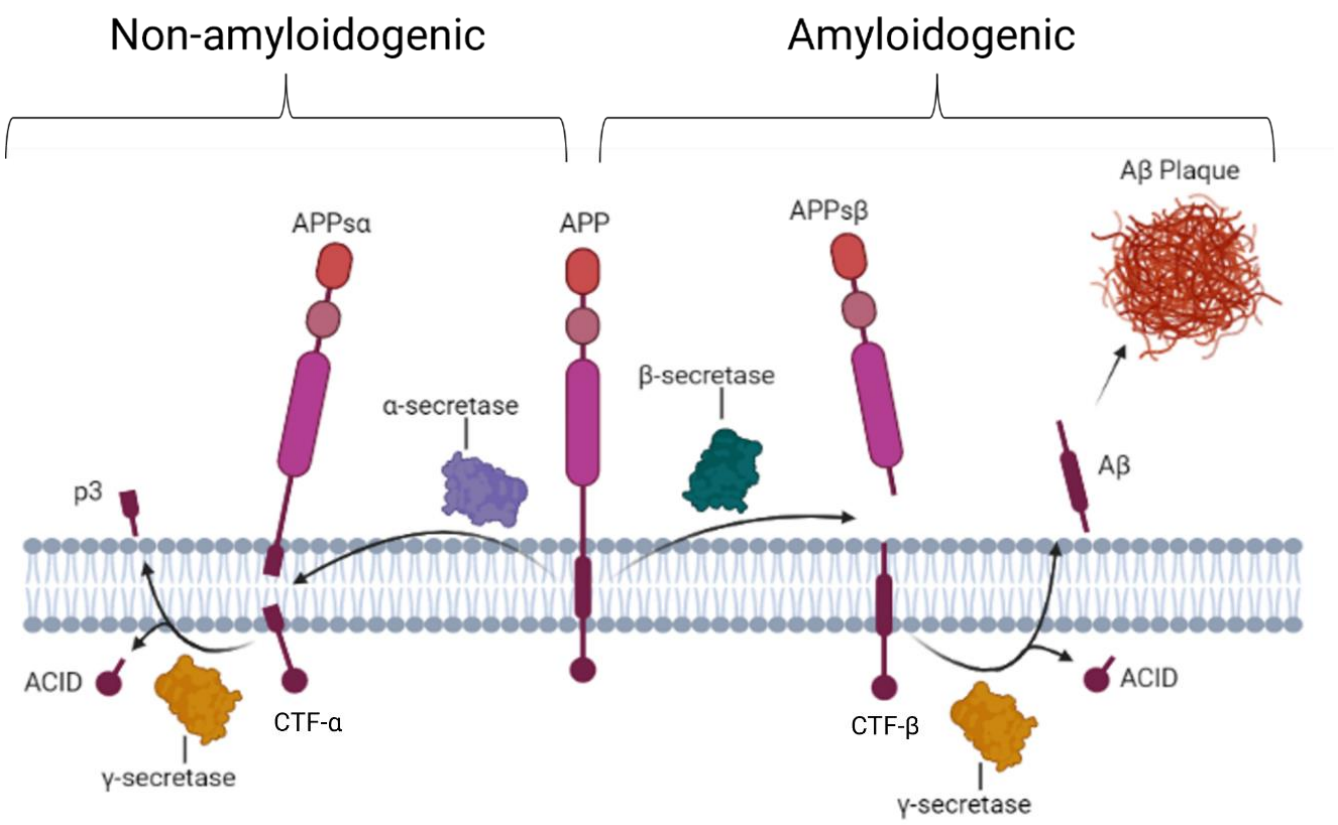

Figure 1.1 The amyloid hypothesis of Alzheimer's disease. *Deposits of extracellular Aβ plaques are a major hallmark of AD and are hypothesised to trigger a cascade of neurotoxicity. APP is a plasma membrane protein which can be cleaved by either α- or β-secretase enzymes. Cleavage by α-secretase initiates the non-amyloidogenic pathway as its cleavage site is within the Aβ region, generating APPsα and CTF-α. CTFα is subsequently cleaved by γ-secretase to produce AICD and the peptide p3. If APP is cleaved by β-secretase however, the amyloidogenic pathway is initiated. The cleavage site of β-secretase enzymes is at the N-terminus of Aβ, generating APPsβ and CTF-β. CTF-β is then also cleaved by γ-secretase, producing AICD and Aβ. Aβ aggregates form, leading to the presence of extracellular plaques. Aβ: amyloid β, APP: amyloid precursor protein, APPsα: α-secretase-generated APP ectodomain fragment, APPsβ: β-secretase-generated APP ectodomain fragment, CTF-α: α C-terminal fragment, CTF-β: β C-terminal fragment β, AICD: AP intracellular domain. Figure adapted from Müller et al. (2017) and created in BioRender.*

similar toxic effects on neurons, occurring at earlier stages than the effects of plaques. It is now thought these oligomers are a more important source of neurotoxicity in AD than the plaques themselves (Cline et al., 2018).

Rare missense mutations in the *APP* gene were identified in cases of familial AD which cause an amino acid substitution at the C-terminal end of APP (Chartier-Harlin et al., 1991, Goate et al., 1991). Mutations in *PSEN1* and *PSEN2* are also linked to

familial AD leading to a shift towards the amyloidogenic pathway in APP cleavage. This results in increased production of Aβ throughout life (Scheuner et al., 1996). However, the majority of AD cases are sporadic and not caused by *APP* or *PS* (PSEN gene) mutations. Hardy and Higgins (1992) suggest that there may be additional causes which induce the shift towards the amyloidogenic pathway, resulting in AD.

Since the introduction of the amyloid hypothesis, *ApoE4* has been identified as the strongest known genetic risk factor for LOAD (see section 1.3.2.1). The global frequency of this allele is 13.7% but is found at a frequency of approximately 40% in individuals with AD (Liu et al., 2013). Risk is gene dose dependent and homozygous individuals have an 8–12-fold increase in risk for AD (Eid et al., 2019). ApoE proteins are known to have roles in lipid transport across plasma membranes via interaction with lipoprotein receptors, though whether isoform-dependent downstream pathways exist remains unclear (Raulin et al., 2022). ApoE4 is associated with earlier and more severe amyloid pathology, possibly due to reduction in Aβ clearance. ApoE is thought to induce Aβ clearance by forming ApoE-Aβ complexes, stimulating uptake of the complex by low-density lipoprotein receptor-related protein 1 (LRP1) (Bilousova et al., 2019). This complex is less stable with ApoE4 compared with other ApoE alleles, suggesting ApoE4 may increase AD risk through both a reduction in Aβ uptake by LRP1 and an increased levels of Aβ oligomers (Tai et al., 2013).

The amyloid hypothesis has also come under criticism as manipulating this system has not led to successful clinical outcomes after showing promising results in reducing plaque counts and improving cognition *in vivo* (Morris et al., 2014). It is possible that these trials failed as disruption to Aβ accumulation must happen in the early stages of AD to resist the toxic effect of Aβ plaques (Selkoe, 2011, Oddo et al., 2004). Due to the factors discussed in section 1.1.1, early diagnosis of AD is difficult and so early intervention is unlikely to be feasible in these trials. Another common criticism of the amyloid hypothesis is that the number of amyloid plaques does not correlate with cognitive decline. Davis et al. (1999) found that 49% of their subjects met the pathological diagnosis for AD at autopsy, based on the number of plaques in the neocortex, though none showed signs of cognitive impairment in life. Significant increases in the accumulation of Aβ also occurs over time in cognitively healthy

elderly populations. In a longitudinal study over 2.5 years, Vlassenko et al. (2011), using positron emission tomography amyloid tracing, found that cognitively normal subjects, with no amyloid plaques initially, showed an increase in plaques of 3.1% per year and cognitively normal carriers of ε4 allele of apolipoprotein E (APOE4; the presence of which is the second strongest risk factor for AD after age, see section 1.3.2.1) had an increased rate of plaque deposition. Levels of Aβ have also been found to plateau in AD patients despite continuing cognitive decline (Jack et al., 2013). It is therefore difficult to determine an individual's outcome based on the prevalence of Aβ plaques. For the amyloid hypothesis, the lack of correlation between Aβ level and cognition poses a challenge. The relationship between cognition and Aβ may, however, be more complex than a simple linear correlation, and potentially moderated by factors such as education and intelligence (Rentz et al., 2010). Higher levels of education are thought to reduce AD risk by creating a 'cognitive reserve' where alternative brain regions and networks are recruited to compensate for age-related degeneration (Larsson et al., 2017).

Alternative interpretations of the role of Aβ in AD have been put forward, including toxic effects of metal ions binding to plaques, soluble Aβ oligomers, and the effect of Aβ on the cerebral vasculature (Morris et al., 2014, Savory et al., 2002, Weller et al., 2008). Other pathological markers of AD have been suggested to have a stronger correlation with cognitive ability, including neurofibrillary tangles, synapse loss, and microglial activation (Ingelsson et al., 2004).

1.1.2.3 Tau Pathology

Tau is a microtubule-associated protein essential for neurite growth by promoting tubulin polymerisation and impairing depolymerisation which stabilises microtubules (Drubin and Kirschner, 1986, Weingarten et al., 1975). Alternative splicing of the product of the *MAPT* (microtubule-associated protein tau) gene produces six isoforms of the human tau protein which range from 37 to 45 kDa (Goedert et al., 1989). Expression of these isoforms is developmentally regulated, and those usually found in the foetal brain appear to be upregulated in AD (Kosik et al., 1989). These foetal isoforms are thought to be associated with a regeneration of neurites and this may underlie the irregular dendritic sprouting observed in early AD (Masliah et al., 1991, Scheibel and Tomiyasu, 1978). Under normal conditions, tau is primarily located in the axon of neurons in the phosphorylated form, which has a reduced

association with tubulin. In AD, hyperphosphorylation of tau occurs, resulting in dissociation from microtubules and intracellular aggregation of the protein (Ittner and Götz, 2011, Hasegawa et al., 1992). Phosphorylation of tau is regulated by proline-directed protein kinases such as glycogen synthase kinase 3β (GSK-3β), cyclin-dependent-like kinase 5 (CDK-5), and dual specificity tyrosine-phosphorylation-regulated kinase 1A (DYRK1A), whereas dephosphorylation is due to tau phosphatases such as protein phosphatase 2A (PP2A) (Iqbal et al., 2016, Avila, 2008). These tau phosphatases show reduced activity in AD which may underlie tau hyperphosphorylation (Gong et al., 1993, Gong et al., 1995). The neurofibrillary tangles (NFTs) that form from hyperphosphorylated tau proteins lead to neuronal death as microtubules are more readily depolymerised This results in the disruption of axonal transport, preventing trafficking of signals and enzymes required to ensure survival. Destabilisation of the cytoskeleton also contributes to cell death. (Grill and Cummings, 2010, Terwel et al., 2002). NFTs may also result in neurodegeneration by forming physical barriers within the cytoplasm of neurons which displaces cytoplasmic organelles as well as preventing protein trafficking (Lin et al., 2003).Compared to Aβ pathology, the progression of NFT accumulation in the brains of AD patients was found to better reflect clinical neurodegeneration and showed less variation between individuals. The Braak stages, defined by Eva Braak and her husband in the 1990s, map this spread from the entorhinal regions, through associative areas of the neocortex and finally to the neocortex (Braak and Del Tredici, 2013, Braak and Braak, 1991). This spread of tau protein has been suggested to occur through neuron-to-neuron transmission in a ‘prion-like’ manner with seeding, the misfolding of tau due to hyperphosphorylation, and propagation and transport of the misfolded protein (Clavaguera et al., 2013, Dujardin et al., 2014). However, this ‘prion-like’ hypothesis of tau progression is debated, as the exact mechanisms of seeding and propagation have yet to be established but hypotheses such as exome-mediated secretion and chaperone by heat shock cognate 70, DnaJ, and synaptosome-associated protein of 25 kDa (SNAP23) have been suggested (Fontaine et al., 2016, Polanco et al., 2016, Colin et al., 2020).

Tau and Aβ pathologies were first linked when mouse models displaying both pathologies showed enhanced numbers of NFTs (Götz et al., 2001, Lewis et al., 2001). This indicated that the presence of extracellular Aβ plaques influenced

intracellular tau pathology, but the mechanistic link was not clear. Reduction of tau in Aβ mouse models prevented behavioural deficits and protected against excitotoxicity without altering the number of Aβ plaques, suggesting that amyloid-induced degeneration is at least partly mediated through tau (Roberson et al., 2007). After exposure of dendritic synapses to Aβ oligomers, tau is found in significantly higher than normal levels in the dendrites. Neurons with missorted tau have a reduced number of dendritic spines, increased activity of tau-targeting kinases, and increased cytosolic calcium. It is proposed that an increase in NMDA receptor-mediated calcium influx results in disruption in phosphorylation of proteins mediated by the calcium-dependent kinase calmodulin. Tau phosphorylation is mediated by calmodulin, meaning dysregulation of intracellular calcium concentrations triggered by interaction of Aβ at the synapse may lead to tau hyperphosphorylation and microtubule destabilisation (Zempel et al., 2010). Reduction of tau in APP23 mice was found to significantly reduce postsynaptic targeting of Fyn kinase, leading to a reduction in excitotoxicity by uncoupling NMDA receptors from excitatory mechanisms (Ittner et al., 2010). Aβ is thought to contribute to neurodegeneration through excitotoxic mechanisms (Mattson et al., 1992, Olney et al., 1997). These data suggest that excitotoxicity in AD may be mediated through dendritic localisation of tau, with NFTs forming due to increased activity of tau kinases.

1.1.2.4 Cholinergic Hypothesis of Alzheimer's Disease

The cholinergic hypothesis of AD is based on the loss of innervation of cholinergic neurons in the limbic system and neocortex. Dysfunction of cholinergic pathways interacts with other pathophysiological markers of AD, including Aβ plaques and NFTs (Hampel et al., 2018). The cholinergic system modulates neural activity through acetylcholine (ACh) receptors and regulates many cognitive functions, including attention, working memory, and planning. Disruption to this system was found to correlate with cognitive decline in AD patients (Blokland, 1995, Darvesh and Hopkins, 2003, Lane et al., 2006, Perry et al., 1999). Reductions in the level of choline acetyltransferase (CAT) in the hippocampus, reduced activity in the cerebral cortex, and degeneration of cholinergic neurons in AD patients compared to controls were originally described in the 1970's (Bowen et al., 1976, Davies and Maloney, 1976, Perry et al., 1977). Later, further evidence for the cholinergic hypothesis of AD was provided, including deficits in acetylcholine (ACh) release and transport, loss of

cholinergic innervation to the cortex, and alterations in nicotinic and muscarinic ACh receptor expression (Figure 1.2) (Nilsson et al., 1986, Rylett et al., 1983, Whitehouse et al., 1982, Lebois et al., 2018). This is also supported by pharmacological studies examining the effect of modulating the cholinergic system on memory performance (Decker and McGaugh, 1991, Newhouse et al., 1994, Elrod and Buccafusco, 1991, Terry et al., 1993, Vitiello et al., 1997). This hypothesis underlies the majority of current treatments for AD, such as acetylcholinesterase (AChE) inhibitors, which attempt to boost cholinergic activity (Doggrell and Evans, 2003). However, though there is agreement that deficits in the cholinergic system impacts cognition, it is not established as a cause of AD (Sanabria-Castro et al., 2017). Many of the changes seen in the cholinergic system have been observed in post-mortem tissue and so

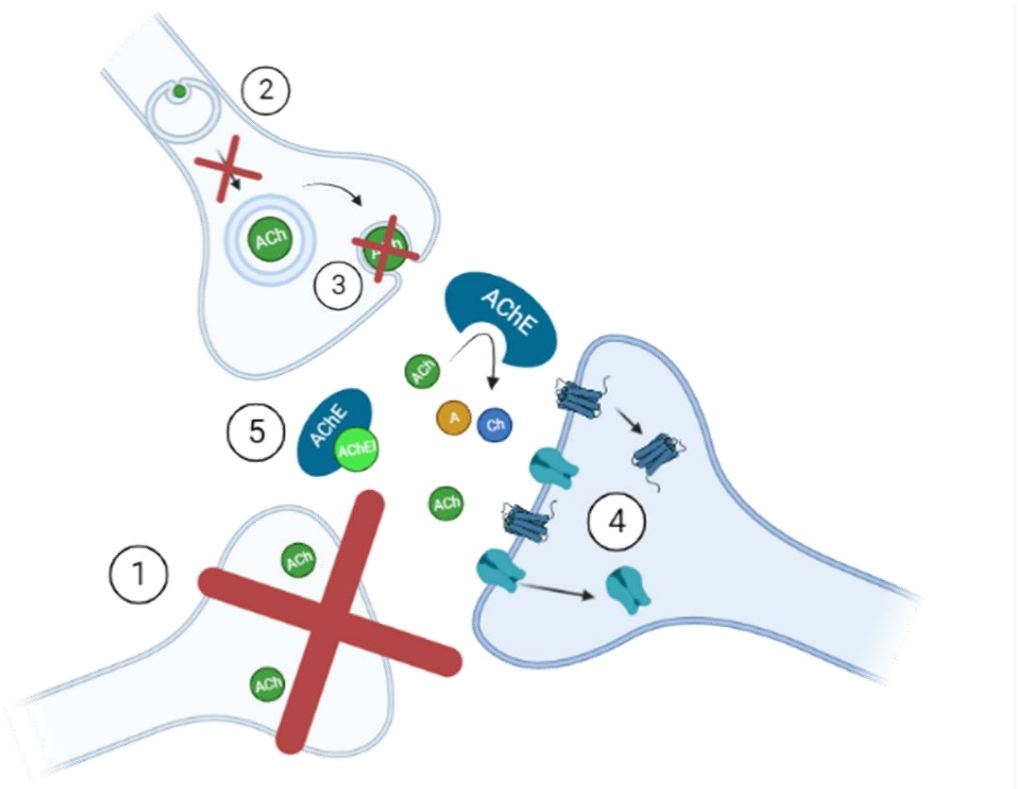

Figure 1.2 The cholinergic hypothesis of Alzheimer's Disease. *Diagram representing deficits in the cholinergic system in AD.* ***1)*** *Loss of cholinergic innervation* ***2)*** *Reduced ACh transport within the pre-synaptic membrane* ***3)*** *Reduced ACh release from the pre-synaptic membrane* ***4)*** *Down-regulation of nicotinic and muscarinic ACh receptors on the post-synaptic membrane. AChE inhibitors* ***(5)*** *are used to block the breakdown of ACh, increasing the concentration in the synaptic cleft, leading to increased receptor stimulation. ACh: Acetylcholine, AChEI: Acetylcholinesterase Inhibitor, A: Acetate, Ch: Choline. Figure created in BioRender.*

represent the brain at the end stages of AD, providing limited insights into the pathology underlying early stages of AD (Terry and Buccafusco, 2003).

1.1.3 Current Treatments

There is no cure for AD and no therapies to stop or reverse progression. The majority of treatments currently available only provide symptomatic relief and attempt to slow the progression of the disease. There are four drugs approved by the Food and Drug Administration (FDA) for use in the treatment of AD. Donepezil, galantamine, and rivastigmine are acetylcholinesterase (AChE) inhibitors which prevent the breakdown of acetylcholine (Ach). Memantine is an NMDA receptor antagonist which relieves symptoms of AD by attempting to block excitotoxicity produced by excessive glutamate signalling (Carvalho et al., 2015). These drugs can provide a small but significant benefit to patients, particularly in the early stages of AD. Patients experience a slower decline in cognitive ability and a delay in admission to full-time care; however, as the disease progresses these treatments become less effective (Deardorff et al., 2015). Drugs such as selective serotonin reuptake inhibitors (SSRIs) and antipsychotics are also prescribed to treat the behavioural symptoms of AD, such as co-morbid depression and psychosis (Yiannopoulou and Papageorgiou, 2013). However, the effectiveness of these treatments is debated, as SSRIs and antipsychotics were not shown to provide any benefit over placebo with increased risk of adverse effects (Banerjee et al., 2011, Zec and Burkett, 2008).

Disease-modifying treatments are being investigated, but none have so far had success in clinical trials. BACE and γ-secretase inhibitors have been considered to inhibit Aβ synthesis (Sharma et al., 2019). Specifically, BACE1 is targeted for inhibition as this isoform is predominantly responsible for APP cleavage in neurons (Cai et al., 2001). A major challenge with this approach is the loss of additional BACE1 functions, such as roles in axon guidance (Hitt et al., 2012). Failure of these drugs to produce clinical benefits have questioned the effectiveness of this strategy, especially as they prevent the formation of new plaques with no effect on existing ones. A successful BACE1 inhibitor may therefore form a preventative rather than curative therapy (Menting and Claassen, 2014). γ-secretase inhibitors have failed in late-stage clinical trials due to negatively affecting cognition and increasing rates of skin cancer (Kelleher and Shen, 2010). Also, as with BACE1 inhibitors, this strategy does not remove existing Aβ plaques so could only form a preventative therapy.

To prevent the aggregation of Aβ, molecules which interfere with Aβ-Aβ interactions have been developed. These molecules have shown promise in *in vitro* and *in vivo* studies but fail in phase II clinical trials (Ma et al., 2012, Caltagirone et al., 2012). Potential druggable targets to increase the clearance of Aβ, such as enzymes and receptors mediating clearance and accumulation, have been described but anti-Aβ immunotherapies are the leading strategy to combat existing plaques (Mathis et al., 2007, Cai et al., 2016, Sharma et al., 2019).

Pharmacological approaches aimed at treating tau pathology have also been explored. Inhibition of GSK-3β has been explored to reduce hyperphosphorylation of tau. Lithium has been suggested to reduce tau phosphorylation by inhibiting GSK-3β *in vitro* and has shown encouraging results in slowing cognitive decline in initial clinical trials (Hong et al., 1997, Forlenza et al., 2012, Morris and Berk, 2016). However, the discontinuation rate of lithium therapy is relatively high and so may not form a feasible long-term treatment (Macdonald et al., 2008). Inhibition of CDK-5 has also been studied and found to restore synaptic functions and cognition *in vivo* although inhibitors have not yet progressed to clinical trials (He et al., 2017, Shukla et al., 2017).

Both active and passive immunisation methods have the trialled as an AD immunotherapy and both utilise the immune system by inducing the phagocytosis of plaques by microglia. This method has shown promising results in clinical trials, with increased clearance of Aβ plaques and slowing of cognitive decline in patients (Weiner and Frenkel, 2006). However, major safety concerns have hampered this research, most clearly demonstrated by the disastrous AN 1792 Alzheimer's vaccine clinical trial where around 6% of participants developed meningoencephalitis (Delrieu et al., 2012, Pride et al., 2008, Robinson et al., 2004, Coman and Nemes, 2017, NCT00021723, 2002). Since this trial, there has been some success in the development of anti-Aβ antibodies. Many have failed in phase III clinical trials which led to criticism of amyloid hypothesis of AD (Doody et al., 2014, Lasser et al., 2016, Moreth et al., 2013). However, Lecanemab, a humanised IgG1 monoclonal antibody against soluble Aβ, was found to reduced amyloid markers and slow cognitive decline in a phase III clinical trial in 2023. The treatment was associated with adverse events, including infusion-related reactions, atrial fibrillation, and angina

pectoris, meaning further trials over a longer period are planned to fully determine the efficacy and safety of Lecanemab (NCT03887455, 2019, van Dyck et al., 2022). Immunotherapies against tau have also been explored in the treatment of AD (Chai et al., 2011, Sharma et al., 2019). Antibodies targeted against structures essential for tau-tau interactions have been successful in reducing tau oligomers in vivo and passed phase I clinical trials (Novak et al., 2019). This vaccine (AADvac1) underwent a phase II clinical trial which showed AADvac1 had a good safety profile but did not significantly improve cognition. The study investigators suggest a phase III trial for AADvac1 is required to make robust conclusions on the clinical efficacy of the vaccine (NCT02579252, 2019, Novak et al., 2021). Other approaches in targeting tau proteins include antibodies against hyperphosphorylated tau as well as specific tau peptides and complete tau (Pedersen and Sigurdsson, 2015).

1.2 Microglia

1.2.1 Microglial Biology

Microglia are cells of myeloid lineage and often referred to as the macrophages of the central nervous system (CNS) (Figure 1.3). Although glia were first described in 1846 by Rudolf Virchow, microglia were not recognised as a unique cell type until 1924 through the work of Pío del Río-Hortega (Tremblay et al., 2015). These cells are derived from myeloid progenitors in the embryonic yolk sac, earlier than other tissue macrophages, and the population is maintained through local self-renewal rather than progenitor recruitment (Ajami et al., 2007, Ginhoux et al., 2010, Alliot et al., 1999, Lenz and Nelson, 2018). Microglia play an important role during development, where they mediate synaptic pruning through phagocytosis of tagged synapses, remove apoptotic cells, and regulate neural precursor and neuronal cell populations (Paolicelli et al., 2011, Cunningham et al., 2013, Marín-Teva et al., 2004). In the adult brain, ‘resting’ microglia survey the environment. In this state the cells have a ramified morphology with a small cell body and thin, motile processes. Activation of surface receptors on ramified microglia signals a threat to CNS homeostasis initiating a pathway resulting in ameboid microglia. This is a graded response where microglia become ‘activated’, coordinating both pro- and anti-inflammatory responses via cytokine release (Nimmerjahn et al., 2005). Microglia

gradually shift from a non-phagocytotic to a phagocytotic state through retraction of branches eventually reaching the ameboid state. These microglia can freely move throughout neural tissue, are phagocytotic, and secrete pro-inflammatory cytokines (Xu et al., 2022). Activation of microglial receptors by neuron-secreted chemokines has also been shown to form a feedback loop mediating synaptic plasticity (Wu et al., 2015, Ragozzino et al., 2006). Microglial activation occurs in response to brain injury and infection in an attempt at damage control. However, this activation can also result in harmful neuroinflammation, now identified as a key component of the pathology of neurodegenerative diseases (Shi and Holtzman, 2018, Jones et al., 2010).

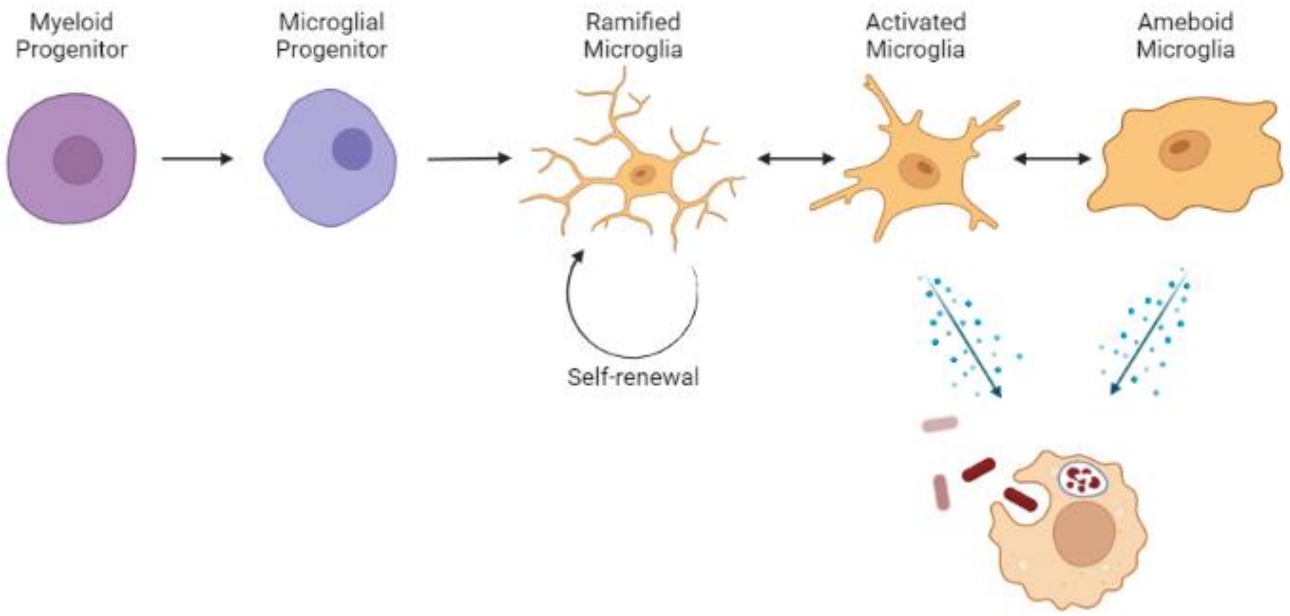

Figure 1.3 Developmental lineage of microglia. *Microglia are derived from myeloid progenitor cells from the embryonic yolk sac. Differentiation of myeloid progenitor cells to microglial progenitor cells occurs in the yolk sac before migration to the developing brain. Once mature, microglia exist in the 'resting' ramified state where the population is sustained by self-renewal. Ramified microglia survey the environment for disruptions to CNS homeostasis. Activation of surface receptors initiates a graded response of microglial activation. Activated microglia begin to retract their branches, release inflammatory cytokines, and become more phagocytotic. At the end of this pathway microglia exist in an ameboid state which is highly phagocytotic and free to move throughout the neural environment. Figure created in BioRender.*

1.2.2 Microglia in Neurodegeneration

The activation states of microglia have classically been grouped into ‘M1’and ‘M2’ based on the classification system of macrophages (Martinez and Gordon, 2014). The M1 phenotype was considered a classically activated state, characterised by secretion of pro-inflammatory mediators. The M2 phenotype defined microglia that were ‘alternatively activated’ which increases phagocytosis and triggers an anti-inflammatory response (Zhou et al., 2017, Shi and Holtzman, 2018). This classification has since been refuted for being too simplistic, as both macrophages and microglia show a broader range of activation types in response to the environment (Ransohoff, 2016, Murray et al., 2014, Mosser and Edwards, 2008). More recently the term ‘disease associated microglia’ (DAM) has been used to describe a subset of microglia with a unique transcriptional profile and functions associated with neurodegenerative diseases. DAM express many of the genes identified in AD genome wide association studies (GWAS) and activation requires expression of Triggering Receptor Expressed on Myeloid cells 2 (human protein: TREM2, mouse protein: Trem2) (Keren-Shaul et al., 2017). This activation has been proposed to be triggered in response to signals common to neurodegenerative diseases, such as apoptotic cells and protein aggregates (Deczkowska et al., 2018). Neuroinflammation has been implicated in many neurodegenerative diseases and altered expression of microglial proteins has been associated with AD (González et al., 2014, Seyfried et al., 2017). GWAS data highlighted an association between pathways of the immune response and late onset AD (LOAD), leading to the investigation of networks of microglial genes. It is thought that disruption to these networks by the presence of AD risk variants may contribute to the pathology of AD (Jones et al., 2010, Efthymiou and Goate, 2017). There is debate over whether these observed changes in microglia in AD are a cause of the disease or a consequence of it, but evidence associating risk variants of microglial genes with LOAD has shifted the prevailing view towards dysfunctional microglia playing a causal role in LOAD (Jones et al., 2010, Sims et al., 2017). In AD, neuroinflammation occurs due to increased activation and proliferation of microglia and expression of inflammatory signals as well as a decrease in phagocytosis (Martin-Estebane and Gomez-Nicola, 2020, Olmos-Alonso et al., 2016, Wendt et al., 2017, Dickson et al., 1993). Increased microglial activation has also been found to correlate with cognitive decline in AD

patients but not with amyloid load (Edison et al., 2008). Understanding the physiological consequences of microglial gene variants associated with AD risk is vital to understand AD pathology and identify potential druggable targets.

1.2.3 In Vitro Microglia Models

One of the most biologically relevant *in vitro* cell models are cultures of primary cells. Rodent primary microglial cultures can be generated by isolating microglia from both neonatal and adult animals and human primary cultures are derived from foetal tissue post-termination or from post-mortem tissue (Baker et al., 2002, Giulian and Baker, 1986, Timmerman et al., 2018). The yield of these cultures, however, is limited, particularly from human sources (Henn et al., 2009). Phenotypic changes due to changing environments influencing gene expression have also been reported (Gosselin et al., 2017). To produce microglial cultures of a sufficient yield for proteomics studies, immortalised cell lines are often used. These cells are initially derived from a primary cell culture and usually immortalised by incorporation of oncogenes allowing for continual proliferation. These cell lines are easier to maintain than a primary culture and allow for growth of large numbers of cells due to abundant proliferation. However, it has been acknowledged that immortalisation may result in a change to the microglial phenotype as these cell lines do show some genetic and functional differences from primary microglia (Butovsky et al., 2014, Melief et al., 2016, Timmerman et al., 2018). Both mouse and human immortalised microglia cell lines are available, although some studies have uncovered issues with the human cell lines. For example, the HMO6 line was originally immortalised by transduction of a v-myc carrying PASK 1.2 retroviral vector to embryonic primary microglia; however, exposure of these cells to lipopolysaccharide (LPS) did not induce expression of the same cytokines as primary microglia (Nagai et al., 2001). Lines developed from CHME-5 cells (including HMC3) have also been claimed to be human microglial immortalised cell lines (Janabi et al., 1995, Dello Russo et al., 2018). However, there is concern that some branches of this line may be cross-contaminated with rat glioblastoma cells (Dello Russo et al., 2018). Genotyping of short tandem repeats and by microsatellite analysis demonstrated these cells to be of rat origin, although were confirmed to be a suitable *in vitro* model of rat microglia, particularly for studying inflammatory signalling (Figueroa-Hall et al., 2017, Garcia-Mesa et al., 2017).

Two of the most commonly used mouse microglia cell lines are the BV2 and N9 lines (Timmerman et al., 2018). N9 cells were generated from embryonic primary microglia and transformed with *v-myc* or *v-mil* oncogenes from MH2, an avian retrovirus (Righi et al., 1989). These cells are positive for microglial markers such as macrophage antigens and glycoprotein F4/80 and negative for astrocytic and oligodendrocytic markers such as glial fibrillary acidic protein (GFAP) and galactocerebroside (GalC) (Timmerman et al., 2018). N9 cells also release pro-inflammatory cytokines in response to LPS and ATP stimulation, indicating the expression of purinergic receptors and similar calcium signalling patterns to primary microglia (Ferrari et al., 1996). BV2 cells were generated by transduction of *v-raf*/*v-myc* oncogenes into mouse neonatal primary microglia (Blasi et al., 1990). As with the N9 cell line, BV2 cells express microglial markers, including macrophage-1 antigen and macrophage-2 antigen (MAC1/2), are negative for GFAP and GalC, release cytokines in response to LPS stimulation, and show phagocytotic activity (Timmerman et al., 2018, Stansley et al., 2012, Boza-Serrano et al., 2014).

A major advantage of immortalised cell lines, particularly for proteomic studies, is the ability of these cells to proliferate quickly and so large numbers of cells can be generated relatively quickly and cheaply. However, as this occurs due to the presence of transduced oncogenes, by their very nature these cell lines are not the same as primary microglia raising questions as to their suitability for *in vitro* assays to determine the biological role of microglia. Due to this, Henn et al. (2009) compared BV2 cells to primary microglia and concluded that the BV2 line were a valid substitute. Proteomic and transcriptomic analysis identified similar patterns of signalling after LPS stimulation and both lines showed similar regulation of nitric oxide. BV2 cells were also able to stimulate other glial cells, including nuclear factor kappa-light-chain-enhancer of activated B cells (NF-κB) translocation and IL-6 production in astrocytes. As the BV2 line is one of the most common microglial cell lines, used in both academic laboratories and within the pharmaceutical industry, they are one of the best characterised *in vitro* models of microglia (Henn et al., 2009). Immortalised human microglial lines are not currently as well characterised, but a reliable line which can form a viable substitute to primary human microglia could be a more translatable *in vitro* assay to human biology and health.

Microglia derived from induced pluripotent stem cells (iPSCs) are potential models hoped to provide more translatable results from *in vitro* studies to clinical applications. iPSC-derived microglia have been found to have similar mRNA/gene expression to human foetal microglia, although cells resembling dendritic cells and macrophages are also generated (Pandya et al., 2017, Muffat et al., 2016, Douvaras et al., 2017, Haenseler et al., 2017). This creates a problem when studying neurodegenerative diseases as these disorders typically appear in old age. Signs of aging in cells, such as senescence and telomere shortening, are reset during the reprogramming of adult donor cells to iPSCs (Timmerman et al., 2018). The microglial cultures produced may then not be completely representative of microglia within the brains of patients. Direct reprogramming which skips the stem cell stage has been described, producing cells which retain signs of aging (Mertens et al., 2015, Prasad et al., 2016). For both of these reasons, and the fact that the shortest of these protocol takes 6-8 weeks and is a relatively costly procedure, means that immortalised microglial lines are the most commonly used *in vitro* models to study the physiology of microglia.

1.3 Genetics

1.3.1 Introduction to Genetics

Knowledge of the genetic factors that influence both physiological and pathological mechanisms is a key foundation in understanding the aetiology of disease. In April of 2003, the Human Genome Project (HGP) was declared complete by the National Human Genome Research Institute (Collins et al., 2003, International Human Genome Sequencing Consortium, 2004). This success provided an invaluable tool for identifying genes responsible for human diseases. When the project began in 1990, 100 disease genes had been identified and by the end over 1400 genes were known to affect human disease. More than 100,000 alleles have since been found to contribute to at least one disorder and genes for most Mendelian disorders have been identified thanks to this significant resource (Hamosh et al., 2005, Stenson et al., 2014). However, it was also discovered that many diseases do not have just one causal gene and therefore no single druggable target (Penrod et al., 2011). Despite this, the HGP has provided a framework for the collection of genomic-scale data and

allowed for advances in functional genomics (Penrod et al., 2011). From this, fields such as transcriptomics, proteomics, and epigenomics stemmed, offering insights into the genotype-phenotype relationship. This has led to the identification of druggable targets in many areas of pathology, including cancer, psychiatric disorders, and Huntington's disease (HD), as well as in AD (Reddy and Kaelin, 2002, Gandal et al., 2016, Albin and Tagle, 1995).

Pathology can be the result of variation in multiple genes (as well as environmental factors), and variants within an individual gene may therefore only account for a small proportion of the phenotype. Therefore, risk for a polygenic disorder varies between individuals due to genetic variation within the population (Lvovs et al., 2012). Risk accumulates with the presence of additional risk alleles meaning polygenic risk scores can be calculated based on the variants an individual possesses. Around 90% of this genetic variation is thought to be due to single nucleotide polymorphisms (SNPs) (Collins et al., 1998). SNPs are common within populations and occur once in every 250-1000 nucleotides on average (Ye et al., 2001). SNPs are defined as a single base pair change when compared to the human reference genome sequence (International Human Genome Sequencing Consortium, 2004, Jackson et al., 2018). Within exons, these can be silent (no amino acid change), missense (base pair change results in an amino acid change), or nonsense (base pair change results in a premature stop codon and truncated protein). SNPs more commonly occur in non-coding regions as only around 1.5% of the genome encodes for proteins. SNPs present in these regions can affect the binding of proteins such as transcription factors and alter gene expression and splicing. SNPs which are known to influence disease are referred to as risk variants. These variants range in frequency and effect size (McCarthy et al., 2008) (Figure 1.4). Mendelian disorders are caused by rare variants with a high effect size and GWAS methods have identified hundreds of common variants with low effect sizes. These variants contribute to many different phenotypes, including AD, schizophrenia (SZ), and even height (Shen and Jia, 2016, Bergen and Petryshen, 2012, Guo et al., 2018). Rare variants with a low effect size are difficult to identify but may act as modifier variants (Hammer et al., 2017). SNPs occur more frequently in non-coding regions of DNA as they are more likely to be selected against in coding regions (Collins et al., 1998, Nickerson et al., 1998). This also complicates the identification

of druggable targets through genetic sequencing, as only a minority of SNPs occur within exons and those within introns are thought to affect gene expression.

Identification of genes affected by SNPs is also complicated by linkage disequilibrium (LD; defined as “the non-random association of alleles at different loci”

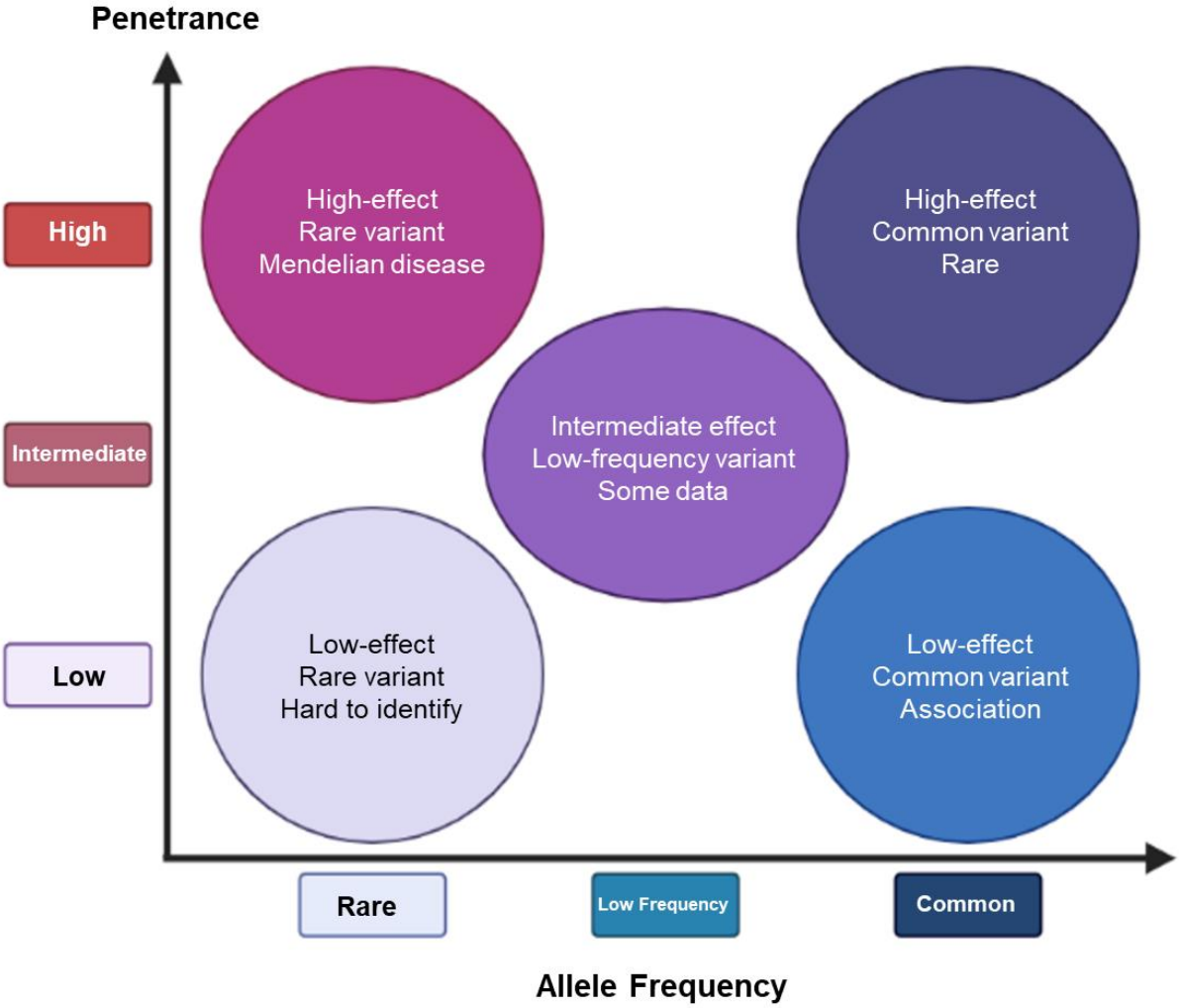

Figure 1.4 Risk variants range in frequency and effect size. *Risk variants have different frequencies amongst a population. Rare alleles have a minor allele frequency between 0.001 and 0.005, low frequency variants between 0.005 and 0.05, and common variants >0.05. Effect size, or penetrance, also differs. The effect size is the contribution of a particular SNP to a particular phenotype. A variant with a high effect size greatly contributes to the specific phenotype. Common variants with a high-effect size are rare as they are generally selected against. Mendelian diseases, such as cystic fibrosis or sickle cell, are caused by rare variants of high effect. Low effect common variants are identified through association studies and are thought to explain 50% of the heritability of late onset Alzheimer’s disease. Low-frequency variants with intermediate effects are also detected through association studies but are harder to identify. Low-effect rare variants are the hardest to identify although can be detected through linkage disequilibrium patterns with common variants. Figure created in BioRender.*

(Slatkin, 2008)) and long-range gene regulation (enhancer-promoter interactions have been identified which span up to 1000 kb (West and Fraser, 2005)).

Another complication in understanding how SNPs affect the function of the proteins they code for is post-transcriptional modifications. Splicing can occur meaning a single gene can encode multiple isoforms of a protein. Exon skipping, intron retention, and alternative 3' and 5' sites can occur, meaning a SNP may affect one isoform but not another or modify the splicing mechanisms themselves.

1.3.2 Genetics of Alzheimer's Disease

Genetic mutations underlying EOAD led to hypotheses for the aetiology of AD. The heritability of EOAD is thought to be around 90% and is estimated to be between 58% and 79% for LOAD (Gatz et al., 2006, Wingo et al., 2012). Genes carrying risk for AD were first identified in linkage studies of multiplex families with EOAD. The development of GWAS, whereby around 1 million SNPs are simultaneously genotyped in large patient and control samples, then allowed for the discovery of common risk variants with a low to moderate effect size (Shen and Jia, 2016, Ertekin-Taner, 2010). Most recently, next generation sequencing (NGS) of the exome and whole genome has been used to identify rare variants contributing to LOAD (Sims et al., 2017, Bis et al., 2020).

Over 50 susceptibility loci for LOAD have been identified at genome-wide significance, including both common and rare variants (Sims et al., 2020). The rapidly growing list of associated genes can be attributed to international co-operation, as large patient and control data sets are required for the identification of both common and rare variants. In 2011, the International Genomics of Alzheimer's Project was formed from a merger of the AD Genetics Consortium, the Cohorts for Heart and Aging Research in Genomic Epidemiology, the European AD Initiative, and the Genetic and Environmental Risk in AD group. The first results from this project identified 11 new risk loci, a list which has grown substantially since (Lambert et al., 2013, Sims et al., 2020). Common risk variants for AD have been identified through GWAS and rare risk variants through NGS, highlighting 'hub genes' which significantly influence AD risk.

1.3.2.1 Linkage Studies

As mentioned above, rare genetic variants with a strong effect on risk for AD were initially identified through linkage studies. Here, co-segregation of the phenotype with particular alleles at highly polymorphic markers is sought in families with a high incidence of the trait to identify the chromosomal location likely to contain the causal genetic variant. This is possible due to linkage of genetic variation within families, where genes in close proximity to one another remain linked during meiosis (Pulst, 1999).

Initially, loci contributing to EOAD were identified through linkage studies (Naj and Schellenberg, 2017). A locus on chromosome 21 was implicated and subsequent investigation identified rare variants of *APP* as a causal factor (Goate et al., 1991, St George-Hyslop et al., 1987). Functional studies showed that mutations in *APP* shifted the cleavage of APP towards the amyloidogenic pathway resulting in greater numbers of Aβ plaques (Suzuki et al., 1994). Variants of *PSEN1* and *PSEN2,* located on chromosomes 14 and 1, respectively, were also found to cause EOAD (Levy-Lahad et al., 1995, Rogaev et al., 1995, Sherrington et al., 1995). The proximal long arm of chromosome 19 was also implicated in EOAD through linkage studies (Pericak-Vance et al., 1991). This location was known to include the gene *APOE* and the protein APOE was found to bind to Aβ in the CSF. The specific isoform APOE4 was subsequently found to be associated with LOAD, the first and strongest genetic risk factor identified (Strittmatter et al., 1993, Saunders et al., 1993b, Saunders et al., 1993a). Three isoforms of *APOE* exist due to point mutations at two sites within the gene, resulting in amino acid changes (LaDu et al., 1994). The ε3 allele is considered the wild-type and the ε2 isoform is associated with a protective effect against AD (Corder et al., 1994). *APOE4* is thought to contribute to risk for AD as the point mutations result in structural changes which negatively affect ligand binding to molecules including Aβ and TREM2 (a receptor also implicated in AD risk, see section 1.3.4). In mouse models this has been shown to disrupt clearance of Aβ plaques, implicating *APOE* in the amyloid cascade hypothesis (Deane et al., 2008). *APOE* has also been found to influence vascular function, neuroinflammation, and synaptic plasticity; functions implicated in AD pathology (Liao et al., 2017). Individuals homozygous for *APOE4* have a 5-times increased risk for AD compared to heterozygous individuals, indicating a dose-dependent risk (Sims et al., 2020).

A major limitation with linkage studies, however, is they only identify risk variants with a high effect size and therefore are often rare, with the notable exception of *APOE* which has unusually high penetrance for a common variant. In order to identify variants of lower effect size, much larger genomic datasets of both case and control groups are required.

1.3.2.2 Genome Wide Association Studies

More recently, disease-associated variants have been identified through GWAS. GWAS is a highly successful method to investigate how genetics influences phenotype, although confounding variables between study groups and distinct genetic variation between ethnic groups can result in reproducibility issues (Jackson et al., 2018, Sazonovs and Barrett, 2018). The development of DNA microarray technology and the completion of the Human Genome and International HapMap Projects paved the way for high-throughput genome comparisons between case and control groups (Bush and Moore, 2012, The International HapMap Consortium, 2005, International Human Genome Sequencing Consortium, 2004, Sazonovs and Barrett, 2018). SNPs which appear more frequently in the case samples compared to controls are determined to be associated with increased risk for the disease. SNPs appearing less frequently in cases compared to controls are likely to be protective against the disease. As typically 1 million independent SNPs are tested, a stringent P-value of $\leq 5.0 \times 10^{-8}$ is used as the threshold for 'genome-wide significance' to control for multiple testing. The first published GWAS identified a polymorphism associated with age-related macular degeneration and as of April 2022 the GWAS Catalog contains 372,752 genome-wide significant associations between genetic variants and phenotypic traits from 5,690 publications (Klein et al., 2005, Buniello et al., 2019). The goal of GWAS is to find associations between allele or genotype frequency and a phenotype. When studying a disease, case and control groups are genotyped by SNP arrays or whole-genome sequencing. Association tests then identify SNPs which show a genome-wide significant association with the disease. Once a locus has been identified, the region is examined for genes which are likely to influence the phenotype. Loci in linkage disequilibrium (LD) with the identified SNP also need to be investigated as they may contain the site of the causal variant. The identified locus may not be the location of the risk gene, as it may influence the expression of a gene many kilobases away. Whilst GWAS have

been responsible for the identification of thousands of disease/trait-associated genetic variants, only a proportion of the heritability of common diseases has been explained. For example, around 50% of the heritability of LOAD has been explained by common variants, variants with a minor allele frequency (MAF) of greater than 0.05 (Sims et al., 2020). This missing heritability may be the failure of GWAS to identify SNPs with a small effect size due to the high significance threshold required to account for multiple testing. Susceptibility to a disease is also influenced by environmental factors and so gene-environment interactions may explain some of the missing heritability, along with rarer risk variants (Tam et al., 2019).

Some of the first genes found to be associated with AD from GWAS were variants in the *clusterin* (*CLU*; also known as *apolipoprotein J or APOJ*), *phosphatidylinositol-binding clathrin assembly protein* (*PICALM*), and *complement receptor 1* (*CR1*) loci (Harold et al., 2009, Lambert et al., 2009). CLU is best known as an extracellular chaperone protein but is also involved in cell death and survival pathways (Humphreys et al., 1999). PICALM is known to play a role in clathrin-mediated endocytosis and CR1 is a receptor involved in the complement pathway in the immune response (Zhu et al., 2015, Ford et al., 2001). Both CLU and PICALM have been linked to the aggregation and clearance of Aβ plaques and the association of CR1 implicates the innate immune system in the pathology of AD (Xu et al., 2015, Foster et al., 2019, Zhu et al., 2015).

GWAS have been a ground-breaking tool for piecing together the genetic architecture of AD risk. However, alone these studies cannot fully explain the heritability of disease. As GWAS identifies trait-associated common variants, rare variants are not generally targeted (Lord et al., 2014). Identification of these variants, for example via whole exome or whole genome sequencing, is required to fully understand the contribution of genetics to the aetiology of LOAD (Sazonovs and Barrett, 2018). GWAS also cannot identify novel sites of genetic variation. Samples are genotyped by microarrays, allowing for the association between known SNPs and a particular disease but does not identify completely novel SNPs which require DNA sequencing. Although, most common variants have been catalogued and known LD patterns can be used for accurate genotype imputation at minor allele frequencies (McCarthy et al., 2016).

1.3.2.3 DNA Sequencing

In order to identify rare variants for diseases, DNA sequencing or targeted microarray technologies are required. Rare coding variants are defined as having a MAF of less than 0.01 and occur in less than 1% of the population (International Human Genome Sequencing Consortium, 2004, Sims et al., 2020). One of the most commonly used methods is NGS, a high throughput sequencing method which can sequence small DNA fragments in parallel (Behjati and Tarpey, 2013). NGS developed from Sanger sequencing, developed in 1977, which utilises labelled dideoxynucleotides to inhibit chain synthesis and produce DNA fragments of different lengths. The fragments are then resolved on a gel and the DNA sequence can be read (Sanger et al., 1977). In NGS, an entire genome can be read by fragmenting the full sequence and analysing them in parallel by either sequencing by hybridisation or sequencing by synthesis methods (Schuster, 2008, Slatko et al., 2018). Exome-wide sequencing can also be used to detect rare variants in protein-coding sequence. As the exome comprises of around 2% of the eukaryotic genome, the cost of exome-wide sequencing is significantly lower than whole-genome sequencing (Cosart et al., 2011).

Sims et al. (2017) used whole-exome microarray to genotype individuals, identifying rare coding variants for *TREM2*, *ABI3*, and *PLCG2* associated with LOAD. Four missense variants were found to be associated with LOAD at genome-wide significance: p.P522R in *PLCG2* (rs72824905, $P=5.38\times10^{-10}$, OR=0.68, MAF in cases=0.0059, MAF in controls=0.0093); p.S209F in *ABI3* (rs616338, $P=4.56\times10^{-10}$, OR=1.43, MAF in cases=0.011, MAF in controls=0.008); R62H (rs143332484, $P=1.55\times10^{-14}$, OR=1.67, MAF in cases=0.0143, MAF in controls=0.0089) and R42H (rs75932628, $P=5.38\times10^{-24}$, OR=2.46, MAF in cases=0.004, MAF in controls=0.002) in *TREM2*, of which the p.R62H variant was novel. The exact mechanism of how these variants influence AD risk is currently unknown, but the *PLCG2* variant is thought to be protective and other *TREM2* variants increase risk of AD due to reduced ligand binding (Magno et al., 2019, Atagi et al., 2015). Understanding the functional biology of these risk genes is paramount in explaining how these variants influence risk for AD. Genomic approaches such as GWAS and NGS can identify associations between the genes and risk for disease, but cell biology and proteomic

studies are required to fully understand the function of risk proteins, consequences of disease associated genetic variants, and to identify potential druggable targets.

1.3.3 ABI3

Abl interacting protein 3 (human protein: ABI3, mouse protein: Abi3) was first characterised by Miyazaki et al. (2000) by cloning from a human placental cDNA library. The gene was initially named new molecule encoding Src homology 3 (NESH) before being added to the ABI family due to similar domain structures and amino acid sequence as ABI1 and ABI2. ABI3 mRNA was found to be expressed in a variety of tissues including the heart, liver, and kidney, as well as low level expression in the brain and skeletal muscle. The ABI3 protein contains a Src homology 3 (SH3) motif, proline-rich regions, and serine rich regions, both of which are intrinsically disordered (Figure 1.5). The presence of an SH3 domain suggests a role as a signalling protein as this region is associated with protein-protein interactions (PPIs) and regulation of many cellular functions (Kurochkina and Guha, 2013, Dionne et al., 2021).

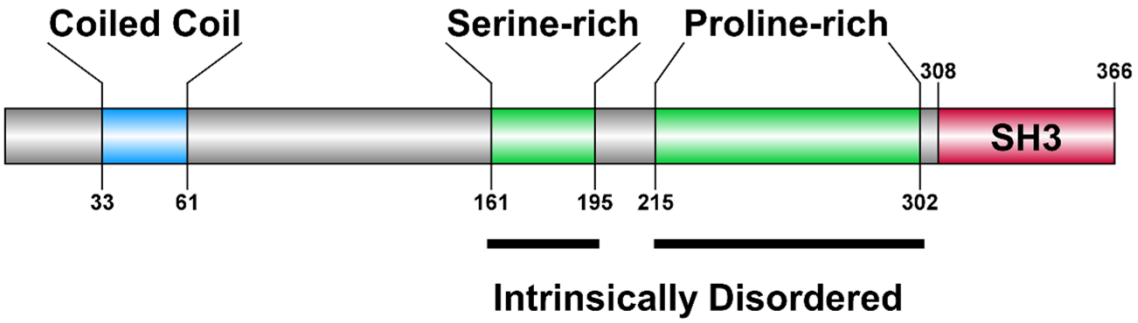

Figure 1.5 ABI3 protein structure. *The protein sequence of ABI3 is 366 amino acids long with an SH3 domain at the C-terminus. The structure also contains a coiled coil domain, a serine-rich, and a proline-rich region. These serine and proline rich regions are intrinsically disordered. Figure created in DOG 2.0.*

1.3.3.1 Function

The exact function of ABI3 is as yet unknown, although it is known to play a role within the Wiskott-Aldrich syndrome protein (WASP)-family verprolin-homologous protein (WAVE) regulatory complex (WRC) (Sekino et al., 2015). The WRC contains five subunits of proteins from the ABI family (ABI1, ABI2, or ABI3), WAVE family (WAVE1, WAVE2, or WAVE3; also known as WASP-family member (WASF) proteins), hematopoietic proteins (HEM1 or HEM2; also known as nucleosome

assembly protein 1 (NAP1)), cytoplasmic fragile X messenger ribonucleoprotein 1 interacting protein (CYFIP) proteins (also known as SRA proteins) and BRICK1 (also known as haematopoietic stem/progenitor cell protein 300 (HSPC300)) (Figure 1.6) (Chen et al., 2014). Different isoforms of the WRC are produced by inclusion of different orthologues of the above proteins. The main function of the WRC is regulation of the actin cytoskeleton through activation of the actin-related proteins 2 and 3 (Arp2/3) complex (Takenawa and Suetsugu, 2007). Arp2/3 nucleates actin filaments, leading to branched actin structures which form lamellipodia at the leading edge of motile cells (Innocenti, 2018). Hirao et al. (2006) found that ABI1 and ABI2 regulated the activity of c-Abl tyrosine kinase (which promotes the formation of the WRC through the phosphorylation of WASF2) but ABI3 did not. All three ABI family members were shown to interact with WASF2, but ABI3 did not interact with c-Abl tyrosine kinase whereas ABI1 and ABI2 did. This suggests that ABI3 functions within the WRC to regulate the cytoskeleton but does not promote actin polymerisation, as ABI1 and ABI2 do. The presence of ABI3 has also been shown to reduce ABI1 levels and, when present in the WRC, inhibited the formation of lamellipodia by preventing the translocation of WASF2 to the plasma membrane (Sekino et al., 2015). Microglia from Abi3 knockout mice show morphological abnormalities, alteration of microglial surveillance, and a reduction in phagocytosis (Simonazzi et al., 2021, Preprint, Karahan et al., 2021).

1.3.3.2 Role of ABI3 in Alzheimer's Disease

Within the CNS, ABI3 is primarily expressed in microglia and has also been observed in hippocampal neurons (Satoh et al., 2017, Bae et al., 2012b). Although the specific function of ABI3 has not been studied, the WRC is known to regulate pathways leading to T-cell activation and microglial migration occurs through the regulation of lamellipodium via the action of the actin-related protein 2/3 (Arp2/3) complex to form branched actin structures (Satoh et al., 2017, Nolz et al., 2006, Vincent et al., 2012). It is likely that due to its association with the WRC and regulation of the actin cytoskeleton, ABI3 plays a role in microglial motility and morphological changes, such as during phagocytosis and cell activation. ABI3 has also been implicated in neuronal dendritic spine and synapse formation (Bae et al., 2012a, Bae et al., 2012b). In AD, ABI3 is highly expressed in microglia associated with Aβ plaques, adding to evidence that ABI3 is involved in mechanisms

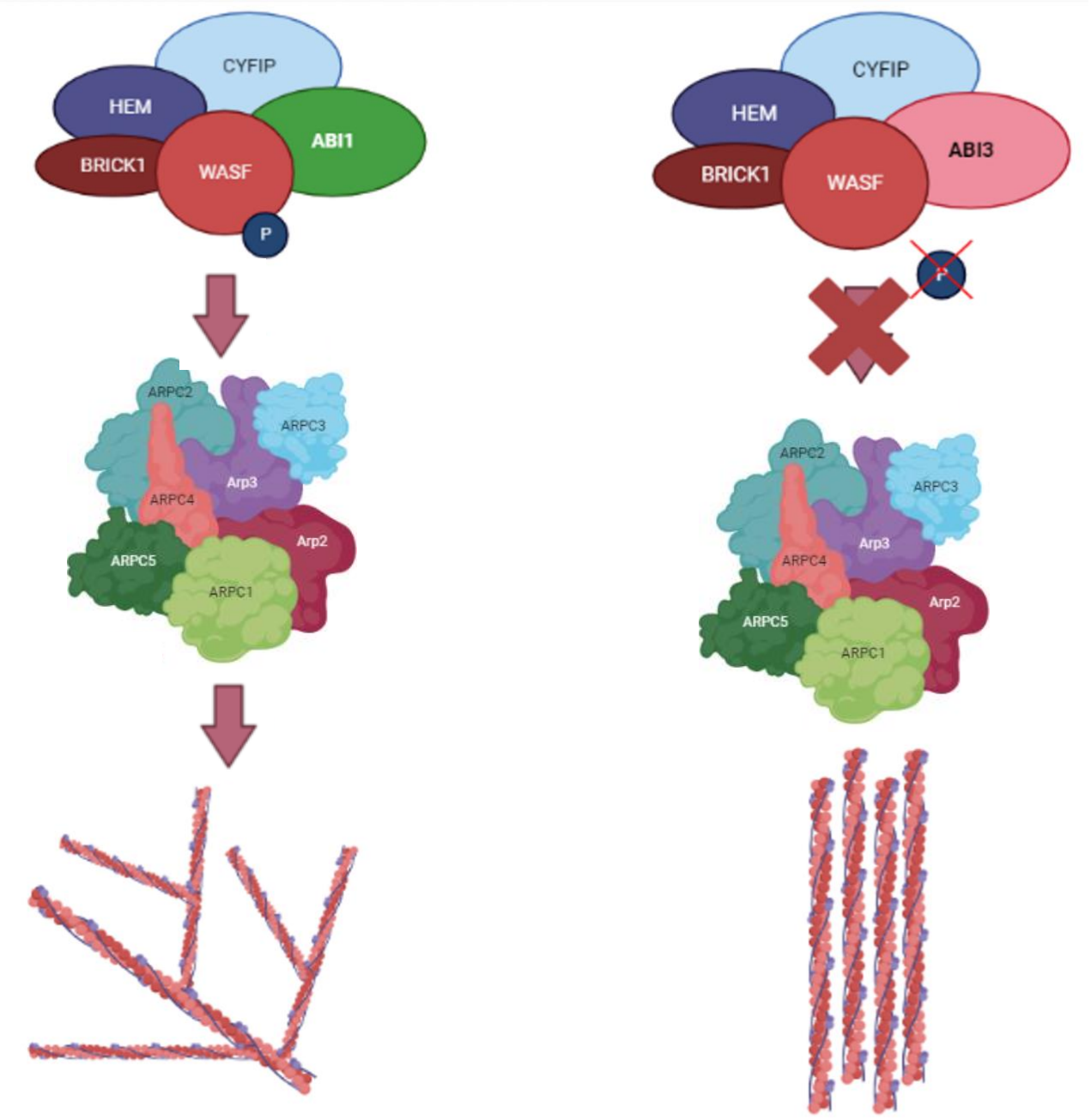

Figure 1.6 Schematic of the Proposed Role of ABI3 in the WAVE Regulatory Complex. *The WRC is a 5-subunit complex consisting of paralogues of Cytoplasmic fragile X messenger ribonucleoprotein 1 interacting protein (CYFIP), Hematopoietic protein (HEM), BRICK1, Wiskott-Aldrich syndrome protein-family member (WASF), and Abl interacting protein (ABI) family members. When the WRC is active, ABI1 is included in the complex resulting in the phosphorylation of WASF, inducing translocation to the plasma membrane and activation of the Arp2/3 complex. This results in nucleation of actin filaments creating branched actin structures. When ABI3 is incorporated into the complex, WASF is not phosphorylated and so the WRC is inactive resulting in reduced activation of the Arp2/3 complex, allowing for parallel actin structures to form. Figure created in BioRender.*

underpinning cell migration and motility (Satoh et al., 2017). The rare ABI3 variant (S209F) was found to be associated with increased AD risk but to date no study has elucidated the molecular mechanisms of this risk (Sims et al., 2017, Dalmasso et al., 2019, Conway et al., 2018). It is possible that the risk is mediated by changes in ABI3 function or interaction with the WRC.

1.3.4 TREM2

TREM2 is a plasma membrane protein expressed in cells of the myeloid lineage, including monocytes, macrophages, and osteoclasts (Paloneva et al., 2003, Klesney-Tait et al., 2006, Turnbull et al., 2006, Bouchon et al., 2000, Daws et al., 2001). Within the brain TREM2 is expressed primarily in microglia, with some expression in a subpopulation of neurons (Schmid et al., 2002, Sessa et al., 2004, Jolly et al., 2019). Expression levels are regulated by microglia stimulation and activation, Toll-like receptors (TLRs), CD33, and micro-RNAs (Sessa et al., 2004, Prada et al., 2006, Schmid et al., 2002, Zhong et al., 2017, Ford and McVicar, 2009, Chan et al., 2015, Bhattacharjee et al., 2016, Han et al., 2017).

1.3.4.1 Protein Life cycle and Trafficking

TREM2 contains an extracellular domain, a transmembrane region, and a short cytoplasmic tail (Figure 1.7) The mouse protein differs only from the human by a shorter cytoplasmic tail, which in both species does not contain any apparent signalling motifs and so cannot mediate signalling alone, although does contain a retromer-binding motif (Paradowska-Gorycka and Jurkowska, 2013, Colonna, 2003, Bouchon et al., 2000). In the trans-Golgi network (TGN), N-glycosylation sites in the extracellular domain are glycosylated (Park et al., 2015). These N-glycans have been shown to play a role in the trafficking of TREM2 to the plasma membrane and cell surface expression is modulated by other proteins, including mitogen-activated protein kinase kinases (Shirotani et al., 2022, Schapansky et al., 2021). The majority of TREM2, however, is located in intracellular pools in the TGN, which translocate to the cell surface after microglial stimulation (Prada et al., 2006, Sessa et al., 2004). Schmid et al. (2002) found that LPS activation of primary murine microglia reduced plasma membrane expression of TREM2, suggesting that activation of microglia by immunogenic ligands has the opposite effect on TREM2 expression than general activation by ionomycin. Zhong et al. (2017) discovered that the LPS-induced

downregulation of plasma membrane TREM2 is mediated through the c-Jun N-terminal kinases (JNK) pathway resulting in activation of the transcription factor nuclear factor kappa-light-chain-enhancer of activated B cells (NF-κB). TREM2 expression is also regulated by Toll-like receptors (which induce the production of inflammatory cytokines), CD33, and micro-RNAs (Bhattacharjee et al., 2016, Chan et al., 2015, Ford and McVicar, 2009, Han et al., 2017).

At the plasma membrane, TREM2 undergoes class 1 regulated intramembrane proteolysis. The ectodomain is first cleaved by ADAM10 (a disintegrin and metalloproteinase domain containing protein 10), the shedding of which results in soluble TREM2 (sTREM2), a form detectable in the CSF (Kleinberger et al., 2014, Schlepckow et al., 2017). The C-terminal fragment remains in the membrane with the short cytoplasmic tail. This fragment is then cleaved by γ-secretase within the membrane to degrade the protein (Wunderlich et al., 2013). Inhibition of γ-secretase results in significantly reduced TREM2-induced increases in intracellular calcium and phagocytotic activity in microglia (Glebov et al., 2016, Schlepckow et al., 2017). Cell surface Trem2 is also recycled via a retromer complex. Yin et al. (2016) found that vacuolar protein sorting 35 (Vsp35) regulates the recycling of Trem2 in microglia. Trem2 is internalised in a clathrin-dependent manner and Vsp35/retromer mediated endosome-to-plasma membrane trafficking. This process is regulated by proteins such as beclin 1, an autophagy-associated protein shown to affect microglial phagocytosis via interactions with the retromer-complex (Lucin et al., 2013).

1.3.4.2 Interactors, Signalling, and Function

Ligands of TREM2 include bacterial products such as LPS, as well as nucleic acids, APOE, anionic phospholipids, and Aβ (Wang et al., 2015b, Kawabori et al., 2015, Atagi et al., 2015, Jendresen et al., 2017, Daws et al., 2003). The only reported intracellular interactor of TREM2 is DNAX-activating protein 12 (DAP12; also known as killer cell activating receptor-associated protein; KARAP, and tyrosine kinases binding protein; TYROBP). DAP12 is a polypeptide containing an immunoreceptor tyrosine-based activation motif (ITAM) region and acts as an accessory protein for receptors in the C-type lectin family and the immunoglobulin superfamily (Ig-SF); indeed the TREM family was discovered by searching for DAP12-associated proteins (Bouchon et al., 2000, Turnbull and Colonna, 2007, Paradowska-Gorycka and Jurkowska, 2013, Olcese et al., 1997, Lanier et al., 1998). DAP12 is recruited to

TREM2 by an electrostatic interaction between the transmembrane domains of each protein (Call et al., 2010, Lanier et al., 1998, Zhong et al., 2017). As the protein interactome of TREM2 has not been systematically explored, it is possible other proteins interact with the intracellular domain of TREM2. There are currently no reported interactors for mouse TREM2 in the Biological General Repository for Interaction Datasets (BioGRID) database (Oughtred et al., 2021).

The TREM2/DAP12 signalling pathway is known to play a role in cell activation, differentiation, and survival, as well as control of the actin cytoskeleton (Peng et al., 2010) (Figure 1.8). The binding of ligands to TREM2 results in phosphorylation of DAP12, triggering intracellular signalling cascades (Lanier et al., 1998). Proteins activated downstream of DAP12 phosphorylation include spleen tyrosine kinase (SYK) and zeta-chain-associated protein kinase 70 (ZAP70), which activate the PI3K/Akt pathway. This pathway promotes cell proliferation and survival as well as phosphorylation of phosphatidylinositol-4,5-biphosphate (PIP2) at the plasma membrane triggering conversion to phosphatidylinositol-3,4,5-triphosphate (PIP3) resulting in the activation of PLCγ enzymes and other secondary messengers which induce the release of calcium from intracellular stores (Smith-Garvin et al., 2009, Paradowska-Gorycka and Jurkowska, 2013, Zheng et al., 2017).

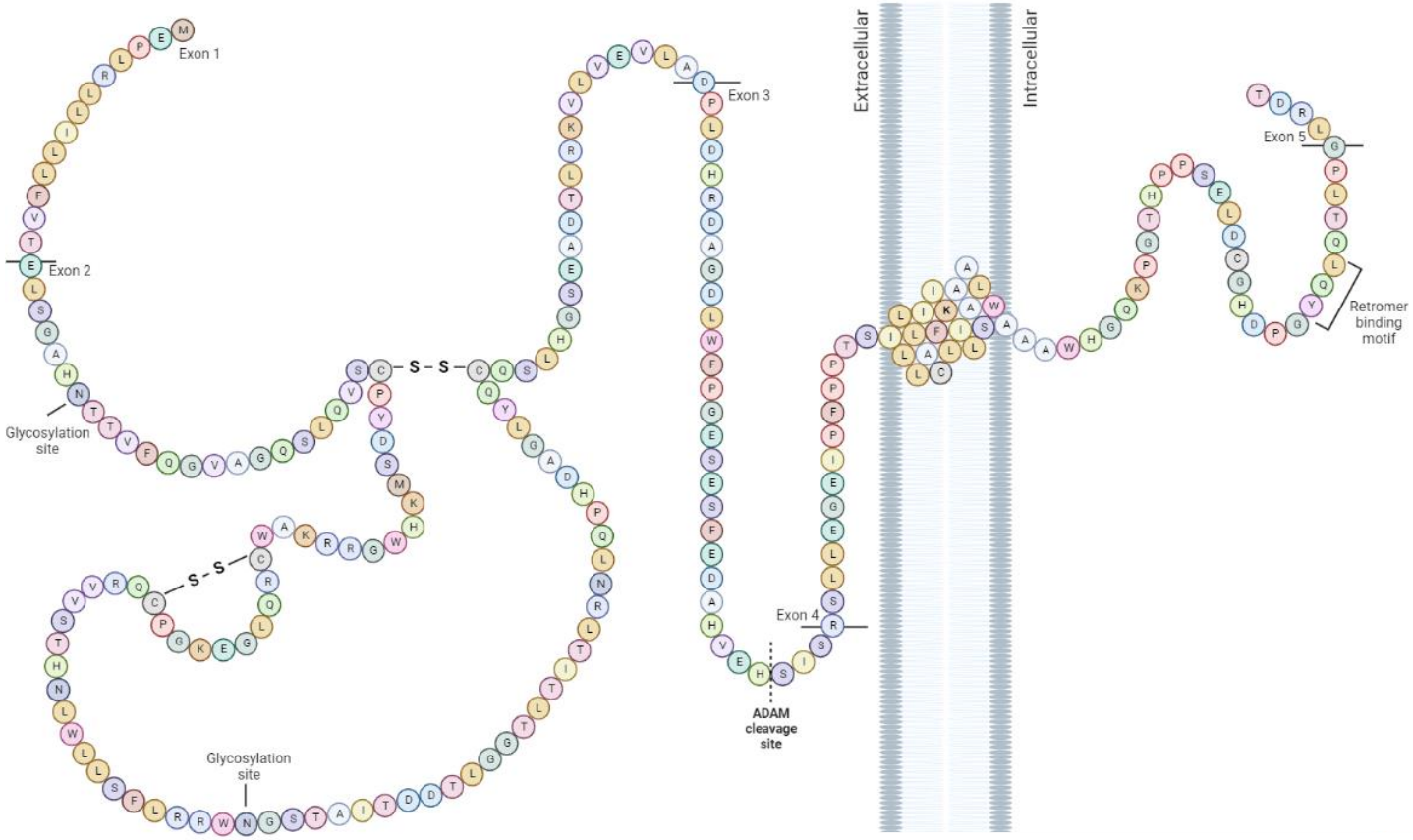

Figure 1.7 TREM2 protein structure. *TREM2 is a 230 amino acid protein with an extracellular domain, transmembrane region, and short cytoplasmic tail. The extracellular domain consists of 156 amino acids and includes a V-type Ig-SF domain (a structure known as the Ig fold; formed by disulphide-linked β-sheets with variable antigen recognition sites) and N-glycosylation sites. These sites are glycosylated within the Golgi complex, creating a 40 kDa protein, then de-glycosylated at the plasma membrane when the ectodomain is shed, leaving a 26 kDa protein. The transmembrane domain contains 21 amino acids including a positively charged lysine residue which mediates the interaction with DAP12. The short cytoplasmic tail of TREM2 consists of 35 amino acids and contains a retromer binding motif. TREM2 undergoes class 1 regulated intramembrane proteolysis by ADAM10, the shedding of which results in soluble TREM2. The C-terminal fragment remains in the plasma membrane with the short cytoplasmic tail which is eventually cleaved by γ-secretase. TREM2: triggering receptor expressed on myeloid cells 2. Adapted from Carmona et al. (2018). Figure created in BioRender.*

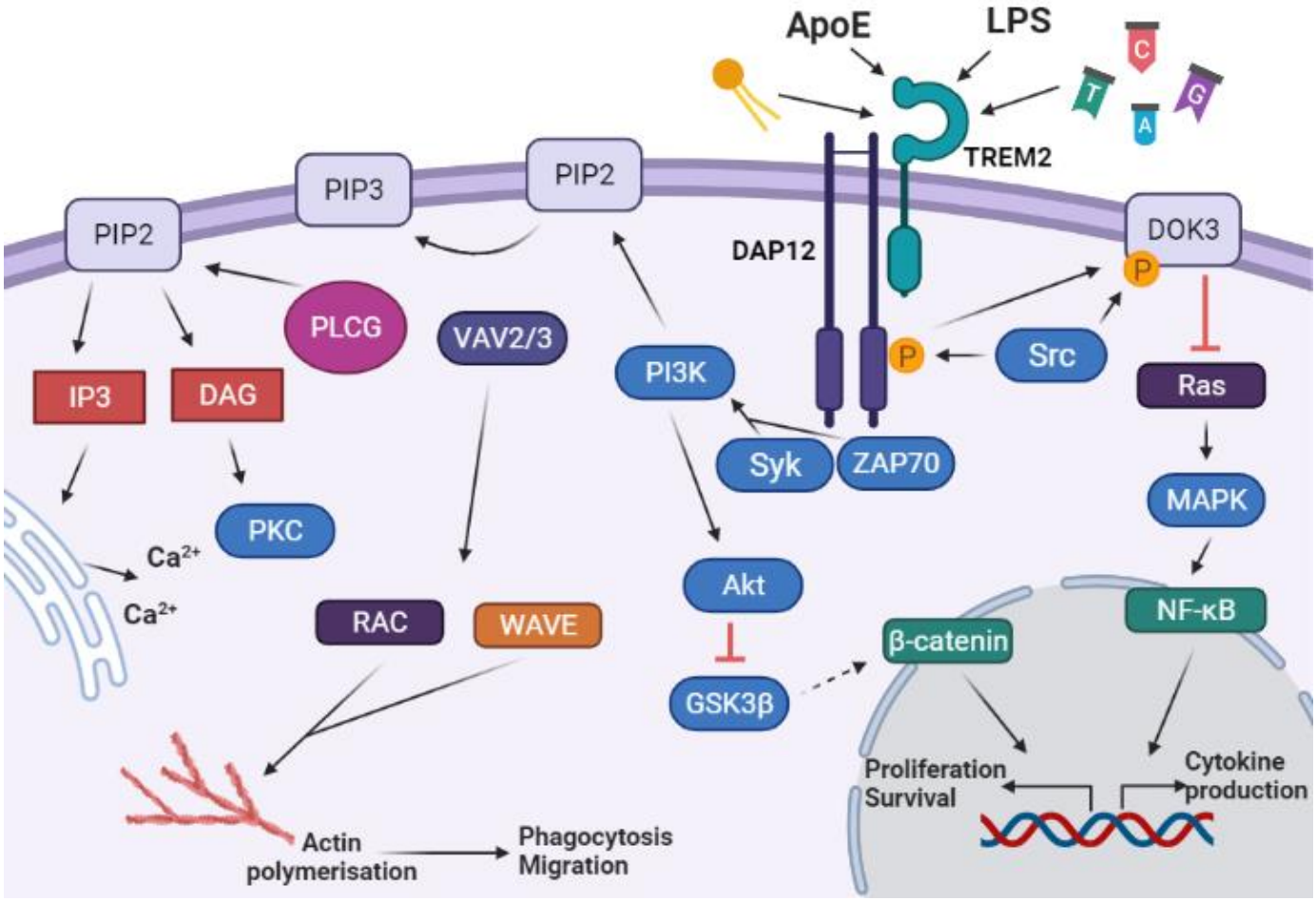

Figure 1.8 TREM2 signalling pathways. *Ligands of TREM2 include lipids, such as APOE and Aβ, bacterial products, such as LPS, and nucleic acids. Activation of the receptor by these ligands induces structural changes leading to an electrostatic attraction between TREM2 and DAP12. The ITAM region of DAP12 is then phosphorylated by Src kinases. This results in the activation of kinases SYK and ZAP170 as well as the phosphorylation of docking protein 3 (DOK3). This reduces the activation of Ras proteins, in turn reducing the activity of MAPK and NF-κB pathways. ZAP170 and SYK kinases activate the PI3K/Akt pathways. Akt inactivates GSK3β inducing translocation of β-catenin to the nucleus where it stimulates the expression of genes promoting cell proliferation and survival. PI3K phosphorylates PIP2 at the plasma membrane resulting in the creation of PIP3, the process of which contributes to the recruitment of PLCG and VAV enzymes. PLCG enzymes cleave PIP2 to form IP3 and DAG. IP3 induces the release of calcium from intracellular stores such as the endoplasmic reticulum whilst DAG activates PKC, both pathways resulting in further downstream cell signalling. VAV2/3 enzymes activate RAC and WAVE proteins which regulate the cytoskeleton through actin polymerisation. This induces changes in cell structure and morphology related to microglia switching to phagocytotic states and migration. TREM2: triggering receptor expressed on myeloid cells 2, APOE: Apolipoprotein E, Aβ: Amyloid β, ITAM: Immunoreceptor tyrosine-based activation motif, SYK: Spleen tyrosine kinase, ZAP170: zeta-chain-associated protein kinase 70, DOK3: Docking protein 3, MAPK: mitogen-activated protein kinase, NF-κB: Nuclear factor kappa-light-chain-enhancer of activated B cells, PI3K: phosphatidylinositol 3-kinase, GSK3β: glycogen synthase kinase 3β, PIP2: phosphorylates phosphatidylinositol-4,5-biphosphate, PIP3: phosphatidylinositol-3,4,5-triphosphate, PLCG: phospholipase-γ, IP3: Inositol trisphosphate, DAG: diacylglycerol, WAVE: WASP-family verprolin-homologous protein. Figure created in BioRender.*

TREM2$^{-/-}$ mice have been found to have a reduced microglial population and an increase in microglial apoptosis (Linnartz-Gerlach et al., 2019, Wang et al., 2015b). In osteoclast precursors, TREM2 deficiency reduces osteoclast proliferation (Otero et al., 2012). Similar mechanisms are known to control microglial cell proliferation and so a comparable pathway is likely to occur in microglia (Jay et al., 2017b).

The role of TREM2 in neuroinflammation has been widely studied as the receptor has been found to co-express with genetic markers of both inflammatory 'M1' and anti-inflammatory 'M2' microglia (Jay et al., 2017b, Konishi and Kiyama, 2018, Neumann and Takahashi, 2007, Carmona et al., 2018, Forabosco et al., 2013). Both up- and downregulation of inflammatory response genes have also been observed in dendritic cells of PLOSL (polycystic lipomembraneous osteodysplasia with sclerosing leukoencephalopathy; also known as Nasu-Hakola disease) patients, who carry mutations in both *TREM2* and *DAP12* (Kiialainen et al., 2007). TREM2 may therefore have opposing effects on the inflammatory response which could depend on disease context and cell-state (Jay et al., 2015).

Part of the immune response is migration of microglia to the site of injury. Levels of TREM2 expression correlate with the amount of microglial migration to apoptotic neurons and Aβ plaques (Wang et al., 2016, Mazaheri et al., 2017, Jay et al., 2015). Pathways known to regulate microglial motility are downstream of TREM2 activation. Rac and WASF proteins regulate the cytoskeleton via actin polymerisation and are activated by the conversion of PIP2 to PIP3 (Kurisu and Takenawa, 2009, Forabosco et al., 2013, Turner and Billadeau, 2002). This pathway also influences the morphology of microglia, allowing for phagocytotic activity. Phagocytosis in microglia is influenced by TREM2 signalling and interaction with APOE (Takahashi et al., 2005, Atagi et al., 2015, Bailey et al., 2015). Both TREM2 knockout and reduced activation have been shown to reduce the phagocytosis of apoptotic neurons by microglia both in vitro and in vivo, with overexpression of TREM2 increasing levels of microglial phagocytosis (Atagi et al., 2015, Takahashi et al., 2005, Kawabori et al., 2015, Hsieh et al., 2009).The cell surface expression of TREM2 is at least partly controlled by the TGN-plasma membrane-endosome cyling of the receptor, as with other phagocytotic receptors (Hall-Roberts et al., 2020).

1.3.4.3 Role in Alzheimer's Disease

TREM2 was first linked to neurodegenerative diseases when mutations in both *TREM2* and *DAP12* were found to be the cause of PLOSL (Paloneva et al., 2002). As progressive dementia is a major symptom of this disease, genes associated with PLOSL were investigated in AD. However, it was not until 2013 that variants of *TREM2* were linked with increased risk of AD in large genome and exome sequencing studies (loss-of-function R47H and D87N mutations) (Guerreiro et al., 2013, Jonsson et al., 2013). Since then, several variants of TREM2 have been associated with AD. Yin et al. (2016) found an interaction between Trem2 and Vps35 which mediated Trem2 endosome-to-plasma membrane recycling which was disrupted by the R47H mutation. Disruption to the trafficking of Trem2 may therefore underlie the AD risk associated with this variant. The H157Y TREM2 variant has been found to increase shedding of Trem2 by ADAM10 and reduce phagocytotic activity (Schlepckow et al., 2017).

Initially, however, studies into the effect of TREM2 variants on AD pathology gave contradictory results. $Trem2^{-/-}$ in Aβ pathology mouse models was found to both reduce and increase Aβ load (Wang et al., 2015b, Jay et al., 2015). It was later confirmed that the effect of Trem2 deficiency on AD-like pathology is dependent on disease stage. In the early stages of AD in this mouse model, reduction in Trem2 reduces Aβ plaques whereas at later stages a lack of Trem2 enhances Aβ pathology (Jay et al., 2017a). In human AD, the relationship between TREM2 expression and stage of disease is less clear although the majority of studies suggest an upregulation of TREM2 in AD patients (Celarain et al., 2016, Martiskainen et al., 2015, Jolly et al., 2019, Zhao et al., 2013). A potential reason for this lack of clarity is failure of these studies to include age-matched control groups or data on disease stage. Though the disease-stage-dependent effect of TREM2 expression is not as clear in human post-mortem studies as in mouse models, it is still an important factor to consider when therapeutically targeting TREM2 in AD.

The molecular role of TREM2 in AD has been widely studied both *in vitro* and *in vivo*. TREM2 was found to facilitate microglial phagocytosis of Aβ oligomers and inhibit inflammatory responses induced by Aβ (Jiang et al., 2014). The role of TREM2 as a negative regulator of TLR, a receptor which mediates Aβ-induced microglial inflammation (Liu et al., 2012). Decreased expression of TREM2 may therefore

contribute to AD pathology by reducing the ability of microglia to clear extracellular Aβ as well as the loss of a mechanism to combat proinflammatory responses. Activation of Trem2 in a mouse model of AD pathology was found to reduce Aβ plaque deposition and increase microglial recruitment to plaques as well as cognitive function (Price et al., 2020).

1.3.5 Indirect interactions between ABI3 and TREM2

ABI3 and TREM2 may be indirectly linked by the downstream effects of TREM2 activation. Modification of the actin cytoskeleton occurs after recruitment of VAV proteins by the conversion of PIP2 to PIP3 by PI3K which then activate WAVE proteins. As ABI3 is suggested to inhibit WRC activity when included in the complex, ABI3 and TREM2 may have opposing roles in the regulation of the actin cytoskeleton. Reduction in TREM2 expression and/or signalling may lead to an increase of ABI3 recruitment to the WRC, decreasing the phagocytotic activity of microglia.

It is possible that plasma membrane expression of TREM2 is influenced by ABI3. Endosomal receptor recycling is an actin-dependent process. Protein complexes, including the retromer complex (VPS35, VPS29, VPS26), retriever complex (C16orf62, VPS29, DSCR3), the copper metabolism MURR1 domain (COMMD)/coiled-coil domain-containing (CCDC) 22/CCDC93 (CCC) complex, and the Wiskott-Aldrich syndrome protein and scar homolog (WASH) complex (WASH1, Strumpellin, FAM21A/C, CCDC53, SWIP) complex interact with intracellular domains of cargo and sorting nexin proteins to drive receptor recycling (Simonetti and Cullen, 2019). The retromer complex has long been known to play a major role in endosomal protein sorting by mediating cargo selection (Seaman, 2012a). More recently, retriever, a retromer-like complex, has been identified which requires the WASH and CCC complexes to mediate endosome localisation and functions (McNally and Cullen, 2018). These processes are reliant on branched actin networks, created through the polymerisation and nucleation of actin by Arp2/3. Arp2/3 is regulated by nucleation promoting factors (NPF) such as the WRC, WASH complex, and cortactin. WASH and cortactin are involved in the remodelling of actin at the endosomal surface by enhancing Arp2/3-dependent actin polymerisation (Chakrabarti et al., 2021). ABI3 may therefore play a role in the regulation of TREM2

recycling by clathrin-mediated endocytosis, as this process is driven by Arp2/3-dependent actin remodelling, which in turn is regulated by the WRC.

1.4 Protein Networks

1.4.1 Protein Interactomes

The term ‘proteome’ was first defined by Wasinger et al. (1995) to describe all proteins expressed by the genome of a cell. However, proteins do not exist in isolation. Basic biological functions within a cell are carried out via protein interactions, from signalling cascades to metabolic reactions, and by the creation of protein and enzyme complexes.

1.4.2 Techniques to Study PPIs

Experimental techniques to study PPIs are designed to investigate protein networks by capturing prey proteins (proteins which interact with the protein of interest, known as the bait protein). A common biochemical technique to analyse PPIs is co-immunoprecipitation (co-IP) where antibodies against the bait protein are used to capture protein complexes and prey proteins are often identified by mass spectrometry (MS). However, as protein complexes must be maintained throughout, gentle lysis and wash conditions are required meaning identification of insoluble proteins or weak/transient interactors is difficult. To overcome this, proximity labelling methods can be used. Biotinylation of prey proteins is catalysed by engineered enzymes to label prey proteins in proximity to a fusion bait protein.

1.4.2.1 BioID

BioID is a proximity labelling technique developed by Roux et al. (2012) which utilises the strong affinity ($K_d = 10^{-14}$ M) between biotin and streptavidin. The bait protein is a fusion protein formed of BirA and the protein of interest, which is then expressed in the relevant cell line. BirA is a 35 kDa protein which regulates the biotinylation by generating biotinoyl-5’-adenosine monophosphate (bioAMP) from biotin and ATP then using this activated form of biotin to biotinylate lysine residues of proteins (Chapman-Smith and Cronan, 1999, Roux et al., 2012). Roux et al. (2012) utilised a mutant form of BirA (R118G, referred to as BirA*) to biotinylate proteins proximal to the bait protein in live mammalian cells. BirA* prematurely releases bioAMP due to a reduced affinity between the enzyme and the substrate resulting in

increased efficiency of biotinylation (Kwon and Beckett, 2000, Kwon et al., 2000). After labelling, biotinylated proteins are captured from cell lysates by addition of streptavidin-conjugated beads and identified by MS (Figure 1.9)

Alternative enzymes for use in biotin proximal labelling have also been produced. These methods include TurboID and miniTurbo, which require much shorter biotin incubation times (Kim et al., 2016, Branon et al., 2018, Samavarchi-Tehrani et al., 2020). However, due to the increased affinity for biotin in these enzymes compared to BirA*, scavenging of biotin from cell media can occur, which may cause toxicity issues during the generation of stable cell lines (Samavarchi-Tehrani et al., 2020).

The BioID technique has advantages over co-IP, primarily as PPIs and organelle integrity do not need to be maintained during the process. Protein complexes do not need to be maintained as prey proteins have been tagged during cell culture. (Samavarchi-Tehrani et al., 2020). BioID can also produce information on specific proximity relationships of protein interactors when captured proteins are analysed by MS. This data can be used to map interaction relationships of bait proteins from synthesis until cell lysis (Samavarchi-Tehrani et al., 2020). BioID can also be applied to *in vivo* studies, although exogenous biotin must be delivered to the site of interest in experiments with mammalian species as biotin is not synthesised endogenously (Dingar et al., 2015, Uezu et al., 2016).

The main limitation of the BioID method is that it relies on expression of an exogenous fusion protein. This may affect the functionality or localisation of the bait protein and so must be assessed in each experiment (Weill et al., 2019). The cellular location of the fusion protein can be established through immunostaining methods to ascertain correct targeting of the protein (Stadler et al., 2013). Expression of bait proteins at near endogenous levels (produced by the generation of stable cell lines) may help to mitigate this problem, but verification of bait protein localisation and function is critical (Samavarchi-Tehrani et al., 2020). Another potential limitation of BioID is the biotinylation itself. As biotin is covalently bonded to lysine residues of interacting proteins, it is possible that the loss of charge on these sites could affect secondary modifications and the behaviour of the affected proteins. It should also be noted that this method alone cannot be used to definitively determine protein interaction. The labelling radius of BirA* is around 10 nm and so proteins do not have to physically interact with the fusion protein to become biotinylated (Kim et al., 2014).

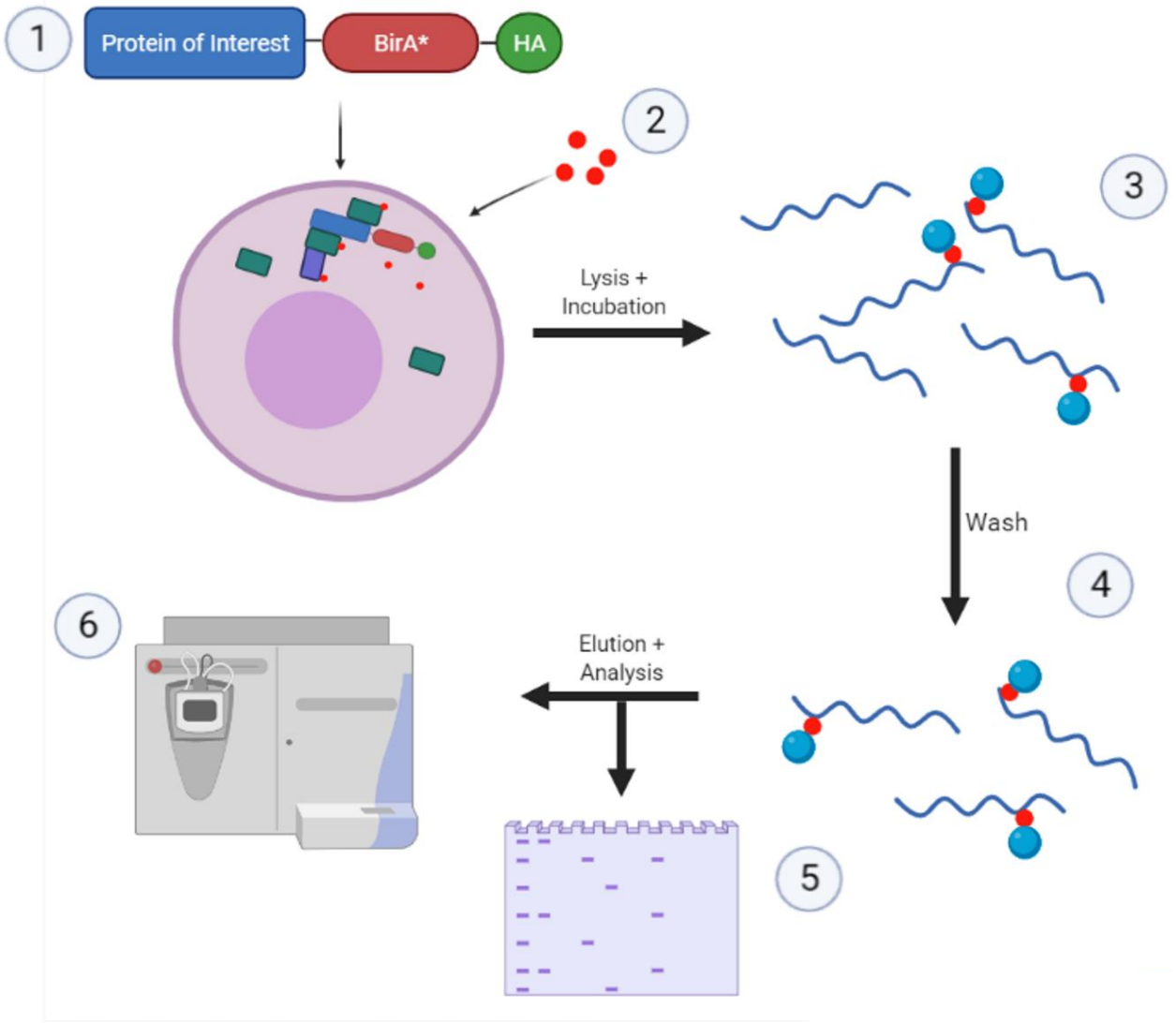

Figure 1.9 BioID labels prey proteins proximal to the bait by biotinylation. ***(1)*** *A fusion protein of the protein of interest, the modified E. coli biotin ligase BirA*, and an epitope tag are expressed in the relevant cell line. Validation of successful expression and localisation of the exogenous protein is paramount at this stage.* ***(2)*** *Biotin is added to the cell media and cells are incubated for at least 16 hours. Biotinylation of proteins within 10 nm of the bait protein occurs during cell culture, therefore even transient interactors are likely to be labelled.* ***(3)*** *Cells are lysed and incubated with streptavidin-conjugated beads. Biotinylated proteins adhere to the beads due to the formation of a high affinity bond between biotin and streptavidin.* ***(4)*** *Beads are washed to remove proteins not adhered to the beads. This should be any proteins in the cell lysate that were not biotinylated and therefore were not proximal to the protein of interest during the biotin incubation in cell culture.* ***(5)*** *Proteins are eluted through use of detergents and biotin displacement and a sample of the proteins are run on an SDS-PAGE electrophoresis gel to confirm capture of biotinylated proteins.* ***(6)*** *Elutions are analysed by MS to identity proteins present in the samples. Further statistical analysis ranks these proteins to identify high-confidence interactors of the protein of interest. See sections 2.2.1 and 2.4.1 for full details of BioID method used in this thesis. Figure created in BioRender.*

It is therefore most useful to use the BioID method to screen for candidate interactors which are either direct or indirect interactors, or proximal proteins and confirm physical interaction with alternative methods, such as co-IP (Roux et al., 2012).

1.4.3 Application of Protein Interaction Analyses to Cell Biology and Disease

The human genome encodes many protein recognition domains highlighting the importance of PPIs to basic cell biology. The function of novel proteins as well as novel functions of known proteins have been identified by studying PPIs. This gives insights into cellular systems under normal physiological conditions, a key foundation in understanding and manipulating disease pathology. The protein interactome of the cystic fibrosis transmembrane conductance regulator (CFTR) protein has been investigated to study pathophysiological mechanisms of cystic fibrosis (CF) and identify druggable targets (Amaral et al., 2020). Hutt et al. (2018) compared the interactomes of CF causing CFTR variants using a proteomic variant approach. This method integrated purification affinity MS with genomic screening to study the impact of each variant on the disease. In the 5 variants looked at, a total of 625 interacting proteins were identified, 588 of which were common to all 5 variants. In total, 528 proteins were found to have significantly different interactions with the CF-variant compared to wild type CFTR, 70 of which were common to all variants. Following on from this, Hutt et al. (2018) identified proteins which bound with high affinity to these CFTR variants and showed that downregulation of these binding proteins improved trafficking of the proteins to the plasma membrane. This suggests that targeting these binding proteins in patients with CF caused by these mutations may form an effective treatment. Comparison of the wild type CFTR and the G551D-CFTR variant interactomes revealed reduced interaction between the variant and proteins involved in trafficking, indicating that the reduced channel activity of this mutation is, at least partly, due to failure to traffic to and be retained at the plasma membrane. This study again highlights the importance of identifying protein networks in understanding how coding variants result in disease, revealing mechanisms that could be targeted therapeutically.

Mapping protein interactions is also a key tool in combating infectious diseases. During the COVID-19 pandemic, the interactome of SARS-CoV-2 was investigated

to aid research into treatments (Gordon et al., 2020). Cellular mechanisms disrupted by SARS-CoV-2 were identified, highlighting potential druggable targets. Proteome comparisons to other known pathogens also highlighted similar pathological mechanisms suggesting which currently approved drugs which may assist in the fight against COVID19.

In AD, PPIs have been studied in an attempt to understand the aetiology and pathology of the disease. Genes and signalling pathways which contribute to AD have been identified through these studies (Krauthammer et al., 2004, Liu et al., 2010). Jensen et al. (2018) characterised seven protein interactions of Munc-18-interacting 2 (Mint2, also known as X11β or Aβ A4 precursor protein-binding family A member 2 (APBA2)), an adaptor protein involved in amyloid pathology which interacts with PSEN and APP. It was discovered that the C-terminal of Mint2 regulates protein interaction and stabilisation of the target protein. Mint1 (X11α or APBA1) and Mint3 (X11γ or APBA3) are also known to interact with the cytoplasmic domain of APP, along with the proteins Fe65 (also known as APP-binding protein 1), Fe65-like1, Fe65-like2, and mammalian homolog of disabled 1 (Swistowski et al., 2009, Mueller et al., 2000, Dumanis et al., 2012). Fe65 has also been shown to facilitate interactions between APOE receptors and APP, providing a mechanistic link between APOE and amyloid pathology (Hoe et al., 2006, Trommsdorff et al., 1998). Overexpression of Mint1 and Mint2 in transgenic mice carrying the APP Swedish mutation were found to have lower levels of Aβ plaques in the cortex and hippocampus and Mint2$^{-/-}$ mice show increased levels of Aβ aggregation in the hippocampus (Lee et al., 2003, Lee et al., 2004, Sano et al., 2006). This suggests that stabilisation of APP by interaction of Mint proteins inhibits production of $A\beta_{40/42}$ peptides. Mint1/2 have also been shown to interact with PSEN1, preventing interactions between PSEN1 and APP (Lau et al., 2000). Therefore, the stabilisation of APP and subsequent reduction in Aβ plaques with overexpression of Mint1/2 may be due to inhibition of cleavage by γ-secretases. Targeting these proteins to increase activity may have beneficial therapeutic effects, particularly in familial AD cases with known APP mutations. These studies provide useful insights into specific interactions of proteins known to influence AD pathology, but do not elucidate the overall genetic architecture of AD. Srinivasa Rao et al. (2013) described an analytical method to construct a PPI map for AD using data on proteins known to be involved

in AD pathology. 1412 interactions were predicted from 969 proteins. This method is hoped to aid drug development to identify pathways which can be targeted to restore normal cellular function. From the building of networks which map all potential PPIs of proteins which influence AD pathology, systematic analysis of the function and interactions of specific proteins in this network can uncover potential druggable targets and highlight pathways enriched in AD pathology.

1.5 Thesis Aims and Structure

Multiple SNPs have been identified which contribute to the risk of developing AD, some of which have a known mechanism of risk whilst for others this mechanism remains unknown. The overarching aim of this thesis was to systematically map the PPI network of two known risk genes for AD: Abi3 and Trem2. Comparison of the interactomes of wild type Abi3 and the variant Abi3-S212F (the mouse equivalent of the human S209F variant) may identify any differences between the normal and pathological protein network, leading to a greater understanding of AD pathology. Novel interactors identified may present new therapeutic targets and highlight cellular mechanisms which underlie AD pathology. The BV2 mouse microglia-like cell line was used as there is little PPI data from microglia despite these cells being highly relevant to both AD and the function of these proteins. Proteomic techniques have been used to determine these interactomes, primarily the proximity-labelling method BioID. The overall hypothesis of this thesis was that BioID is a suitable technique to define PPIs and study the functional effects of genetic risk variants for AD. To answer this question, experiments with the following aims are outlined in this thesis:

1. Define the interactome of Abi3 in microglia-like cells (Chapter 3)
2. Define and compare the interactome of Abi3-S212F in microglia-like cells to the interactome of Abi3 (Chapter 4)
3. Define the intracellular interactome of Trem2 in microglia-like cells (Chapter 5)

Novel findings presented in this thesis are summarised and discussed in Chapter 6.

Chapter 2 – Methods

2.1 Cell Biology

2.1.1 Cell Culture

Human embryonic kidney 293T (HEK-293T) cells were cultured in Thermo Fisher Scientific 25cm^2 (T25) flasks in 5 ml of Dulbecco's modified eagle medium (DMEM, GIBCO©, stored at 4°C and warmed to 37°C before use) with 4% (volume/volume (v/v)) foetal bovine serum (FBS) and 2% (v/v) L-glutamine. BV2 cells were cultured in T25 flasks in 25 ml Roswell Park Memorial Institute 1640 medium (RPMI, GIBCO©, stored at 4°C and warmed to 37°C before use) with 10% (v/v) FBS and 2% (v/v) L-glutamine. Cultures were incubated in a humidified atmosphere of 5% CO_2 and 95% air at 37°C. Cells were passaged at around 80% confluence to maintain healthy, viable cultures. During passage media was removed and, in the case of BV2 cells, RPMI media was centrifuged at 1000 rpm for 3 min to collect detached cells. To detach adherent cells, 3 ml of Accutase © (Sigma-Aldrich) was added and cells were incubated for 5 min at 37°C. Detachment of adhered cells was verified via microscope and Accutase© was inactivated by addition of 3 ml of media. Cells were then centrifuged at 1000 rpm for 3 min at room temperature to form a pellet. The supernatant was removed, and all pellets were resuspended in 10 ml of fresh medium. Cells were then counted using a haemocytometer and seeded at an appropriate density in the appropriate medium in new flasks. The amount of medium was dependent on flask size (Table 2.1).

Table 2.1 Cell culture seeding densities and volumes for culture reagents.

Flask Type	Seeding Density	Cell Density at Confluency	Volume of Medium (ml)	Volume of Accutase© (ml)
T-25 (25cm^2)	0.7 x 10^6	2.8 x 10^6	5	3
T-75 (75cm^2)	2.1 x 10^6	8.4 x 10^6	10	5
T-175 (175cm^2)	0.7 x 10^6	23.3 x 10^6	25	17

2.1.1.1 Transient Transfection of HEK-293T Cells

On day 1, cells were seeded at a density of 500,000 cells per well in 1.5 ml DMEM, with 4% FBS in a six-well plate. Cells were incubated at 37°C to grow to a confluence of around 70% for approximately 24 h. On day 2, cells were transfected with an appropriate amount of plasmid DNA using Lipofectamine© 2000 (Lipo2000) Transfection Reagent (Invitrogen). Per transfection, plasmid DNA and Lipo2000 was added in a 1:3 ratio to the appropriate amount of Opti-MEM© Reduced Serum Medium (GIBCO) to create a transfection mix of 150 µl (10% of total media volume). Transfection mixes were then left at room temperature for 20 min to allow the plasmids to be taken up by the lipid. The mix was then added directly to each well. The plate was then incubated overnight at 37°C.

2.1.1.2 Generation of BV2 Stable Cell Lines

Plasmids were designed and packaged into a lentivirus vector by VectorBuilder (VectorBuilder Inc, Chicago, IL; see sections 3.2.1, 4.2.1, and 5.2.1 for plasmid details and vector maps). On day 0, BV2 cells were seeded in a 6-well plate at a density of 250,000 cells per well in RPMI media with 10% FBS. On day 1, media was changed to RPMI with 10% FBS containing the appropriate amount of lentivirus with 5 µg/ml polybrene and incubated at 37°C, 5% CO_2 for 24 h. For a multiplicity of infection (MOI) of 20 from a virus titre of 10^8 TU/ml, 50 µl of virus contained $5x10^6$ viral particles. On day 2 media was changed to fresh RPMI with 10% FBS to remove polybrene. Selection began on day 3 with 5 µg/ml puromycin per well and continued until green fluorescent protein (GFP) expression remained consistent. At this point the polyclonal lines were expanded, frozen at -80°C for long term storage, and culture continued as described in section 2.1.1 with the addition of 2.5 µg/ml puromycin and 1% penicillin/streptomycin to the media.

2.2 Protein Analysis

2.2.1 Sample Preparation for Protein Analysis

Western Blot

Media was removed from cells, and cells were washed in phosphate-buffered saline

(PBS) prior to lysis in 100 µl SDS-sample buffer (0.125 M Tris pH 6.8, 4% sodium dodecyl sulphate (SDS), 20% (v/v) glycerol, 5% (v/v) β-mercaptoethanol, 0.001 (weight/volume (w/v)) bromophenol blue). A cell scraper was used to break up the viscous material formed after lysis, allowing the lysate to be pipetted into a 1.5 ml microcentrifuge tube. Lysates were stored at -20°C for long term storage.

Immunocytochemistry

Cells were grown on 3-triethoxysilylpropylamine (TESPA) coated coverslips (22 mm x 22 mm) in 35 mm TC-treated culture dishes (Corning) at a density of 250,000 cells per well in appropriate media and incubated at 37°C to grow to a confluence of around 70% for approximately 24 h. Medium was removed and cells were fixed for 10 min in 2 ml 3.7% formal saline (150 mM NaCl, 90% H_2O, 3.7% (v/v) formaldehyde). After fixing, cells were incubated in 2 ml 100% ethanol to aid fixing then washed with PBS for 5 min. Coverslips were either processed for immunocytochemistry immediately or stored in 2 ml sucrose storage medium (125 mM sucrose, 1.62 mM MgCl, 25% (v/v) PBS, 25% (v/v) glycerol) at -20°C.

BioID

BV2 stable cell lines were grown to full confluency in two T-175 cell culture flasks per cell line in RPMI media with 10% (v/v) FBS. Biotin (Sigma-Aldrich) was added to the media to make a final concentration of 50 µM and cells were incubated at 37°C for a further 12-16 h. Media was then removed and centrifuged at 1000 rpm for 3 min to collect suspended cells while adherent cells were detached with Accutase and centrifuged at 1000 rpm for 3 min in cold PBS. All cell pellets were resuspended combined in cold PBS and incubated on ice for 5 min to slow biotinylation reactions, then pelleted again by centrifugation. Cells were washed a total of 3 times by resuspension in cold PBS and centrifugation to remove excess biotin. Cells were then lysed in 1 ml 1x lysis buffer (Cell Signal Technology 10x; 20 mM Tris-HCl, 150 mM NaCl, 1 mM Ethylenediaminetetraacetic acid disodium salt dehydrate (Na_2EDTA), 1 mM ethylene glycol-bis(β-aminoethyl ether)-N,N,N′,N′-tetraacetic acid (EGTA), 1% Triton, 2.5 mM sodium pyrophosphate, 1 mM β-glycerophosphate, 1 mM Na_3VO_4, 1µg/ml leupeptin, additional 0.4% SDS). Lysates were stored in 1.5 ml microcentrifuge tubes and either stored at -20˚C for long term storage or immediately processed for capture of biotinylated proteins by BioID.

2.2.2 Sodium Dodecyl Sulphate-Polyacrylamide Gel Electrophoresis

For western blot or Coomassie staining, samples were separated on 12% (v/v) acrylamide gels by Sodium Dodecyl Sulphate-Polyacrylamide Gel Electrophoresis (SDS-PAGE) using a Mini-PROTEAN© Treat System (Bio-Rad). The resolving gel contained 1.5 M Tris pH 8.8, 12% (v/v) acrylamide (30% (w/v) acrylamide, 0.8% bis-acrylamide stock solution (37.5:1)), 0.1% (w/v) SDS, 0.075% (w/v) ammonium persulphate (APS) and 0.06% N,N,N',N-Tetramethylethylenediamine (TEMED). The gel was left under a layer of distilled water to polymerise to exclude air from the gel and allow for a smooth surface. The stacking gel was then prepared containing 1.5 M Tris pH 6.8, 5% (v/v) acrylamide (30% (w/v) acrylamide, 0.8% bis-acrylamide stock solution (37.5:1)), 0.1% (w/v) SDS, 0.1% (w/v) APS, 0.1% (v/v) TEMED. The stacking gel was then poured onto the set resolving gel after the distilled water layer was removed. A comb was directly inserted into the stacking gel and left to polymerise at room temperature. Prior to loading, samples were heated to 95°C for 5 min and sonicated if required using a UP50H Ultrasonic Processor. As a protein standard, a Precision Plus Dual Xtra (Bio-Rad) protein ladder was used. Gels were secured into a tetra cell which was placed in a tank then submerged in 1X SDS-PAGE running buffer (10x: 0.25 M Tris base, 1.92 M glycine, 0.1% (w/v) SDS, pH 8.3). Gels were run at 150 V for approximately 75 min.

Sample were prepared for mass spectrometry, by separation on NuPAGE™ 4 to 12%, bis-Tris, 1.0 mm, Mini Protein Gels (Thermo Fisher Scientific) using an XCell SureLock Mini-Cell Electrophoresis System (Thermo Fisher Scientific). Samples containing biotinylated protein after elution from streptavidin beads (as verified by western blotting) were run for a total of 15 min in 1x NuPAGE™ MOPS SDS running buffer (Thermo Fisher Scientific).

2.2.3 Western Blot

In order to detect specific proteins with antibodies, following SDS-PAGE gel electrophoresis, proteins were transferred to a 0.2 µm pore size nitrocellulose membrane (Amersham™ Protran™) for 1 h at 100 V in transfer buffer (25 mM Tris-base, 192 mM glycine, 20% (v/v) methanol) using the Mini Trans-Blot© Electrophoretic Transfer Cell (Bio-Rad). For western blots not requiring biotin or

streptavidin, membranes were blocked in 5% (w/v) dried skimmed milk powder (Marvel) in 1x Tris-buffered saline with Tween (10x TBST; 100 mM Tris-Base, 1 M NaCl, 0.5% (v/v) Tween 20, pH 7.6) for 1 h. For BioID experiments, membranes were blocked in 2.5% (w/v) bovine serum albumin (BSA, Sigma) in 1x TBST for 30 min. BSA was chosen over dried milk powder to block membranes in BioID experiments to avoid contamination of the membrane with endogenous biotin from milk. Blocking with non-fat dry milk has also been reported to inhibit biotin-streptavidin interactions (Pillai-Kastoori et al., 2020). Blocking steps were performed to prevent non-specific binding and reduce background signal by blocking unoccupied sites on the membrane prior to antibody incubation. Membranes were then washed in 1x TBST and incubated with either streptavidin IR800CW (LI-COR Biosciences, 1:10000) in 5 ml 1x TBST, 2.5% (w/v) BSA and 0.1% (w/v) SDS or appropriate primary antibody (Table 2.2) in 1% (w/v) dried skimmed milk powder in 1x TBST. All membranes were incubated overnight at 4°C with 1 h incubation at room temperature. When incubating with streptavidin, blots were kept in the dark from this stage on. For addition of secondary antibodies, blots were washed in 1x TBST for 5 min, 3 times, then incubated with appropriate secondary antibody for 1 h (Table 2.2). All blots were then washed in 1x TBST for 30 min and visualised with the two-colour Odyssey© Infrared Imaging System (LI-COR Biosciences).

2.2.4 Coomassie Staining

Coomassie blue staining was used to directly visualise proteins separated by SDS-PAGE. Following electrophoresis, the gel was directly stained with Coomassie blue stain (0.025% (w/v) Coomassie Brilliant Blue R, 40% (v/v) methanol, 7% (v/v) acetic acid) for 40 min at room temperature on a platform shaker. The gel was then de-stained for at least 1 h in 40% (v/v) methanol, 10% (v/v) acetic acid at room temperature. Gels were imaged using a Molecular Imager® Gel Doc™ XR+ Imaging System (BioRad) or two-colour Odyssey© Infrared Imaging System (LI-COR Biosciences).

For mass spectrometry analysis, NuPAGE™ gels were fixed in 50% methanol and 7% acetic acid for 15 min. Gels were then washed in dH_2O and stained with GelCode™ Blue Stain Reagent (Thermo Fisher Scientific) for 1 h followed by de-staining in dH_2O overnight.

2.2.5 Immunocytochemistry

Cells were fixed on coverslips with a PFA fix as described above. If stored in sucrose storage medium, cells were washed in PBS 3 times. Cells were permeabilised with 0.2% Triton X-100 for 15 min. Coverslips were then washed three times in PBS, dipped in 0.02% Tween-20, then incubated with the appropriate primary antibody (Table 2.2) overnight in a humidified chamber. Coverslips were then washed 3 times in PBS and incubated with the appropriate secondary antibody (Table 2.2) for 1 h in a dark, humidified chamber. Cells were then washed 3 times in PBS then mounted onto slides using DAPI-Vectashield® mounting medium (Vector Laboratories). Coverslips were sealed and slides left to dry. Coverslips were visualised and images captured using the Leica TCS SP8 confocal microscope (Leica Microsystem) with a 40x oil immersion objective. The pinhole was set at 1 AU (Airy Unit) for all channels giving an optical slice thickness of approximately 0.89 µm. Excitation, beamsplitter, and emission collection settings varied by channel (Table 2.3). Emission collection in all channels was via photomultiplier tube. Images were processed to create merged figures in ImageJ (Schindelin et al., 2012).

Table 2.2 Antibodies and probes used in this thesis.

Marker	Fluorophore	Assay and Dilution	Type	Dilution	Species	Source
Streptavidin	IRDye 800CW	Western blot (1:10000)	Primary	1:10000	N/A	Li-cor 926-32230
Anti-myc	N/A	Western blot (1:20)	Primary	1:20	Mouse monoclonal	In house 9E10 from Professor Derek Blake
Anti-mouse	Alexa Fluor 680	Western blot (1:15000)	Secondary	1:15000	Donkey polyclonal	Thermo Fisher Scientific A10038
Anti-mouse	Alexa Fluor 800	Western blot (1:15000)	Secondary	1:15000	Donkey polyclonal	Thermo Fisher Scientific A32730
Anti-rabbit	Alexa Fluor 568	Immunocytochemistry (1:1000)	Secondary	1:1000	Donkey polyclonal	Thermo Fisher Scientific A11011
Anti-rabbit	Alexa Fluor 680	Western Blot (1:15000)	Secondary	1:15000	Goat polyclonal	Thermo Fisher Scientific A21109
Anti-mouse	Alexa Fluor 594	Immunocytochemistry (1:1000)	Secondary	1:1000	Goat polyclonal	Abcam ab150120
Anti-HA	N/A	Western Blot (1:1000)	Primary	1:1000	Mouse monoclonal	Biolegend 901501

		Immunocytochemistry (1:1000)				
Anti-FLAG	N/A	Western Blot (1:1000)	Primary	1:1000	Mouse monoclonal	Merck F1804

Table 2.3. Leica TCS SP8 confocal microscope setting for DAPI, A488, and A568 channels.

Channel	**Colour**	**Excitation**		**Beamsplitter**	**Emission Collection**	
		Laser (nm)	Intensity* (%)		nm	Gain
DAPI	Blue	405	31.8	Reflector	421–610	804
A488	Green	488	24.5	DD 488/522	501–702	804
A568	Red	552	69.3	DD 488/552	562–740	800

*Intensity measures are estimates based on metadata of images captures and known laser intensities of the Leica TCS SP8 microscope at first ever use.

2.3 Plasmid Preparation

2.3.1 Plasmid Vectors

Plasmid vectors used for cloning are described in Table 2.4.

Table 2.4 Details of plasmid vectors used for DNA cloning and expression. *Details of the BioID expression constructs and vector maps can be found in the relevant chapters (Abi3: Section 3.2.1, Abi3-S212F: Section 4.2.1, Trem2: Section 5.2.1).*

Vector Backbone	Description	Antibiotic Selection
pLV[Exp]-EGFP-mPGK	Mammalian gene expression lentiviral vector with EGFP. Lentiviral vectors are derived from the retrovirus HIV and are constructed as a plasmid in E. coli then transfected into packaging cells to produce viral particles. Vector DNA, located between two long terminal repeats (LTRs,) is transcribed into RNA. When the virus is added to target cells, the RNA is shuttled into the cells where it is turned into DNA by reverse transcription. This DNA is randomly integrated into the host genome. Any genes between the LTRs during vector cloning inserted into host DNA with the rest of viral genome.	Puromycin
pcDNA3.1+	A mammalian expression vector derived from pcDNA3 and designed for stable and transient expression in mammalian cell lines. The vector contains the CMV promoter, a multiple cloning site, BGH pA/SV40 pA to terminate transcription, neomycin and ampicillin resistance, and pUC origin of replication to produce high copy numbers.	Ampicillin

2.3.2 Plasmid Construction

All plasmids were constructed by Genscript Biotech Corp (Piscataway, NJ) or Vectorbuilder (VectorBuilder Inc, Chicago, IL). Constructs are detailed in Table 2.5.

2.3.3 Plasmid DNA Isolation

Bacterial cultures were made from glycerol stocks of DH5α E. coli transformed with the appropriate plasmid and contained 5 ml LB and the appropriate antibiotic. Plasmid DNA was isolated from the cultures using Monarch® Plasmid Miniprep Kit (New England Biolabs), following the manufacturer's instructions. DNA was subsequently quantified using a Nanodrop spectrophotometer (DeNovix® DS-11 FX+) and stored at -20°C.

Table 2.5 Constructs used in BioID and interactor validation.

Construct	Species	Insert	Vector	Restriction Sites	Construction	Use
HA-BirA*	Mouse	Full BirA* sequence with N-terminus HA tag	Mammalian gene expression lentiviral vector	N/A	Constructed by VectorBuilder	Stable cell line generation for BioID
HA-BirA*-Abi3	Mouse	Full Abi3 sequence fused to the N-terminus to the C-terminus of BirA*, the N-terminus of which was fused to an HA tag The biotin ligase was fused to the N-terminus of Abi3 so as not to interfere with the SH3 domain, a major interaction site	Mammalian gene expression lentiviral vector	N/A	Constructed by VectorBuilder	Stable cell line generation for BioID
HA-BirA*-Abi3S212F	Mouse	Full Abi3S212F sequence fused to the C-terminus of BirA*, the N-terminus of which was fused to an HA tag	Mammalian gene expression lentiviral vector	N/A	Constructed by VectorBuilder	Stable cell line generation for BioID

Trem2-BirA*-HA	Mouse	Full Trem2 sequence fused at the C-terminus to the N-terminus of BirA*, the C-terminus of which was fused to a HA tag The biotin ligase was fused to the C-terminus of Trem2 to ensure biotinylation of intracellular signalling partners	Mammalian gene expression lentiviral vector	N/A	Constructed by VectorBuilder	Stable cell line generation for BioID
Myc-Abi3	Mouse	Full length Abi3 sequence with N-terminus myc tag	pcDNA3.1	EcoRI/SalI	Constructed by Genscript	Immunoprecipitation for interaction validation
Trem2-myc	Mouse	Full length Trem2 sequence with C-terminus myc tag	pcDNA3.1	EcoRI/SalI	Constructed by Genscript	Immunoprecipitation for interaction validation
Cep170-FLAG	Mouse	Full length Cep170 sequence with C-terminus flag tag	pcDNA3.1	EcoRI/SalI	Constructed by Genscript	Immunoprecipitation for interaction validation
Dap12-FLAG	Mouse	Full length Dap12 sequence with C-terminus flag tag	pcDNA3.1	EcoRI/SalI	Constructed by Genscript	Immunoprecipitation for interaction validation

2.4 Proteomics

2.4.1 Biotin-Affinity Capture

After cell lysis, 10% of each sample was saved and stored at -20°C as an input sample. Triton X-100 (Sigma-Aldrich) was added to the remainder of the lysates (final concentration 1%) and lysates were sonicated for 2 sessions using a UP50H Ultrasonic Processor. Samples were kept on ice for 2 min between sessions. Samples were then diluted 1:2 with cold lysis buffer to create optimal conditions for affinity capture. Samples then underwent a final session of sonication and were centrifuged for 10 min at 16,500 g at 4°C. Meanwhile, 25 µl of the stock of streptavidin-conjugated beads (Dynabeads™ MyOne™ Streptavidin C1, Thermo Fisher Scientific) per condition was washed in 1 ml lysis buffer. Beads were then resuspended in cleared supernatant and rotated overnight at 4°C to allow for streptavidin-biotin binding. Samples were placed in a magnet rack for 1 min and supernatant was collected without disturbing the beads. Beads were resuspended in 1 ml of 50 mM Tris with 2% SDS, rotated for 8 min, then placed on the magnet for 1 min and supernatant removed. Samples were then washed 3 times with 1 ml lysis buffer and underwent a final wash in 1 ml 50 mM Tris. The washing buffer was removed and the remaining pellet was resuspended in 50 µl of elution buffer (4x Laemmli buffer (4% SDS 20% glycerol 0.004% bromphenol blue 0.125M Tris-Cl, pH 6.8 10% 2-mercaptoethanol), 50 mM tris(2-carboxyethyl)phosphine (TCEP), 2 mM biotin) per condition. The elution step was repeated a further three times sequentially, to obtain a total of four subsequent elution samples to assess elution efficiency. All samples were stored at -20°C.

2.4.2 Mass Spectrometry

After gel electrophoresis and staining with GelCode™ Blue, bands were excised from the gel with a sterile razor blade, stored in 1.5 ml microcentrifuge tubes, and sent to the Fingerprints Proteomics Facility at the University of Dundee for MS.

2.4.3 Immunoprecipitation

HEK-293T cells were transfected with the appropriate plasmids (see Table 2.5) in 6-well plates and 24 h later were washed with 1 ml of ice-cold PBS. Cells were then lysed in 1.2 ml radioimmunoprecipitation assay (RIPA) buffer (150 mM NaCl, 50 mM

Tris pH 8.0, 1% (v/v) Triton X-100, 0.5% (w/v) sodium deoxycholate, EDTA-free protease inhibitors). Lysates were passed through a 23G hypodermic needle then centrifuged at 13,000 rpm for 10 min at 4°C to remove cell debris. 50 µl of each lysate was saved and stored at -20°C as an input sample. Meanwhile, 20 µl per sample of Anti-FLAG® M2 magnetic beads (M8823, Sigma) were washed in 1 ml RIPA buffer and resuspended in 50 µl RIPA buffer with protease inhibitors. 50 µl of beads were then added to each sample and incubated overnight at 4°C with rotation. The next day, the beads were recovered with a magnet and 50 µl of the supernatant from each sample was retained to assess efficiency of capture. Beads were then washed four times in 300 µl RIPA buffer with protease inhibitors. Reducing buffer (1x NUPAGE LDS sample buffer; 4x: 106 mM Tris HCL, 141 mM Tris Base, 2% LDS, 10% Glycerol, 0.51 mM EDTA, 0.22 mM SERVA Blue G250, 0.175 mM Phenol Red, + 50 mM TCEP) was added to each sample (input/wash sample: 50 µl, recovered beads: 70 µl). All samples were then boiled for 5 min at 95°C and eluted proteins isolated by recovery of magnetic beads and supernatant transferred to new 1.5 ml microcentrifuge tubes. Samples were taken immediately for SDS-PAGE western blot analysis.

2.5 Bioinformatics

2.5.1 General

Gene and protein sequences were obtained from the National Center for Biotechnology Information (NCBI) databases. Nucleotide and protein sequence alignment were performed with Clustal Omega (Madeira et al., 2019) and Jalview v. 2.11.2.4 (Waterhouse et al., 2009). DNA to protein translation was carried out with ExPASy (Expert Protein Analysis System) proteomic server from the Swiss Institute of Bioinformatic (http://www.expasy.org/). Protein/peptide molecular weight and DNA reverse strand prediction was carried out with the Sequence Manipulation Suite (http://www.bioinformatics.org/sms) (Stothard, 2000).

2.5.2 Mass Spectrometry Data Analysis

Previously known protein interactors were obtained from the NCBI database, which collates interaction data from other databases including the BioGRID and the Human Protein Reference Database (HRPD). RStudio (R Core Team, 2022) ("Spotted

Wakerobin" Release (7872775e 2022-07-22) for Windows, R version 4.2.1 (2022-06-23 “Funny-Looking Kid”)) was used to sort and filter the data with the `dplyr` package. Data were visualised in plots and charts created in RStudio: bubble plots with the `ggplot` package and UpSet plots with the `UpSetR` package. Venn diagrams were created with DeepVenn (Hulsen, 2022, Preprint).

2.5.2.1 Filtering Methods

Both true interactors and contaminating proteins are pulled down during BioID experiments therefore comparison to proteins captured in the BirA* control experiments is crucial. Using the Abi3 dataset, two filtering approaches were investigated as methods to determine putative interactors.

The hard filter method assumed any protein identified in the control data is a background contaminant and therefore not a true interactor of Abi3. Proteins from each Abi3 BioID replicate were filtered against the BirA control data, resulting in a list of 5 putative interactors of Abi3. However, labelling of proximal proteins in BioID occurs in live cell culture and both the Abi3 and BirA fusion proteins are expressed in the same cellular compartments. It is therefore possible that proteins which interact with Abi3 may also be in proximity of BirA only and therefore appear in both datasets. A filtering method which takes relative abundance of proteins between the two datasets was therefore required.

The Significance Analysis of INTeratome (SAINTexpress v3.4) (Teo et al., 2014) is a statistical method which scores protein-protein interaction data from affinity purification MS experiments. The probability of prey proteins being ‘true’ interactors is based on the relative abundance of each protein in each dataset. A putative interactor must appear in the Abi3 data at a significantly higher level than the control data. This is determined by the fold change, which is calculated by dividing the average spectral count of each interaction in the Abi3 data by the average spectral count of the corresponding interaction in the control. Based on the fold-change, a SAINT score is assigned to each prey protein and, along with the fold change, is then used to estimate the Bayesian false discovery rate (BFDR). Here, proteins with a BFDR < 0.05 were considered to be putative interactors of Abi3. Using this method, 10 proteins were identified as putative interactors.

As expected, the SAINTexpress method identified more putative interactors (10) compared to the hard filtering method (5) and 100% of the proteins identified with the

hard filtering were also identified by SAINTexpress. Both methods therefore identify similar proteins of interest as interactors of Abi3. However, due to the mechanism of BioID, the SAINTexpress method is more advantageous as proteins which are at a low level of abundance in the BirA control data are not automatically excluded from the analysis. This method has also been utilised by a number of previous studies analysing BioID data (Coyaud et al., 2015, Dingar et al., 2015, Khan et al., 2018, Madeira et al., 2019, Qiu et al., 2021). SAINTexpress was therefore used as the final filtering methods of Abi3 (section 3.2.3.1), Abi3-S212F (section 4.2.3.1), and Trem2 (section 5.2.3.1) BioID data.

2.5.2.2 STRING and Metascape

To investigate known functional relationships between the putative interactors identified by SAINTexpress, the Search Tool for the Retrieval of Interacting Genes/Proteins (STRING) database (v11.5, https://string-db.org/) and Metascape (https://metascape.org/) databases were used. Networks of the putative interactors, as well as the known interaction network of the bait proteins, were visualised with STRING. Over 25 million physical and functional associations between known and predicted PPIs are stored in the STRING database, collected from five main sources: genomic context predictions, high-throughput lab experiments, (conserved) co-expression, automated text mining, and other databases (Szklarczyk et al., 2021). For this analysis, physical interaction data from high-throughput lab experiments and other databases were used as prediction methods, with a medium confidence threshold (0.4). All proteins were also converted to their human orthologues as there is a greater availability of complete data and PPIs are relatively well conserved between species (Pérez-Bercoff et al., 2013, Qian et al., 2011, Sharan et al., 2005).

Biological functions of the putative interactors were investigated using Metascape's gene ontology enrichment analysis (Zhou et al., 2019). Gene ontology terms which are over-represented within a set of genes determine which biological processes these genes are likely involved in. The analysis uses 11 ontology sources to determine the biological processes enriched within a dataset: KEGG Pathway, GO Biological Processes, Reactome Gene Sets, Canonical Pathways, CORUM, TRRUST, DisGeNET, PaGenBase, Transcription Factor Targets, WikiPathways and COVID. All genes in the genome were used as the enrichment background. Terms with a p-value <0.01, a minimum count of three, and an enrichment factor of >1.5

(the ratio between the observed counts and the counts expected by chance) are grouped into clusters based on their similarities. The cluster was represented by the most statistically significant term.

2.5.2.3 Statistical Analysis

Normality of data was determined with Kolmogorov-Smirnov tests. All data were found to be non-normally distributed. Non-parametric tests were therefore used to determine significant differences in the data. Differences in spectral counts of putative interactors between genotypes were analysed by Mann Whitney U tests with a 1% false detection rate in GraphPad Prism. Differences were determined to be statistically significant at $p<0.05$. Graphs to visualise the differences in spectral count of putative interactors were created with GraphPad Prism.

Chapter 3 – Investigation of the Abi3 Protein Interactome

3.1 Introduction

3.1.1 Abi3

ABI3 encodes the cytoplasmic protein Abl interacting protein 3 (referred to from here on as ABI3, or Abi3 when referring to the mouse protein) and is highly expressed in microglia (Satoh et al., 2017, Zhang et al., 2014b). The exact molecular function of ABI3 is unknown but it is expected to play a role in the WRC due to the similarities with its paralogues ABI1 and ABI2 (Sekino et al., 2015). As discussed in section 1.3.3, ABI3 is known to influence cell motility in cancer cell lines via the WRC (Latini et al., 2011, Sekino et al., 2015). In AD, ABI3-positive microglia have been found to cluster around Aβ plaques while the ABI3-S209F variant is associated with increased risk of AD (Satoh et al., 2017, Sims et al., 2017). In AD mouse models, *Abi3* knockout has been found to exacerbate amyloid pathology and impair microglial migration and phagocytosis (Karahan et al., 2021). The biochemical mechanism of how this variant influences AD pathology is unknown but may be mediated by disruption to WRC signalling. Elucidating the protein interactome of wild type Abi3 in microglia will provide evidence for the function of Abi3 under normal physiological conditions, which can then be used as a foundation when investigating the influence of risk variants.

RNA sequencing data for both mouse and human primary cells show high levels of Abi3 expression in microglia compared to other CNS cell types (mouse data shown in Figure 3.1a) (Zhang et al., 2014b). As discussed in section 1.2.3, BV2 cells are a murine microglia-like immortalised cell line. Immortalised cell lines are ideal for proteomic studies due to their rapid proliferation rate and ease of culture. Although immortalisation does raise questions of the suitability of these cell lines as a substitute for primary microglia, BV2 cells are well characterised and deemed a valid *in vitro* microglial model (Henn et al., 2009). Expression of Abi3 in BV2 cells has been confirmed by RNA sequencing and so they are a suitable model for investigating the protein interactome of microglial Abi3 (Figure 3.1b) (Carrillo-Jimenez et al., 2019).

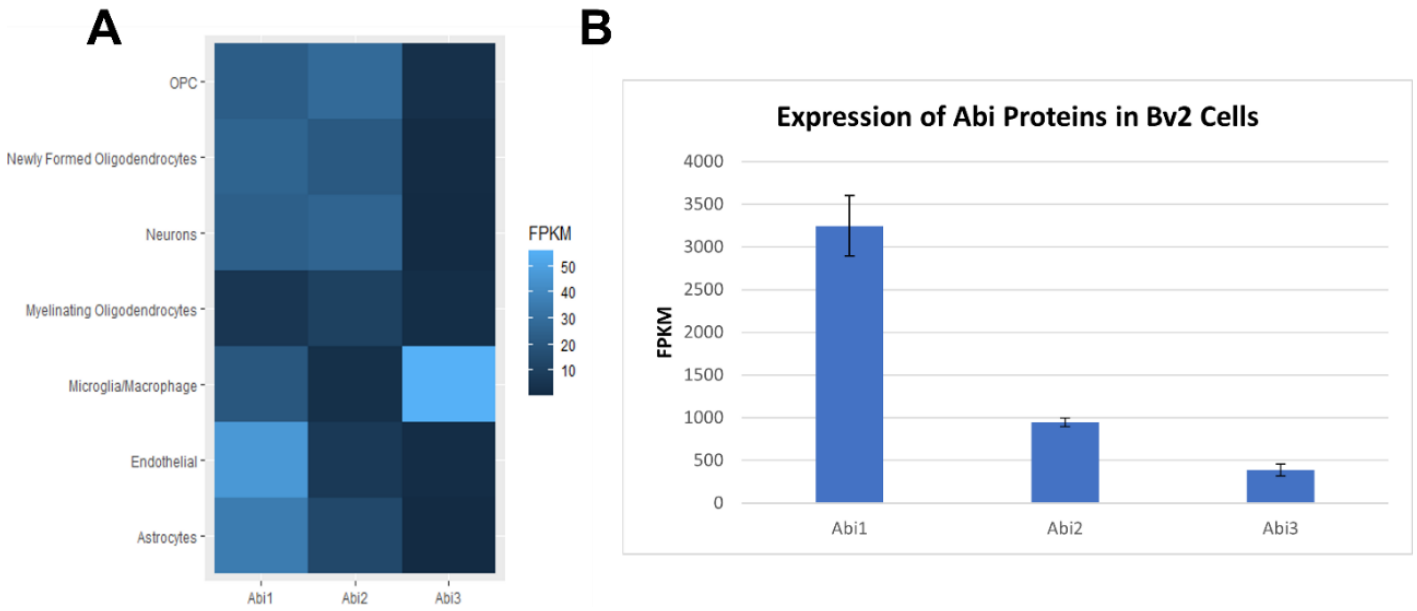

Figure 3.1 Expression of Abi proteins in neural and glial cell types. ***A)*** *Heat map of RNA sequencing data from Zhang et al. (2014b) showing relative expression of Abi proteins in different neural cell types. Abi3 is most highly expressed in microglia/macrophages compared to other cell types as well as to Abi1 and Abi2.* ***B)*** *RNA sequencing data from Carrillo-Jimenez et al. (2019) was replotted and confirms expression of Abi3 in BV2 cells. FPKM: Fragments Per Kilobase of transcript per Million fragments mapped.*

The protein interactome of Abi3 was elucidated with the proximity labelling method BioID (a full explanation of this technique is detailed in section 1.4.1). BioID has several advantages over AP-MS. Firstly there is no requirement to maintain PPI integrity meaning harsh lysis and wash conditions can be used. BioID is therefore well suited to investigating the interactomes of both plasma membrane-associated and cytoskeletal proteins which can be difficult to solubilise. Secondly, there is no reliance on a high-quality antibody against the protein of interest. Cross-reactivity, the non-specific binding of antibodies to seemingly unrelated proteins, contributes to the difficulty in replicating results when using these techniques. It is critical that only the intended bait protein and any physically interacting prey proteins are captured. As BioID is an antibody-free technique, this limitation of more traditional protein interactor capture methods is eliminated.

3.1.2 Aims

The aim of the work covered in this chapter was to validate BioID as a suitable method to investigate protein interactions and define the protein interactome of Abi3 in BV2 cells. This was achieved by the generation of two stable BV2 cell lines expressing HA-BirA* and HA-BirA*-Abi3 fusion proteins. The lines were validated by immunocytochemical and western blot analysis to confirm expression and localisation of the fusion protein. Proximal proteins were captured by BioID and identified by MS then filtered to identify putative Abi3 interactors.

3.2 Results

3.2.1 Generation and Validation of BV2 Cells Stably Expressing HA-BirA* and HA-BirA*-Abi3

BV2 cells stably expressing BioID fusion proteins HA-BirA* or HA-BirA*-Abi3 were generated by lentiviral transduction (Figure 3.2). Fusion proteins and the puromycin resistance gene were expressed under the control of the mouse phosphoglycerate kinase 1 (mPGK1) promoter. The mPGK1 promoter has relatively low expression levels but these levels are fairly consistent between cell types (Qin et al., 2010). An internal ribosome entry site (IRES) preceding the puromycin resistance gene allows for translation of the mRNA independent of the 5’ cap. The presence of an IRES in the untranslated regions of the mRNA causes IRES trans-acting factors to recruit ribosome 40S downstream of the 5’ cap and eukaryotic translation initiation factor (eIF) 4F recruitment of ribosome 40S (Figure 3.3). This ensured that both the HA-BirA* or HA-BirA*-Abi3 and puromycin resistance genes could be expressed under the same promoter (Renaud-Gabardos et al., 2015). The viral vector also contained GFP, expressed under the control of the human cytomegalovirus (CMV) promoter. The CMV promoter shows varied expression levels between cell types but expression levels are generally high (Qin et al., 2010). The full DNA sequences encoding the fusion proteins can be found in appendix 1.

Successful lentiviral transduction was validated by expression of GFP in BV2 cells and the expression and localisation of the fusion proteins were assessed by immunocytochemical staining of the protein containing the HA epitope (Figure 3.4a). In both the BirA* control and Abi3 BV2 cell lines, HA was located in the cytoplasm of

GFP positive cells and did not overlap with nuclear DAPI staining. This is consistent with reports of the location of endogenous Abi3 in the literature suggesting the fusion protein targeted the same cellular compartment as endogenous Abi3 (Satoh et al., 2017). The percentage of cells expressing HA-BirA*-Abi3 appeared to be lower than the proportion of cells expressing HA-BirA*. Not all GFP positive cells appeared to express the HA epitope. This may be because the GFP and HA-BirA*/HA-BirA*-Abi3 genes were expressed under different promotors. It was decided that the fusion protein genes should be expressed under the same promotor as the puromycin gene rather than GFP as cell selection was achieved by resistance to puromycin. Expression and proper biotinylation functioning of the biotin ligase in both lines was assessed via western blot using fluorophore-conjugated streptavidin to label biotinylated proteins (Figure 3.4b). Streptavidin labelling was successful in both cell lines. The highest levels of fluorescence were seen in the elution 1 samples, confirming enrichment of biotinylated proteins after pull-down and efficient removal of proteins from the streptavidin beads in the first elution. Low fluorescence in the unbound protein samples suggest successful capture of the majority of biotinylated proteins during incubation with streptavidin beads. The high fluorescent bands at approximately 75 kDa and 125–150 kDa likely represent the endogenously biotinylated carboxylases β-methylcrotonyl-CoA carboxylase (72 kDa), propionyl-CoA-carboxylase (74 kDa), and pyruvate carboxylase (128 kDa) (Grant et al., 2019). These results suggest successful expression of both exogenous proteins and fully functioning BirA*.

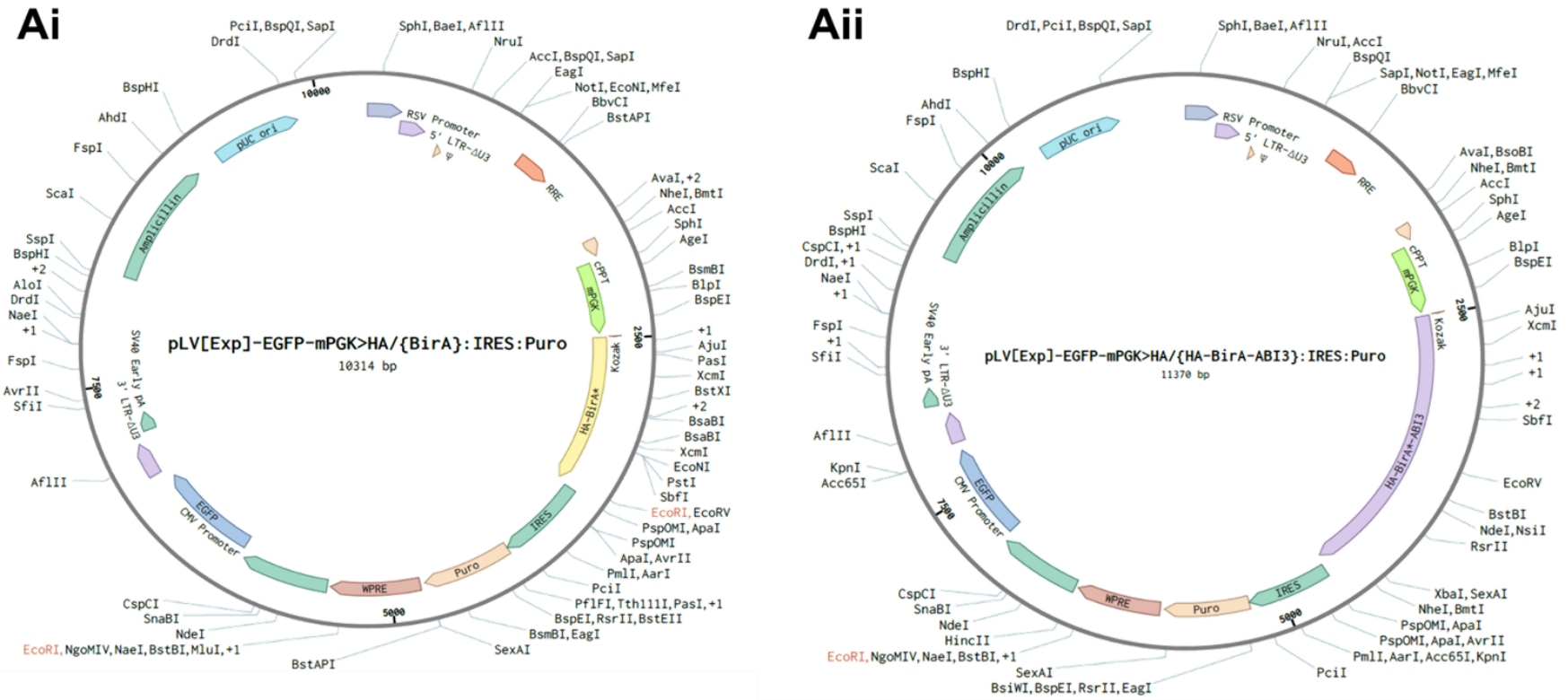

[65]

Figure 3.2 Schematics of structure of lentiviral vectors and fusion proteins. ***A)*** *Lentiviral vectors were used to transduce the sequences of fusion proteins expressed in the BirA* control* ***(i)*** *and Abi3* ***(ii)*** *stable BV2 cell lines. BirA* is the mutated form of the E. coli biotin ligase BirA* which prematurely releases bioAMP, resulting in promiscuous biotinylation of surrounding proteins.* ***B)*** *The BioID proteins were designed with an HA epitope joined to the N-terminus of the BirA* sequence via a linker. In the Abi3 fusion protein the HA-BirA* sequence was joined to the N-terminus of full length Abi3, also via a linker.*

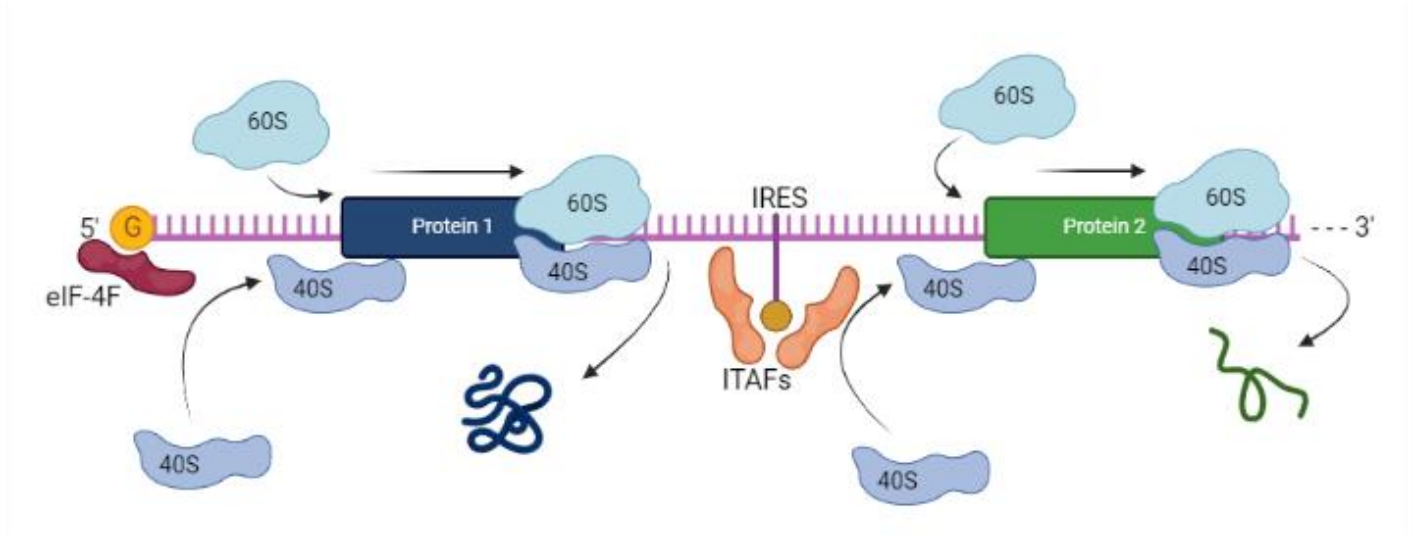

Figure 3.3 Mechanism of cap-dependent and IRES-dependent initiation of translation. *Cap-dependent initiation of translation requires the recruitment of ribosome 40S by initiation factor 4F (eIF-4F) at the 5' cap of the mRNA, and ribosome 60S when the start codon is recognised. Protein synthesis continues until the stop codon is recognised and a protein is produced. An internal ribosome entry site (IRES) located in an untranslated region of mRNA also recruits ribosome 40S and initiates protein synthesis via IRES trans-acting factors (ITAFs). This structure allows multiple proteins to be translated from the same strand of mRNA as two independent ribosome recruitment mechanisms exist. Figure adapted from Renaud-Gabardos et al. (2015), created in Biorender.*

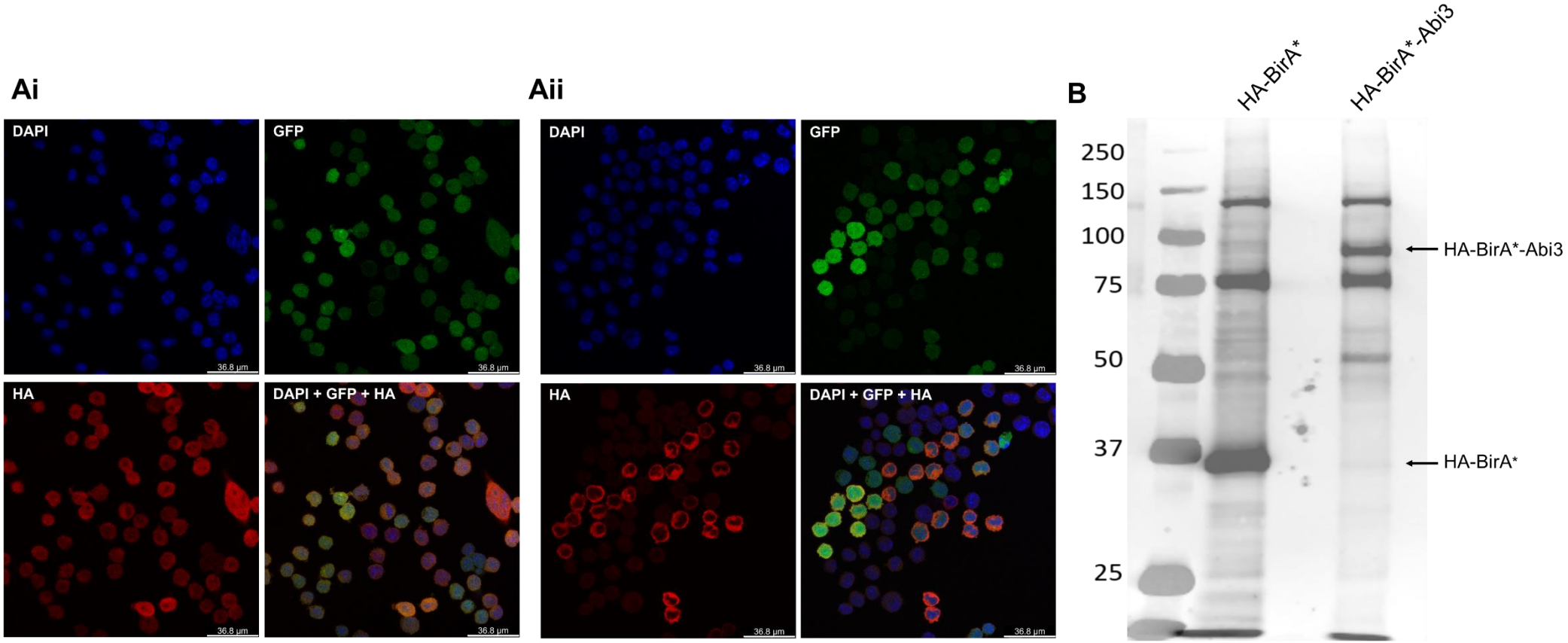

Figure 3.4 Characterisation of BV2 cells stably expressing HA-BirA* and HA-BirA*-Abi3 ***A)*** *Immunocytochemistry confirms successful transduction of exogenous proteins and cytoplasmic localisation of BirA** ***(i)*** *and Abi3* ***(ii)*** *fusion proteins. GFP and HA-epitope expression do not correlate as these genes were expressed under different promotors. Blue = DAPI, red = HA (BirA* (A), Abi3 (B)), green = GFP* ***B)*** *Streptavidin western blot shows successful expression of exogenous proteins (HA-BirA*: 37 kDa lane 1, HA-BirA*-Abi3: ~80 kDa lane 2) in BV2 cells and functioning of biotin ligase. Bands at 72 kDa, 74 kDa, and 128 kDa in both lanes likely represent the endogenously biotinylated carboxylases β-methylcrotonyl-CoA carboxylase, propionyl-CoA-carboxylase, and pyruvate carboxylase, respectively.*

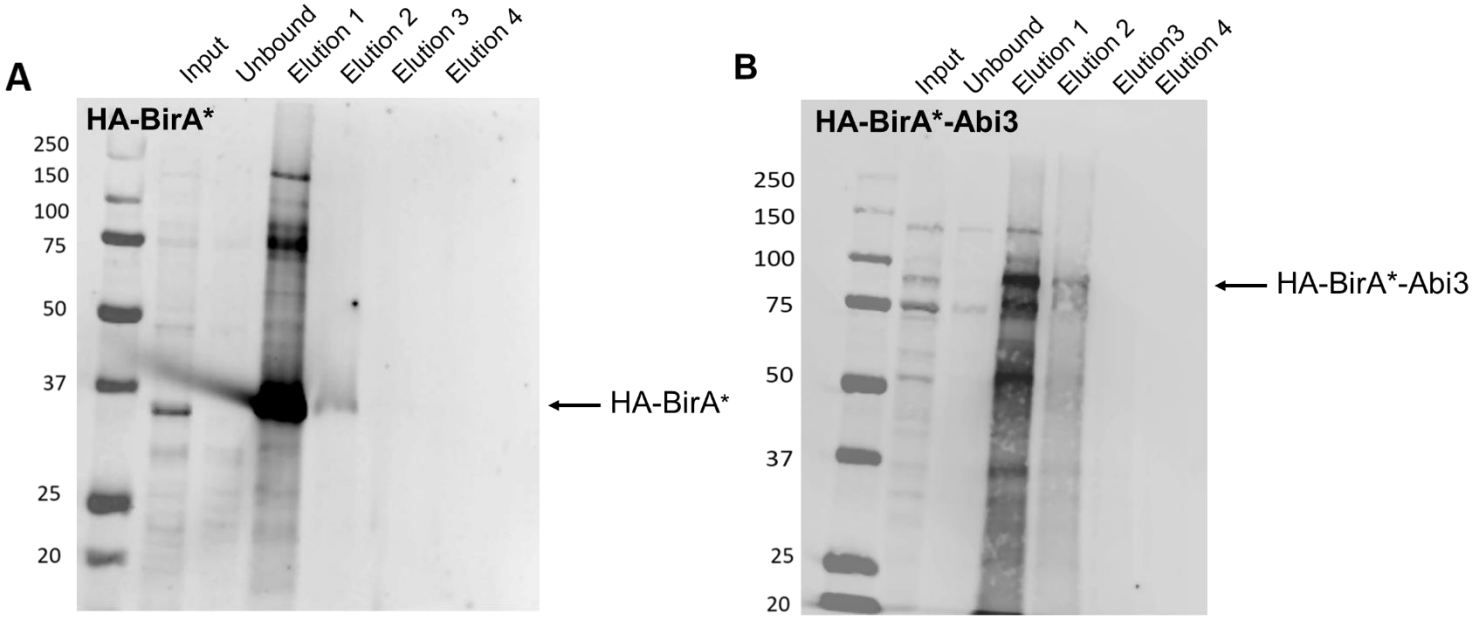

Figure 3.5 Biotin affinity capture of HA-BirA* and HA-BirA*-Abi3 associated proteins. *Capture of interacting proteins of HA-BirA* (37 kDa)* ***(A)*** *and HA-BirA*-Abi3 (~80kDa)* ***(B)*** *by BioID. Enrichment of proteins in elution 1 compared to the input sample indicates higher concentration of biotinylated proteins in the elution. Low fluorescence in the unbound (lane 2) and subsequent elution samples (lanes 4-6) confirmed capture and elution of biotinylated proteins. A unique labelling profiles of HA-BirA*-Abi3 elution 1 compared to HA-BirA* elution 1 suggests different bait proteins capturing unique interactors.*

3.2.2 Biotin-Affinity Capture of the Abi3 Interactome in BV2 Stable Cell Line

The proximity labelling method BioID was used to capture protein interactors of Abi3 in BV2 cell lines stably expressing HA-BirA*-Abi3. Background proteins were captured by streptavidin affinity chromatography in the control cell line expressing HA-BirA*. BV2 cells expressing HA-BirA* or HA-BirA*-Abi3 were incubated with 50 µM biotin for around 16 hours before lysis. Lysates were then incubated with streptavidin Dynabeads to capture biotinylated proteins. After incubation, the beads were washed with lysis buffer to remove non-biotinylated proteins. Biotinylated proteins were eluted then were resolved by SDS-PAGE and detected by western blotting with Streptavidin IR800 (Figure 3.5).

Enrichment of the first elution sample (lane 3) compared to the input (lane 1) indicated a higher concentration of biotinylated proteins in the elution due to removal of non-biotinylated proteins during wash stages. Low fluorescence in the unbound (lane 2) and subsequent elution samples (lanes 4-6) confirmed capture and elution

of biotinylated proteins. Strong fluorescence can be seen in the BirA* control which likely indicates endogenously biotinylated carboxylases as well as self-biotinylation of the fusion protein (Grant et al., 2019). These results confirm expression of each fusion protein, proper functioning of the biotin ligase, and successful capture of biotinylated proteins.

3.2.3 Proteomic Analysis of Protein Interactome

To identify the biotinylated proteins, samples were sent for MS analysis by the Fingerprints Proteomics Facility at the University of Dundee. The biotinylated proteins were run for 15 minutes on a 4-12% polyacrylamide gel. Proteins were visualised with GelCode™ Blue stain reagent (Coomassie Blue; Figure 3.6). As the de-staining process in this method does not fix the protein, it is therefore suitable for MS. For each condition the protein bands were excised from the gel in a single sample and sent for MS (see Figure 3.7 for full workflow). At the proteomics facility, the samples were reduced and trypsinised to digest the proteins. Trypsin is a serine protease which digests proteins by cleaving the C-terminal end of lysine and arginine residues, producing peptides. These peptides are then separated by liquid chromatography (LC) coupled to the mass spectrometer and the mass and charge (m/z) of each peptide was determined by tandem MS (MS/MS) allowing the sequence of each peptide to be assigned and mapped to an individual protein.

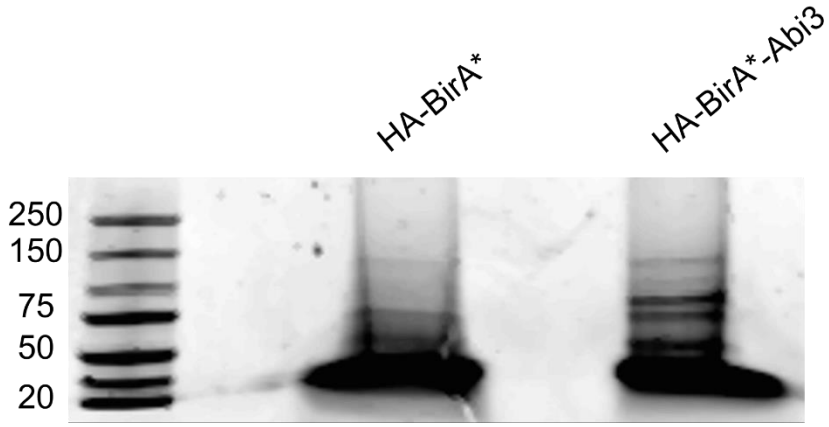

Figure 3.6 Separation of proteins for MS analysis. *A representative gel of proteins from elution 1 separated by SDS-PAGE. Proteins were run on the gel for 15 minutes and visualised with GelCode™ Blue stain reagent. HA-BirA* and HA-BirA*-Abi3 lanes were individually excised from the gel and sent to the FingerPrints Proteomics Facility at the University of Dundee for MS analysis.*

Proteins in the original samples were identified by matching the peptide sequences to the Swiss-Prot protein database for *Mus musculus* proteins to identify proteins present in the original sample. At least two unique peptides from a protein must be present to verify the presence of a protein.

BioID and MS were used to identify the protein interactome of Abi3 in BV2 cells. Two stable cell lines were generated, one expressing Abi3 fused to the biotin ligase BirA* and a control line expressing BirA* only. The data generated from the control cell line formed a list of background proteins which was used during data analysis to identify putative interactors of Abi3. For each condition, five replicates were performed to increase the statistical power of identifying putative interactors. The reproducibility of these replicates is assessed in Figure 3.8. In the control data a total of 1,273 proteins were identified, 304 of which were found in all five replicates. In the Abi3 data, a total of 1,120 proteins were identified, 197 of which were found in all five replicates, although presence of a protein in all replicates was not required to be determined a putative interactor. 859 proteins were found in both control and test conditions and 261 were exclusively identified in the Abi3 data.

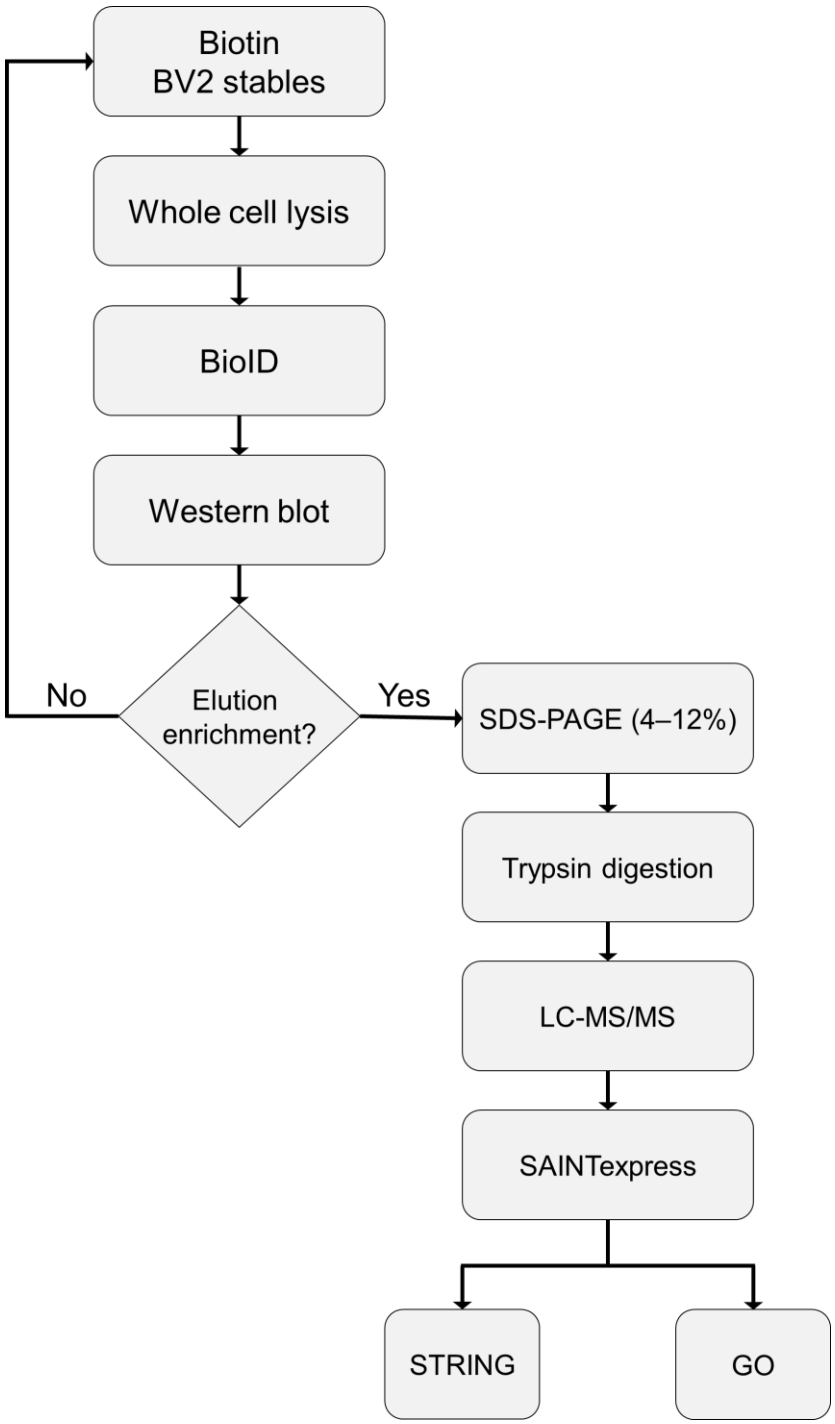

Figure 3.7 Workflow of BioID from cell culture to data analysis. *Stable cell lines were grown in culture and biotin added to the media. Whole cell lysates were then generated for BioID pull-down, and enrichment of captured proteins was assessed by western blot. If successful, proteins in BioID elution samples were separated by SDS-PAGE gel electrophoresis and gel plugs sent to the Fingerprints Proteomics Facility at the University of Dundee where samples were reduced and digested ready for liquid chromatography tandem MS. A list of proteins detected in the samples was generated and interactors of Abi3 were identified by SAINTexpress analysis. These data then underwent further analysis to investigate known interactions (STRING annotation) and functional roles (Gene Ontology) to determine proteins of interest for further investigation.*

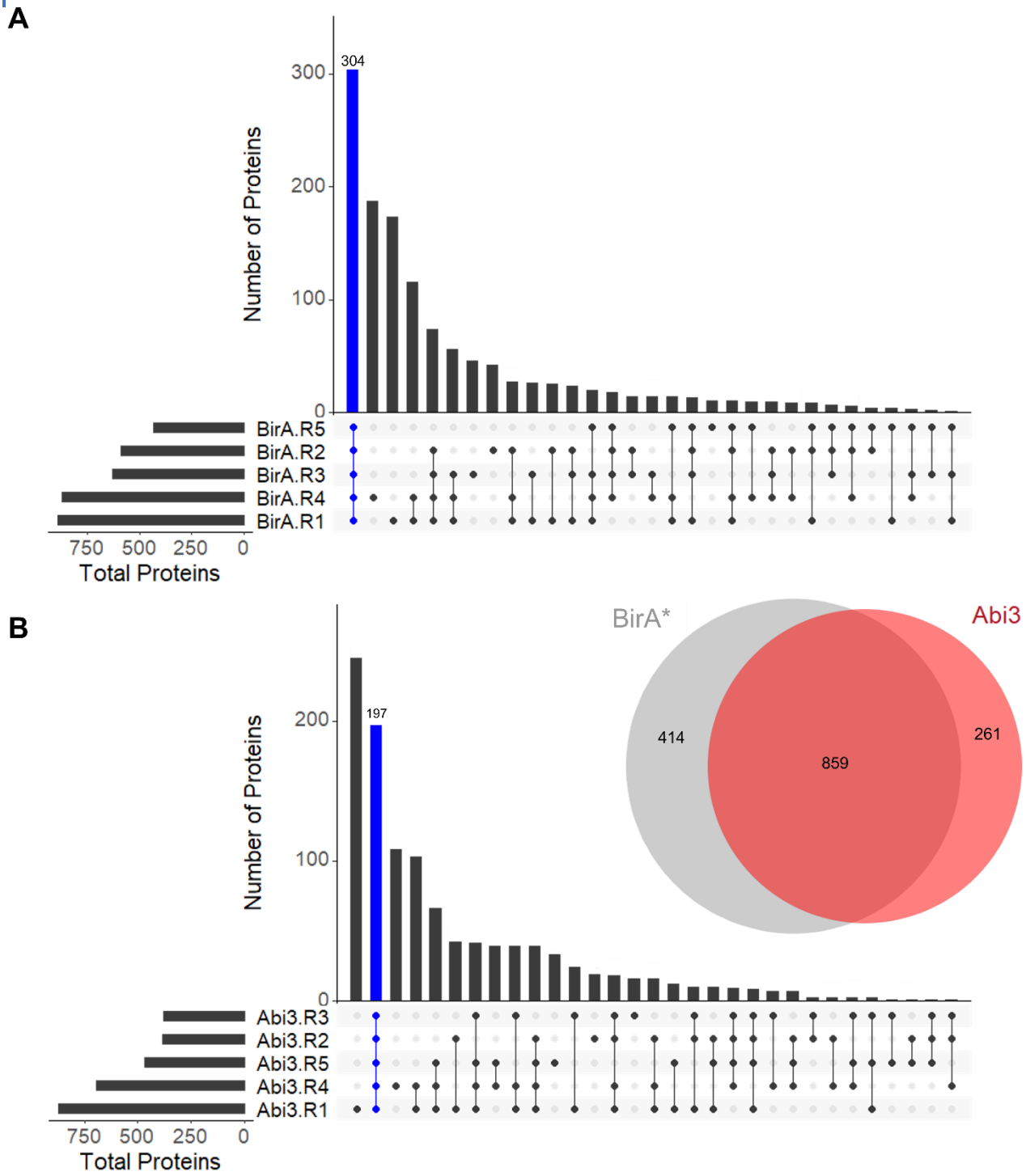

Figure 3.8 Reproducibility of BioID replicates. ***A)*** *Number of proteins identified in each replicate from BirA* control BioID data. Of the 1,273 proteins identified in the data, 304 proteins were found in all 5 replicates. The first dataset (BirA.R1) contained the largest number of proteins of all the replicates, 173 of which were unique to this sample.* ***B)*** *Number of proteins identified in each replicate from Abi3 BioID data. Of the 1,120 proteins identified, 197 were found in all 5 replicates. The first dataset (Abi3.R1) contained the largest number of proteins of all the replicates, 245 of which were unique to this sample.* ***Inset)*** *Overlap of proteins between all BirA* control and Abi3 data. In total 1,535 proteins were identified, 859 of which appeared in both the control and the Abi3 datasets. 414 were unique to the control data and 261 were unique to the Abi3 dataset. Bar highlighted in blue represents the proteins identified in all replicates.*

3.2.3.1 SAINTexpress

Putative interactors were identified by significance analysis of interactome (SAINT) express (Choi et al., 2011). SAINTexpress is a method of scoring protein interactions in AP-MS data. The model assesses the probability of prey proteins being either 'true' or 'false' interactors of the bait based on the abundance of the prey in the test and control conditions. For a protein to be identified as a putative interactor it must appear in the test condition at a significantly higher level than in the control, calculated by division of the average spectral count of each interaction in the bait condition by the average spectral count in the control to give the fold change (Teo et al., 2014). From this, a SAINT score is assigned to each prey protein which is then used with the fold change to estimate the BFDR (Choi et al., 2011). The BFDR uses a Bayesian approach to control the false discovery rate. The posterior error probability (PEP) is calculated which gives the probability that a protein is not an interactor. The sum of the PEP for each protein gives the expected value of the total number of false positives. The cumulative mean of the PEP values gives the q-value, the threshold of which was here defined as $q<0.05$ to determine the total number of proteins identified as interactors with a 5% false positive rate. A prey protein with a BFDR value of less than 0.05 was considered to be a putative interactor. These proteins were then taken for further analysis: gene ontology analysis (GO), STRING annotation and identification of proteins of interest.

10 proteins of the 1,120 captured were found to be putative interactors of Abi3 (Table 3.1). The SAINT score for each of the 1,120 captured proteins was plotted against $\log_2$ of the fold change to visualise the putative interactors of Abi3 (Figure 3.9). The abundance (total sum of spectral counts from HA-BirA*-Abi3 cells) of each protein is represented by the size of the bubble and putative interactors are highlighted in red.

The peptide data for all identified putative interactors of Abi3 can be found in Supplementary table 1.3 in appendix 1.

Table 3.1 Abi3-associated proteins prioritised by SAINTexpress. *The identified proteins were detected by MS of BioID samples from HA-BirA*-Abi3 stable BV2 lines. Proteins which passed the significance threshold <0.05 BFDR after probabilistic scoring of protein-protein interaction by SAINTexpress are above the black line. SAINT determines putative interactors from non-specifically bound proteins by calculating the fold change between the data and a negative control affinity-purification sample. Counts of 0 were considered as 1 to calculate a fold-change. To be considered a putative interactor, the prey protein must appear in the Abi3 dataset at a significantly higher level than in the BirA* control data. Proteins are sorted first by BFDR value (lowest to highest) then by fold change (highest to lowest). The bait protein is highlighted in bold. Title annotations: Spec: spectral counts for the bait-prey pair in each replicate. SpecSum: sum of spectral counts across all replicates. AvgSpec: mean spectral count. crtlCounts: spectral count in each negative control replicate. SaintScore: probability of being an interactor. FoldChange: average spectral count in test interaction divided by the average in controls. BFDR: Bayesian false discovery rate.*

#	Protein	Accession	Spec	SpecSum	AvgSpec	ctrlCounts	SaintScore	FoldChange	BFDR
1	Cyfip1	Q7TMB8	46|12|25|14|2	99	19.8	0|0|0|0|0	0.98	198	0
2	Mtss1	Q8R1S4	8|9|12|5|9	43	8.6	0|0|0|0|0	1	86	0
3	**Abi3**	**Q8BYZ1**	**322|103|125|113|92**	**755**	**151**	**9|0|0|0|0**	**1**	**83.89**	**0**
4	Ccdc22	Q9JIG7	24|4|5|3|2	38	7.6	0|0|0|0|0	0.97	76	0
5	Wasf2	Q8BH43	53|35|30|22|29	169	33.8	2|0|2|0|0	1	42.25	0
6	Cep170	Q6A065	243|146|156|136|101	782	156.4	20|4|12|5|4	1	17.38	0
7	Pi3kap1	Q9EQ32	14|5|3|2|2	26	5.2	0|0|0|0|0	0.95	52	0.01
8	Tanc1	Q0VGY8	55|19|19|16|3	112	22.4	4|0|2|0|0	0.83	18.67	0.01

9	Gigyf2	Q6Y7W8	14|3|3|3|0	23	4.6	0|0|0|0|0	0.79	46	0.03
10	Ripk3	Q9QZL0	6|3|2|2|0	13	2.6	0|0|0|0|0	0.75	26	0.05
11	Homer3	Q99JP6	0|2|5|3|2	12	2.4	0|0|0|0|0	0.75	24	0.07
12	Sec16a	E9QAT4	21|11|3|4|4	43	8.6	3|0|0|0|0	0.73	14.33	0.09
13	Cbl	P22682	12|6|3|5|2	28	5.6	3|0|0|0|0	0.66	9.33	0.1
14	Ruvbl2	Q9WTM5	25|16|16|5|8	70	14	7|0|0|4|0	0.65	6.36	0.12
15	Arhgap12	Q8C0D4	6|6|4|0|0	16	3.2	0|0|0|0|0	0.6	32	0.14
16	Rpl39	P62892	13|0|3|4|0	20	4	0|0|0|0|0	0.6	40	0.16
17	Exoc4	O35382	6|0|3|4|0	13	2.6	0|0|0|0|0	0.6	26	0.17
18	Hist2h2bb	Q64525	26|21|0|70|48	165	33	10|20|0|0|0	0.59	5.5	0.18
19	Wdr62	Q3U3T8	13|2|6|0|0	21	4.2	0|0|0|0|0	0.58	42	0.2
20	Dvl2	Q60838	11|4|0|0|2	17	3.4	0|0|0|0|0	0.58	34	0.21

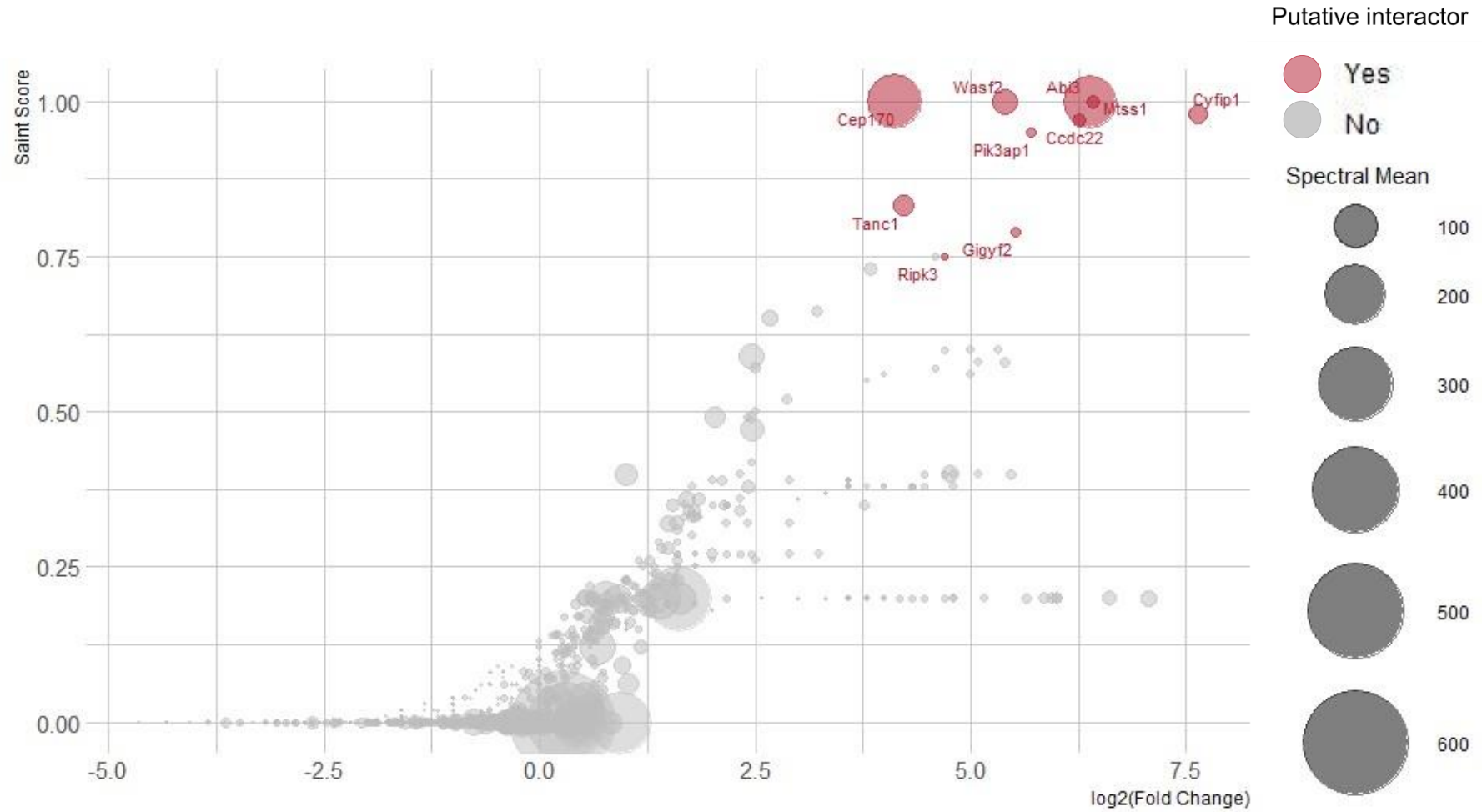

Figure 3.9 Fold change and SAINT score from SAINTexpress. *Proteins identified by MS in Abi3 BioID samples. Data are represented at log_2 of the fold change (difference in protein count from control data) and are plotted against the SAINT score (probability of protein being a putative interactor). Each bubble on the plot denotes an individual protein. The size of the bubble represents the abundance of each protein in the data, calculated by the mean of the spectral counts. Proteins identified as being putative interactors of Abi3 (BFDR < 0.05) are labelled. Red = putative interactor, grey = non-interactor.*

3.2.3.2 STRING Annotation

For all further analysis, proteins were converted to their human orthologues as there is more complete human data and PPIs are relatively well conserved between species (Sharan et al., 2005, Qian et al., 2011, Pérez-Bercoff et al., 2013).

Known relationships between the identified putative Abi3 interactors were investigated using the STRING database (version: 11.5; https://string-db.org/) (Szklarczyk et al., 2021). Physical interaction data from high-throughput experiments and previous databases were extracted from the STRING database with a medium confidence interaction score (0.4) for the putative Abi3 interactors (Figure 0.10a). The known ABI3 PPI network was also extracted (Figure 0.10b).

Part of the WRC network (WASF2, CYFIP1) was identified in the MS data (identified in blue in Figure 0.10). The other orthologues of the putative interactors of Abi3 identified by BioID were not previously known to have direct interactions with either ABI3 or other members of the network.

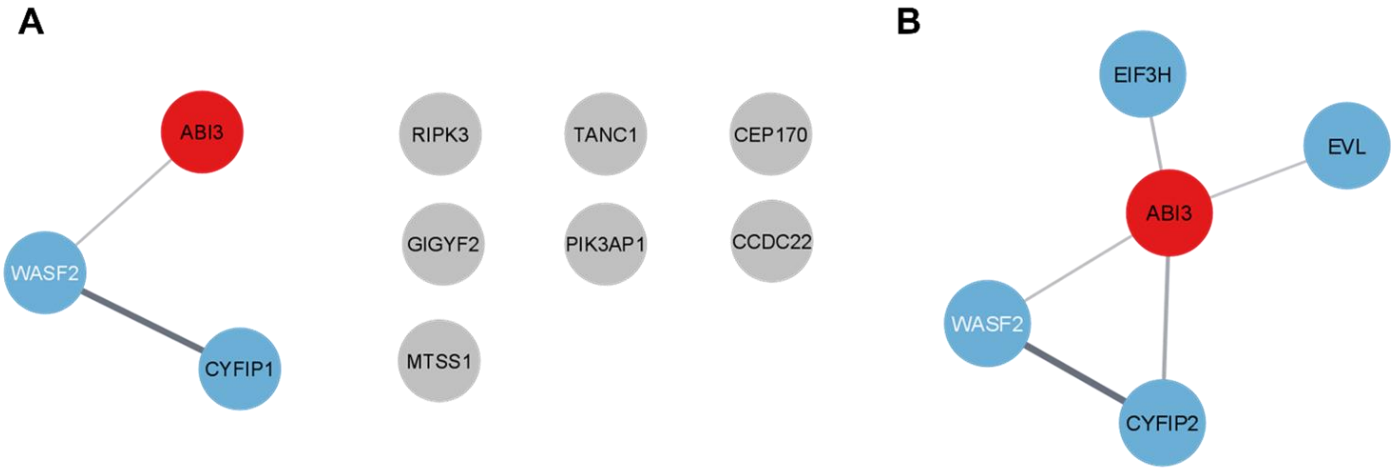

Figure 0.10 Protein-protein interaction network of Abi3-associated proteins. *Known interactions between the human orthologues of the high-confidence Abi3-associated proteins (**A**) and previously identified ABI3 interactions **(B)** obtained from the STRING v11.5 database. ABI3 is highlighted in red with known interacting network members in blue. Proteins with no known interactions within the set are marked in grey. Known physical interactors of ABI3 also identified as high-confidence interactors of HA-BirA*-Abi3 are labelled in white.*

3.2.3.3 Known Interactors

Comparison of the Abi3 interactors identified here with known interactors listed in the NCBI database revealed only one previously characterised interaction: WASF2 (Supplementary table 1.1 in appendix 1). ABI3 and WASF2 are known to form part of

the WRC along with cytoplasmic FMR1 Interacting Protein 1 and 2 (CYFIP1, CYFIP2), although direct interaction between CYFIP1 and ABI3 has not been previously identified (Chen et al., 2014). Interaction between ABI3 and centrosomal protein of 170 kDa (CEP170) has been suggested, reported in a pre-publication dataset on the Bioplex Interactome database and reported by BioGRID (Huttlin et al., 2021). Associations with CEP170P1 (CEP170-like protein, a transcribed pseudogene of CEP170) have also been suggested (Rual et al., 2005).

3.2.4 Functional Annotation of Interactors

Functional annotation of the putative Abi3 interactors was carried out with the Metascape enrichment analysis (http://metascape.org) (Zhou et al., 2019). The majority of the identified biological processes play roles in cell structure and morphology, with the top processes being the ABI3-WAVE2-CYFIP1 complex and lamellipodium formation. Synapse organisation and actin and cytoskeleton regulation processes are also enriched in the identified Abi3 interactors (Figure 3.11, Table 3.2).

Table 3.2 Protein-protein interaction network of Abi3-associated proteins. *Known interactions between the human orthologues of the high-confidence Abi3-associated proteins (**A**) and previously identified ABI3 interactions **(B)** obtained from the STRING v11.5 database. ABI3 is highlighted in red with known interacting network members in blue. Proteins with no known interactions within the set are marked in grey. Known physical interactors of ABI3 also identified as high-confidence interactors of HA-BirA*-Abi3 are labelled in white.*

Category	Description	Count	Percentage
CORUM	ABI3-WAVE2-CYFIP1 complex	3	30.00
GO Biological Processes	Regulation of actin cytoskeleton organization	4	40.00
GO Biological Processes	Cell junction organization	4	40.00
GO Biological Processes	Regulation of synapse organization	3	30.00

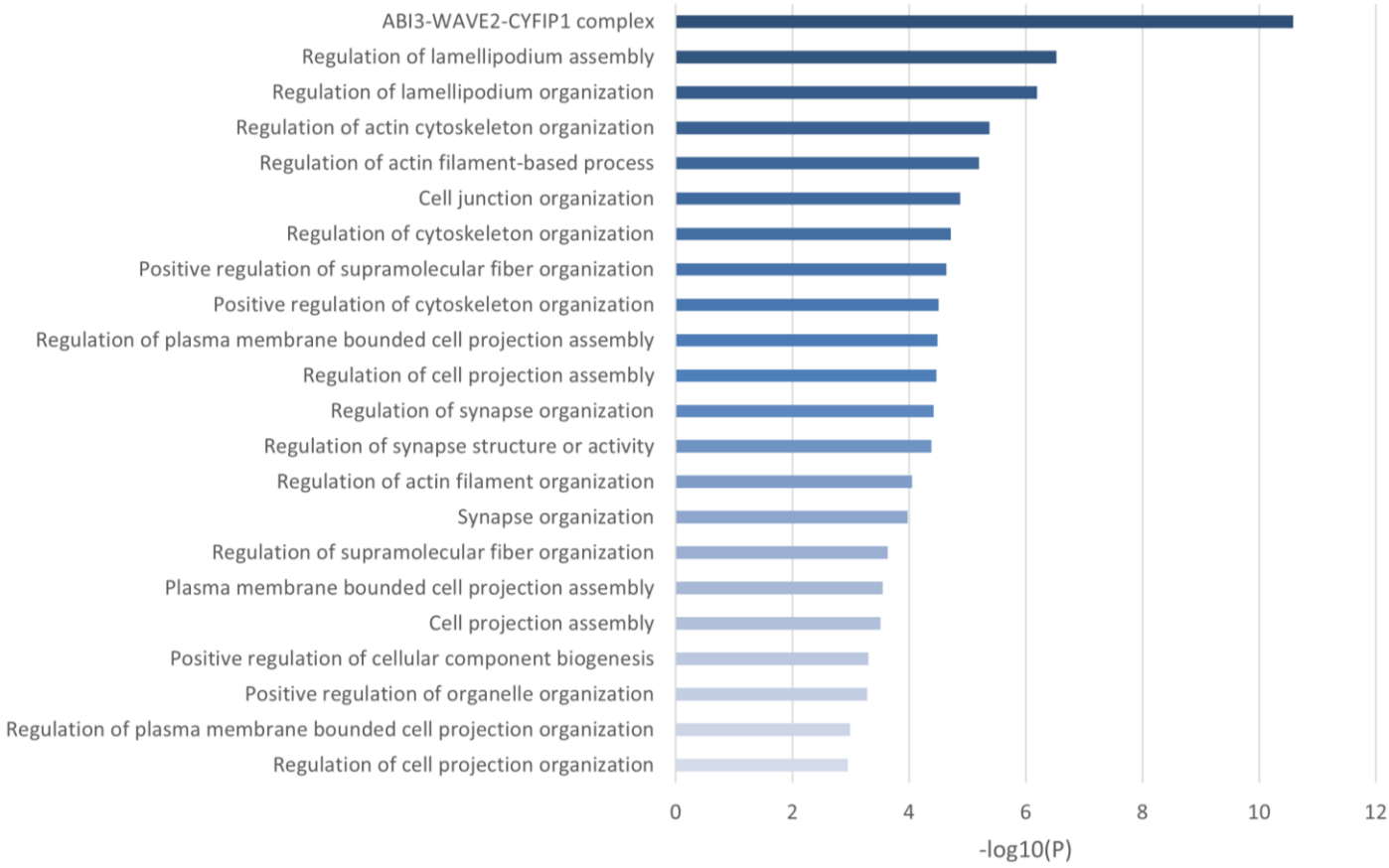

Figure 3.11 Biological process annotations for Abi3-associated proteins identified by BioID. *Enrichment analysis from Metascape was used to identity biological processes enriched in the human orthologues of the identified putative interactors of Abi3. The heatmap is coloured according to p-value and plotted with the -log$_{10}$(P) score.*

3.2.5 Proteins of Interest

The above analysis has identified 9 potential novel interactors of Abi3 to investigate (peptide data found in appendix 1, Supplementary table 1.3). From the STRING analysis, the WRC was highlighted as the major network involving Abi3. Wasf2 was the only previously identified Abi3 protein interactor identified by BioID. Cyfip1 is a paralogue of Cyfip2, a known Abi3 interactor and important component of the WRC, so confirmation of physical interaction would strengthen evidence that a major role of Abi3 is within this complex, regulating the actin cytoskeleton.

Centrosomal protein of 170 kDa (Cep170) is of interest to confirm as an interactor of Abi3. After Abi3 itself, Cep170 was the most abundant protein identified in the bait

samples, with a mean spectral count of 129.25. Cep170 is a centrosomal protein associated with microtubules during cell growth and division. As of May 2023, human CEP170 is listed as an interactor of ABI3 on the BioGRID database, sourced from a pre-publication dataet from the BioPlex Network (Huttlin et al., 2021). A variant at the CEP170 locus has also recently been associated with risk of AD (Kulminski et al., 2022).

Metastasis suppressor-1 (Mtss1) is reported to be down-regulated in AD (Rangaraju et al., 2018). Mtss1 was initially identified as a suppressor of metastasis and also has roles as a scaffold protein and regulator of actin dynamics (Xie et al., 2011). Confirming interaction between Mtss1 and Abi3 may elucidate a common pathway for AD risk.

3.2.6 Validating Putative Interactors

As the biotin ligase BirA* has a biotinylation range of around 10 nm, it is possible that proteins which are proximal but that do not interact with the bait protein are captured. To validate the putative interactors identified by SAINT after BioID, co-IPs can be used to confirm physical interaction. However, the reasons for using BioID over IPs for identifying protein interactions is often due to the need for harsher lysis conditions to extract the bait proteins. These conditions disrupt protein interactions and so any interactors are lost before capture can begin. To assess whether co-IP was a suitable method to validate putative interactors, the proteins HA-BirA*-Abi3, Abi3-myc, and Cep170-Flag were transfected into HEK-293T cells and lysed under different conditions. The harshest lysis was done with a 4% SDS lysis buffer and the gentlest with RIPA buffer (a lysis buffer commonly used to prepare samples for IP). RIPA buffer with 0.1% SDS and 0.5% SDS were also tested as intermediate buffers. Myc-Abi3 was successfully extracted with all lysis buffers tested, however Cep170-FLAG was only recovered using the 4% SDS lysis buffer (Figure 3.12). Under these harsh lysis conditions, PPIs are disrupted and so this buffer is not suitable to prepare samples for IP. Validation of physical interaction between Abi3 and Cep170 was therefore unable to be completed using this method. Additionally, extraction of Abi3 appeared to be less effective with the RIPA buffers compared to the 4% SDS buffer, implicating that Abi3 may also be difficult to solubilise. Protocols requiring gentle lysis conditions may therefore not be suitable for validating physical interaction of any of the putative interactors identified here. Interestingly, two bands can be seen

around the expected molecular weight of myc-Abi3. These may represent the phosphorylated and unphosphorylated forms of Abi3. ABI3 has been suggested to be phosphorylated by protein kinase B (PKB) at residue S342 as inhibiting PKB led to a reduction in the amount of phosphorylated ABI3 captured by immunoprecipitation (Moraes et al., 2017). Further characterisation of the HA-BirA*-Abi3 BV2 line could be achieved by similar inhibition of phosphorylation during cell culture. If the higher molecular weight band is not present when phosphorylation is inhibited, this would indicate that these bands do represent Abi3 at different phosphorylation states.

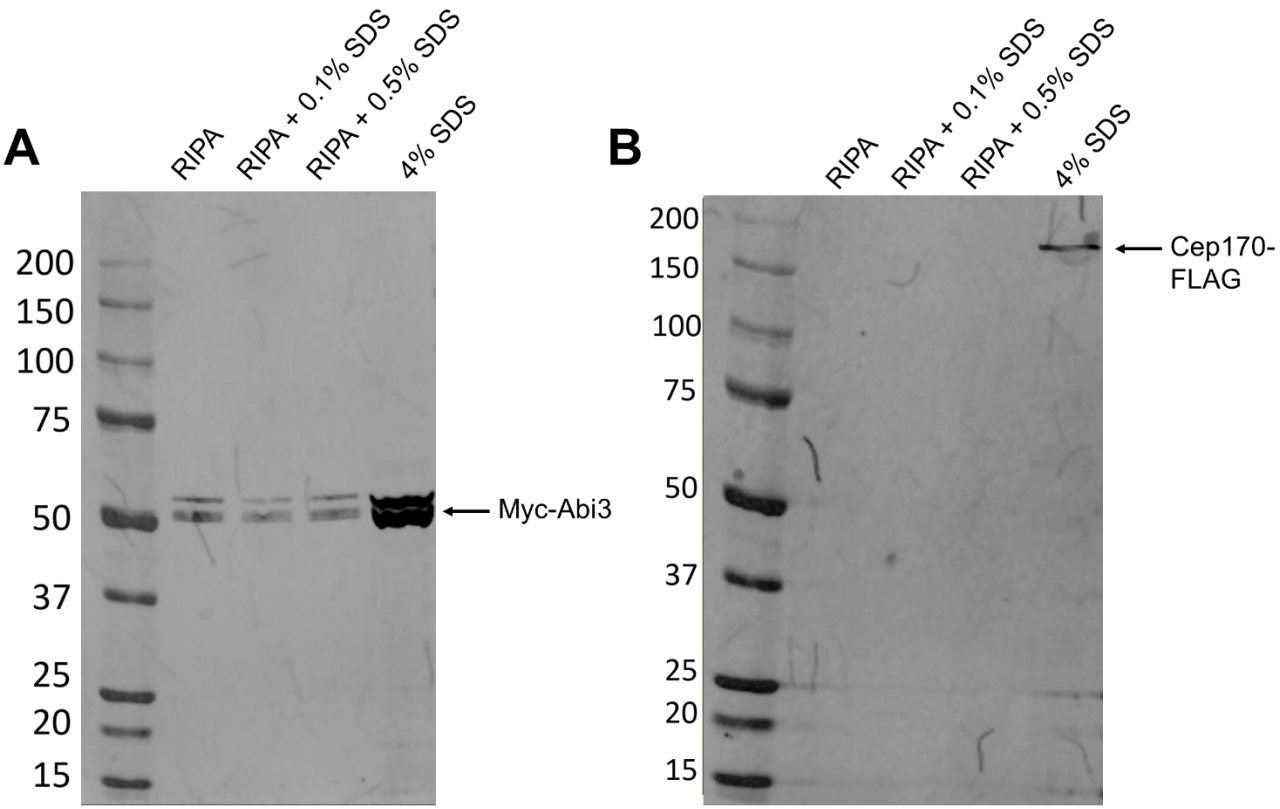

Figure 3.12 Comparison of protein extraction with different strength lysis buffers. *HEK-293T cells transfected with myc-Abi3* ***(A)*** *or Cep170-FLAG* ***(B)*** *were lysed with either RIPA buffer (lane 1), RIPA buffer with 0.1% SDS (lane 2), RIPA buffer with 0.5% SDS (lane 3) or a lysis buffer containing 4% SDS (lane 4). For myc-Abi3, protein was successfully extracted with all lysis buffers. For Cep170-FLAG protein was only successfully extracted with the harshest lysis protocol*

3.3 Discussion

The main aims of the experiments described in this chapter were to establish the BioID technique for use in the detection of protein interactomes of AD risk genes and, with this, identify the protein interactome of Abi3. The exact function of Abi3 is unknown although it has been proposed to be part of the WRC due to the known functions of its paralogues Abi1 and Abi2. BioID was successfully used to produce a potential Abi3 protein interactome in a microglial cell line. Previously identified interactors of ABI3 and Abi3 were mostly identified in Y2H assays or AP-MS experiments in non-microglial lines (Supplementary table 1.1 and Supplementary table 1.2). The results presented here represent the first interactome of Abi3 in a cell line physiologically relevant for study of the role of Abi3 in microglia and AD pathology.

The National Center for Biotechnology Information (NCBI) lists 84 protein interactors of human ABI3 (Supplementary table 1.1, appendix 1) (Human ABI3 NCBI; interactions sourced from the HPRD and BioGRID databases). Four interactors of mouse Abi3 are listed (Mouse Abi3 NCBI; interactions sourced from BioGRID database), 3 of which overlap with the human data (Supplementary table 1.2, appendix 1). The majority of these interactions were identified by two-hybrid studies, which detect binary interactions, with some detected by affinity capture with either MS or western blotting. At present, there have not been many studies of the Abi3 interactome in physiologically relevant systems. HEK, Chinese hamster ovary (CHO), and yeast were the most prevalent cell lines in studies listed in Supplementary table 1.1 and Supplementary table 1.2 (appendix 1). The results presented here were obtained from a microglial cell line and therefore are more applicable to the identification of the microglial protein interactome.

3.3.1 Confirmed and Novel Protein Interactors of Abi3

3.3.1.1 HA-BirA-Abi3 Interacts with the WRC*

Of the putative interactors identified, three of the top five proteins were Abi3, Wasf2, and Cyfip1. These proteins are members of the WRC and Wasf2 is a known interactor of Abi3. This, along with the cytoplasmic labelling seen with immunocytochemistry (Figure 3.4), suggests that the addition of the biotin ligase did not appear to affect the localisation of the exogenous Abi3 as the fusion protein was

located in the same subcellular compartment as endogenous Abi3. It is not possible to determine if the detection of Abi3 in these samples was due to interaction with endogenous Abi3 or capture of the HA-BirA*-Abi3 protein due to self-biotinylation. The identification of known Abi3 interactors is also evidence of correct localisation of HA-BirA*-Abi3 as well as suggesting normal functioning of the protein. Cyfip1 is not identified as an interactor of Abi3 in databases such as BioGRID or NCBI although its paralogue Cyfip2 is. Previous studies have shown expression of the Cyfip proteins to vary between neural cell types, with Cyfip2 mostly expressed in neurons and Cyfip1 in glial cells in addition to neurons (Zhang et al., 2019b, Drew et al., 2020, Preprint) It is possible that in microglia, Cyfip1 is the more common component of the WRC, hence its identification as a putative interactor of HA-BirA*-Abi3 rather than Cyfip2. Drew et al. (2020, Preprint) also identified a “canonical microglial WRC” comprising of Cyfip1, Abi3, Nap1l, and Wave2 and Moraes et al. (2017) also identified CYFIP1 as an interactor of ABI3 by IP.

No other proteins known to make up the WRC were identified as putative interactors of Abi3 by BioID. The WRC comprises of five proteins from the Abi, Cyfip, Wasf, and Hem families, as well as Brick1. From these proteins, a large dimer of Cyfip and Hem proteins and a smaller trimer comprising of Wasf, Abi, and Brick1 proteins join to form the WRC (Rottner et al., 2021). Neither Brick1 nor any Hem proteins were identified as putative interactors of Abi3. Brick1 was not identified in RNA sequence data of BV2 cells, which may explain why this protein was not identified here but does raise the question of how the WRC is formed in BV2s (Carrillo-Jimenez et al., 2019). Hem-like proteins were identified in RNA sequencing which may replace Hem proteins in the WRC of BV2 cells. The Hem-Cyfip dimer is known to be around 10 x 10 x 20 nm in size, and so the positioning of Hem-like proteins and HA-BirA*-Abi3 may explain why these were not identified if they are outside of the 10 nm labelling radius of BirA*. Hem proteins may not form direct interactions with Abi proteins within the WRC whereas Cyfip proteins may. An interaction between Abi and Cyfip proteins may induce the formation of the WRC by bringing together the Hem-Cyfip dimer and the Wasf-Abi-Brick1 trimer.

The identification of two WRC proteins as putative interactors of Abi3 strengthens the evidence that at least one role of Abi3 in microglia is as part of this complex, regulating actin polymerisation and cell motility. These results also confirm that BioID

is a suitable method for identifying candidate protein interactors, although further validation is required for confirmation of physical interaction.

3.3.1.2 HA-BirA-Abi3 Potentially Interacts with Other Cytoskeleton-Associated Proteins*

The proteins of the WRC are not the only ones to interact with the cytoskeleton to regulate cell morphology. Both Cep170 and Mtss1 play roles in cytoskeletal regulation and were here identified as putative interactors of Abi3.

Cep170 is a centrosomal protein responsible for microtubule organisation. This protein is phosphorylated during mitosis and associates with centrioles (Guarguaglini et al., 2005). If Cep170 is validated as a physical interactor of Abi3, this could suggest a role for Abi3 in microtubule, as well as actin, organisation. CEP44 and kinesin family members KLC3 and KLC4 of kinesin-1, and KIFC3 are listed as interactors of ABI3 on the BioGRID database. These proteins are also associated with microtubules; however, these interactions have not been verified in microglia or other relevant cell types and were not identified as putative interactors in the BioID experiments detailed here. A variant of CEP170 has also been associated with AD risk in a recent GWAS. Kulminski et al. (2022) identified the variant rs71537331 in cytogenic region 1q43. However, this locus also contains *Serologically defined colon cancer antigen 8* (also known as *CCCAP* or *NPHP10*) which encodes the protein serologically defined colon cancer antigen 8. Fine mapping and functional analyses, such as expression quantitative trait loci mapping and genome editing, is needed to confirm if CEP170 is indeed an AD risk gene.

Mtss1 was first identified as a metastasis suppressor protein and was found to regulate the actin cytoskeleton (Saarikangas et al., 2011, Kawabata Galbraith et al., 2018). Inhibition of cell motility occurs via interaction of Mtss1 with G-actin as this antagonises WASP-mediated actin polymerisation. However, Mtss1 also increases actin polymerisation via interaction with cortactin, an Arp2/3 positive regulator (Lin et al., 2005). Mtss1 interacts with the SH3 domain of cortactin, a domain also found in Abi3. Therefore, it is likely that Mtss1 has the ability to physically interact with Abi3, although experimental validation of this is needed. The effect of Mtss1 interaction with Abi3 is unclear, although identification of this interaction suggests a novel route for these proteins to regulate the actin cytoskeleton.

Rangaraju et al. (2018) found Mtss1 to be downregulated in the microglia of AD mouse models and Bossers et al. (2010) found MTSS1 mRNA in post-mortem human brain tissue to be downregulated at Braak stages 0-III and upregulated at stages IV-VI. If Abi3 is confirmed as a physical interactor of Mtss1, this may uncover a new route for Abi3 to influence the actin cytoskeleton as well as link it to a potential AD pathology pathway.

3.3.1.3 HA-BirA-Abi3 Potentially Interacts in Inflammatory Signalling Pathways*

A completely novel pathway for Abi3 suggested by this interactome is as part of inflammatory signalling pathways. Ccdc22 is known to regulate NF-κB signalling via the CCC complex and Phosphoinositide-3-Kinase adaptor protein 1 (Pi3kap1; also known as BCAP) links TLR activation to Pi3k signalling.

CCDC22 forms part of the CCC complex and reduction in expression or functioning of the complex has been shown to affect NF-κB signalling. NF-κB is a transcription factor which promotes proinflammatory pathways. Activation is regulated by ubiquitination of IκB (inhibitor of NF-κB) proteins, which prevents the translocation of NF-κB to the nucleus. Starokadomskyy et al. (2013) showed that CCDC22 is required for the ubiquitination and, therefore degradation, of IκB proteins. If Abi3 is validated as a physical interactor of Ccdc22 this may suggest a role for Abi3 in regulating the NF-κB pathway and influencing microglial responses to inflammatory stimuli. Interestingly, both Commd2 and Ccdc93 appear in the list of proteins identified by MS after proximal protein capture at, slightly but not significantly, higher levels than in the control data (Commd2 average spectral count: 3.2 in Abi3 data, 0.6 in control; Ccdc93 average spectral count: 0.4 in Abi3, 0 in control). It is possible that Abi3 can affect the CCC complex via interaction with Ccdc22 and the proximity of Commd2 and Ccdc93 within the complex led these proteins to be biotinylated to a slightly greater extent in the HA-BirA*-Abi3 cell line compared to HA-BirA* only.

The CCC complex also plays a key role in protein trafficking and endosomal recycling. The recruitment of the CCC complex to endosome membranes is dependent on the WASH complex (Singla et al., 2019). WASH proteins are members of the WASP family, of which WASF (or WAVE) proteins also belong, which regulate actin polymerisation via ARP2/3 at the endosomal membranes. Interactions between the WASH complex subunit WASHC2 (also known as FAM21) and CCDC22 lead to CCC complex recruitment to endosomes. With retriever, these proteins mediate

endosomal localisation and are reliant on the branching of actin networks. Interactions between Abi3 and Ccdc22 may therefore play a role in endosomal functions, mediating intracellular transport. As with Ccdc93 and Commd2, Washc2 was identified in the list of proteins identified by BioID at a slightly higher, but again not significant, level in the Abi3 interactome data compared to control. Abi3 may therefore be interacting with Ccdc22 as part of CCC complexes involved in both NF-κB signalling and actin remodelling at endosomes.

Pi3kap1 was also identified as a putative interactor of HA-BirA*-Abi3. This protein is a TLR signalling adaptor required for Pi3k signalling after TLR activation. TLRs reside in the cell and endosome membranes. In microglia, TLR activation initiates inflammatory signalling pathways resulting in phagocytosis and cytokine release (Heidari et al., 2022). TLRs have been linked to AD due to their activation of inflammatory pathways, overexpression in both patients and mouse models, and inhibition of specific types of TLR has shown to be protective against neuroinflammation (Su et al., 2016). Pi3k pathway activation regulates multiple inflammatory response mechanisms by propagating intracellular signalling (Cianciulli et al., 2020). PI3KAP1 negatively regulates proinflammatory cytokine release and cell proliferation (Troutman et al., 2012, Duggan et al., 2017). Chai et al. (2021, Preprint) found that the protein was highly correlated with oxidative damage and the immune response in AD patient brains at Braak stages 0-IV and suggested its use as a biomarker of AD. If Abi3 is confirmed to physically interact with Pi3kap1 this may suggest a new role in regulating Pi3k signalling downstream of TLR activation. Abi3 has not previously been reported to have any role in intracellular signalling pathways outside of the WRC. If these putative interactors are validated as physical interactors of Abi3, this would suggest novel roles for Abi3 in inflammatory signalling in microglia and provide links to other known AD pathology mechanisms.

3.3.1.4 HA-BirA-Abi3 May Interact with Translation Repressor Proteins*

Growth factor receptor-bound protein interacting glycine-tyrosine phenylalanine domain protein 2 (Gigyf2) was initially linked to tyrosine kinase receptors, such as insulin-like growth factor receptor, by interaction with growth factor receptor-bound protein 10 (Giovannone et al., 2003). Later studies identified a role of GIGYF2 in translation repression as part of a complex with 4EHP, a mRNA 5'-cap binding protein (Morita et al., 2012). GIGYF2 is proposed to connect RNA binding proteins

and 4EHP forming an mRNA closed loop which inhibits translation. GIGYF2 however has also been shown to independently repress translation by direct mRNA binding (Amaya Ramirez et al., 2018). Abi3 has not previously been linked to regulation of translation, so this is a potentially novel role for Abi3 provided physical interaction is confirmed.

As well as being a critical subunit of the WRC, CYFIP1 has also been shown to repress translation through binding to eIF4E (Napoli et al., 2008). BNDF-Rac1 signalling initiates the translocation of CYFIP1 from eIF4E binding to the WRC, mediating the transport of CYFIP1 between the two complexes. Disruption of binding to eIF4E or the WRC caused dendritic spine defects in neurons, and it is therefore possible that changes in the interaction between CYFIP1 and ABI3 in microglia may adversely affect microglial projections (Amaya Ramirez et al., 2018). As the putative interactors identified by BioID from HA-BirA*-Abi3 cells were not enriched for processes relating to translation, it is more likely that the Cyfip1 interacting with Abi3 in these cells was located in the WRC.

3.3.1.5 HA-BirA-Abi3 Potentially Interacts in Cell Death Pathways*

Receptor-interacting protein kinase-3 (Ripk3) is a serine/threonine-protein kinase, the activation of which promotes both apoptotic and necrotic cell death pathways. Ripk3 has been shown to influence neuroinflammation and microglial death post ischemic stroke, in Gaucher's disease, and preceding remyelination post CNS injury (Lloyd et al., 2019, Vitner et al., 2014, Yang et al., 2018). Interaction of Ripk3 with mixed lineage kinase domain-like protein promotes necrosis via calcium influx through damage to the plasma membrane, and interaction with Ripk1, FAS-associated death domain protein and caspase-8 promotes apoptosis. Abi3 has no known roles in these pathways, but potential interaction with Ripk3 may suggest a role in cell death pathways, possibly via disruption of cytoskeletal structures or a new, unknown role.

3.3.1.6 HA-BirA-Abi3 Potentially Interacts in Other Protein Complexes*

Tetratricopeptide Repeat, Ankyrin Repeat and Coiled-Coil Containing 1 (Tanc1) is a scaffold protein mostly reported in the post-synaptic density although its specific molecular functions remain unknown (Wu et al., 2021). Scaffold proteins are mediators of PPIs. They bind multiple proteins to physically assemble them into a

protein complex. Scaffold proteins have been suggested as the mechanism of spatial and temporal organisation of signalling cascades as well as regulators of selectivity within these pathways (Good et al., 2011). Interaction of Abi3 with Tanc1 may suggest a role for Abi3 in other protein complexes, although the nature of those complexes is not clear from this data.

3.3.2 Strengths and Limitations of BioID

The results discussed above provide evidence that the proximity labelling method BioID is able to successfully capture protein interactors of the exogenous bait protein. A suitable control line is required to create a list of background proteins which include endogenously biotinylated proteins and proteins biotinylated by the ligase due to proximity rather than interaction. It is therefore important that the ligase only control protein be expressed in the same cellular compartment as the bait protein. This was confirmed in the HA-BirA* and HA-BirA*-Abi3 stable BV2s by immunocytochemistry where the HA epitope was shown to be cytoplasmic in both cell lines (Figure 3.4a). With this background protein list, appropriate statistical analysis can be performed to identify putative interactors of the bait protein. Due to the nature of BioID, fully excluding all proteins from the background list is likely to remove genuine Abi3 interactors from the analysis. As Figure 3.4a shows, both HA-BirA* and HA-BirA*-Abi3 were located in the same cellular compartment. Therefore, any cytoplasmic protein which falls within the 10 nm labelling radius of the biotin ligase is likely to be biotinylated by HA-BirA*, which may include cytoplasmic interactors of Abi3. The HA-BirA*-Abi3 protein is likely to be more specifically targeted to areas where endogenous Abi3 functions and therefore proteins interacting with Abi3 will have higher levels of biotinylation than those which transiently fall within the labelling radius. It is for this reason that SAINTexpress was chosen as the method of statistical analysis of the MS data as the relative abundance of each protein is assessed.

A major advantage of the BioID method is its reproducibility. The lack of a requirement for a high-quality antibody against the bait protein removes many challenges faced when studying PPIs with more traditional techniques such as co-IP. The high affinity bond between biotin and streptavidin means fewer non-specifically bound proteins will be captured. From a practical point of view, once the lysis and

capture have been optimised, the method is easily translated to different cell lines and bait proteins.

As discussed above, the biotin ligase has a 10 nm labelling radius and so it is possible that proteins which are proximal to, but do not interact, with the bait protein are biotinylated. Proteins which are transiently proximal to the bait, and therefore have low levels of biotinylation, are not likely to be deemed putative interactors. However, proteins within the same complex, but which do not directly bind to the bait, may be highly biotinylated by the biotin ligase. Physical interaction between bait and prey proteins therefore must be verified with alternative methods. One such method is IP, however the lack of a specific antibody or harsh lysis conditions required to solubilise the protein are major disadvantages of this technique. As shown in Figure 3.12, only the harsh lysis conditions created by the 4% SDS lysis buffer successfully extracted Cep170. Under these conditions, protein complexes would no longer be maintained as a negatively charged SDS-protein complex is formed, disrupting hydrophobic interactions as well as ionic and hydrogen bonds between proteins. Alternative methods of validation could include Y2H however, this is not a physiologically relevant system for expressing proteins and often criticised for producing many false positive and false negative results (Stellberger et al., 2010). Label transfer protein interaction analysis could be a potential method to validate the putative Abi3 interactors described here. A labelled crosslinking reagent is attached to the bait protein which then crosslinks the bait and prey proteins during interaction. The crosslink is then cleaved leaving the label attached to the prey protein, which can then be captured and detected by western blot (Liu et al., 2007). This method has similar advantages to BioID as weak and transient interactors can be identified and labelling occurs before lysis meaning protein complexes do not need to be maintained. Biotin can be used as the label in this protocol, which can be captured and detected by streptavidin in a similar way to the BioID protocol. By expressing Abi3 linked to this labelled crosslinker and the putative interactor in the same cell line, the requirement for gentle lysis is removed and detection of the label on the putative interactor would strengthen evidence that the identified protein is a true interactor of Abi3.

An innate limitation of BioID is the requirement of an exogenous bait protein. In order to label the protein interactome, the biotin ligase must be attached to the bait. This

addition may cause incorrect folding of the bait protein, affecting its localisation and function. It is therefore important to validate the cell lines before performing BioID experiments to confirm the bait protein is as similar to the endogenous protein as possible. HA-BirA*-Abi3 was confirmed to be expressed in the same cellular compartment as endogenous Abi3 and the identification of WRC proteins infers normal functioning of the protein, although does not confirm it. In this respect, IPs have an advantage over BioID as endogenous bait proteins are captured. However, difficulty in extracting proteins with gentle lysis and the requirement for a highly specific antibody against the endogenous protein to avoid cross-reactivity are major limitations.

3.3.3 Conclusions

Using BioID, 10 putative interactors of Abi3 were identified in this chapter, including 8 novel interactions. As discussed in sections 3.2.6 and 3.3.2, validation of physical interaction of these putative interactors was not achieved due to difficulty in protein extraction with gentle lysis. If these interactions are confirmed, this interactome suggests previously unknown functions of Abi3, including alternative mechanisms of actin regulation via Mtss1, a role in inflammatory signalling pathways via Ccdc22 and Pi3kap1, and possible regulation of translation via Gigyf2. The results presented here also show that BioID can give novel insights into the functional mechanism of proteins based on enriched functional processes within the putative interactome, building a foundation for further investigation.

Chapter 4 – Investigation of the Protein Interactome of the AD Risk Variant Abi3-S212F

4.1 Introduction

4.1.1 ABI3 AD-Associated Risk Variants

ABI3 was first associated with AD risk by Sims et al. (2017) using whole-exome microarray genotyping of LOAD patients and age-matched controls. The SNP rs616338 was identified and mapped to *ABI3* where it was found to be a g.624C>T substitution resulting in a p.S209F amino acid missense substitution (Figure 4.1a-b). While the mechanism of risk of ABI3-S209F is unknown, changes to the primary sequence of the protein can alter its function through a range of mechanisms, including the loss or gain of PPIs. The association of ABI3-S209F with AD has been replicated since the first report but has not yet been linked to specific AD phenotypes (Olive et al., 2020, Conway et al., 2018). Elucidating the mechanism by which this risk variant influences AD pathology will enhance our understanding of how ABI3-S209F contributes to overall AD risk, highlighting pathways that may be targets for therapeutic intervention.

Multiple sequence alignment confirms the mouse equivalent variant as p.S212F (Figure 4.1c). The work undertaken in this chapter uses the Abi3-S212F variant as BV2 cells are of mouse origin and interactions between human ABI3 and mouse prey proteins may not be physiologically relevant. The reasons for the use of the BV2 cell line over human immortalised microglial lines are explored in chapter 1 (section 1.2.3). As evidenced in chapter 3, BioID is an effective method to identify protein interactomes. By characterising the Abi3-S212F interactome and comparison with the Abi3 interactome described in chapter 3, a potential mechanism of AD risk may be uncovered. Coding SNPs can influence protein interactions by loss or gain of interactions as well as complete node removal for more disruptive variants. The work described here investigates the protein interactome of Abi3-S212F in BV2 cells using BioID and MS.

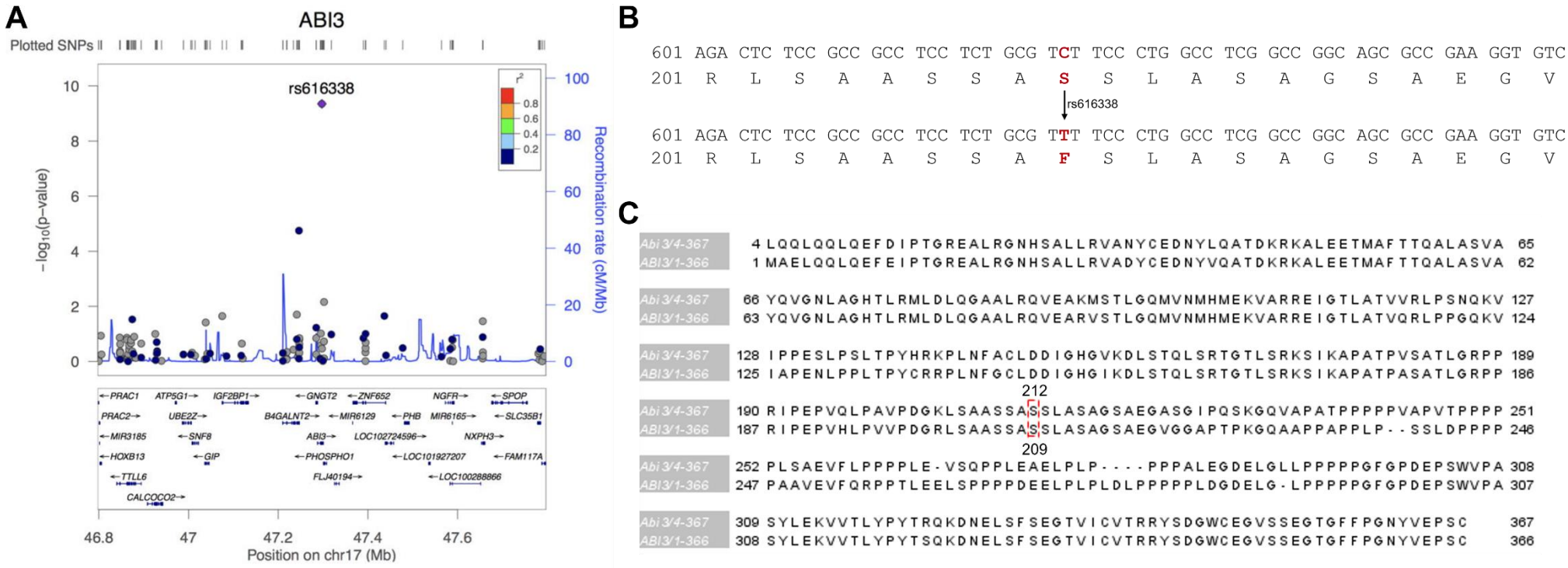

Figure 4.1 Identification of ABI3-S209F association with AD and sequence alignment to mouse orthologue. A) The rs616338 SNP was associated with increased AD risk by Sims et al. (2017) and mapped to the ABI3 gene. **B)** The g.624C>T substitution results in a p.S209F amino acid missense substitution in the protein sequence. **C)** Multiple sequence alignment with the mouse orthologue of ABI3 (Abi3) shows the equivalent change results in a p.S212F amino acid missense mutation. Figure adapted from Sims et al. (2017).

4.1.2 Aims

The aim of the work covered in this chapter was to define the protein interactome of the AD risk variant Abi3-S212F in BV2 cells. This was achieved by capture and identification of proximal proteins by BioID and MS in BV2 cells stably expressing HA-BirA* and HA-BirA*-Abi3-S212F fusion proteins. The interactome determined here was then compared to the interactome of wild type Abi3 determined in chapter 3 to investigate possible functions disrupted by the p.S212F amino acid substitution.

4.2 Results

4.2.1 Generation and Validation of BV2 Cells Stably Expressing HA-BirA*-Abi3-S212F

Stable BV2 lines expressing HA-BirA*-Abi3-S212F were generated by lentiviral transduction (Figure 4.2; see section 3.2.1 for generation and validation of HA-BirA* line). The fusion protein sequence and the puromycin resistance gene were separated by an IRES enabling both genes to be expressed under the control of the mPGK promoter. By contrast, GFP was expressed under the control of the CMV promoter. The full DNA sequence encoding HA-BirA*-Abi3-S212F can be found in appendix 2 (see appendix 1 for HA-BirA* DNA sequence).

Expression and localisation of the fusion protein was validated with immunocytochemical staining of the protein containing the HA epitope (Figure 4.3a). Anti-HA-immunoreactivity was detected in the cytoplasm of GFP^+ cells and did not overlap with nuclear DAPI staining. This is consistent with reports of the cellular localisation of Abi3 in the literature and the localisation of the HA-BirA*-Abi3 protein in chapter 3 (Satoh et al., 2017). These data also show that the Abi3-S212F variant does not cause gross mislocalisation of the protein. As with the HA-BirA*-Abi3 cell line, not all GFP positive cells appeared to express the HA epitope as they were not expressed under the same promoter. This was so HA-BirA*-Abi3-S212F and puromycin could be expressed under the same promoter. Expression and function of the BirA* biotin ligase was validated with streptavidin labelling of biotinylated proteins by western blot (Figure 4.4). Biotinylated proteins were successfully detected with streptavidin suggesting that the biotin ligase was successfully expressed and functional.

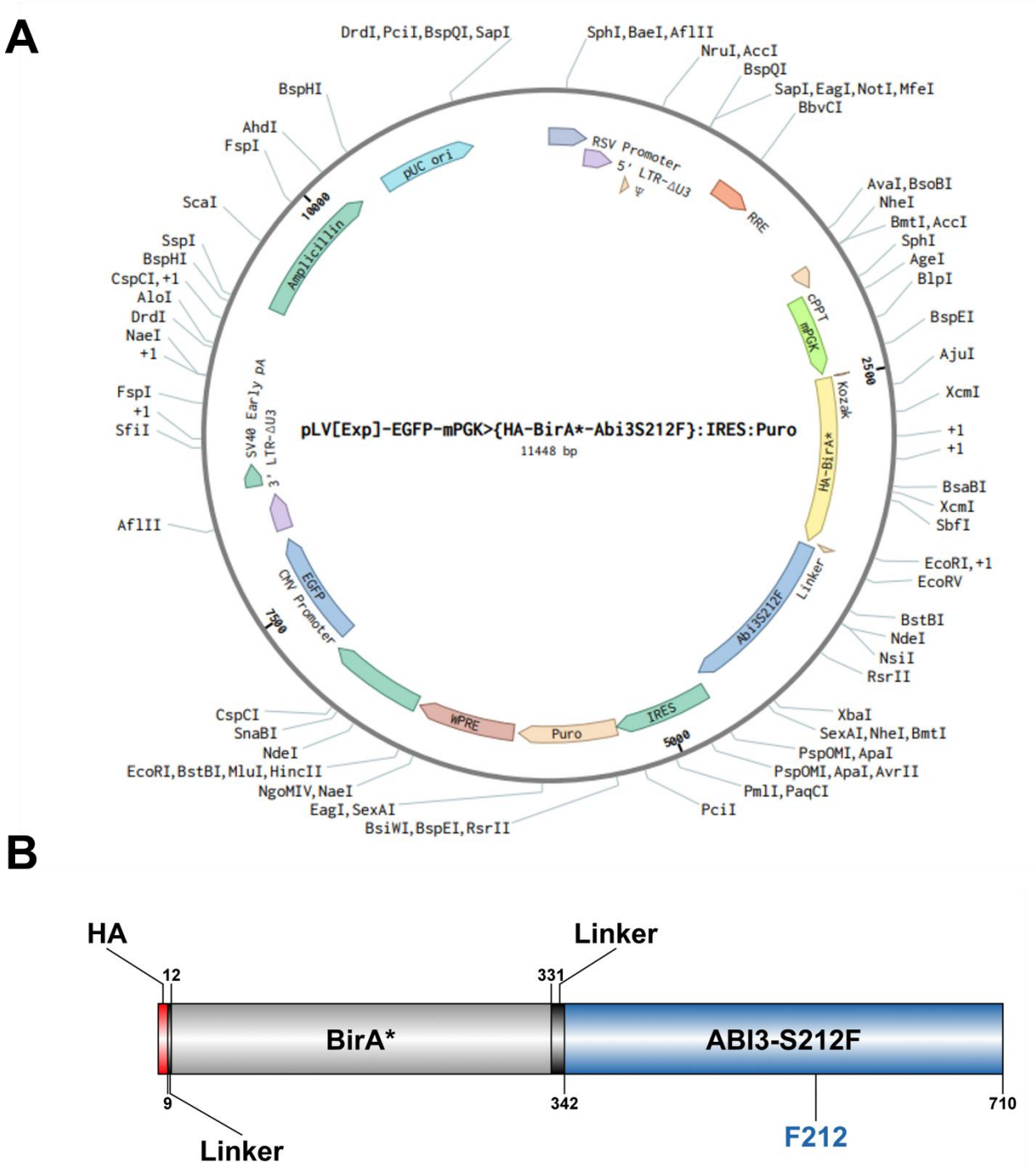

Figure 4.2 Schematic of structure of lentiviral vector and fusion protein. ***A)*** *A lentiviral vector was used to transduce the Abi3-S212F sequence to generate a stable BV2 cell line. BirA* is the mutated form of the E. coli biotin ligase BirA* which prematurely releases bioAMP, resulting in promiscuous biotinylation of surrounding proteins.* ***B)*** *The BioID protein was designed with an HA epitope joined to the N-terminus of the BirA* sequence via a linker. The HA-BirA* sequence was joined to the N-terminus of full length Abi3-S212F, also via a linker.*

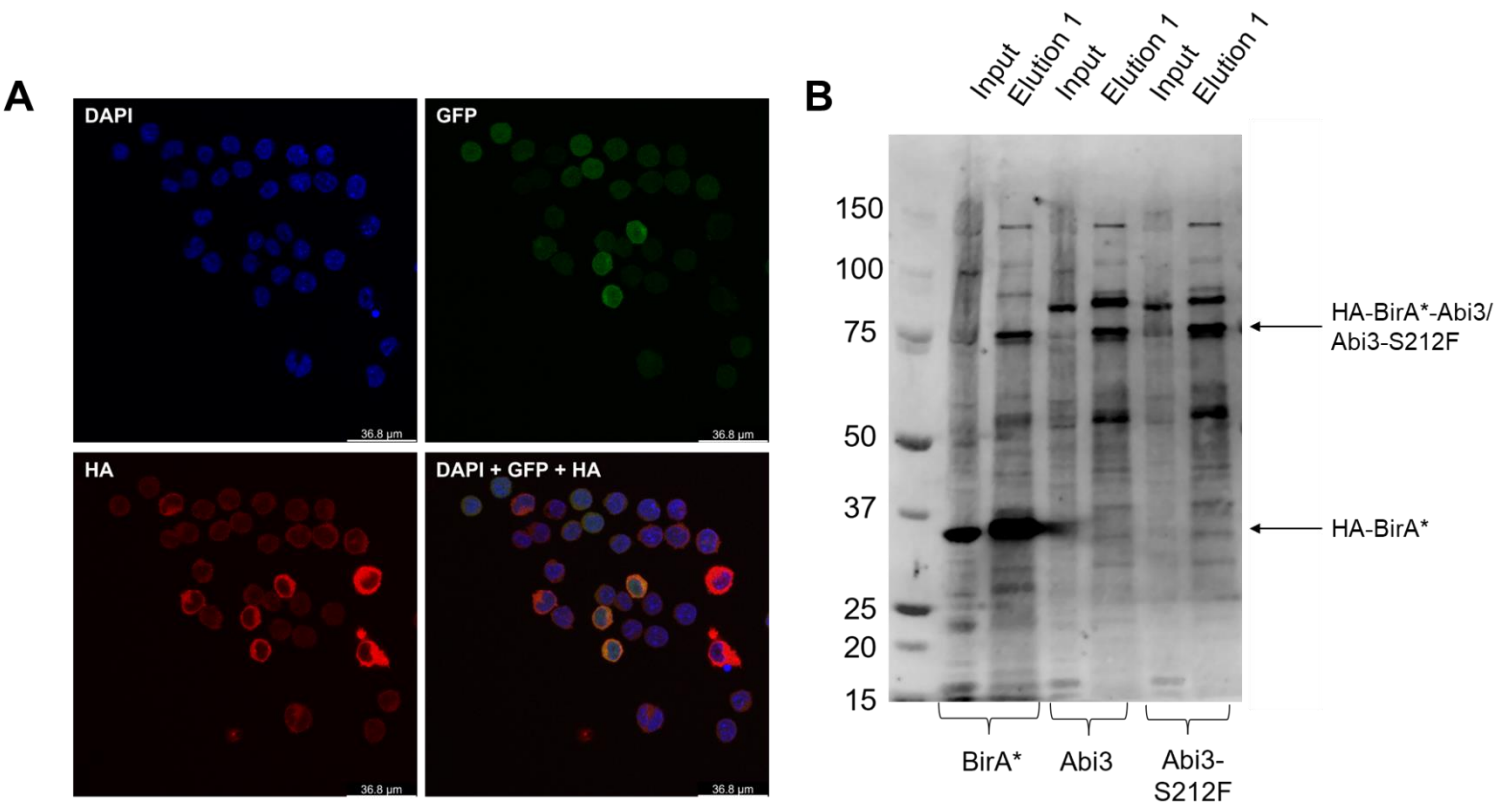

Figure 4.3 Characterisation of BV2 cells stably expressing HA-BirA*-Abi3-S212F A) *Immunocytochemistry confirms successful transduction of exogenous protein and cytoplasmic location of Abi3-S212F. The lack of correlation between GFP positive and HA positive cells is likely due to these genes being expressed under different promoters. Blue = DAPI, red = HA (Abi3-S212F), green = GFP.* ***B)*** *Streptavidin western blot shows successful expression of exogenous protein in BV2 cells and functioning of biotin ligase. Labelling of biotinylated proteins captured with BirA* control bait and Abi3 wild type bait for comparison.*

4.2.2 Biotin-Affinity Capture of the Abi3-S212F Interactome in BV2 Stable Cell Line

Protein interactors of Abi3-S212F were captured in BV2 cells expressing HA-BirA*-Abi3-S212F by streptavidin affinity chromatography. Cells were incubated with 50 µM biotin then lysed and incubated with streptavidin Dynabeads to capture biotinylated proteins. Non-biotinylated proteins were removed by washing the beads and remaining biotinylated proteins and denatured and eluted. Protein in the eluted samples were resolved by SDS-PAGE and detected by western blotting with

Streptavidin IR800 (Figure 4.4). Compared to the input (lane 1) the first elution (lane 3) showed higher fluorescence confirming enrichment of biotinylated proteins. Low fluorescence in the unbound protein sample (lane 2) indicated successful capture of biotinylated proteins during bead incubation. The second, third, and fourth elutions (lanes 4-6) also show low fluorescence confirming successful elution of biotinylated proteins from the beads. These results confirm expression of the HA-BirA*-Abi3-S212F, proper functioning of the biotin ligase, and successful capture of biotinylated proteins.

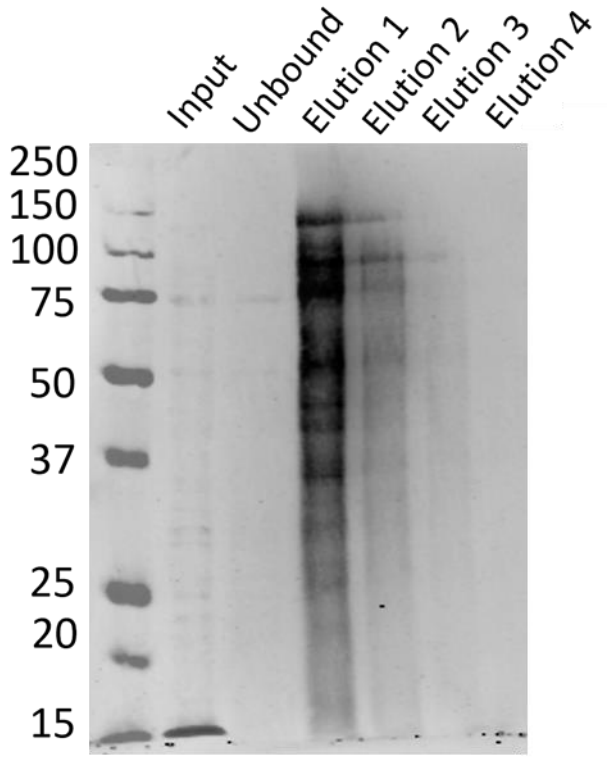

Figure 4.4 Biotin affinity capture of HA-BirA*-Abi3-S212F associated proteins. *Enrichment of protein in elution 1 compared to the input sample indicates higher concentration of biotinylated proteins in the elution. Low fluorescence in the unbound (lane 2) and subsequent elution samples (lanes 4-6) confirmed capture and elution of biotinylated proteins.*

4.2.3 Proteomic Analysis of Protein Interactome

Biotinylated proteins from elution 1 were run on a 4-12% polyacrylamide gel for 15 minutes (Figure 4.5). Proteins were visualised with GelCode™ Blue stain reagent and bands excised from the gel before being sent for MS analysis. These proteins were identified by MS at the Fingerprints Proteomics Facility at the University of Dundee. After trypsinisation and peptide separation by LC, the mass and charge

(m/z) of each peptide was determined by MS/MS allowing the sequence of each peptide to be assigned and mapped to individual proteins. Proteins in the original samples were identified by matching the peptide sequences to the Swiss-Prot protein database for *Mus musculus*. At least two unique peptide sequences were required to verify the identity of a protein.

The data generated from the control cell line (HA-BirA*, described in chapter 3) was

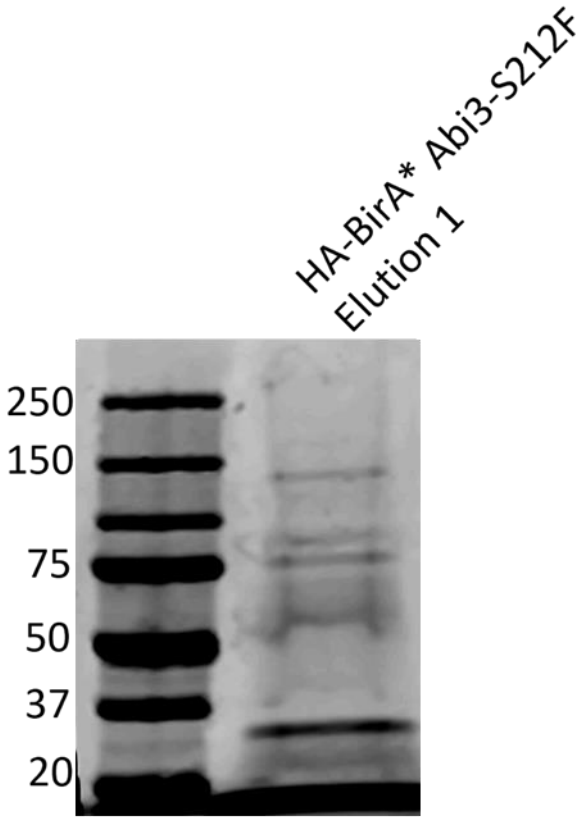

Figure 4.5 Separation of proteins for MS analysis. *A representative gel of proteins from elution 1 separated by SDS-PAGE. Proteins were run on the gel for 15 minutes and visualised with GelCode™ Blue stain reagent. HA-BirA*-Abi3-S212F lanes were individually excised from the gel and sent to the FingerPrints Proteomics Facility at the University of Dundee for MS analysis.*

used to create a list of background proteins. This list was used to determine putative interactors of Abi3-S212F by SAINTexpress. Five replicates were performed to increase the statistical power of identifying putative interactors, the reproducibility of which are assessed in Figure 4.6. A total of 891 proteins were identified in the Abi3-S212F data, 230 of which were present in all five replicates. 695 proteins captured in the HA-BirA*-Abi3-S212F cells were also present in the control data and 196 were unique to the Abi3-S212F data.

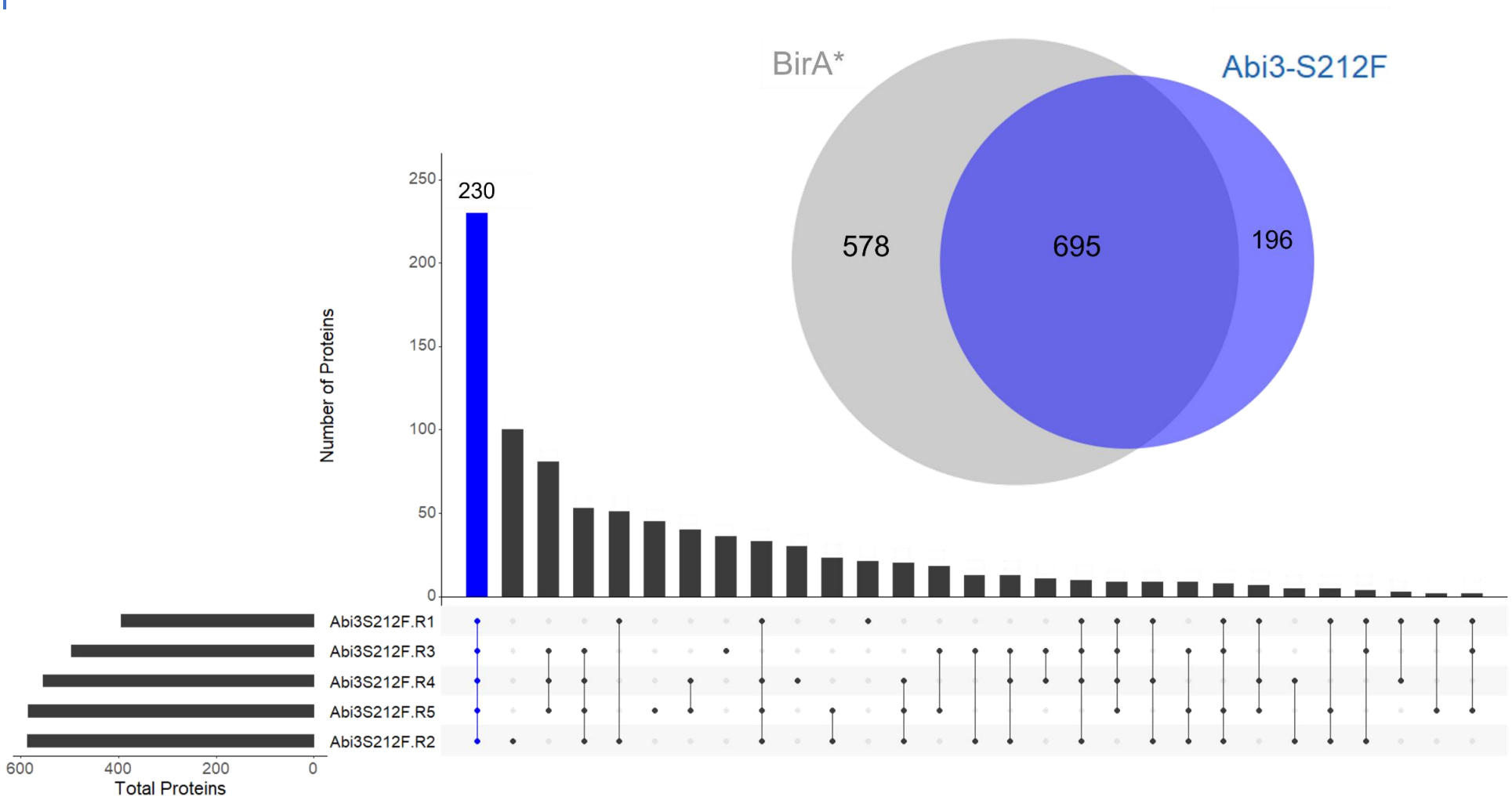

Figure 4.6 Reproducibility of BioID replicates. *Number of proteins identified in each replicate from the Abi3-S212F BioID data. Of the 891 proteins identified in the data, 230 proteins were found in all 5 replicates. The second dataset (Abi3-S212F.R2) contained the largest number of proteins of all the replicates, 100 of which were unique to this sample.* ***Inset)*** *Overlap of proteins between all BirA* control and Abi3-S212F data. In total 1,469 proteins were identified, 695 of which appeared in both the control and the Abi3-S212F datasets. 578 were unique to the control data and 196 were unique to the Abi3-S212F dataset. Blue bar represents the proteins identified in all replicates.*

4.2.3.1 SAINTexpress

Putative interactors were identified by SAINTexpress, as described in section 3.2.3.1 (Choi et al., 2011). Proteins determined to be putative interactors of Abi3-S212F were taken for GO, STRING, and POI analysis.

Of the 892 proteins identified by BioID, 21 were found to be putative interactors by SAINTexpress. These data were visualised by plotting the SAINT score for each protein captured against $\log_2$ of the fold change (Figure 4.7, Table 4.1). Putative interactors are shown in blue. The abundance of each protein is represented by the size of the bubble.

The peptide data for all identified putative interactors of Abi3-S212F can be found in Supplementary table 2.1 in appendix.

4.2.3.2 STRING Annotation

For all further analyses, protein IDs were converted to their human orthologues as there is more complete human data and PPIs are relatively well conserved between species (Sharan et al., 2005, Qian et al., 2011, Pérez-Bercoff et al., 2013).

Known interactions between proteins identified as putative interactors of Abi3-S212F were downloaded from the STRING database (v11.5; https://string-db.org/) (Szklarczyk et al., 2021). Physical interactions from high-throughput experiments and other existing databases were obtained from the STRING database using a medium confidence interaction score (0.4) (Figure 4.8).

Part of the WRC network was identified among the putative interactors of Abi3-S212F (WASF2, CYFIP1), as well as the tyrosine-protein kinase ABL2 (Abelson 2, also known as Abelson-related gene). The only other known interaction identified was between CEP170 and WDR62 (WD repeat-containing protein 62). No other previously determined interactions were found between the remaining putative interactors of Abi3-S212F identified by BioID

Table 4.1 Abi3-S212F-associated proteins prioritised by SAINTexpress. *The identified proteins were detected by MS of BioID samples from HA-BirA*-Abi3-S212F stable BV2 lines. Proteins which passed the significance threshold <0.05 BFDR after probabilistic scoring of protein-protein interaction by SAINTexpress are above the black line. SAINT determines putative interactors from non-specifically bound proteins by calculating the fold change between the data and a negative control affinity-purification sample. To be considered a putative interactor, the prey protein must appear in the Abi3-S212F dataset at a significantly higher level than in the BirA* control data. Proteins are sorted first by BFDR value (lowest to highest) then by fold change (highest to lowest). The bait protein is highlighted in bold. Title annotations: Spec: spectral counts for the bait-prey pair in each replicate. SpecSum: sum of spectral counts across all replicates. AvgSpec: mean spectral count. crtlCounts: spectral count in each negative control replicate. SaintScore: probability of being an interactor. FoldChange: average spectral count in test interaction divided by the average in controls. BFDR: Bayesian false discovery rate.*

#	Protein	Accession	Spec	SpecSum	AvgSpec	ctrlCounts	SaintScore	FoldChange	BFDR
1	Cyfip1	Q7TMB8	21|33|72|24|25	175	35	0|0|0|0|0	1	350	0
2	Mtss1	Q8R1S4	18|31|18|16|21	104	20.8	0|0|0|0|0	1	208	0
3	Arhgap12	Q8C0D4	4|12|8|5|9	38	7.6	0|0|0|0|0	1	76	0
4	Evi2b	Q8VD58	3|9|9|6|6	33	6.6	0|0|0|0|0	1	66	0
5	Pik3ap1	Q9EQ32	3|7|6|7|8	31	6.2	0|0|0|0|0	1	62	0
6	Wasf2	Q8BH43	46|54|30|38|35	203	40.6	2|0|2|0|0	1	50.75	0
7	**Abi3**	**Q8BYZ1**	**125|130|63|76|61**	**455**	**91**	**9|0|0|0|0**	**1**	**50.56**	**0**
8	Abl2	Q4JIM5	2|4|3|3|7	19	3.8	0|0|0|0|0	0.98	38	0

9	Mtmr1	Q9Z2C4	3|3|4|3|3	16	3.2	0|0|0|0|0	0.99	32	0
10	Tanc1	Q0VGY8	22|49|33|31|30	165	33	4|0|2|0|0	1	27.5	0
11	Cep170	Q6A065	167|214|139|131|120	771	154.2	20|4|12|5|4	1	17.13	0
12	Ruvbl2	Q9WTM5	18|26|20|20|16	100	20	7|0|0|4|0	0.95	9.09	0
13	Usp15	Q8R5H1	9|13|14|11|12	59	11.8	3|0|2|3|0	0.99	7.38	0
14	Glmn	Q8BZM1	3|2|2|2|2	11	2.2	0|0|0|0|0	0.93	22	0.01
15	Cbl	P22682	6|24|11|8|10	59	11.8	3|0|0|0|0	0.95	19.67	0.01
16	Eif4g2	Q62448	8|16|13|11|15	63	12.6	4|2|2|4|0	0.94	5.25	0.01
17	Dbt	P53395	4|7|21|18|14	64	12.8	4|0|0|2|0	0.83	10.67	0.02
18	Stat3	P42227	0|3|4|6|9	22	4.4	0|0|0|0|0	0.8	44	0.03
19	Wdr62	Q3U3T8	0|6|3|4|4	17	3.4	0|0|0|0|0	0.8	34	0.04
20	Arfgap1	Q9EPJ9	2|14|15|12|11	54	10.8	4|2|0|0|0	0.8	9	0.04
21	Ripk3	Q9QZL0	0|4|4|2|4	14	2.8	0|0|0|0|0	0.78	28	0.05
22	Cyld	Q80TQ2	0|4|3|2|5	14	2.8	0|0|0|0|0	0.78	28	0.06
23	Pcm1	Q9R0L6	4|7|2|2|0	15	3	0|0|0|0|0	0.77	30	0.07
24	Ccdc22	Q9JIG7	5|5|2|2|0	14	2.8	0|0|0|0|0	0.77	28	0.07

25	Zwint	Q9CQU5	3|5|2|2|0	12	2.4	0|0|0|0|0	0.76	24	0.08
26	Trio	Q0KL02	0|2|2|2|2	8	1.6	0|0|0|0|0	0.74	16	0.09
27	Gapvd1	Q6PAR5	2|10|3|4|4	23	4.6	2|0|0|0|0	0.76	11.5	0.09
28	Apbb1ip	Q8R5A3	7|4|2|6|5	24	4.8	3|0|0|0|0	0.73	8	0.1
29	Sorbs1	Q62417	5|7|6|5|5	28	5.6	3|0|2|0|0	0.72	5.6	0.11
30	Limd1	Q9QXD8	5|13|7|9|7	41	8.2	4|3|2|0|0	0.68	4.56	0.11

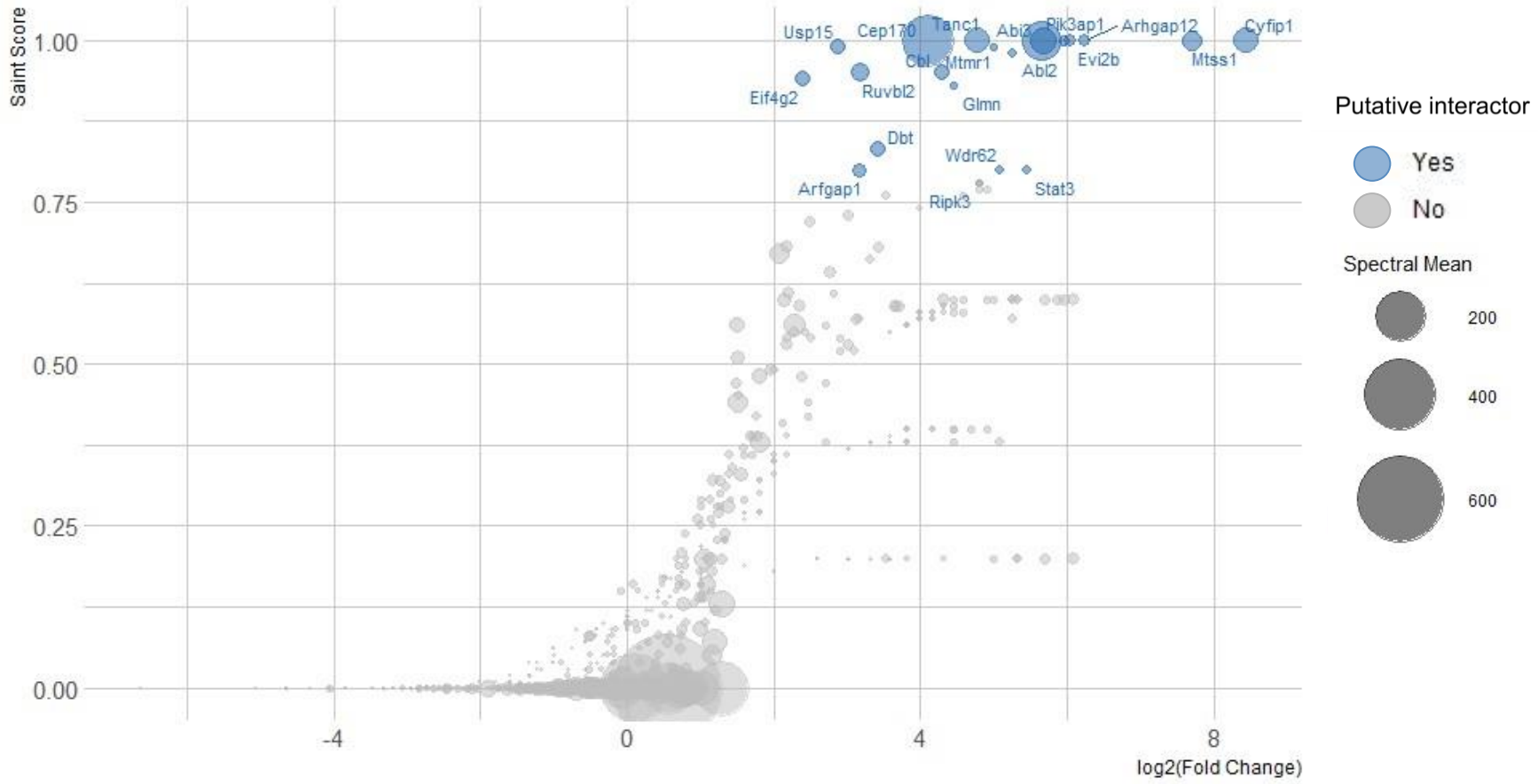

Figure 4.7 Fold change and SAINT score from SAINTexpress. *Proteins identified by MS in Abi3-S212F BioID samples. Data are represented as log_2 of the fold change (difference in protein count from control data) plotted against the SAINT score (probability of protein being a putative interactor). Each bubble on the plot denotes an individual protein. The size of the bubble represents the abundance of each protein in the data, calculated by the sum of the spectral counts. Proteins identified as being putative interactors of Abi3-S212F (<0.05 BFDR) are labelled. Blue = putative interactor, grey = non-interactor.*

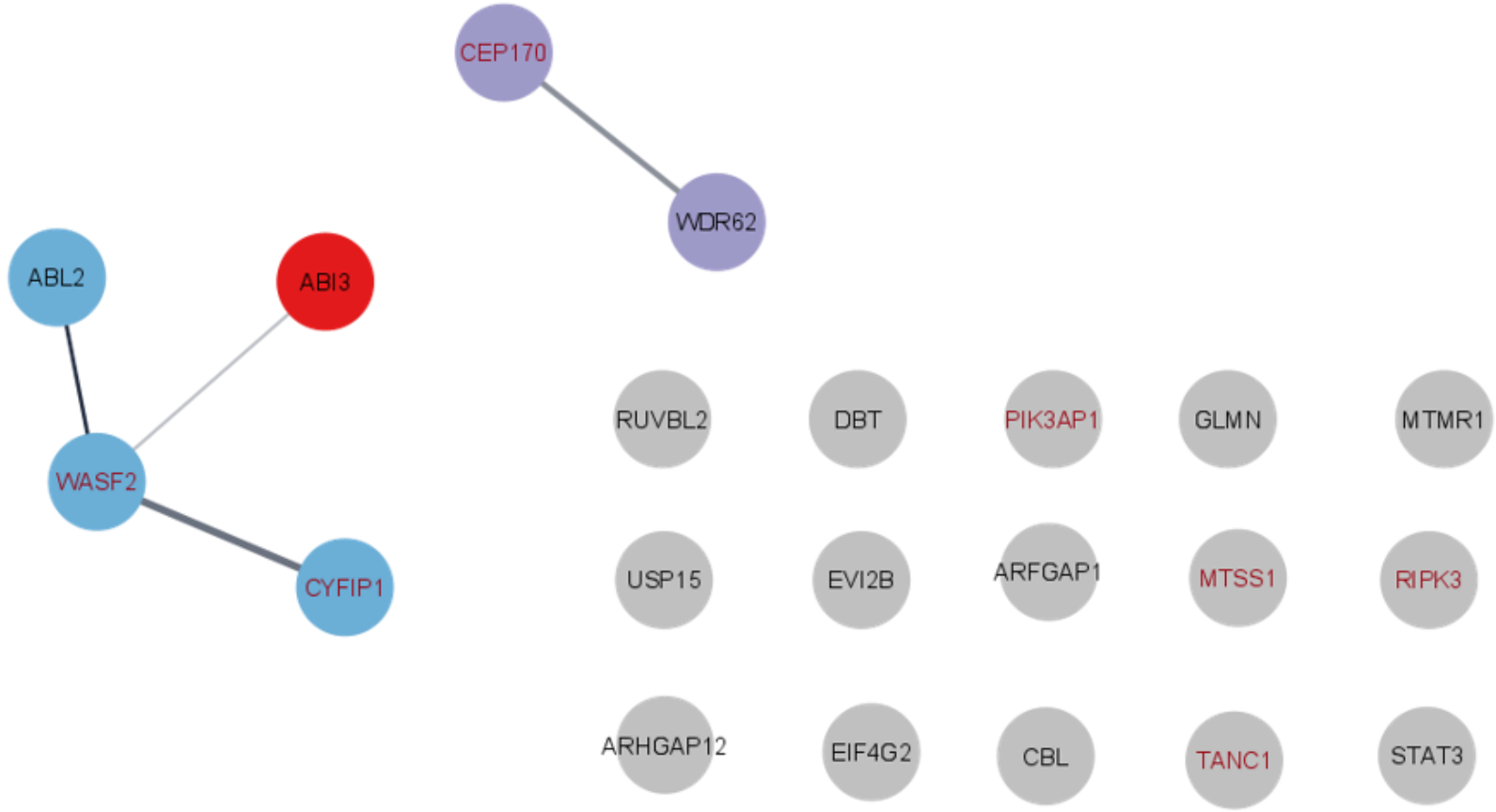

Figure 4.8 Protein-protein interaction network of Abi3-S212F-associated proteins. *Known interactions between the human orthologues of the high-confidence Abi3-S212F interactors obtained from the STRING v11.5 database. ABI3 is highlighted in red with known interacting network members in blue. A known interaction between CEP170 and WDR62 was identified (purple). Proteins with no known interactions within the set are marked in grey. Putative interactors of Abi3-S212F also identified as putative interactors of Abi3 in chapter 3 are labelled in red.*

4.2.4 Functional Annotation of Interactors

Metascape enrichment analysis (http://metascape.org) (Zhou et al., 2019) was used to functionally annotate the putative interactors of Abi3-S212F. The top process identified was the ABI3-WAVE2-CYFIP1 complex while many of the enriched functions related to cell motility and morphology (Figure 4.9, Table 4.2). Processes such as regulation of endocytosis and tyrosine kinase and guanosine triphosphate-ase (GTPase) signalling were also enriched among the functions of the putative interactors of Abi3-S212F.

Table 4.2 Summary of functional terms enriched in the list of genes encoding Abi3-S212F-associated proteins from Metascape. *All annotations are grouped into functional clusters with one representative enriched term presented. Count: number of genes with membership in identified gene ontology term. Percentage: percentage of genes with at least one annotation found in identified gene ontology term.*

Category	Description	Count	%
CORUM	ABI3-WAVE2-CYFIP1 complex	3	14.29
WikiPathways	Acute viral myocarditis	3	14.29
GO Biological Processes	regulation of small GTPase mediated signal transduction	4	19.05
Canonical Pathways	PID PDGFRB PATHWAY	3	14.29
GO Biological Processes	hemopoiesis	4	19.05
GO Biological Processes	regulation of T cell activation	3	14.29
GO Biological Processes	response to radiation	3	14.29
GO Biological Processes	morphogenesis of an epithelium	3	14.29

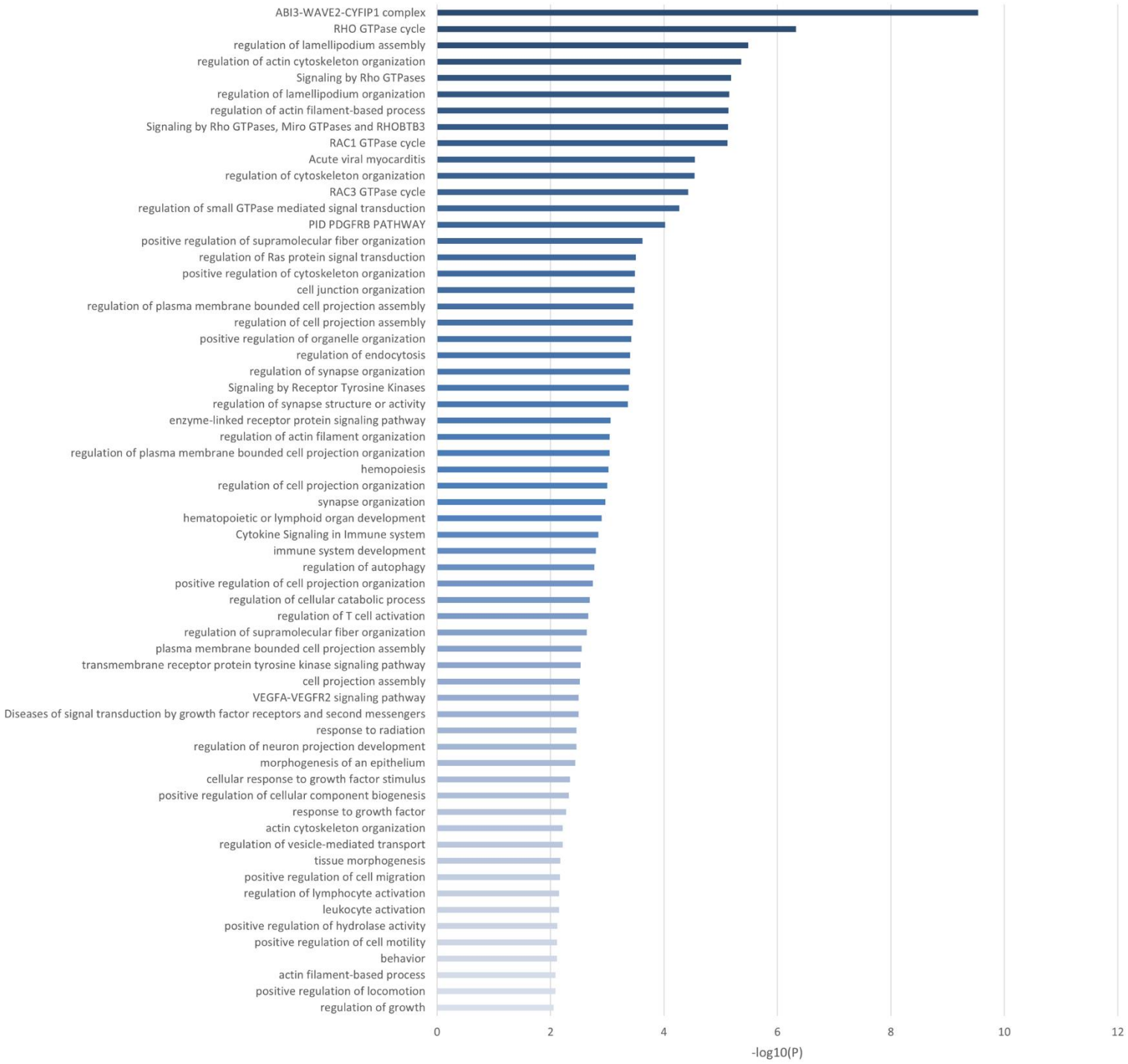

Figure 4.9 Biological process annotations for Abi3-S212F-associated proteins identified by BioID. *Enrichment analysis from Metascape was used to identity biological processes enriched in the human orthologues of the identified putative interactors of Abi3-S212F. The heatmap is coloured according to p-value and plotted with the -log$_{10}$(P) score.*

4.2.5 Proteins of Interest

The interactors detailed above are all novel interactors of Abi3-S212F as no data on the interactome of this Abi3 variant has previously been published. Protein interactors of Abi3, both confirmed in the literature replicated in this study (chapter 3), were also identified as putative interactors of Abi3-S212F. The majority of Abi3-S212F putative interactors were however found to be interactors of wild type Abi3. Comparison of these protein interactomes may elucidate mechanistic differences between the variants.

4.3 Discussion

The main aim of the experiments described in this chapter was to identify the protein interactome of the AD risk variant Abi3-S212F in BV2 cells using BioID and MS. As the exact molecular role of wild type Abi3 is not yet established, comparison of the interactome detailed here to the wild type Abi3 interactome (chapter 3) both strengthens evidence for the role of Abi3 in the WRC regulating actin polymerisation as well as potential novel roles discussed in section 3.3.1. Here, processes in which multiple putative interactors of Abi3-S212F are associated are discussed along with comparisons to the Abi3 interactome defined in chapter 3.

Of all the proteins captured from cells expressing either HA-BirA*-Abi3 or HA-BirA*-Abi3S212F, 748 were identified in both conditions. 372 were found only in HA-BirA*-Abi3 expressing cells and 144 were unique to HA-BirA*-Abi3S212F cells (Figure 4.10a). Of the proteins determined to be putative interactors, 7 were identified as putative interactors of both Abi3 and Abi3-S212F (Figure 4.10b).

4.3.1 Abi3-S212F Exists in Similar Pathways to Abi3

Seven of the putative interactors of Abi3 were also identified as putative interactors of Abi3-S212F (Figure 4.11). This suggests that Abi3-S212F participates in similar cell processes as wild type Abi3, although novel protein interactors for Abi3-S212F were also identified.

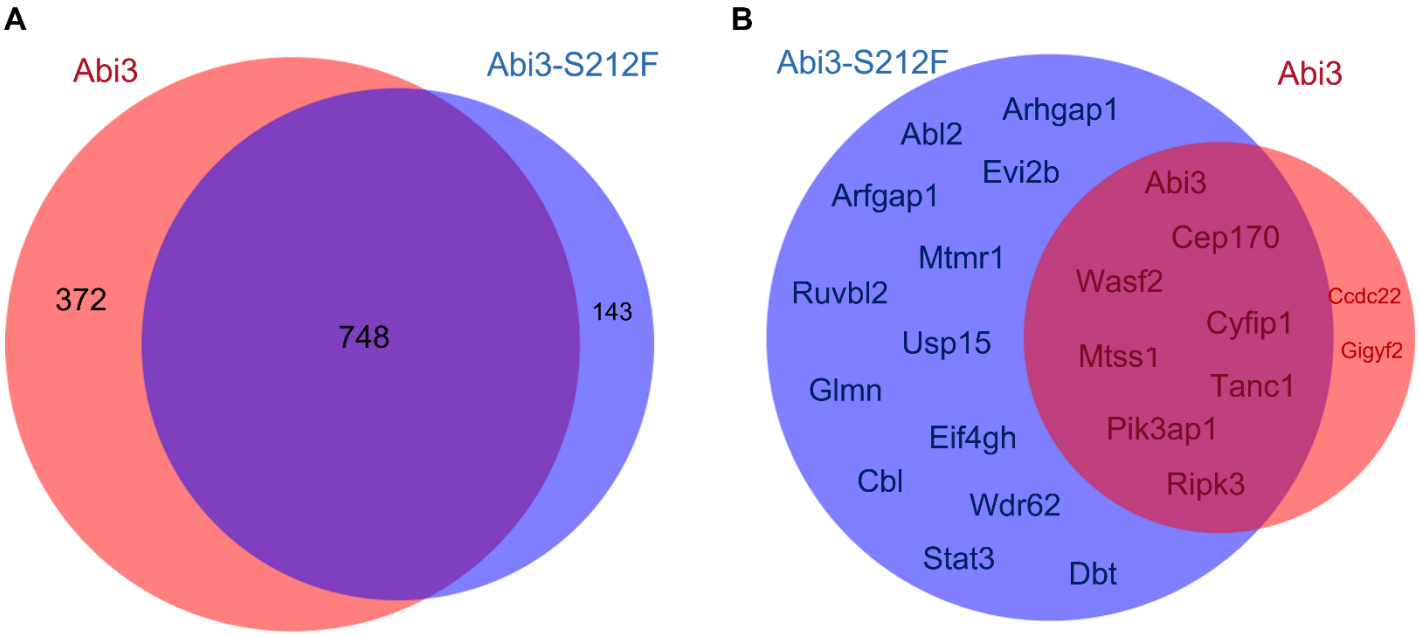

Figure 4.10 Overlap of proteins captured from Abi3 and Abi3-S212F expressing cells. ***A)*** *748 proteins were identified by MS in both HA-BirA*-Abi3 and HA-BirA*-Abi3-S212F expressing cells. 372 were unique preys of Abi3 and 144 were unique to Abi3-S212F.* ***B)*** *8 proteins were determined to be putative interactors of both HA-BirA*-Abi3 and HA-BirA*-Abi3-S212F by SAINTexpress. 2 proteins were determined to be putative interactors of Abi3 only and 12 were unique to Abi3-S212F.*

4.3.1.1 HA-BirA-Abi3-S212F Interacts with the WRC*

Among the putative interactors of Abi3-S212F identified by SAINTexpress was a network of proteins involved in the WRC (Cyfip1, Wasf2, Abi3). The ABI3-WAVE2-CYFIP1 complex was also the top process enriched for this list of proteins using the Metascape enrichment analysis. WASF2 and CYFIP proteins are known interactors of ABI3 within the WRC, and the data presented herein suggests that they also interact with Abi3-S212F.

4.3.1.2 HA-BirA-Abi3-S212F May Interact with Other Cytoskeleton Associated Proteins*

Mtss1, Abl2, Cep170, and Wdr62 have roles regulating the cytoskeleton. As discussed in section 3.3.1.2, Cep170 is a centrosomal protein responsible for organising microtubules while Mtss1 regulates the actin cytoskeleton via Arp2/3 independently of the WRC.

Abl2 is a tyrosine kinase essential for the stability of actin structures. The protein contains two filamentous actin binding domains and Abl2 deficiency impairs the formation of lamellipodia (Bradley and Koleske, 2009). Phosphorylation of cortactin by Abl2 is a key mechanism in actin regulation. Cortactin is enriched within lamellipodia and activates the Arp2/3 complex, causing branching of actin filaments (Wang et al., 2015a, Weaver et al., 2001). As Abl2 is a putative interactor of Abi3-S212F but not Abi3, the variant may contribute to AD risk by disrupting the normal function of Abl2 and thereby impacting lamellipodia formation and cell motility and morphology independent of the WRC.

Wdr62 is a microtubule-associated protein which regulates centriole duplication, glial cell development, and spindle assembly. Wdr62 interacts with Cep170 during spindle assembly and Wdr62 knockout results in downregulation of Cep170, impacting spindle organisation (Zhang et al., 2019a, Qin et al., 2019, Zhi et al., 2021). The identification of Cep170 as a putative interactor of both Abi3 and Abi3-S212F supports a novel role of Abi3 in microtubule and spindle regulation, however verification of physical interaction between these two is required. The detection of Wdr62 as a putative interactor of Abi3-S212F only could suggest that interaction with Wdr62 can only occur with the variant, for example if the amino acid substitution produces a confirmational change exposing sites in the protein structure able to bind Wdr62. Alternatively, it is possible that Wdr62 was captured at higher levels with expression of the HA-BirA*-Abi3-S212F bait if interaction between Abi3-S212F and Cep170 was stronger or more frequent than between Abi3 and Cep170. Interestingly, Wdr62 was identified as a potential interactor of HA-BirA*-Abi3 but was fell below the statistical criterion (fold change: 42, BFDR: 0.2) for putative interactors. Abi3 may form a physical interaction with Cep170 as part of a Cep170-Wdr62 complex, but not with Wdr62 itself. This may explain higher levels of biotinylation and therefore capture of Wdr62 compared to the BirA* control. A stronger interaction between Abi3-S212F and Cep170 may also explain the increase in biotinylation and capture of Wdr62 in these cells compared to HA-BirA*-Abi3 cells. Investigation of physical interactions between Abi3/Abi3-S212F and Cep170 and Wdr62 may elucidate the mechanism of the potential role of Abi3 in spindle assembly.

4.3.1.3 HA-BirA-Abi3-S212F May Interact in Inflammatory Signalling Pathways*

Microglia are key cellular regulators of inflammatory responses within the brain and neuroinflammation has been implicated in AD pathology (see section 1.2.2 for further discussion). Two proteins, Pik3ap1 and Stat3, involved in the inflammatory response were identified as putative interactors of Abi3-S212F.

Pik3ap1, also identified as a putative interactor of Abi3, links Toll-like receptor signalling to Pi3k activation and prevents excessive inflammatory cytokine production. Higher spectral counts for Pik3ap1 were found in Abi3-S212F expressing cells compared with Abi3 expressing cells but this was not determined to be statistically significant.

Signal transducer and activator of transcription 3 (Stat3) is a regulator of the immune response that was also identified as a putative interactor of Abi3-S212F. Stat3 was initially studied as a transcription factor but was later discovered to have roles in pathways regulating immune processes (Hillmer et al., 2016). In microglia, STAT3 has been found to mediate cell activation, proinflammatory processes, and upregulate proinflammatory genes (Przanowski et al., 2014, Huang et al., 2008, Chen et al., 2017b). Given the cytoplasmic location of Abi3 in BV2 cells, a physical association between Abi3-S212F and Stat3 in microglia is more likely to be involved in inflammatory signalling rather than transcription regulation.

4.3.1.4 p.S212F May Cause Increased Association of Abi3 with the WRC

Abi3 has previously been identified as a component of the WRC, and data presented in chapter 3 provides evidence of Abi3 interaction with known WRC proteins in BV2 cells. These proteins were also identified as putative interactors of Abi3-S212F but at an apparently increased level of abundance when spectral counts for each protein were compared. Spectral counts for each protein were normalised to the spectral count of the bait protein (Abi3 and Abi3-S212F) to account for differences in expression level of the bait protein and capture of biotinylated proteins. Normalised average spectral counts were compared and levels of both Wasf2 and Cyfip1 captured in Abi3-S212F cells were significantly higher than those from cells expressing Abi3 (Mann-Whitney U test, $p<0.05$; Figure 4.11). Apparent increases in abundance of Wasf2 and Cyfip1 may have occurred if higher levels of these proteins were proximal to HA-BirA*-Abi3-S212F compared to HA-BirA*-Abi3. The most likely

explanation for this is that Abi3-S212F forms a tighter association with the WRC than wild type Abi3.

These data may be explained by the phosphorylation state of Abi3. It is thought that the non-phosphorylated form of Abi3 is incorporated into the WRC and phosphorylation by PKB at residue S342 results in an inactive form of Abi3 (Moraes et al., 2017). ABI3-S209F is predicted to disrupt phosphorylation, with some evidence showing a lack of phosphorylated ABI3 in cells transfected with ABI3-S209F (Ibanez et al., 2022, Turner et al., 2022). WRC activation in microglia expressing this variant would be lower than cells expressing wild type Abi3 and may therefore show reduced Arp2/3 activation and actin filament branching (Figure 4.12). Branched actin filaments form lamellipodia, thin cytoplasmic sheets at the leading-edge of the plasma membrane are thought to be the main driver of microglial movement. From lamellipodia, parallel actin filament structures known as filopodia form which contribute to cell-to-cell signalling, environment sensing, and extra-cellular matrix adhesion (Franco-Bocanegra et al., 2019). As the expression of Abi3-S212F may reduce actin branching by outcompeting other Abi paralogues the formation of lamellipodia is likely to be disrupted, thereby impairing microglial migration. Filopodia however would not be affected as parallel actin structures can still form through actin polymerisation.

Based on the data presented herein, the proposed reduction in WRC activation may be a mechanism of AD risk conferred by Abi3-S212F. A non-phosphorylated Abi3 variant would outcompete other Abi paralogues for incorporation into the WRC, reducing Arp2/3 activation, actin branching, and lamellipodia formation resulting in less motile microglia (Franco-Bocanegra et al., 2019). Migration of microglia to Aβ plaques could therefore be negatively affected.

Activation of Arp2/3 by the WRC is also required for morphological changes associated with phagocytosis through actin nucleation (Kim et al., 2018). Reduction of WRC activity by incorporation of Abi3 may therefore also reduce the ability of microglia to phagocytose Aβ plaques and apoptotic neurons. The presence of a variant of Abi3 that leads to hypo-phosphorylation of Abi3 may therefore influence risk for AD by disrupting both microglial motility and morphological dynamics.

4.3.1.5 p.S212F May Cause Increased Association of Abi3 with Cep170

The amount of Cep170 captured and identified in Abi3-S212F expressing BV2 cells was significantly higher compared to the levels of Cep170 captured in Abi3 expressing cells (Figure 4.11). This suggests a stronger or more frequent interaction of Abi3-S212F with Cep170 compared to Abi3. As Cep170 is known to organise microtubules in centrioles and play key roles in spindle organisation during mitosis, it is possible that Abi3 influences this pathway via interaction with Cep170.

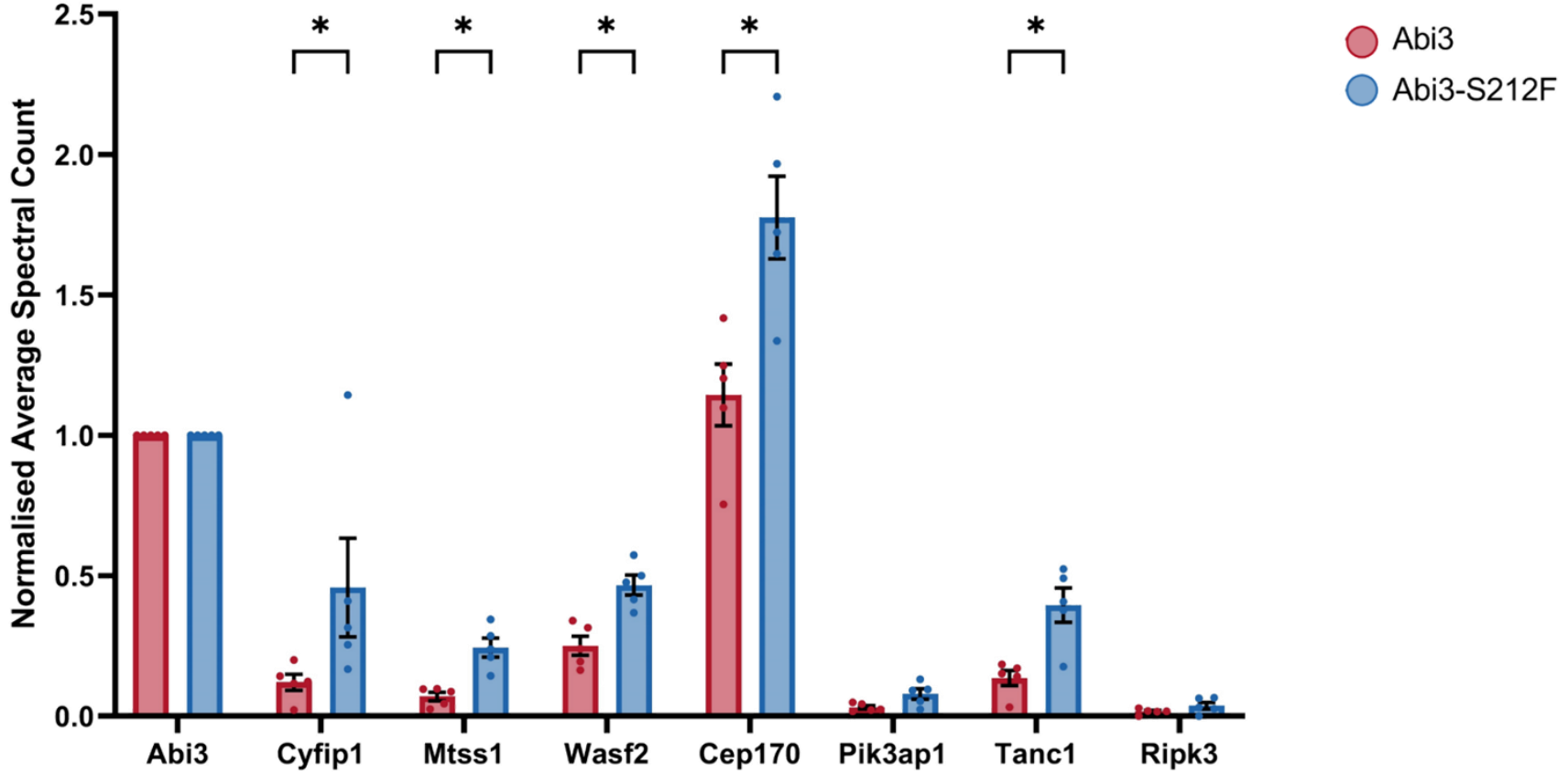

Figure 4.11 Relative abundance of putative interactors of both Abi3 and Abi3-S212F. *Average spectral counts of each putative interactor were normalised to the average spectral count of the bait protein (Abi3 and Abi3-S212F) to account for differences in expression levels and capture of biotinylated proteins. Cyfip1, Mtss1, Wasf2, Cep170, and Tanc1 were found to be significantly more abundant in samples from Abi3-S212F expressing cells compared to Abi3 cells (Mann Whitney U Test, p<0.05). Red bars represent normalised average spectral count of putative interactor from HA-BirA*-Abi3 expressing cells. Normalised spectral counts of putative interactor from each replicate are represented by red dots. Blue bars represent normalised average spectral count of putative interactor from HA-BirA*-Abi3-S212F expressing cells. Normalised spectral counts of putative interactor from each replicate are represented by blue dots. Error bars = standard error of the mean.*

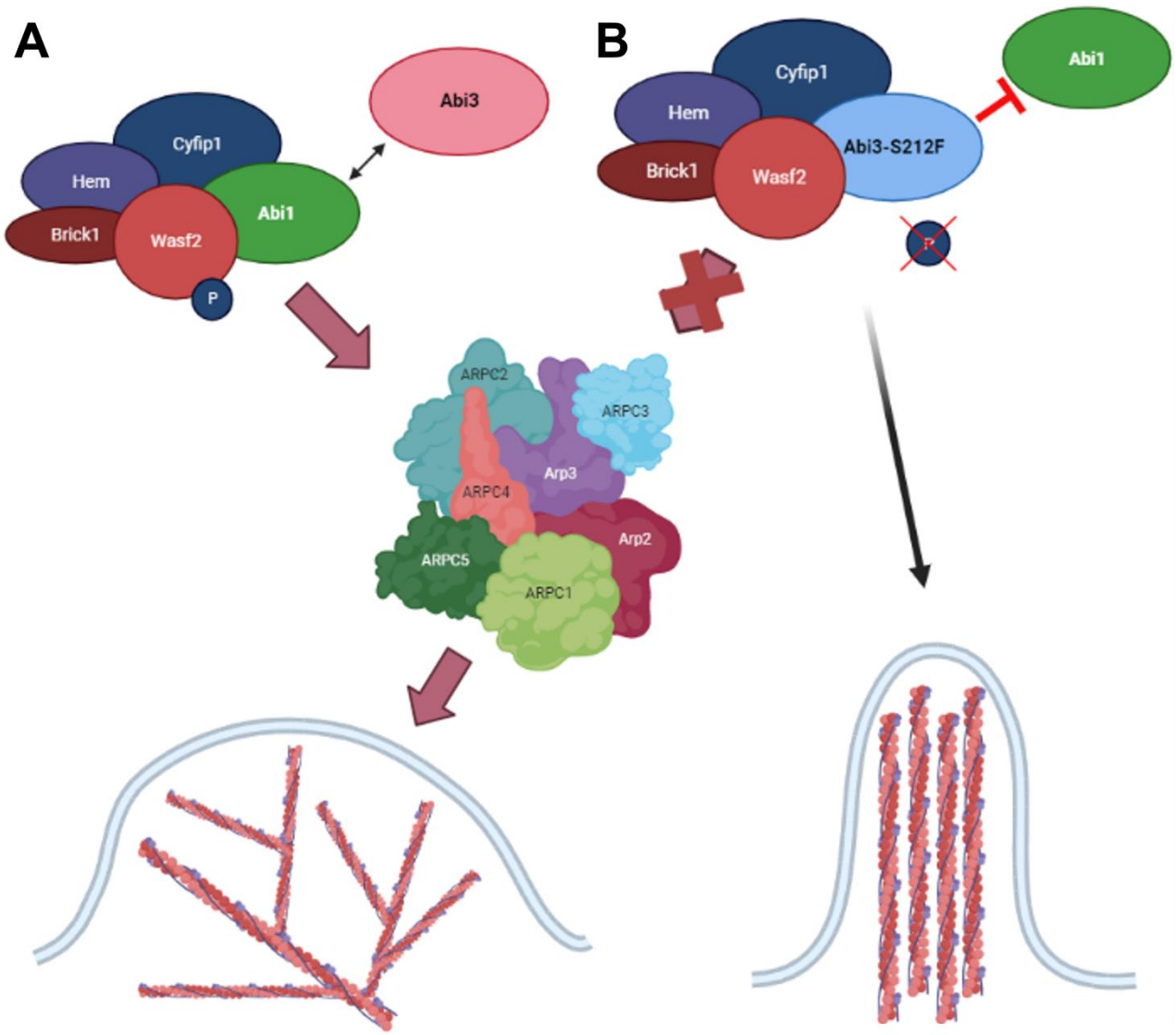

Figure 4.12 Proposed model of Abi3-S212F function in microglia. ***A)*** *In cells expressing wild type Abi3, Abi1 and Abi3 can compete for interaction with the WRC. When Abi1 is part of the complex, phosphorylation of Wasf2 occurs causing the translocations of the WRC to the plasma membrane where it activates the Arp2/3 complex. Arp2/3 mediates the nucleation of actin filaments resulting in branched actin structures. These structures cause lamellipodia to form, the main drivers of microglial movement. When Abi3 is part of the WRC, Wasf2 is not phosphorylated and so the Arp2/3 complex is not activated. Actin filaments are then free to form parallel structures resulting in filopodia formation, structures key to the environmental scanning roles of microglia.* ***B)*** *In cells expressing Abi3-S212F, tighter associations form between Abi3-S212F and Wasf2/Cyfip1. This may cause Abi3-S212F to out compete Abi1 for interaction with the WRC, resulting in an inhibition of Wasf2 phosphorylation leading to less actin nucleation mediated by the Arp2/3 complex and an increase in filopodia formation. Figure created in BioRender.*

4.3.2 p.S212F Results in Gain of Interactions

The most obvious difference between the protein interactomes of Abi3 and Abi3-S212F was the greater number of putative interactors of Abi3-S212F. 13 proteins were identified as putative interactors of Abi3-S212F only. Proteins within the ubiquitin system, regulators of Rho GTPases, the cytoskeleton, and immune responses were associated with Abi3-S212F but not Abi3. The effect of these gains of interaction remains to be determined empirically, along with validation of direct interaction. Both gains and losses of interaction may be due to variability between biological replicates and so confirming direct interaction, or lack thereof, is required. Defining the differences in microglial phenotypes due to expression of Abi3-S212F may also highlight which specific pathways are likely to be altered and this interactome can then be used to identify specific proteins for further investigation.

4.3.2.1 HA-BirA-Abi3-S212F May Interact with the Ubiquitin System*

The ubiquitin system is responsible for protein degradation and plays critical roles in signal transduction, immune response, and cell development and death. Ubiquitin ligases are responsible for the addition of ubiquitin to lysine residues of proteins and deubiquitinases (DUB) remove ubiquitin from proteins. HA-BirA*-Abi3-S212F was found to potentially interact with the E3 ubiquitin-protein ligase Casitias B-lineage lymphoma (Cbl), the DUB Usp15, and the ubiquitin ligase inhibitor glomulin (Glmn). Abi3-S212F appears to interact with proteins involved in both the addition and removal of ubiquitin from proteins. Both ubiquitination and de-ubiquitination are important processes in the degradation of proteins by the proteosome, with ubiquitination resulting in aggregation of proteins and de-ubiquitination removing the ubiquitin tag for recycling. The identification of these proteins as putative interactors of Abi3-S212F but not Abi3 may reflect greater degradation of Abi3-S212F, possibly as a protective mechanism.

4.3.2.2 HA-BirA-Abi3-S212F May Interact with Rho GTPase Regulators*

Finally, the Rho GTPase-activating protein Arhgap12 was determined to be a putative interactor of Abi3-S212F. This protein negatively regulates Rac1 signalling by increasing GTP hydrolysis, resulting in inactive GDP-bound GTPases (Gentile et al., 2008). Rac1 is known to bind and activate the WRC and was identified as a central protein in a protein domain network associated with AD (Chen et al., 2017a,

Kikuchi et al., 2020). An interaction with Abi3-S212F may disrupt Arhgap12 function, affecting regulation of the WRC and the ability of microglia to control the actin cytoskeleton. A decrease in Arhgap12 function would likely result in increased activation of the WRC due to a reduction in GDP-bound Rac1. Conversely, if Abi3-S212F interaction increases Arhgap12 activity, this may be an additional pathway by which this variant reduces WRC activation, contributing to less motile microglia.

4.3.3 p.S212F Results in Loss of Interactions

The p.S212F substitution in Abi3 may have resulted in the loss of two interactors, Gigyf2 and Ccdc22, with Abi3. Gigyf2, a repressor of protein translation, and Ccdc22, an NF-κB and endosomal sorting regulator, were both identified by MS in samples from Abi3 and Abi3-S212F expressing cells but were determined to be putative interactors of Abi3 only. If these proteins are validated as direct or indirect interactors of Abi3, this suggests that the p.S212F substitution may prevent Abi3 associating with these proteins.

Gigyf2 inhibits protein translation to prevent the translation of defective mRNAs (Hickey et al., 2020). If loss of Abi3 interaction reduces the function of Gigyf2 there may be a disruption of ribosomal quality control in protein synthesis. Alternatively, if loss of Abi3 interaction causes an increase in Gigyf2-mediated translation repression then this mechanism may become overactive, reducing overall protein synthesis.

Ccdc22 forms part of the CCC complex, which has roles in both NF-κB signalling and endosomal sorting. A possible interaction between Abi3 and the CCC complex implicates a role for Abi3 in these pathways, disruption to which may contribute to the increased AD risk of Abi3-S212F. Proinflammatory signals may be dysregulated if Abi3/CCC interaction impacts the inhibition of IκB proteins. Disruption of this interaction may also impact protein trafficking/recycling if Abi3 influences the role of the CCC complex in mediating endosome localisation.

4.3.3 Limitations

As discussed in section 3.3.2, the same limitations of the BioID method apply to the data discussed in this chapter. In particular, the lack of validation of physical interaction means these novel protein interactors cannot be definitively confirmed. However, the capture of known Abi3 interactors, both confirmed in the literature and identified in chapter 3, highlights the reliability of BioID in revealing interactors of the

bait protein. Even so, evidence of physical interaction is a key to identifying direct protein interactors of Abi3 and Abi3-S212F.

The mechanism of AD risk conferred by Abi3-S212F was investigated by comparison of the wild type and variant interactomes. The difference between the normalised average spectral count of the putative interactors between the cell lines was assessed as a proxy for changes in interaction between the bait and prey proteins. The spectral count is a label-free quantification technique to estimate the abundance of proteins in a sample from the frequency of all peptides corresponding to the matched protein. The more abundant the protein, the more peptides are available for sequencing post-trypsinisation and therefore a higher spectral count. A positive linear correlation has been shown between spectral count and protein abundance (Liu et al., 2004, Old et al., 2005). However, longer proteins are more likely to have a higher number of tryptic peptides. The spectral counts were therefore normalised to protein length (known as the normalised spectral abundance factor) by SAINTexpress to account for this. One of the limitations of using spectral counts as a measure of protein abundance is this creates a bias against low-abundance proteins (average spectral count <5) due to a larger variation in the spectral counts (Zhou et al., 2010). This results in underestimating true protein levels which may introduce biases into the data. Differences in protein abundance also does not necessarily equate to changes in affinity of protein interaction. Protein binding assays are required to confirm if Abi3-S212F does indeed form tighter associations with protein interactors than Abi3.

Finally, the variance between the biological replicates is not assessed. The reproducibility of the technical replicates (n=5, Abi3: Figure 3.8, Abi3-S212F: Figure 4.6) increases the confidence of determining which proteins are putative interactors of the bait protein. Whether the differences identified between the interactomes of Abi3 and Abi3-S212F are solely due to the genotype or vary between the biological replicates remains unknown. To fully repeat these experiments was not viable within the scope of this thesis.

4.3.4 Conclusions

The data presented herein suggest a putative protein interactome for Abi3-S212F. In total, 21 proteins were identified as putative interactors. Comparison to the identified wild type Abi3 protein interactors shows that these proteins have different

interactomes though both have functional roles within the WRC. Both proteins were found to interact in the WRC, strengthening evidence for the role of Abi3 in actin organisation as well as the ability of BioID to reliably capture protein interactors. Novel interactors were also identified, suggesting that Abi3-S212F influences many more pathways than its wild-type counterpart, which may contribute to the mechanism of AD risk. Validation of physical interaction is required to present a definitive protein interactome of Abi3-S212F, but the data presented here can be used as a foundation to refine the interactome and to focus research on likely pathological pathways associated with increased risk of AD.

Chapter 5 – Investigation of the Trem2 Protein Interactome

5.1 Introduction

5.1.1 Trem2

Variants of *TREM2* are associated with an increased risk of AD although the mechanism of this risk for some identified variants is unknown (see section 1.3.4.2) The *Trem2* gene encodes the protein Trem2 (Daws et al., 2001). Trem2 is expressed in cells of the myeloid lineage and was first described in dendritic cells (Bouchon et al., 2000, Daws et al., 2001). Since then, the protein has also been found in other myeloid cells including monocytes, macrophages, and osteoclasts (Paloneva et al., 2003, Klesney-Tait et al., 2006, Turnbull et al., 2006). Within the brain Trem2 is expressed primarily in microglia (Figure 5.1a) (Schmid et al., 2002, Sessa et al., 2004, Jolly et al., 2019).

Intracellularly, Trem2 is found in two pools: the Golgi complex and exocytic vesicles. Stimulation of microglia with ionomycin induces translocation of TREM2 from these intracellular pools to the plasma membrane via retromer-mediated protein trafficking (Sessa et al., 2004, Prada et al., 2006, Yin et al., 2016). Ionomycin stimulates similar activation pathways to LPS in microglia by increasing intracellular calcium concentrations but does not induce release of nitric oxide (NO) or cytokines, indicating TREM2 activation in response to bacterial infection (Hoffmann et al., 2003). TREM2 expression is also regulated by TLRs, CD33, and micro-RNAs (Bhattacharjee et al., 2016, Chan et al., 2015, Ford and McVicar, 2009, Han et al., 2017).Ligands of Trem2 were first identified in a mouse lymphoma cell line and include bacterial components such as LPS, as well as nucleic acids, ApoE, anionic phospholipids, and Aβ (Wang et al., 2015b, Kawabori et al., 2015, Atagi et al., 2015, Jendresen et al., 2017, Daws et al., 2003). Upon ligand binding, Dap12 is recruited to Trem2, stimulating intracellular signalling pathways (Call et al., 2010, Lanier et al., 1998) (see section 1.3.4.1). As the protein interactome of Trem2 has not been systematically explored, it is possible there are other extracellular ligands and intracellular proteins that interact with Trem2.

The pathological effect of many rare *TREM2* coding variants is currently unknown, but TREM2-R47H has been one of the most widely studied. The SNP causes an

amino acid substitution in the extracellular domain of TREM2 which has been shown to negatively affect the receptor's ability to bind APOE as well as altering glycosylation in the TGN and endoplasmic reticulum (Atagi et al., 2015, Bailey et al., 2015, Park et al., 2016). The R62H and D87N variants have also been shown to reduce APOE binding as well as impair uptake of Aβ-lipid complexes (Yeh et al., 2016). APOE triggers TREM2-mediated phagocytosis of apoptotic neurons tagged with APOE (Atagi et al., 2015).Protein aggregates, including Aβ plaques are also coated with APOE therefore these variants may increase AD risk by reducing microglia's ability to clear both cellular debris and Aβ plaques (Liao et al., 2015).

TREM2 is recycled from the plasma membrane by internalisation via clathrin-mediated endocytosis and trafficked to the TGN by VSP35 in the retromer complex. Reduction in Vsp35 was shown to increase accumulation of Trem2 in lysosomes, leading to a reduction in proinflammatory responses (Yin et al., 2016). This interaction is likely to occur at the retromer recruitment motif in the intracellular region of Trem2. Disruption of this region may affect the interaction of TREM2 and endocytic proteins, possibly leading to reduced expression of Trem2 through impaired receptor recycling. The retromer complex is regulated by proteins such as

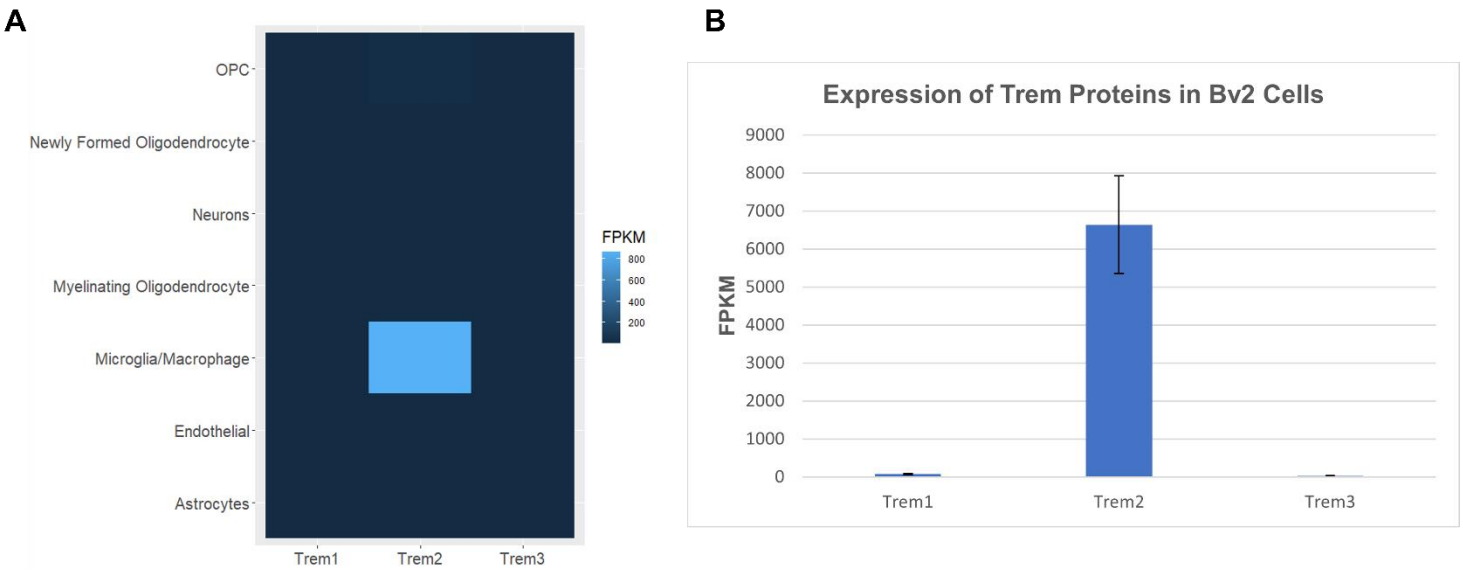

Figure 5.1 Expression of Trem2 proteins in neural and glial cell types. A) *Heat map of RNA sequencing data from Zhang et al. (2014b) showing relative expression of Trem proteins in different neural cell types. Trem2 is almost exclusively expressed in microglia/macrophages compared to other cell types as well as to Trem1 and Trem3.* ***B)*** *RNA sequencing data from Carrillo-Jimenez et al. (2019) confirms expression of Trem2 in BV2 cells.*

beclin 1, an autophagy protein, reduction of which was found to impair phagocytosis via disruption to receptor recycling mechanisms (Lucin et al., 2013). Determining intracellular interactors of TREM2 throughout its lifecycle is therefore vital to understand the role of TREM2 in microglia.

As previously discussed in section 1.2.3, BV2 cells are a suitable *in vitro* microglial model. RNA sequencing confirms endogenous expression of Trem2 in this cell line, making them suitable for investigating the protein interactome of Trem2 (Figure 5.1b) (Carrillo-Jimenez et al., 2019).

The proximity labelling method BioID was used to determine the protein interactome of Trem2 in BV2 cells (see section 1.4.1 for explanation of BioID). A major advantage of BioID over AP-MS is its suitability for investigating PPIs involving membrane proteins. During cell or tissue lysis, plasma membranes are, by necessity, disrupted by detergent treatment along with protein complexes formed at the membrane. By labelling interactors during cell culture, disruption of protein complexes does not hinder capture of prey proteins. Covalent interactions between biotin and lysine residues ensures that biotinylation of proteins is stable throughout lysis and subsequent washes. BioID is therefore more suited to the investigation of protein interactors of plasma membrane proteins such as Trem2 than other affinity purification methods which rely on detergent extraction methods that are known to destroy PPIs for plasma membrane-associated proteins.

5.1.2 Aims

The aim of the work described in this chapter was to define the intracellular protein interactome of Trem2 in BV2 cells. Two stable cell lines expressing the fusion proteins HA-BirA* and Trem2-BirA*-HA were generated and validated by immunocytochemical and western blot analysis to confirm expression and localisation of exogenously expressed proteins. Proximal proteins were identified by MS and filtered to identify putativeTrem2 interactors.

5.2 Results

5.2.1 Generation and Validation of BV2 Cells Stably Expressing Trem2-BirA*-HA

Generation of the control cell line stably expressing the fusion protein HA-BirA* is described in section 3.2.1. The same lentivirus plasmid backbone was used to generate the Trem2-BirA*-HA cell line. The fusion protein sequence and puromycin resistance gene were expressed under the control of the mPGK promoter, joined by an IRES-containing linker, while GFP was expressed under the control of the CMV promoter (Figure 5.2). The full DNA sequence encoding the Trem2 fusion protein can be found in appendix 3.

Expression and localisation of the fusion proteins for both the Trem2 and control cell lines were validated by immunocytochemical staining of the protein containing the HA epitope tag (Figure 5.3b). The BirA* control cell line showed cytoplasmic labelling, similar to results generated from this line in chapter 3 (section 3.2.1) In the Trem2 stable cell line, HA seemed to be concentrated both at the plasma membrane and in a perinuclear pool. This distribution suggests that the Trem2-BirA*-HA protein may be located both at the cell surface as well as in and around the Golgi complex within intracellular vesicles, though higher power imaging co-localisation with a range of intracellular markers, including the Golgi complex, would be needed to confirm this (Prada et al., 2006). Again, there was a lack of correlation between GFP positive and HA-expressing cells as these genes were expressed under different promoters, with the fusion protein gene expressed under the same promoter as the puromycin resistance gene.

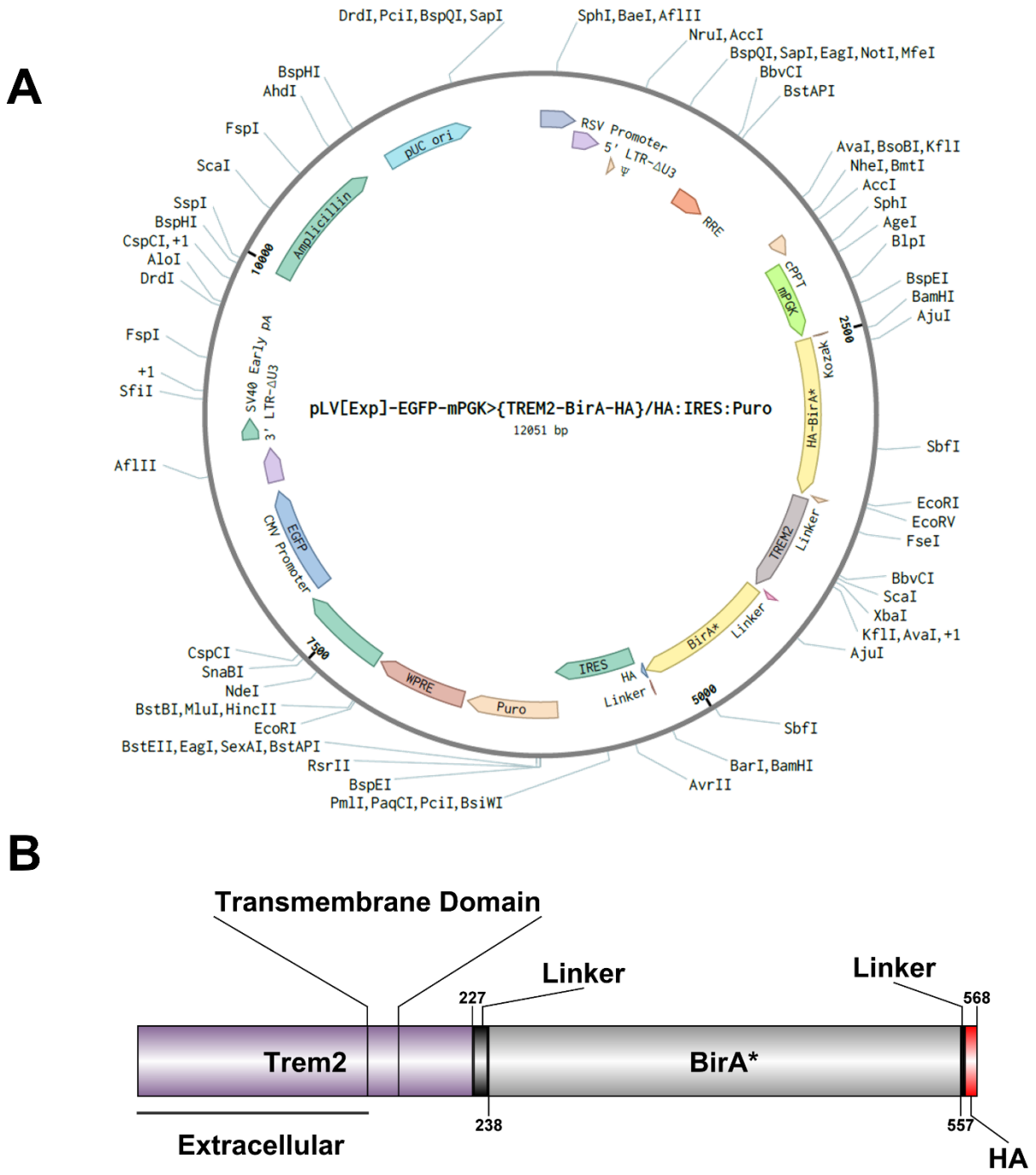

Figure 5.2 Schematic of structure of lentiviral vector and fusion protein. ***A)*** *The lentiviral vector used to transduce the sequence of the Trem2 fusion protein expressed in stable BV2 cell lines.* ***B)*** *The Trem2 fusion protein was designed with the BirA* sequence joined via a linker to the C-terminus of full length Trem2. This end of the sequence was chosen as the C-terminus resides within the cytoplasm and the aim was to capture intracellular interactors of Trem2 rather than extracellular ligands. The HA epitope was joined to the C-terminus of the BirA* sequence, also via a linker.*

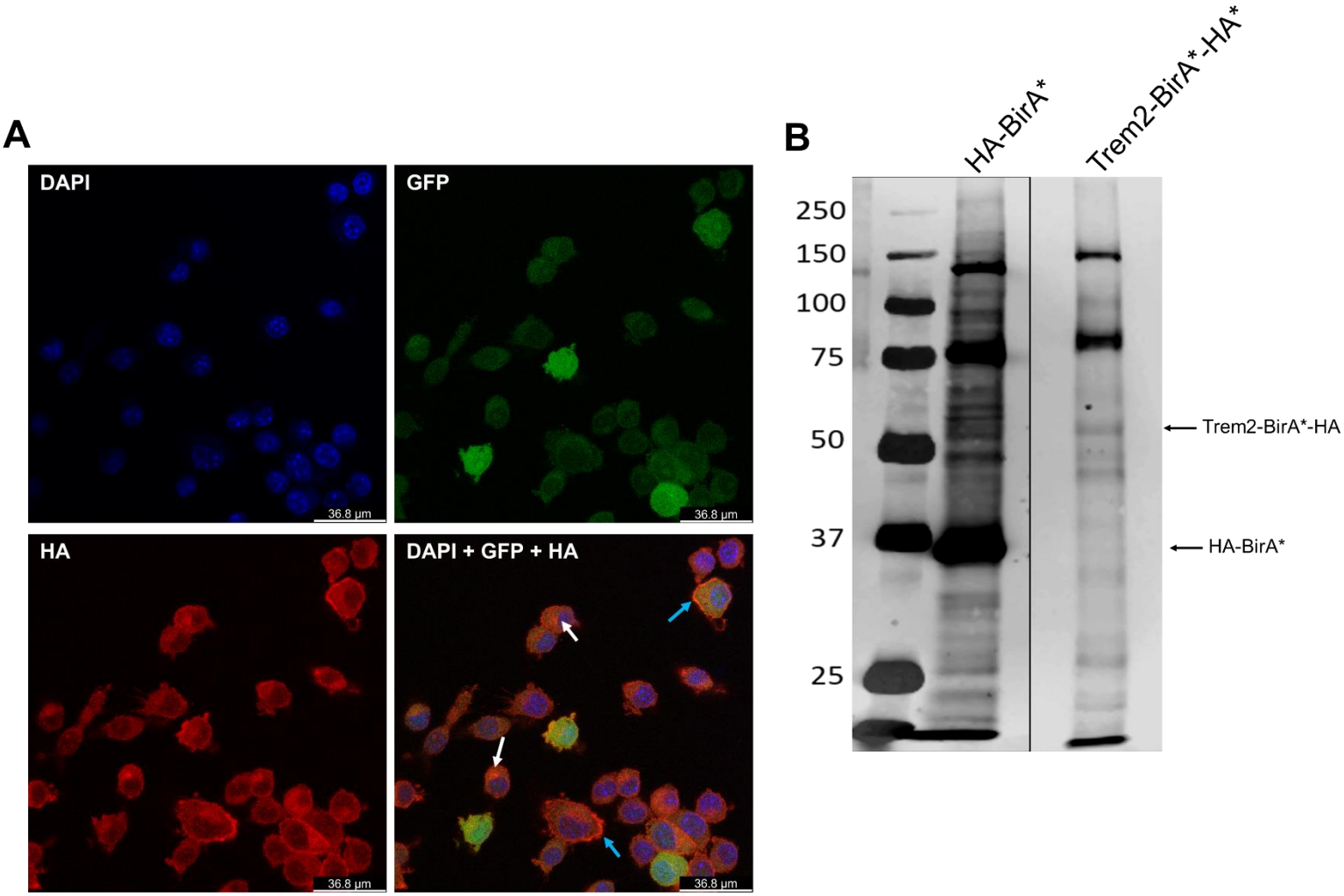

Figure 5.3 Characterisation of BV2 cells stably expressing Trem2-BirA*-HA. ***A)*** *Immunocytochemistry confirms successful transduction and expression of the exogenous proteins. White arrows highlight intracellular localisation of the HA epitope. Blue arrows highlight plasma membrane localisation of HA epitope. Lack of co-localisation of GFP positive and HA-epitope positive cells is likely due to expression of these genes under different promoters. Blue = DAPI, red = HA (Trem2), green = GFP* ***B)*** *Streptavidin western blot shows successful expression of exogenous proteins (HA-BirA*: 37 kDa, Trem2-BirA*-HA: 60 kDa) in BV2 cells and functioning of biotin ligase.*

5.2.2 Biotin-Affinity Capture of the Trem2 Interactome in BV2 Stable Cell Line

Protein interactors of Trem2 in BV2 stable cell lines expressing Trem2-BirA*-HA were captured by streptavidin affinity chromatography. Cells were incubated with 50 µM biotin, lysed, and biotinylated proteins were captured by incubation of lysates with streptavidin Dynabeads. Non-biotinylated proteins were removed during the washing stages and the remaining biotinylated proteins were eluted. Proteins were resolved by SDS-PAGE and detected by western blotting with streptavidin IR800 (Figure 0.4).

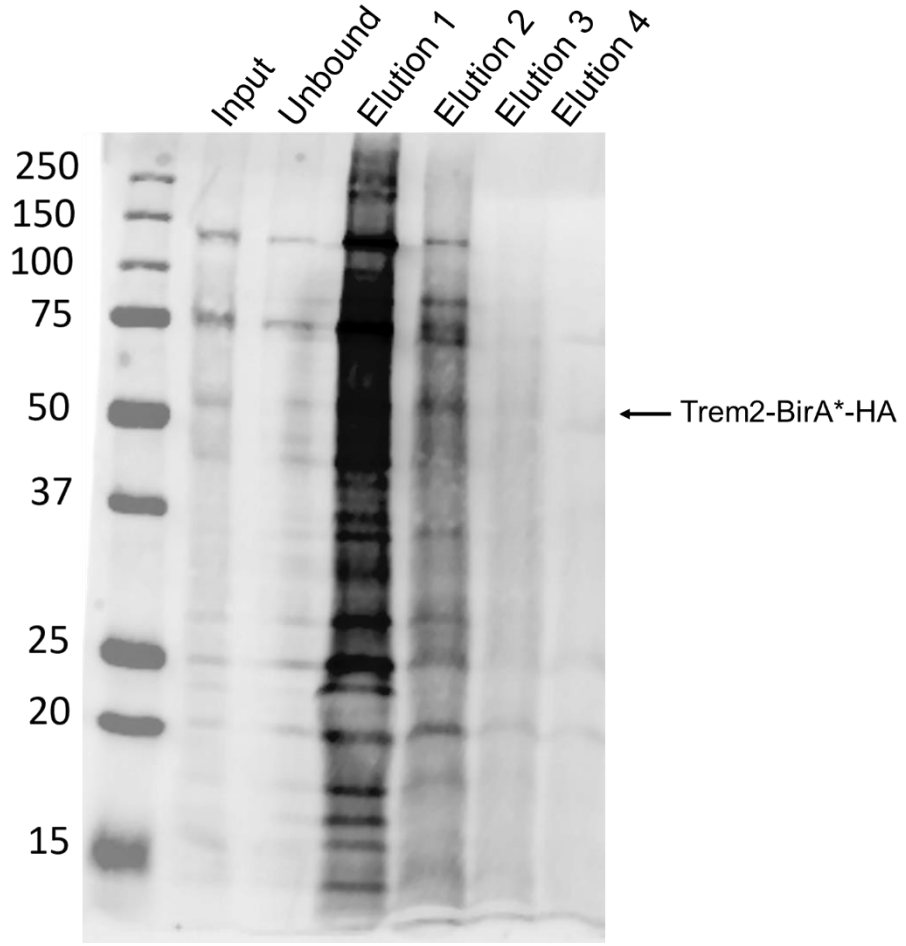

Figure 0.4 Biotin affinity capture of Trem2-BirA*-HA and associated proteins. *Enrichment of proteins from elution 1 compared to the input sample indicates higher concentration of biotinylated proteins. Low fluorescence in the unbound (lane 2) and subsequent elution samples (lanes 4-6) confirmed capture and elution of biotinylated proteins.*

The first elution sample (lane 3) was enriched compared to the input sample (lane 1) showing a higher concentration of biotinylated samples in elution 1. Low

fluorescence was observed in the unbound sample (lane 2) and in subsequent elution samples (lanes 4-6). This indicated successful capture of the majority of biotinylated protein during streptavidin affinity chromatography and efficient removal of these proteins from the beads during elution. These results confirm the expression and proper functioning of BirA* and successful capture of biotinylated proteins.

5.2.3 Proteomic Analysis of Trem2 Interactome

Identification of biotinylated proteins captured by BioID was done by MS analysis at the Fingerprints Proteomics Facility at the University of Dundee. Samples were sent as polyacrylamide gel plugs with proteins visualised by GelCode™ Blue Stain Reagent (Coomassie Blue, Figure 5.5) (see section 3.2.3 and Figure 3.7 for full workflow). After trypsinisation, peptides were separated by LC and the mass and charge (m/z) of each peptide was determined by MS/MS allowing the sequences of each peptide to be assigned and mapped to an individual protein. Proteins in the original samples were identified by matching the peptide sequences to the Swiss-Prot protein database for *Mus musculus* proteins.

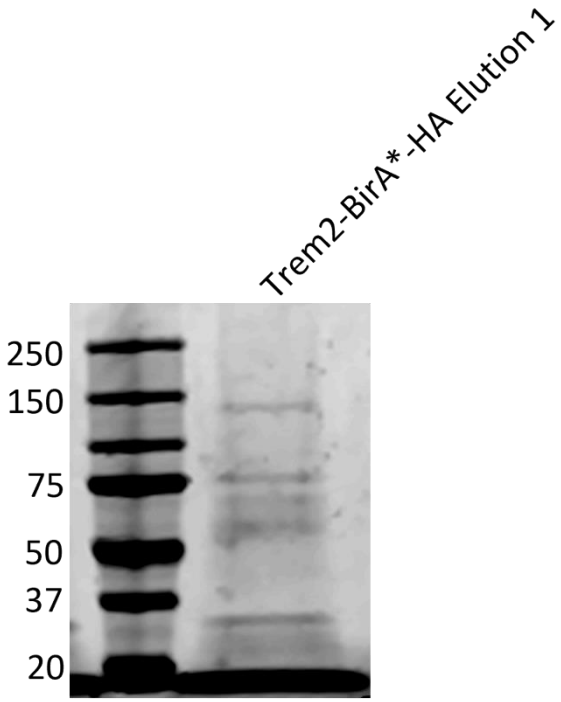

Figure 5.5 Separation of proteins for MS analysis. *A representative gel of proteins from elution 1 separated by SDS-PAGE. Proteins were run on the gel for 15 minutes and visualised with GelCode™ Blue Stain Reagent. Trem2-BirA*-HA lanes were individually excised from the gel and sent to the FingerPrints Proteomics Facility at the University of Dundee for MS analysis.*

MS was used to identify biotinylated proteins in the Trem2-BirA*-HA expressing cells. As described previously, two stable cell lines were generated: one expressing the Trem2-BirA*-HA fusion protein and a control line expressing HA-BirA*. The data generated from the control cell line was used to create a list of background proteins which was used during data analysis to identify putative interactors of Trem2. For Trem2, 5 replicates were analysed and for the BirA* control 4 replicates were analysed. The reproducibility of these replicates is assessed in Figure 5.6. For Trem2, a total of 1,003 proteins were identified, 181 of which were found in all five replicates. 499 proteins overlapped with the control data and 504 were identified exclusively in the Trem2 data sets.

As discussed in section 3.2.3.1, the nature of the BioID protocol means potential cytoplasmic interactors of Trem2 may also be biotinylated by the promiscuous activity of HA-BirA* in the control. Therefore, SAINTexpress analysis was employed to assess the likelihood of interaction with Trem2 by highlighting prey proteins with significantly higher levels in the Trem2-BirA*-HA data compared to the HA-BirA* control.

5.2.3.1 SAINTexpress

Putative interactors of Trem2 were identified by SAINTexpress (Choi et al., 2011) (see section 3.2.3.1 for more detail on SAINT analysis). Prey proteins with a BFDR less than 0.05 were considered to be putative interactors of Trem2. These proteins were then taken for protein of interest identification, GO analysis, and STRING annotation.

70 of the 1003 captured proteins were found to be putative interactors of Trem2 (Table 5.1). The SAINT score for each of the captured proteins was plotted against $\log_2$ of the fold change (Figure 5.7). The abundance of each protein in the Trem2 dataset is represented by the size of the bubble. The peptide data for all identified putative interactors of Trem2 can be found in Supplementary table 3.2 in appendix 3.

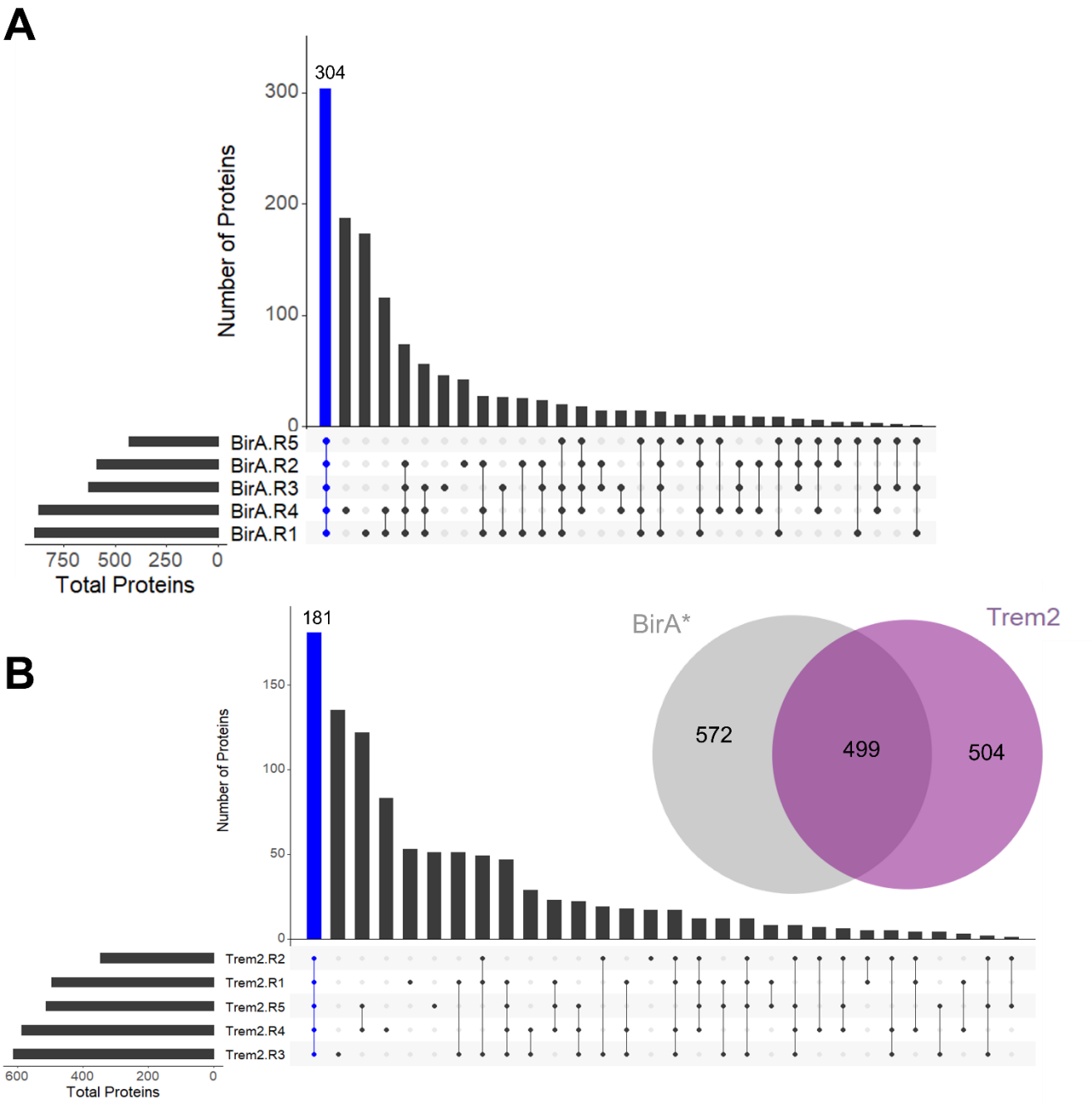

Figure 5.6 Variability of BioID replicates. *Number of proteins identified in each replicate from the **A)** BirA* and **B)** Trem2 BioID data. **A)** Of the 1,071 proteins identified in the BirA* datasets, 304 were found in all 4 replicates. The first dataset (BirA.R1) contained the largest number of proteins, 185 of which were unique to this replicate. **B)** Of the 1,003 proteins identified in the Trem2 datasets, 181 proteins were found in all 5 replicates. The third dataset (Trem2.R3) contained the largest number of proteins of all the replicates, 135 of which were unique to this replicate. **Inset)** Overlap of proteins between all BirA* control and Trem2 datasets. In total 1,575 proteins were identified, 499 of which appeared in both the control and the Trem2 datasets. 572 were unique to the control data and 504 were unique to the Trem2 dataset. Blue bar represents the proteins identified in all replicates.*

Table 5.1 Trem2-associated proteins prioritised by SAINTexpress. *The identified proteins were detected by MS of BioID samples from Trem2-BirA*-HA stable BV2 lines. Proteins which passed the significance threshold <0.05 BFDR after probabilistic scoring of protein-protein interaction by SAINTexpress are above the black line. SAINT determines putative interactors from non-specifically bound proteins by calculating the fold change between the data and a negative control affinity-purification sample. To be considered a putative interactor, the prey protein must appear in the Trem2 dataset at a significantly higher level than in the BirA* control data. Proteins are sorted first by BFDR value (lowest to highest) then by fold change (highest to lowest). The bait protein is highlighted in bold. Title annotations: Spec: spectral counts for the bait-prey pair in each replicate. SpecSum: sum of spectral counts across all replicates. AvgSpec: mean spectral count. crtlCounts: spectral count in each negative control replicate. SaintScore: probability of being an interactor. FoldChange: average spectral count in test interaction divided by the average in controls. BFDR: Bayesian false discovery rate.*

#	Prey	PreyGene	Spec	SpecSum	AvgSpec	NumReplicates	ctrlCounts	SaintScore	FoldChange	BFDR
1	Q07113	Igf2r	50|24|44|52|53	223	44.6	5	0|0|0|0	1	446	0
2	Q99K01	Pdxdc1	36|19|33|53|52	193	38.6	5	0|0|0|0	1	386	0
3	Q9QYE6	Golga5	35|15|20|34|41	145	29	5	0|0|0|0	1	290	0
4	P01901	H2-K1	27|14|22|17|11	91	18.2	5	0|0|0|0	1	182	0
5	P11835	Itgb2	15|9|16|23|17	80	16	5	0|0|0|0	1	160	0
6	Q9WV55	Vapa	13|4|18|14|19	68	13.6	5	0|0|0|0	1	136	0
7	O89001	Cpd	6|2|15|21|17	61	12.2	5	0|0|0|0	0.99	122	0
8	Q8BLU0	Flrt2	6|9|9|18|15	57	11.4	5	0|0|0|0	1	114	0
9	O08579	Emd	8|4|14|12|12	50	10	5	0|0|0|0	1	100	0
10	Q9ERB0	Snap29	9|3|7|16|13	48	9.6	5	0|0|0|0	1	96	0
11	Q99K28	Arfgap2	13|3|8|8|15	47	9.4	5	0|0|0|0	1	94	0

12	Q62351	Tfrc	5|8|10|16|8	47	9.4	5	0|0|0|0	1	94	0
13	Q5SYH2	Tmem199	10|10|5|7|14	46	9.2	5	0|0|0|0	1	92	0
14	Q9D024	Ccdc47	4|2|11|13|13	43	8.6	5	0|0|0|0	0.99	86	0
15	**Q99NH8**	**Trem2**	**7|8|6|9|11**	**41**	**8.2**	**5**	**0|0|0|0**	**1**	**82**	**0**
16	P09055	Itgb1	8|2|7|17|6	40	8	5	0|0|0|0	0.99	80	0
17	P70297	Stam	8|2|5|12|12	39	7.8	5	0|0|0|0	0.99	78	0
18	Q3TZZ7	Esyt2	4|2|10|17|4	37	7.4	5	0|0|0|0	0.99	74	0
19	Q8K2P7	Slc38a1	13|6|8|5|5	37	7.4	5	0|0|0|0	1	74	0
20	Q8VBW1	Slc6a8	11|5|7|9|5	37	7.4	5	0|0|0|0	1	74	0
21	Q8CFE6	Slc38a2	11|3|4|7|10	35	7	5	0|0|0|0	1	70	0
22	P63024	Vamp3	7|4|9|8|7	35	7	5	0|0|0|0	1	70	0
23	Q8K1E0	Stx5	8|2|7|8|9	34	6.8	5	0|0|0|0	0.99	68	0
24	Q9JJZ4	Ube2j1	7|3|4|7|11	32	6.4	5	0|0|0|0	1	64	0
25	Q9DB43	Zfpl1	6|2|4|7|12	31	6.2	5	0|0|0|0	0.99	62	0
26	P18572	Bsg	6|3|9|7|4	29	5.8	5	0|0|0|0	1	58	0
27	Q9CZE3	Rab32	3|3|8|7|8	29	5.8	5	0|0|0|0	1	58	0
28	P35279	Rab6a	8|3|4|8|6	29	5.8	5	0|0|0|0	1	58	0
29	Q62313	Tgoln1	5|2|6|8|8	29	5.8	5	0|0|0|0	0.99	58	0
30	Q64281	Lilrb4	8|2|5|7|5	27	5.4	5	0|0|0|0	0.99	54	0
31	O88630	Gosr1	6|3|4|3|10	26	5.2	5	0|0|0|0	1	52	0

32	Q8R1F1	Niban2	3|4|2|13|4	26	5.2	5	0|0|0|0	0.99	52	0
33	P70452	Stx4	5|2|5|7|7	26	5.2	5	0|0|0|0	0.99	52	0
34	Q99LR1	Abhd12	4|2|4|5|10	25	5	5	0|0|0|0	0.99	50	0
35	Q9Z127	Slc7a5	7|2|2|10|4	25	5	5	0|0|0|0	0.98	50	0
36	G5E829	Atp2b1	4|2|3|9|5	23	4.6	5	0|0|0|0	0.99	46	0
37	Q3UQN2	Fcho2	2|2|2|9|6	21	4.2	5	0|0|0|0	0.98	42	0
38	Q99JY8	Plpp3	6|3|4|2|2	17	3.4	5	0|0|0|0	0.98	34	0
39	P97797	Sirpa	18|7|17|16|13	71	14.2	5	0|2|0|0	1	28.4	0
40	Q3U7R1	Esyt1	7|5|8|16|7	43	8.6	5	2|0|0|0	0.98	17.2	0
41	Q9CQW1	Ykt6	15|16|33|28|20	112	22.4	5	0|4|2|2	1	11.2	0
42	Q80UU9	Pgrmc2	35|12|10|21|31	109	21.8	5	2|2|2|2	1	10.9	0
43	P16110	Lgals3	8|9|10|6|6	39	7.8	5	0|0|2|2	0.98	7.8	0
44	P10852	Slc3a2	48|22|29|39|21	159	31.8	5	8|6|5|4	1	5.53	0
45	Q61334	Bcap29	2|2|3|2|4	13	2.6	5	0|0|0|0	0.97	26	0.01
46	P32507	Nectin2	2|3|2|2|4	13	2.6	5	0|0|0|0	0.97	26	0.01
47	P43252	Ptgir	4|2|2|2|3	13	2.6	5	0|0|0|0	0.97	26	0.01
48	Q05CL8	Larp7	6|6|9|20|21	62	12.4	5	3|0|0|0	0.96	16.53	0.01
49	O70480	Vamp4	7|3|12|12|12	46	9.2	5	0|3|0|0	0.91	12.27	0.01
50	Q76LS9	Mindy1	5|5|5|8|7	30	6	5	0|2|0|0	0.96	12	0.01
51	P27773	Pdia3	7|3|12|5|2	29	5.8	5	0|0|2|0	0.86	11.6	0.01

52	Q9JIF7	Copb1	4|4|4|6|4	22	4.4	5	0|0|2|0	0.9	8.8	0.01
53	O88811	Stam2	22|9|13|25|23	92	18.4	5	3|4|2|2	0.97	6.69	0.01
54	Q99JX3	Gorasp2	39|11|26|22|34	132	26.4	5	7|4|2|4	0.87	6.21	0.01
55	B9EJ86	Osbpl8	2|2|6|9|5	24	4.8	5	0|0|2|0	0.81	9.6	0.02
56	P62331	Arf6	4|4|4|6|7	25	5	5	3|0|0|0	0.84	6.67	0.02
57	Q8C2K5	Rasal3	23|22|7|26|18	96	19.2	5	10|0|2|0	0.8	6.4	0.02
58	P48678	Lmna	14|6|12|14|15	61	12.2	5	4|0|5|0	0.83	5.42	0.02
59	Q60738	Slc30a1	9|0|11|20|23	63	12.6	5	0|0|0|0	0.8	126	0.03
60	Q9DCD5	Tjap1	12|5|14|0|27	58	11.6	5	0|0|0|0	0.8	116	0.03
61	Q8K021	Scamp1	11|0|12|13|9	45	9	5	0|0|0|0	0.8	90	0.03
62	Q9D0V7	Ebag9	6|0|31|5|26	68	13.6	5	0|0|0|0	0.8	136	0.04
63	A2A5R2	Arfgef2	16|0|4|13|24	57	11.4	5	0|0|0|0	0.8	114	0.04
64	Q8BP48	Metap1	5|0|5|15|25	50	10	5	0|0|0|0	0.8	100	0.04
65	P97390	Vps45	12|5|0|12|9	38	7.6	5	0|0|0|0	0.8	76	0.04
66	O70252	Hmox2	5|0|3|13|22	43	8.6	5	0|0|0|0	0.8	86	0.05
67	G3X9K3	Arfgef1	10|3|0|10|11	34	6.8	5	0|0|0|0	0.8	68	0.05
68	P42082	Cd86	7|0|8|6|3	24	4.8	5	0|0|0|0	0.8	48	0.05
69	O70492	Snx3	4|5|6|0|4	19	3.8	5	0|0|0|0	0.8	38	0.05
70	Q9D4H2	Gcc1	5|3|0|4|5	17	3.4	5	0|0|0|0	0.8	34	0.05
71	Q91VW5	Golga4	15|2|0|23|36	76	15.2	5	0|0|0|0	0.79	152	0.06

72	Q61830	Mrc1	8|2|11|13|0	34	6.8	5	0|0|0|0	0.79	68	0.06
73	Q3UPL0	Sec31a	11|2|5|10|11	39	7.8	5	0|0|4|0	0.79	7.8	0.06
74	O88983	Stx8	3|0|3|4|6	16	3.2	5	0|0|0|0	0.8	32	0.06
75	Q9EQP2	Ehd4	4|0|2|7|5	18	3.6	5	0|0|0|0	0.79	36	0.07
76	O35516	Notch2	4|0|2|4|4	14	2.8	5	0|0|0|0	0.79	28	0.07
77	Q9Z0P4	Palm	4|0|4|4|2	14	2.8	5	0|0|0|0	0.79	28	0.07
78	P37040	Por	6|2|5|7|0	20	4	5	0|0|0|0	0.79	40	0.07
79	Q8VDS8	Stx18	6|0|2|7|10	25	5	5	0|0|0|0	0.79	50	0.07
80	Q9Z1Z0	Uso1	3|2|0|6|10	21	4.2	5	0|0|0|0	0.79	42	0.07

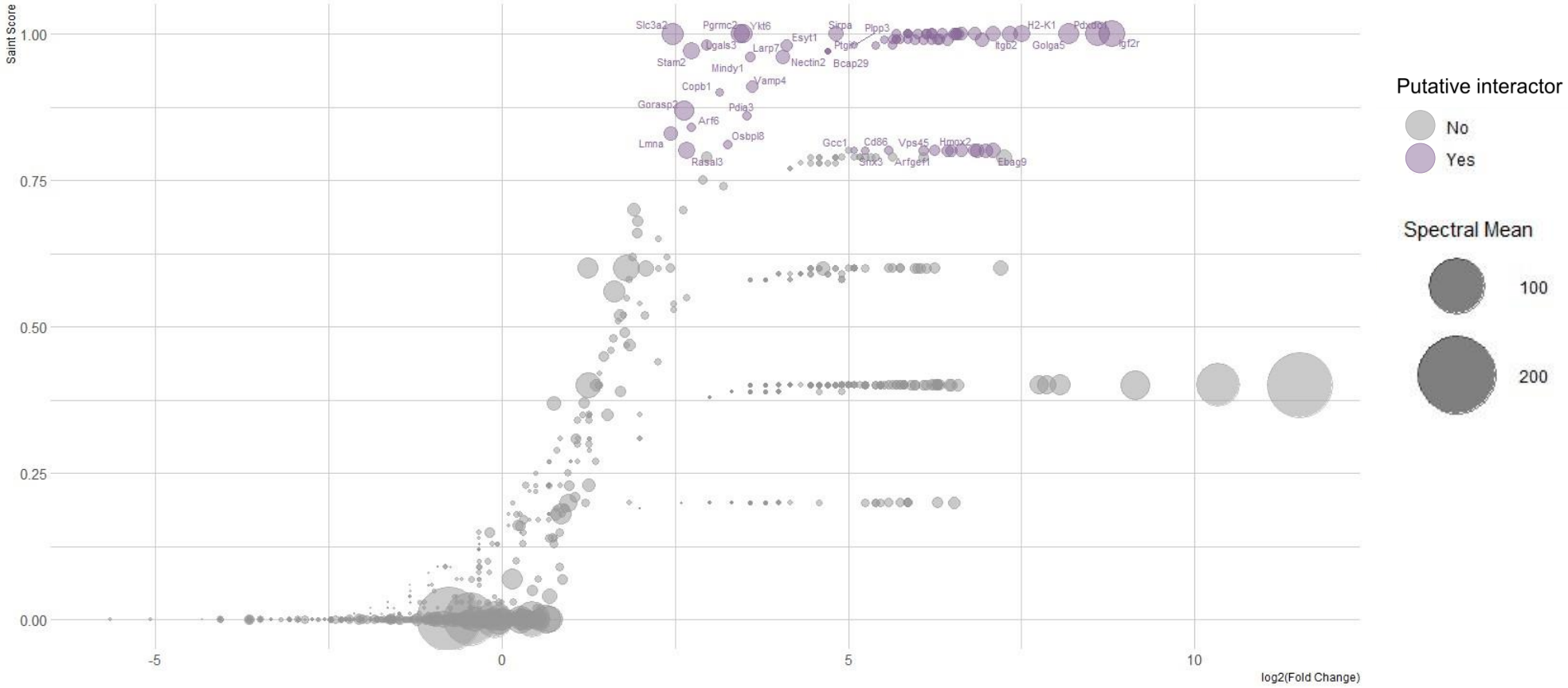

Figure 5.7 Fold change and SAINT score from SAINTexpress. *Proteins identified by MS in Trem2 BioID samples. Data are represented by log_2 of the fold change (difference in protein count from control data) is plotted against the SAINT score (probability of protein being a putative interactor). Each bubble on the plot denotes an individual protein. The size of the bubble represents the abundance of each protein in the data, calculated by the mean of the spectral counts. Proteins identified as being putative interactors of Trem2 (BFDR < 0.05) are labelled. Purple = putative interactor, grey = non-interactor.*

5.2.3.2 STRING Annotation

Known relationships between the identified putative Trem2 interactors were investigated using the STRING database (v11.5; https://string-db.org/) (Szklarczyk et al., 2021) (Figure 5.8).

No known interactors of Trem2 were identified in the BioID data, but some protein complexes were identified in the data set. A network of proteins involved in Golgi complex structure and trafficking (identified in blue in Figure 5.8a) was identified by STRING analysis. A network of plasma membrane proteins was also identified (purple in Figure 5.8a) although it cannot be determined if these proteins were proximal to Trem2-BirA*-HA at the membrane or during trafficking in the secretory pathway. Known interactions between cytoplasmic (green), ER (orange), and nuclear (pink) were also identified (Figure 5.8a).

No known physical interactors of TREM2 were captured by BioID, including Dap12, the major intracellular interactor of Trem2 (Figure 5.8b). As Dap12 contains 2 lysine residues it is capable of being biotinylated, however no biotinylation of Dap12 occurred in these experiments. This could be explained by limited expression of Trem2-BirA*-HA at the plasma membrane, although the identification of plasma membrane proteins from the STRING database and GO analysis may suggest some expression. It is also possible that Trem2-BirA*-HA was not activated by endogenous Trem2 ligands in the BV2 cells, possibly due to the activation state of the cells under basal conditions, and therefore Dap12 was not recruited.

5.2.4 Functional Annotation of Interactors

For all further analysis, proteins were converted to their human orthologues as there is more complete human data and PPIs are relatively well conserved between species (Sharan et al., 2005, Qian et al., 2011, Pérez-Bercoff et al., 2013).

Functional annotation of the human orthologues of the putative Trem2 interactors was carried out with the Metascape enrichment analysis (http://metascape.org) (Zhou et al., 2019). A total of 286 biological processes were found to be enriched in this dataset. Out of the top 10 processes 7 were involved with protein trafficking and transport. Of the top 10 pathway analysis clusters the top 4 clusters were summarised by plasma membrane and vesicle transport and organisation (Figure

5.9 and Table 5.2). The full list of enriched terms can be found in Supplementary table 3.3 in Appendix 3.

5.2.5 Proteins of Interest

The above analysis identified a total of 70 putative interactors of Trem2. STRING analysis identified a network of Golgi proteins, mostly involved in protein transport, and two of the top 10 enriched functions by the Metascape enrichment analysis were Golgi vesicle transport and intra-Golgi and retrograde Golgi-to-ER traffic. A network of plasma membrane-associated proteins was also identified by STRING, and three of the top 10 Metascape enrichment analysis functions were involved in membrane trafficking, docking, and vesicle transport. This suggests that the most abundant interactions of the Trem2-BirA*-HA fusion protein were during the trafficking of the protein within and to/from the Golgi and ER, as well as trafficking to the plasma membrane.

Of the 70 putative interactors identified above, 7 have previously been associated with AD risk in meta-analyses of GWAS data with different levels of supporting data. The functions of these proteins are discussed in section 5.3.2.

5.2.6 Validation of Interaction

As the BirA* ligase will biotinylate any protein within a 10 nm radius, it is possible that the identified putative interactors may not physically interact with Trem2. Validation of physical interaction was attempted using IPs. However, lysis in RIPA buffer was not sufficient to solubilise Trem2 or Dap12 for detection via western blot (Figure 5.10). Extraction of Dap12 was tested in order to assess suitability for co-IP with Trem2 to investigate activation states in which Trem2-Dap12 interaction occurs. Dap12 was only successfully extracted with a lysis buffer containing 4% SDS, conditions too harsh for IP protocols as protein complexes will be disrupted. Trem2 was not detected in any sample. This is likely to be due to a lack of expression of the transfected Trem2-myc protein in the HEK-293T cells. Solubilisation of membrane proteins whilst keeping PPIs intact is a challenge as transmembrane proteins are often relatively insoluble and therefore require harsh lysis conditions. Protocols requiring gentle lysis of cells may not be appropriate to further investigate the interaction between Trem2 and the putative interactors described here.

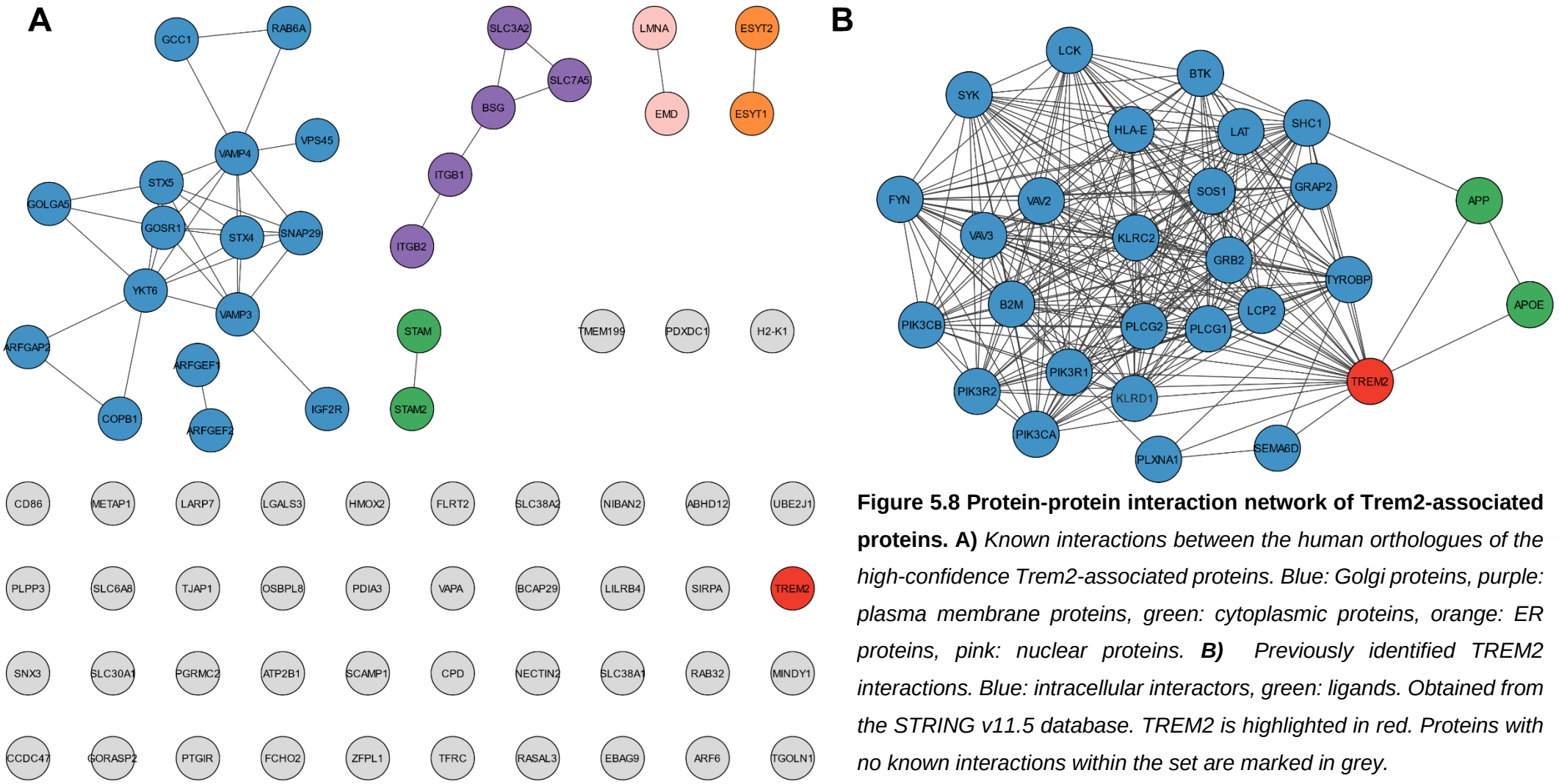

Figure 5.8 Protein-protein interaction network of Trem2-associated proteins. A) *Known interactions between the human orthologues of the high-confidence Trem2-associated proteins. Blue: Golgi proteins, purple: plasma membrane proteins, green: cytoplasmic proteins, orange: ER proteins, pink: nuclear proteins.* ***B)*** *Previously identified TREM2 interactions. Blue: intracellular interactors, green: ligands. Obtained from the STRING v11.5 database. TREM2 is highlighted in red. Proteins with no known interactions within the set are marked in grey.*

Table 5.2 Summary of functional terms enriched in the list of genes encoding Trem2-associated proteins from Metascape. *Top 20 clusters with one representative enriched term presented. Count: number of genes with membership in identified gene ontology term. Percentage: percentage of genes with at least one annotation found in identified gene ontology term.*

GO	Description	Protein Count	Percentage of Interactome
R-HSA-199991	Membrane trafficking	22	31.43
GO:0061024	Membrane organization	21	30
GO:0048193	Golgi vesicle transport	14	20
hsa04130	SNARE interactions in vesicular transport	7	10
R-HSA-9013408	RHOG gtpase cycle	8	11.43
hsa04144	Endocytosis	11	15.71
GO:0051668	Localization within membrane	13	18.57
GO:0002697	Regulation of immune effector process	11	15.71
GO:0051640	Organelle localization	12	17.14
GO:0044000	Movement in host	7	10
GO:0032328	Alanine transport	4	5.71
GO:1905477	Positive regulation of protein localization to membrane	6	8.57
R-HSA-6798695	Neutrophil degranulation	10	14.29
GO:0006897	Endocytosis	10	14.29
GO:0006886	Intracellular protein transport	11	15.71

R-HSA-199992	Trans-Golgi Network Vesicle Budding	5	7.14
GO:0007030	Golgi organization	6	8.57
GO:1903555	Regulation of tumor necrosis factor superfamily cytokine production	6	8.57
GO:0010324	Membrane invagination	4	5.71
R-HSA-9609523	Insertion of tail-anchored proteins into the endoplasmic reticulum membrane	3	4.29

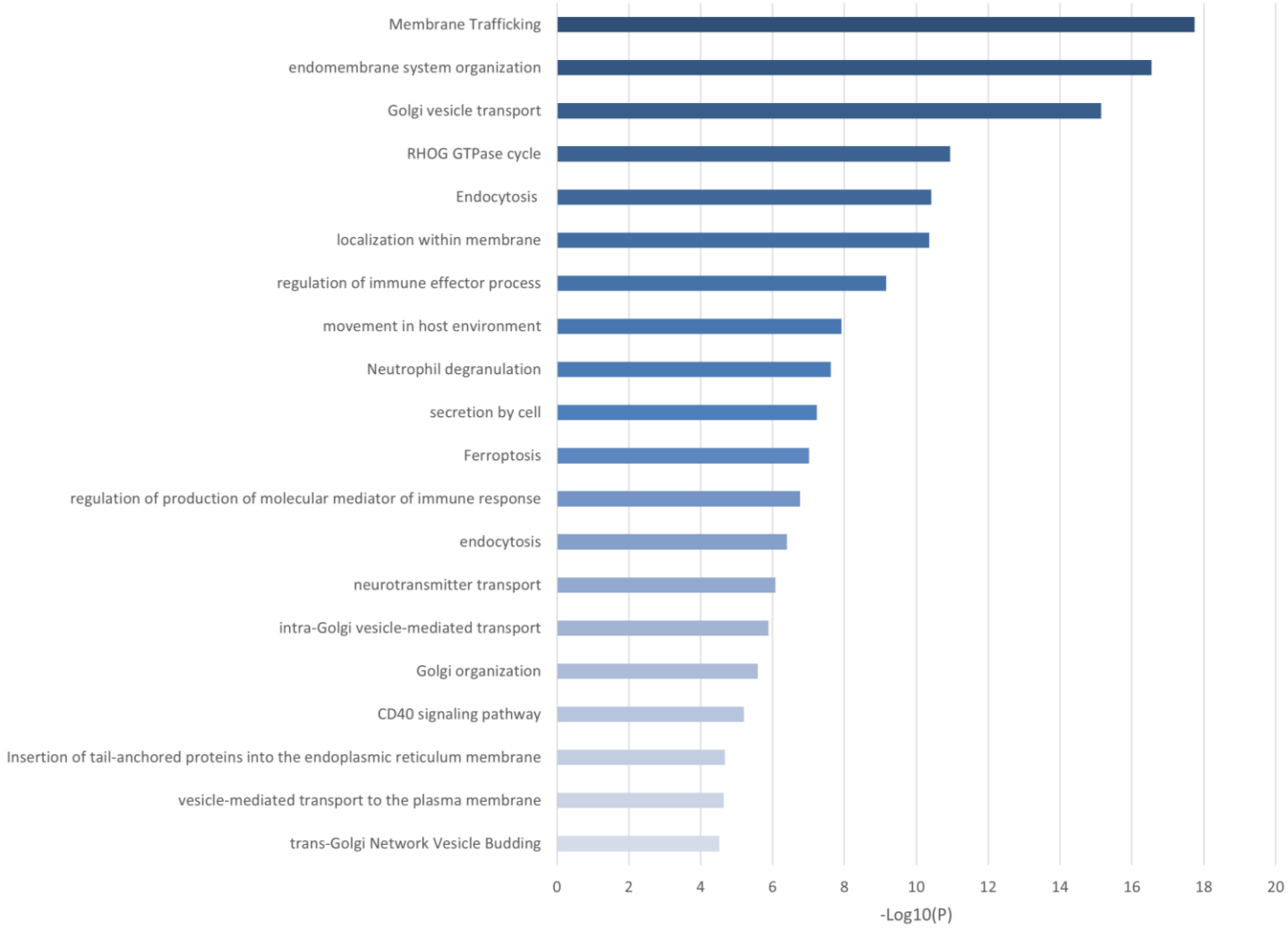

Figure 5.9 ***Summary of biological process annotations for Trem2-associated proteins identified by BioID.*** *Enrichment analysis from Metascape was used to identify biological processes enriched for the human orthologues of the identified putative interactors of Trem2. All annotations are grouped into functional clusters with one representative enriched term presented from the GO, Reactome, and KEGG pathway databases. The heatmap is coloured according to p-value and plotted with the -log$_{10}$(P) score.*

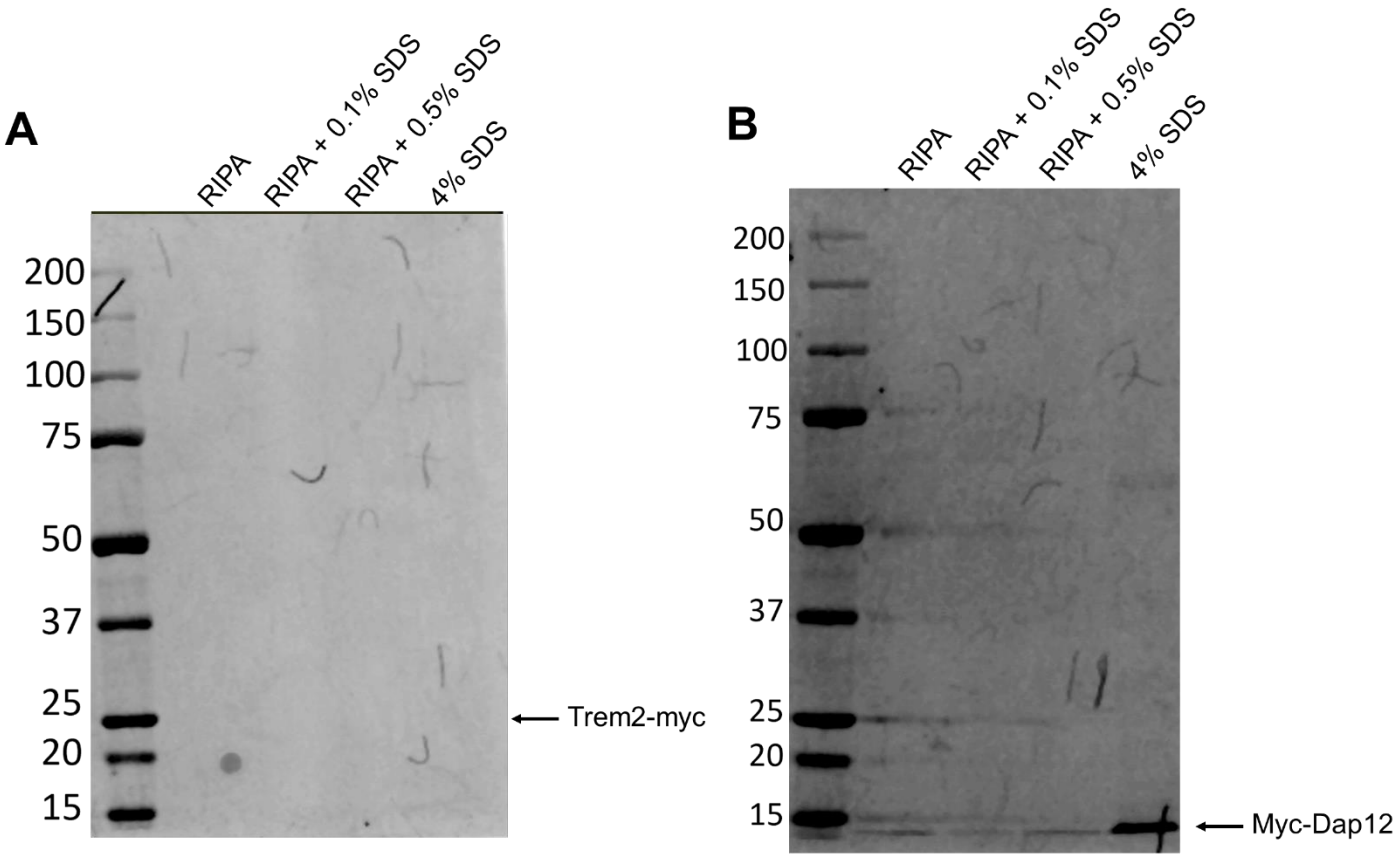

Figure 5.10 Comparison of protein extraction with different strength lysis buffers. *HEK-293T cells transfected with Trem2-myc **(A)** or Dap12-FLAG **(B)** were lysed with either RIPA buffer (lane 1), RIPA buffer with 0.1% SDS (lane 2), RIPA buffer with 0.5% SDS (lane 3) or a lysis buffer containing 4% SDS (lane 4). Trem2-myc was not detected in any sample. For Dap12-FLAG protein was only successfully extracted with the harshest lysis protocol.*

5.3 Discussion

The mechanism by which many TREM2 variants contribute to AD risk is unknown. Some variants are known to disrupt ligand binding, and some have shown a reduction in receptor expression. The identification of intracellular signalling partners of TREM2 is a key step in identifying potential mechanisms of risk by first understanding the normal TREM2 function. In this chapter, BioID and MS was used to identify the repertoire of intracellular proteins that could potentially interact with Trem2 in microglia-like cells.

The NCBI lists 11 protein interactors of human TREM2 (Supplementary table 3.1, appendix 3) (Human TREM2 NCBI; interactions sourced from the HPRD and BioGRID databases). There are no protein interactors listed for mouse Trem2. The majority of these interactions were identified by protein microarray assays with some identified by affinity purification with MS. Ligands of Trem2 were mostly identified using Trem2-Fc fusion proteins and only one study identified in Supplementary table 3.1 used cells of the myeloid lineage. The results presented here were obtained from a microglial cell line and therefore are more relevant to the identification of physiologically relevant interactors, where the majority of Trem2 is expressed in the CNS.

5.3.1 Trem2-BirA*-HA is Located in the Endosomal and Secretory Pathways

From immunocytochemical staining (Figure 5.3a), Trem2-BirA*-HA appeared to be located both intracellularly in perinuclear pools and at the plasma membrane in transduced BV2 cells. The MS analysis of biotinylated proteins captured putative Trem2 interactors involved in the endosomal and secretory pathways. In total, 70 putative interactors of Trem2 were identified, including interactions with Golgi structural and transport proteins, and vesicle transport proteins. The largest network of proteins identified consisted of 14 Golgi proteins with roles including intra-Golgi transport, Golgi structure, and transport between the Golgi and the endoplasmic reticulum. Endogenous TREM2 is known to be stored at the Golgi complex as well as in exocytic vesicles (Sessa et al., 2004). The next largest network identified in the MS data was a group of five plasma membrane proteins. This suggests that the Trem2-BirA*-HA protein was captured at stages throughout its lifecycle.

5.3.1.1 ER-Golgi Trafficking

Five proteins known to be involved in protein trafficking from the ER to the Golgi complex were identified as putative interactors of Trem2-BirA*-HA. Syntaxin-5 (Stx5), Golgi synaptosomal-associated protein (SNAP) receptor complex member 1 (Gosr1), Gors2, and synaptobrevin homolog Ykt6 (Ykt6) are known to form a complex medicating vesicle docking to the cis-Golgi membrane during protein trafficking from the ER (Linders et al., 2019). The putative interactor zinc finger protein-like 1 (Zfpl1) is also an integral cis-Golgi protein, both for Golgi structure and protein trafficking (Chiu et al., 2008). Tight junction-associated protein 1 (Tjap1), Brefeldin A-inhibited guanine nucleotide-exchange protein 1 (Arfgef1, also known as Big1 and plays a role in vesicular trafficking), and GRIP and coiled-coil domain-containing protein 1 (Gcc1) are also involved in maintenance of Golgi complex structure and identified as putative interactors of Trem2-BirA*-HA. Transmembrane protein 199 (Tmem199) was also identified as a putative interactor and is known to maintain Golgi homeostasis. Additionally, TMEM199 deficiency has been shown to result in abnormal glycosylation. Interaction between TMEM199 and TREM2 may mediate TREM2 glycosylation, disruption to which may underlie the impaired glycosylation of TREM2 AD risk variants (Jansen et al., 2016).

5.3.1.2 Trans-Golgi Network

Proteins involved in transport via the TGN were also identified as putative interactors of Trem2-BirA*-HA. The protein coatomer subunit β (Copb) associates with Golgi non-clathrin-coated vesicles mediating transport through the Golgi and TGN. Knockdown of coatomer proteins has been shown to impact the trafficking of Trem2 to the membrane (Sirkis et al., 2017). It is possible that the interaction between Trem2 AD risk variants and coatomer proteins is disrupted, reducing Trem2 membrane expression. ADP-ribosylation factor GTPase-activating protein 2 (Arfgap2) is also implicated in coatomer-mediated protein transport and was found to be a putative interactor of Trem2-BirA*-HA. The soluble N-ethylmaleimine-sensitive factor attachment protein receptors (SNARE) vesicle-associated membrane protein 4 (Vamp4) was determined to be a putative interactor of Trem2-BirA*-HA and is thought to mediate transport from the TGN to endosomes. The TGN-endosomal system is involved in the transport of both newly synthesised proteins and receives recycled proteins from the endocytic pathway (Steegmaier et al., 1999). Trem2 may

therefore interact with Vamp4 at the start of its life cycle or after recycling from the plasma membrane.

5.3.1.3 Golgi-Plasma Membrane Trafficking

From the Golgi, plasma membrane proteins are trafficked to the cell surface in vesicles. Proteins involved in the vesicle transport, insertion, folding, and docking were found to be putative interactors of Trem2-BirA*-HA. Brefeldin A-inhibited guanine nucleotide-exchange protein 2 (Arfgef2, also known as Big2) regulates the formation of vesicles by recruiting coat proteins at the TGN (Shinotsuka et al., 2002). Docking of vesicles at the plasma membrane is regulated by SNARE proteins. The t-SNARE Syntaxin-4 (Stx4) was found to be a putative interactor of Trem2-BirA*-HA and is known to play a key role in cell surface vesicle docking (Zhao et al., 2022). The SNAREs Snap29 and Vamp3 were also determined to be putative interactors. Snap29 has well-characterised roles in protein trafficking and has been found to interact with YKT6 to mediate the fusion of lysosomes and autophagosomes (Matsui et al., 2018, Mastrodonato et al., 2018). Vamp3 is known to interact with Stx4 to facilitate vesicle fusion and docking.

At the plasma membrane, proteins are inserted via chaperone proteins. CCDC47 forms part of the PAT (protein associated with the translocon) complex which assists with the insertion of plasma membrane proteins (Culver and Mariappan, 2020). Potential interaction with Trem2-BirA*-HA suggests that Trem2 may be inserted into the plasma membrane via the PAT complex and provides further evidence of expected trafficking and localisation of Trem2-BirA*-HA.

5.3.1.4 Receptor Internalisation

Down-regulation of cell surface receptors occurs via internalisation of the proteins. Ubiquitination of proteins can mark them for degradation and deubiquitination pushes proteins along the recycling pathway. Ubiquitin-conjugating enzyme E2 J1 (Ube2j1) and signal transducing adaptor molecule 1 and 2 (Stam1, Stam2) were identified as putative Trem2-BirA*-HA interactors. Ube2j1 catalyses the attachment of ubiquitin to proteins and Stam1/2 form part of the endosomal sorting complexes required for transport 0 (ESCRT-0) complex which directs ubiquitinated proteins to multivesicular bodies. The ESCRT-0 complex clusters ubiquitinated proteins at the

plasma membrane in preparation for endocytosis via ubiquitin-binding domains on the Stam proteins (Wollert and Hurley, 2010).

TREM2 is known to be internalised via clathrin-mediated endocytosis (Yin et al., 2016). Secretory carrier membrane protein 1 (Scam1) is known to play a role in the recycling of receptor proteins through recruitment of the clathrin coats to endosomes (Fernández-Chacón et al., 2000). F-BAR domain-containing Fer/Cip4 homology domain-only protein 1 (Fcho1) also contributes to clathrin recruitment by initiating the formation of clathrin-coated pits in early stages of endocytosis (Henne et al., 2010). Possible interaction of these proteins with Trem2-BirA*-HA suggests the fusion protein was recycled from the plasma membrane in the same pathway as endogenous Trem2. ADP-ribosylation factor 6 (Arf6) was also determined to be a putative interactor of Trem2-BirA*-HA and regulates both clathrin-dependent and -independent endocytic membrane trafficking (D'Souza-Schorey and Chavrier, 2006).

5.3.1.5 Endosomal Sorting

Once endosomes are formed encasing their cargo, endosomal sorting occurs to traffic specific proteins to specific intracellular locations. Trem2 is recycled to the TGN and stored in intracellular pools before being recycled to the membrane. Trem2-containing endosomes interact with the retromer complex, triggering recycling to the TGN. Sorting nexin 3 (Snx3) contributes to retromer recruitment to the endosomal membrane and was found to be a putative interactor of Trem2-BirA*-HA (Seaman, 2012b). Endocytic sorting is also regulated by post-translational modification of both cargo and sorting proteins, such as ubiquitination. Trem2-BirA*-HA was found to potentially interact with the deubiquitinating enzyme Ubiquitin carboxyl-terminal hydrolase MINDY-1 (Mindy1). This interaction may shift Trem2 to the endocytic recycling pathway, away from lysosomal degradation (Abdul Rehman et al., 2016).

5.3.2 Trem2-BirA*-HA May Interact with Other Proteins Implicated in AD Pathology

Of the 70 putative interactors of Trem2 identified in section 5.2.3.1, the human orthologues of seven have been implicated in AD pathophysiology (Table 5.3). All seven proteins are expressed in microglia, though their specific microglial functions are not well understood (Carrillo-Jimenez et al., 2019). These genes have been identified with analyses such as polygenic risk score analysis and pleiotropic meta-analysis rather than identified through GWAS, therefore may not themselves be risk variants for AD. Association of these genes with known AD risk genes, such as *TREM2*, may point to common pathways which confer AD risk. Here, the cellular functions of these proteins are discussed to highlight potential networks.

The functions of Arfgef2 and Arfgap2 have been described in section 5.3.1. ARFGEF2 is reported to be downregulated in AD (Wang et al., 2018). Possible mechanisms for AD risk from ARFGAP2 variants are yet to be elucidated.

At the plasma membrane, BSG (Basigin, also knowns as extracellular matrix metalloproteinase inducer (EMMPRIN) or cluster of differentiation 147 (CD147)), FLRT2 (Fibronectin leucine-rich repeat transmembrane protein), Niban2 (also known as family with sequence similarity 129, member B (FAM129B) or maternally expressed gene 3 (MEG3)) and Nectin-2 (also known as CD112) also have AD risk associated variants.

BSG is a transmembrane glycoprotein of the immunoglobulin super-family of proteins which is involved in many cellular functions including lymphocyte activation, extracellular matrix metalloproteinase induction, and nervous system development. The protein is also known to influence Aβ levels by regulation of γ-secretase and amyloid clearance and has been suggested as a therapeutic target to modulate Aβ (Kanyenda et al., 2011).

FLRT2 is involved in synaptic plasticity memory in neurons as well as axon guidance and cell adhesion (Li et al., 2021). Heterozygous knockout of Flrt2 increased synaptic plasticity and spatial memory functions but interestingly only in female mice, a finding which may contribute to the increased prevalence of AD in women compared to men (Cicvaric et al., 2018). This protein is known to be highly expressed in microglia although its influence in this specific cell type has not been well studied.

Niban2 is a negative regulator of apoptosis. Phosphorylation of Niban2 upregulates Akt (PKB) which inhibits Gsk3β allowing for β-catenin translocation to the nucleus and increased expression of genes promoting cell proliferation and survival. As discussed in section 1.3.3.1, this pathway is downstream of Trem2 activation and Dap12 signalling, mediated through Syk and Pi3k activation. If Niban2 is validated as a physical interactor of Trem2, this may suggest a more direct regulation of this pathway by Trem2, either by activation of Niban2 after ligand binding or by inhibition by the inactive form of Trem2.

Nectin-2 is known to modulate T-cell signalling, proliferation, and cytokine production as well as cell adhesion. Expression of nectin-2 AD risk variants may play a role in increasing susceptibility to environmental factors linked with AD pathology. A network of AD risk variants, including those at the *NECTIN2* locus, were linked to susceptibility to herpes viruses which induce an AD-like pathology (Qin and Li, 2019, Licastro et al., 2011). The association between *NECTIN2* risk variants and AD has also been suggested to be mediated by disruption of neural vascular functions, although nectin-2 expression has so far been characterised in neurons and astrocytes rather than in microglia or perivascular macrophages (Mizutani et al., 2022).

Variants in the LPS ligase *ABHD12* (alpha/beta-hydrolase domain containing 12) have also been associated with AD risk (Gouveia et al., 2022). LPS is a known ligand of Trem2 and regulates immune cell responses. Endogenous cannabinoids derived from arachidonic acids (AA) are also known substrates of ABHD12 and AA levels have been found to be increased in the AD brain (Furman et al., 2018, Leishman et al., 2019). SNPs which decrease the enzymatic function of ABHD12 may contribute to these increased AA levels and disruption to the lipidome. TREM2 has also been linked to regulation of lipid metabolism (Li et al., 2022).

Table 5.3 Putative interactors of Trem2-BirA*-HA identified in the EBI GWAS Catalog as associated with AD. *The protein name, cellular location and function was extracted from the UniProt entry for each protein. The gene and paper identifying the variant was extracted from the EBI GWAS Catalog. *For NECTIN2, the variant given is the most significant variant from the 63 variants reported. For a full list of NECTIN2 AD risk variants see Supplementary table 3.4 in appendix 3.*

Mapped Gene	Protein	Location	Function	Risk Variant	Paper and Method
ABHD12	Lysophosphatidylserine lipase abhydrolyse domain containing 12	ER membrane	Mediates lysis of LPS	rs746748 (MAF 0.01837)	Gouveia et al. (2022) – Polygenic risk score analysis
ARFGAP2	ADP-ribosylation factor GTPase-activating protein 2	Cytoplasm Golgi membrane	Implicated in coatomer-mediated protein transport between Golgi and ER	rs75290815 (MAF 0.02117)	Gouveia et al. (2022) – Polygenic risk score analysis
ARFGEF2 (ARGEP2, BIG2)	Brefeldin A-inhibited guanine nucleotide-exchange protein 2	Cytoplasm Vesicles Endosome Cytoskeleton	Promotes guanine-nucleotide exchange on ARF1/3 Trafficking from trans-Golgi network to endosomes and	rs140589268 (MAF 0.02256)	Kulminski et al. (2022) – Pleiotropic meta-analysis

			membrane translocation		
BSG	Basigin (extracellular matrix metalloproteinase inducer (EMMPRIN), cluster of differentiation 147 (CD147))	Membrane Endosome Golgi membrane ER	Transmembrane cell surface glycoprotein Stimulator of IL6 secretion Angiogenesis Targeting of monocarboxylate receptors to membrane	rs201850688 (MAF 0.000399)	Sims et al. (2017) – Exome genotyping array
FLRT2	Fibronectin leucine-rich repeat transmembrane protein	Membrane ER membrane	Cell-cell adhesion Cell migration Mediates axon growth	rs12434216 (MAF 0.2538)	Gouveia et al. (2022) – Polygenic risk score analysis
NECTIN2 (HVEB, PRR2, PVRL2)	Nectin-2	Membrane	Modulates T-cell signalling via CD226 binding	rs146275714* (MAF 0.005192)	Schwartzentruber et al. (2021) – Genome-wide genotyping array

			T-cell proliferation and cytokine production		
NIBAN2 (C9orf88, FAM129B)	Protein Niban 2	Cytoplasm	Suppression of apoptosis	rs2247361 (MAF 0.4816)	Gouveia et al. (2022) – Polygenic risk score analysis

5.3.3 Limitations

A limitation of the experiments described above is that the interactome of Trem2-BirA*-HA does not contain Trem2 signalling partners. Dap12, the major intracellular signalling partner of Trem2, was not captured, indicating that any Trem2-BirA*-HA expressed at the plasma membrane was not activated. To determine this interactome, the BioID experiments described here could be performed in the presence of Trem2-activating antibodies. This would elucidate interacting proteins immediately downstream of Trem2 signalling, providing further insight into the microglial function of Trem2. Proximity-labelling experiments performed under conditions of microglial stimulation, for example by ionomycin, may also provide insights into the mechanisms of Trem2 trafficking from the intracellular vesicle pools to the plasma membrane. Repetition of these experiments with Trem2 AD risk variants and comparison to the wild type interactome may highlight disrupted interactions possibly contributing to AD risk.

Further validation of the localisation of Trem2-BirA*-HA could also be performed to increase the confidence in the correct functioning of the exogenous protein. Antibody internalisation assays could be performed to capture the life cycle of Trem2-BirA*-HA and confirm internalisation and recycling of the protein.

Finally, further analysis of the potential AD risk networks highlighted is needed to establish if these pathways are indeed associated with AD pathology. Gene-set analysis tools such as MAGMA (Multi-marker Analysis of GenoMic Annotation) could determine if these networks show a statistically significant association with AD compared to a random control network (de Leeuw et al., 2015). The networks described above only suggest possible pathways which may be associated with AD risk based on potential interactions between the known AD risk protein TREM2 and other proteins implicated in AD pathophysiology. Robust statistical analysis is required to confidently associate these networks with AD genetic risk.

5.3.4 Conclusions

Overall, the results presented here define a possible protein interactome of Trem2 in unstimulated BV2 cells. The life cycle of Trem2-BirA*-HA through the secretory and endocytic pathways was captured. Trem2-BirA*-HA appeared to interact with known

ER and Golgi proteins involved in both organelle structure and vesicle trafficking. The fusion protein also appeared to exist within the TGN and be trafficked to the plasma membrane. Potential interaction with ubiquitinating enzymes and proteins involved in clathrin vesicle formation suggests Trem2-BirA*-HA was internalised by clathrin-mediated endocytosis. Deubiquitinating enzymes and proteins involved in the retromer complex were also putative interactors, suggesting that at endosomal sorting Trem2-containing vesicles are recycled to the Golgi.

Interactions with other proteins implicated in AD pathophysiology may elucidate common pathways affected by disease, however more robust gene-set analysis is required to fully identify AD risk networks. Further validation of the Trem2-BirA*-HA cell line, particularly concerning the activation state of BV2s, as well as verification of physical interaction with identified putative interactors is required.

Chapter 6 – General Discussion

Coding variants of both *ABI3* and *TREM2* have been identified as risk factors for AD (Sims et al., 2017). ABI3 is a cytoplasmic protein which is part of the WRC, affecting microglial motility and morphology (Moraes et al., 2017). The exact function of ABI3 is not fully understood but is proposed to inhibit activity of the WRC resulting in a reduction of Arp2/3 activity and actin branching (Sekino et al., 2015, Ichigotani et al., 2002, Latini et al., 2011, Hirao et al., 2006). This may promote the formation of parallel actin structures and microglial ramifications. Knockout of Abi3 has been shown to impact microglial morphology and reduce phagocytotic activity (Simonazzi et al., 2021). In AD, ABI3-expressing microglia cluster around Aβ plaques, suggesting that this population of microglia may be recruited to plaques as part of the complex cellular responses involved in neurodegeneration (Satoh et al., 2017). The variant ABI3-S209F (mouse equivalent Abi3-S212F) is associated with a higher risk of AD compared to the wild type, though the mechanism of this risk and molecular link to AD pathology are unknown (Sims et al., 2017).

TREM2 is a transmembrane receptor which influences many cellular functions including inflammation, cell proliferation and survival, and phagocytosis. Nearly 50 variants have been associated with AD (Carmona et al., 2018). Activating ligands of TREM2 are well-documented, but few intracellular binding partners are known. TREM2 intracellular signalling occurs via interaction with DAP12, influencing signalling pathways including MAPK, NF-κB, and PI3K/Akt.

The experiments described in this thesis were designed to elucidate the protein interactomes of Abi3, Abi3-S212F, and Trem2 in BV2 cells. No full protein interactome of these proteins have previously been described in a physiologically relevant cell model. The use of a mouse microglia-like cell line aimed to determine PPIs in a cell system which endogenously expresses binding partners of the bait proteins in BV2 microglia-like cell line.

To achieve this, three major aims were pursued:

1) To determine the protein interactome of Abi3 in microglia-like cells (Chapter 3)
2) To determine the protein interactome of the AD risk variant Abi3-S212F in microglia-like cells (Chapter 4)

3) To determine the intracellular protein interactome of Trem2 in microglia-like cells (Chapter 5)

Investigation of PPIs is important to understand the physiological role and molecular mechanisms of proteins. Discovery of protein interactors has elucidated potential therapeutic targets in disease and identified networks of risk genes highlighting mechanisms of pathology and disease risk (Goehler et al., 2004, Liu et al., 2018, Chojnowski et al., 2015).

6.1 Abi3 and Abi3-S212F Interactomes Give Insights into Mechanisms in Physiology and Disease

The first protein interactome of Abi3 in microglia-like cells was identified in chapter 3 by BioID. Abi3 was found to interact with proteins of the WRC (Wafs2 and Cyfip1), confirming a previously identified role of Abi3 in forming part of this complex. The identification of known Abi3 interactors highlights the efficacy of BioID for detecting interacting proteins. As noted in section 3.3.1.1, although Brick1 and Hem family proteins also form the WRC, neither were identified as putative interactors of Abi3. RNA sequencing showed that while Brick1 was not expressed, transcripts encoding Hem-like proteins were found in BV2 cells (Carrillo-Jimenez et al., 2019). Whether the subunits of the WRC in BV2 cells are identical to the ‘canonical’ microglial WRC remains to be determined (Drew et al., 2020, Preprint).

Abi3 was also found to interact with other cytoskeletal regulatory proteins, including Cep170, a centrosomal protein, and Mtss1 which regulates the actin cytoskeleton independently of the WRC. These data suggest novel roles for Abi3 beyond the WRC, including in inflammatory pathways, possibly through NF-κB signalling via interaction with Ccdc22 or TLR signalling through interaction with Pi3kap1 in the Pi3k signalling pathway. Interaction with Ccdc22 may also suggest a possible role in the regulation of endocytic recycling via the CCC complex and alternative mechanisms of actin regulation. Possible interactions with Gigyf2 and Cyfip1 may implicate Abi3 in translation repression and interactions with Ripk3 may implicate Abi3 in cell death pathways influencing neuroinflammation.

As BioID labels proximal proteins in live cell culture, weak and transient interactions can be detected which may have assisted in the discovery of these novel interactors. However, as physical interaction cannot be confirmed with this method, alternative

techniques to validate these interactions are required. These data however do form a foundation to further explore these specific interactions and illuminate the molecular function by which Abi3 genetic variation increases AD risk in microglia-like cells.

In order to investigate potential mechanisms of AD risk conferred by Abi3-S212F, the protein interactome of the variant was determined by the same method as Abi3 in microglia-like cells. Of the 9 proteins identified as putative interactors of Abi3, 7 were also putative interactors of Abi3-S212F demonstrating the reproducibility of BioID. Interestingly, 14 additional proteins were found to be putative interactors of Abi3-S212F, and 2 interactions were lost. This suggests that the amino acid substitution may influence the ability of Abi3 to bind to specific proteins. The presence of a phenylalanine at position 212 may cause a confirmational change in Abi3, revealing or hiding interaction surfaces in the protein structure. Alternatively, the substitution may unmask post-translational modifications which regulate PPIs. These differences in interactions may explain the increase in AD risk associated with Abi3-S212F by altering cellular responses to external stimuli.

There is limited published research into the functional effects of Abi3-S212F (or the human equivalent S209F), and the results presented here are the first protein interactome of both Abi3 and Abi3-S212F in physiologically relevant cells. The role of ABI3 in microglia has been investigated through ABI3 knockout, which may provide insights into the normal physiological role of the protein but is unlikely to elucidate mechanisms of disease risk (Karahan et al., 2021, Ibanez et al., 2022).The interactomes presented here build on these data by confirming recognised functions of Abi3 via interaction with WRC proteins and provide insights into other possible roles. Comparison of the wild type interactome with that of Abi3-S212F presents possible mechanisms of disease risk through a variety of cellular pathways. Most studies of Abi3-S212F/ABI3-S209F have confirmed the association between the variant and increased risk for AD but have not elucidated mechanisms (Olive et al., 2020, Sims et al., 2017, Dalmasso et al., 2019).

6.2 Trem2 Interactome Highlights the Importance of the Secretory Pathway and Receptor Recycling

The intracellular protein interactome of Trem2 was investigated in chapter 5. The Trem2-BirA*-HA protein was found to primarily reside within the secretory and endocytic pathways. Many of the putative interactors were involved in protein trafficking, Golgi structure, and vesicle transport. The interactome described likely represents the life cycle of Trem2 in BV2 cells under basal conditions and is the first intracellular protein interactome described in a physiologically relevant cell line. Some Trem2 variants are known to be subject to aberrant processing in the ER/Golgi complex resulting in alteration of the glycosylation of Trem2 affecting the trafficking of the protein to the plasma membrane (Hall-Roberts et al., 2020). Comparison of the interactome of wild type Trem2 and that of AD risk variants may elucidate possible mechanisms of risk, potentially by altering interactions of Trem2 with the secretory or endosomal pathways.

Using the proximity labelling technique Turbo ID, TREM2 was found to interact with mitochondria-ER contact sites and expression of TREM2-R47H altered the inter-organelle distance iPSC microglia (Kwak et al., 2023). Overall, 47 novel intracellular interactors were identified in this study, five of which were determined to be putative interactors of Trem2-BirA*-HA here (Hmox2, Emd, Pgrmc2, Gors1, Stam) and 21 were identified by mass spectrometry but not deemed to be putative interactors by SAINTexpress. The difference in these results is likely due to differences between BioID and TurboID, particularly as TurboID has been shown to be more effective in organelles such as the ER (May et al., 2020). This highlights the need for multiple techniques to identify PPIs to determine the full interactome of a protein.

6.3 Abi3 may Influence the Life Cycle of Trem2 via the Endocytic Pathway

Abi3 is known to regulate actin dynamics through inclusion in the WRC. The interactome described in chapter 3 of this thesis included the protein Ccdc22 which is known to form part of the CCC complex. This complex regulates endosomes through association with the cargo recognition complex retriever (Singla et al., 2019). The interactome of Trem2 did not identify putative interactions with proteins known to

associate with retriever, but retromer-interacting proteins were identified along with other endosomal proteins. If interaction between Abi3 and Ccdc22 can be validated and shown to functionally affect the role of the CCC complex in endosomal regulation, it is possible the functioning of Abi3 may impact Trem2 receptor recycling. This putative interaction was lost with Abi3-S212F, meaning any potential role of Abi3 in endosomal recycling may be disrupted with this variant. AD risk may be increased if Trem2-containing endosomes are no longer properly trafficked, reducing Trem2 recycling. Risk could be further increased if a Trem2 variant affecting protein trafficking is also expressed, causing either further disruption of the endosomal pathway, or reducing Trem2 trafficking to the plasma membrane. Comparison of the wild type Trem2 interactome described in chapter 5 with that of a Trem2 AD risk variant may elucidate further mechanisms of risk within the secretory or endosomal pathways. The AD risk variant TREM2-R47H has increased terminal glycosylation which has been suggested to resist proteasomal degradation (Park et al., 2016). This variant has also been shown to disrupt the interaction between Trem2 and Vps35 (Yin et al., 2016). Disruption to protein trafficking is an identified potential mechanism of AD risk conferred by Trem2 variants, an effect which may be compounded by the expression of Abi3-S212F.

Comparison of the Abi3 and Trem2 interactomes also highlights the success of BioID. The efficacy of BioID has been demonstrated by the identification of known protein interactors of Abi3. Additionally, the lack of overlap in the protein interactomes of Abi3 and Trem2 highlights the specificity of BioID in capturing proteins proximal to the bait protein. The exogenous proteins were successfully localised to the cellular compartments in which the endogenous protein is known to reside. Secretory pathway proteins were not identified as putative interactors of Abi3 or Abi3-S212F as SAINTexpress did not determine these proteins to have spectral counts significantly higher than the control. For Trem2, however, these proteins were identified as putative interactors, indicating closer proximity of these proteins to Trem2-BirA*-HA. This agrees with the findings of Go et al. (2021) who concluded that even with bait proteins localised to the same cellular compartment, interactions specific to a particular bait protein could be identified. The BioID technique is therefore suitable to determine interactomes of specific bait proteins.

The results presented in this thesis show that the identification of PPIs with BioID is scalable and could therefore be used to construct a complete map of AD-risk gene in microglia or other relevant cell types.

6.4 Future Directions

The work presented in this thesis defined the first protein interactomes of Abi3 and Trem2 in a physiologically relevant microglial line and the first protein interactome of the AD risk variant Abi3-S212F. However, validation of physical interaction between the putative interactors and the bait proteins could not be demonstrated due to technical difficulties in solubilising the bait and prey proteins and time constraints. To strengthen the conclusions made from the data presented here, pairwise co-IPs in HEK-293T cells expressing both the bait protein and a putative interactor could be used to verify physical interaction. This was attempted in chapters 3 and 5 (sections 3.2.6 and 5.2.6) but conditions for optimal protein extraction that were gentle enough to retain protein complexes could not be achieved. Further investigation and optimisation of the protocol could not be completed due to time constraints. Other techniques to confirm physical interaction, such as Y2H screens of binary interactions or label transfer protein interaction analysis could also be performed.

As discussed in section 3.3.2, an innate limitation of BioID is the requirement of an exogenous bait protein. An interactome determined using endogenous Abi3 and Trem2 is likely to be more physiologically relevant but does require high-quality antibodies against the bait proteins as well as optimisation of protein extraction conditions. Membrane proteins in particular are difficult to solubilise with gentle lysis, therefore an IP with Trem2 as the bait protein may prove particularly difficult. Weak and transient interactions are also likely to be disrupted during lysis whereas they can be captured using BioID. Therefore, comparison of interactors determined by proximity labelling techniques and pull-down of endogenous bait proteins may provide the most accurate protein interactome.

In chapter 5 of this thesis, the cellular localisation of Trem2-BirA*-HA was discussed (section 5.3.1). It was unclear whether the exogenous protein was retained intracellularly alongside endogenous Trem2 or if plasma membrane trafficking was disrupted. Trem2 is known to be stored in Golgi-associated pools and endosomes

(Prada et al., 2006) and immunocytochemical staining combined with the identified protein interactomes presented in chapter 5 suggested that Trem2-BirA*-HA may have been localised to these compartments in a similar way to endogenous Trem2. However, additional analysis such as co-labelling with Golgi markers or more effective visualisation of plasma membrane expressed proteins, is required to fully confirm the cellular location of Trem2-BirA*-HA. Also, as suggested in section 5.3.1, stimulation of microglia by ionomycin increases plasma membrane trafficking of Trem2 (Hoffmann et al., 2003, Prada et al., 2006). Comparison of the location of the HA epitope between stimulated and unstimulated Trem2-BirA*-HA expressing BV2s may confirm if the endogenous protein is able to be trafficked to the plasma membrane. It is possible that the addition of BirA* to the C-terminus of Trem2 hindered the recognition of trafficking signals. The use of a BirA* control protein tagged to a protein known to traffic through the secretory pathway to the plasma membrane may also elucidate the location of Trem2-BirA*-HA. As discussed in section 5.3.3, only proteins on the cytoplasmic face of secretory pathways membranes are likely to be biotinylated by HA-BirA*. By localising the control protein to the secretory pathway, a list of background proteins more accurately reflecting the specific cellular compartment can be generated.

Additionally, Dap12, the main intracellular interactor of Trem2, was not identified as a putative interactor of Trem2-BirA*-HA. This lack of identification of Dap12 may be explained by a lack of exogenous Trem2 expression at the plasma membrane, although some plasma membrane localisation of the HA epitope was possibly identified (Figure 5.3 in section 5.2.1). It is possible that some plasma membrane expression of Trem2-BirA*-HA occurred in the BV2 cells, but Trem2 was not activated. Trem2-Dap12 interaction occurs after Trem2 ligand binding and so BioID experiments conducted on these stable BV2 cells in the presence of a Trem2-activating antibody may identify a protein interactome involved in Trem2 signalling. It is also possible that the addition of BirA* to the short cytoplasmic tail of Trem2 prevented Dap12 interaction. Co-IP experiments in HEK-293T cells transfected with Trem2-BirA*-HA and Dap12 were attempted to assess if direct interaction was possible, however protein extraction was not successful, as described in section 5.2.6.

Comparison of Trem2 interactomes in unstimulated verses stimulated BV2 cells could identify a range of different proteins that interact with Trem2 throughout its life cycle. These same experiments could then be performed on BV2 cells expressing Trem2 AD risk variants and compared to wild type interactomes to highlight possible mechanisms of AD risk.

As discussed above, the capture of prey proteins from an endogenous bait protein would provide a more physiologically relevant protein interactome. To improve this further, an even more physiologically relevant system could be used. The suitability of BV2 cells as a model of microglia was discussed in section 1.2.3 and were deemed to be an appropriate cell line to determine protein interactions as they express the relevant macrophage markers and are negative for other glial cell type markers. BV2 cells are also widely used in research into neurodegeneration. They are freely available and are relatively simple to culture and maintain in large numbers. (Timmerman et al., 2018, Gao et al., 2013, Griciuc et al., 2013, Henn et al., 2009). However, there are inherent limitations with immortalised cells. In the case of BV2 cells, immortalisation was achieved by retroviral transduction of an oncogene, causing increased proliferation and adhesion of immortalised microglia compared to primary cells. The morphology of immortalised and primary microglia also differs (Stansley et al., 2012, Horvath et al., 2008). The results presented here must therefore be interpreted with this in mind as BV2 cells do not accurately reflect the exact state of microglia *in vivo*. Future work should aim to investigate Abi3 and Trem2 interactomes, as well as interactomes of other AD risk variants, in cell types more reflective of *in vivo* states, such as primary or iPSC-derived microglia. The gene editing technique CRIPSR (clustered regularly interspaced short palindromic repeats) could also be used to endogenously tag genes of interest with BirA* through genome editing. This would allow for endogenous expression of the BirA*-tagged bait protein.

6.5 Final Conclusions

The most important findings from the experiments described and results presented in chapters 3 to 5 have been discussed in this final chapter. Protein interactomes of Abi3, Abi3-S212F, and Trem2 from a microglia-like cell line have been generated. For Abi3, interactions with the WRC have been confirmed alongside potential novel

interactions which suggest possible roles for Abi3 in microglia not previously identified, including inflammatory signalling and microtubule organisation. Comparison of this interactome with that of the AD risk variant Abi3-S212F has highlighted possible mechanisms to induce or influence AD pathology. Increased association of Abi3-S212F with the WRC may suggest a reduced ability of these microglia to migrate and regulate their morphology and function. Loss and gain of interactions highlight cellular pathways which may be disrupted by the p.S212F substitution, contributing to AD risk. These data highlight specific proteins and pathways which may provide therapeutic avenues to combat AD pathology.

The protein interactome of Trem2 presented here may reflect the trafficking state of Trem2 in unstimulated BV2 cells. The identification of secretory pathway proteins suggests that Trem2-BirA*-HA may be retained in intracellular pools in unstimulated BV2 cells. Comparison of the interactomes from stimulated verses unstimulated BV2 cells and active verses inactive Trem2 will further elucidate the protein interactors of Trem2 throughout its life cycle as well as increase confidence that the expression of the exogenous protein is comparable to endogenous Trem2.

Together, these results confirm the suitability of BioID to capture protein interactomes in physiologically relevant cells. Although independent validation of the physical interactions between proteins in each interactome is still required, the potential functional consequences of these interactions provide unique insights into the roles of Abi3 and Trem2 in microglia as well as cellular mechanisms of AD risk mediated by Abi3-S212F. Overall, these data present the first protein interactomes of Abi3, Abi3-S212F, and Trem2 in microglia-like cells, contributing to our understanding of the cellular processes involved in AD pathology.

References

ABDUL REHMAN, S. A., KRISTARIYANTO, Y. A., CHOI, S. Y., NKOSI, P. J., WEIDLICH, S., LABIB, K., HOFMANN, K. & KULATHU, Y. 2016. MINDY-1 Is a Member of an Evolutionarily Conserved and Structurally Distinct New Family of Deubiquitinating Enzymes. *Mol Cell,* 63**,** 146-55.

ABRAHAM, R., MOSKVINA, V., SIMS, R., HOLLINGWORTH, P., MORGAN, A., GEORGIEVA, L., DOWZELL, K., CICHON, S., HILLMER, A. M., O'DONOVAN, M. C., WILLIAMS, J., OWEN, M. J. & KIROV, G. 2008. A genome-wide association study for late-onset Alzheimer's disease using DNA pooling. *BMC Med Genomics,* 1**,** 44.

AJAMI, B., BENNETT, J. L., KRIEGER, C., TETZLAFF, W. & ROSSI, F. M. 2007. Local self-renewal can sustain CNS microglia maintenance and function throughout adult life. *Nat Neurosci,* 10**,** 1538-43.

ALBIN, R. L. & TAGLE, D. A. 1995. Genetics and molecular biology of Huntington's disease. *Trends Neurosci,* 18**,** 11-4.

ALLIOT, F., GODIN, I. & PESSAC, B. 1999. Microglia derive from progenitors, originating from the yolk sac, and which proliferate in the brain. *Brain Res Dev Brain Res,* 117**,** 145-52.

ALZHEIMER'S RESEARCH UK 2017. Deaths Due to Dementia. *In:* UK, A. S. R. (ed.).

AMARAL, M. D., HUTT, D. M., TOMATI, V., BOTELHO, H. M. & PEDEMONTE, N. 2020. CFTR processing, trafficking and interactions. *J Cyst Fibros,* 19 Suppl 1**,** S33-s36.

AMAYA RAMIREZ, C. C., HUBBE, P., MANDEL, N. & BÉTHUNE, J. 2018. 4EHP-independent repression of endogenous mRNAs by the RNA-binding protein GIGYF2. *Nucleic Acids Res,* 46**,** 5792-5808.

ANANDATHEERTHAVARADA, H. K., BISWAS, G., ROBIN, M. A. & AVADHANI, N. G. 2003. Mitochondrial targeting and a novel transmembrane arrest of Alzheimer's amyloid precursor protein impairs mitochondrial function in neuronal cells. *J Cell Biol,* 161**,** 41-54.

APOSTOLOVA, L. G. 2016. Alzheimer Disease. *Continuum (Minneap Minn),* 22**,** 419-34.

ASHLEIGH, T., SWERDLOW, R. H. & BEAL, M. F. 2023. The role of mitochondrial dysfunction in Alzheimer's disease pathogenesis. *Alzheimer's & Dementia,* 19**,** 333-342.

ATAGI, Y., LIU, C. C., PAINTER, M. M., CHEN, X. F., VERBEECK, C., ZHENG, H., LI, X., RADEMAKERS, R., KANG, S. S., XU, H., YOUNKIN, S., DAS, P., FRYER, J. D. & BU, G. 2015. Apolipoprotein E Is a Ligand for Triggering Receptor Expressed on Myeloid Cells 2 (TREM2). *J Biol Chem,* 290**,** 26043-50.

AVILA, J. 2008. Tau kinases and phosphatases. *J Cell Mol Med,* 12**,** 258-9.

BAE, J., SUNG, B. H., CHO, I. H., KIM, S. M. & SONG, W. K. 2012a. NESH regulates dendritic spine morphology and synapse formation. *PLoS One,* 7**,** e34677.

BAE, J., SUNG, B. H., CHO, I. H. & SONG, W. K. 2012b. F-actin-dependent regulation of NESH dynamics in rat hippocampal neurons. *PLoS One,* 7**,** e34514.

BAILEY, C. C., DEVAUX, L. B. & FARZAN, M. 2015. The Triggering Receptor Expressed on Myeloid Cells 2 Binds Apolipoprotein E. *J Biol Chem,* 290**,** 26033-42.

BAKER, C. A., MARTIN, D. & MANUELIDIS, L. 2002. Microglia from Creutzfeldt-Jakob disease-infected brains are infectious and show specific mRNA activation profiles. *J Virol,* 76**,** 10905-13.

BANERJEE, S., HELLIER, J., DEWEY, M., ROMEO, R., BALLARD, C., BALDWIN, R., BENTHAM, P., FOX, C., HOLMES, C., KATONA, C., KNAPP, M., LAWTON, C., LINDESAY, J., LIVINGSTON, G., MCCRAE, N., MONIZ-COOK, E., MURRAY, J., NUROCK, S., ORRELL, M., O'BRIEN, J., POPPE, M., THOMAS, A., WALWYN, R., WILSON, K. & BURNS, A. 2011. Sertraline or mirtazapine for depression in dementia (HTA-SADD): a randomised, multicentre, double-blind, placebo-controlled trial. *Lancet,* 378**,** 403-11.

BEECHAM, G. W., HAMILTON, K., NAJ, A. C., MARTIN, E. R., HUENTELMAN, M., MYERS, A. J., CORNEVEAUX, J. J., HARDY, J., VONSATTEL, J. P., YOUNKIN, S. G., BENNETT, D. A., DE JAGER, P. L., LARSON, E. B., CRANE, P. K., KAMBOH, M. I., KOFLER, J. K., MASH, D. C., DUQUE, L.,

GILBERT, J. R., GWIRTSMAN, H., BUXBAUM, J. D., KRAMER, P., DICKSON, D. W., FARRER, L. A., FROSCH, M. P., GHETTI, B., HAINES, J. L., HYMAN, B. T., KUKULL, W. A., MAYEUX, R. P., PERICAK-VANCE, M. A., SCHNEIDER, J. A., TROJANOWSKI, J. Q., REIMAN, E. M., SCHELLENBERG, G. D. & MONTINE, T. J. 2014. Genome-wide association meta-analysis of neuropathologic features of Alzheimer's disease and related dementias. *PLoS Genet,* 10**,** e1004606.

BEHJATI, S. & TARPEY, P. S. 2013. What is next generation sequencing? *Arch Dis Child Educ Pract Ed,* 98**,** 236-8.

BELL, K. F. 2013. Insight into a neuron's preferential susceptibility to oxidative stress. *Biochem Soc Trans,* 41**,** 1541-5.

BERGEN, S. E. & PETRYSHEN, T. L. 2012. Genome-wide association studies of schizophrenia: does bigger lead to better results? *Curr Opin Psychiatry,* 25**,** 76-82.

BHATTACHARJEE, S., ZHAO, Y., DUA, P., ROGAEV, E. I. & LUKIW, W. J. 2016. microRNA-34a-Mediated Down-Regulation of the Microglial-Enriched Triggering Receptor and Phagocytosis-Sensor TREM2 in Age-Related Macular Degeneration. *PLoS One,* 11**,** e0150211.

BILOUSOVA, T., MELNIK, M., MIYOSHI, E., GONZALEZ, B. L., POON, W. W., VINTERS, H. V., MILLER, C. A., CORRADA, M. M., KAWAS, C., HATAMI, A., ALBAY, R., 3RD, GLABE, C. & GYLYS, K. H. 2019. Apolipoprotein E/Amyloid-β Complex Accumulates in Alzheimer Disease Cortical Synapses via Apolipoprotein E Receptors and Is Enhanced by APOE4. *Am J Pathol,* 189**,** 1621-1636.

BIS, J. C., JIAN, X., KUNKLE, B. W., CHEN, Y., HAMILTON-NELSON, K. L., BUSH, W. S., SALERNO, W. J., LANCOUR, D., MA, Y., RENTON, A. E., MARCORA, E., FARRELL, J. J., ZHAO, Y., QU, L., AHMAD, S., AMIN, N., AMOUYEL, P., BEECHAM, G. W., BELOW, J. E., CAMPION, D., CANTWELL, L., CHARBONNIER, C., CHUNG, J., CRANE, P. K., CRUCHAGA, C., CUPPLES, L. A., DARTIGUES, J. F., DEBETTE, S., DELEUZE, J. F., FULTON, L., GABRIEL, S. B., GENIN, E., GIBBS, R. A., GOATE, A., GRENIER-BOLEY, B., GUPTA, N., HAINES, J. L., HAVULINNA, A. S., HELISALMI, S., HILTUNEN, M., HOWRIGAN, D. P., IKRAM, M. A., KAPRIO, J., KONRAD, J., KUZMA, A., LANDER, E. S., LATHROP, M., LEHTIMÄKI, T., LIN, H., MATTILA, K., MAYEUX, R., MUZNY, D. M., NASSER, W., NEALE, B., NHO, K., NICOLAS, G., PATEL, D., PERICAK-VANCE, M. A., PEROLA, M., PSATY, B. M., QUENEZ, O., RAJABLI, F., REDON, R., REITZ, C., REMES, A. M., SALOMAA, V., SARNOWSKI, C., SCHMIDT, H., SCHMIDT, M., SCHMIDT, R., SOININEN, H., THORNTON, T. A., TOSTO, G., TZOURIO, C., VAN DER LEE, S. J., VAN DUIJN, C. M., VALLADARES, O., VARDARAJAN, B., WANG, L. S., WANG, W., WIJSMAN, E., WILSON, R. K., WITTEN, D., WORLEY, K. C., ZHANG, X., BELLENGUEZ, C., LAMBERT, J. C., KURKI, M. I., PALOTIE, A., DALY, M., BOERWINKLE, E., LUNETTA, K. L., DESTEFANO, A. L., DUPUIS, J., MARTIN, E. R., SCHELLENBERG, G. D., SESHADRI, S., NAJ, A. C., FORNAGE, M. & FARRER, L. A. 2020. Whole exome sequencing study identifies novel rare and common Alzheimer's-Associated variants involved in immune response and transcriptional regulation. *Mol Psychiatry,* 25**,** 1859-1875.

BLASI, E., BARLUZZI, R., BOCCHINI, V., MAZZOLLA, R. & BISTONI, F. 1990. Immortalization of murine microglial cells by a v-raf/v-myc carrying retrovirus. *J Neuroimmunol,* 27**,** 229-37.

BLOKLAND, A. 1995. Acetylcholine: a neurotransmitter for learning and memory? *Brain Res Brain Res Rev,* 21**,** 285-300.

BOSSERS, K., WIRZ, K. T. S., MEERHOFF, G. F., ESSING, A. H. W., VAN DONGEN, J. W., HOUBA, P., KRUSE, C. G., VERHAAGEN, J. & SWAAB, D. F. 2010. Concerted changes in transcripts in the prefrontal cortex precede neuropathology in Alzheimer's disease. *Brain,* 133**,** 3699-3723.

BOUCHON, A., DIETRICH, J. & COLONNA, M. 2000. Cutting edge: inflammatory responses can be triggered by TREM-1, a novel receptor expressed on neutrophils and monocytes. *J Immunol,* 164**,** 4991-5.

BOUCHON, A., HERNÁNDEZ-MUNAIN, C., CELLA, M. & COLONNA, M. 2001. A Dap12-Mediated Pathway Regulates Expression of Cc Chemokine Receptor 7 and Maturation of Human Dendritic Cells.

BOWEN, D. M., SMITH, C. B., WHITE, P. & DAVISON, A. N. 1976. Neurotransmitter-related enzymes and indices of hypoxia in senile dementia and other abiotrophies. *Brain,* 99**,** 459-96.

BOZA-SERRANO, A., REYES, J. F., REY, N. L., LEFFLER, H., BOUSSET, L., NILSSON, U., BRUNDIN, P., VENERO, J. L., BURGUILLOS, M. A. & DEIERBORG, T. 2014. The role of Galectin-3 in α-synuclein-induced microglial activation. *Acta Neuropathol Commun,* 2**,** 156.

BRAAK, H. & BRAAK, E. 1991. Neuropathological stageing of Alzheimer-related changes. *Acta Neuropathol,* 82**,** 239-59.

BRAAK, H. & DEL TREDICI, K. 2013. Evolutional aspects of Alzheimer's disease pathogenesis. *J Alzheimers Dis,* 33 Suppl 1**,** S155-61.

BRADLEY, W. D. & KOLESKE, A. J. 2009. Regulation of cell migration and morphogenesis by Abl-family kinases: emerging mechanisms and physiological contexts. *J Cell Sci,* 122**,** 3441-54.

BRANON, T. C., BOSCH, J. A., SANCHEZ, A. D., UDESHI, N. D., SVINKINA, T., CARR, S. A., FELDMAN, J. L., PERRIMON, N. & TING, A. Y. 2018. Efficient proximity labeling in living cells and organisms with TurboID. *Nat Biotechnol,* 36**,** 880-887.

BUNIELLO, A., MACARTHUR, J. A. L., CEREZO, M., HARRIS, L. W., HAYHURST, J., MALANGONE, C., MCMAHON, A., MORALES, J., MOUNTJOY, E., SOLLIS, E., SUVEGES, D., VROUSGOU, O., WHETZEL, P. L., AMODE, R., GUILLEN, J. A., RIAT, H. S., TREVANION, S. J., HALL, P., JUNKINS, H., FLICEK, P., BURDETT, T., HINDORFF, L. A., CUNNINGHAM, F. & PARKINSON, H. 2019. The NHGRI-EBI GWAS Catalog of published genome-wide association studies, targeted arrays and summary statistics 2019. *Nucleic Acids Res,* 47**,** D1005-d1012.

BURDICK, D., SOREGHAN, B., KWON, M., KOSMOSKI, J., KNAUER, M., HENSCHEN, A., YATES, J., COTMAN, C. & GLABE, C. 1992. Assembly and aggregation properties of synthetic Alzheimer's A4/beta amyloid peptide analogs. *J Biol Chem,* 267**,** 546-54.

BUSH, W. S. & MOORE, J. H. 2012. Chapter 11: Genome-wide association studies. *PLoS Comput Biol,* 8**,** e1002822.

BUTOVSKY, O., JEDRYCHOWSKI, M. P., MOORE, C. S., CIALIC, R., LANSER, A. J., GABRIELY, G., KOEGLSPERGER, T., DAKE, B., WU, P. M., DOYKAN, C. E., FANEK, Z., LIU, L., CHEN, Z., ROTHSTEIN, J. D., RANSOHOFF, R. M., GYGI, S. P., ANTEL, J. P. & WEINER, H. L. 2014. Identification of a unique TGF-β-dependent molecular and functional signature in microglia. *Nat Neurosci,* 17**,** 131-43.

BUTTERFIELD, D. A., DRAKE, J., POCERNICH, C. & CASTEGNA, A. 2001. Evidence of oxidative damage in Alzheimer's disease brain: central role for amyloid beta-peptide. *Trends Mol Med,* 7**,** 548-54.

CAI, H., WANG, Y., MCCARTHY, D., WEN, H., BORCHELT, D. R., PRICE, D. L. & WONG, P. C. 2001. BACE1 is the major beta-secretase for generation of Abeta peptides by neurons. *Nat Neurosci,* 4**,** 233-4.

CAI, Z., LIU, N., WANG, C., QIN, B., ZHOU, Y., XIAO, M., CHANG, L., YAN, L. J. & ZHAO, B. 2016. Role of RAGE in Alzheimer's Disease. *Cell Mol Neurobiol,* 36**,** 483-95.

CALL, M. E., WUCHERPFENNIG, K. W. & CHOU, J. J. 2010. The structural basis for intramembrane assembly of an activating immunoreceptor complex. *Nat Immunol,* 11**,** 1023-9.

CALTAGIRONE, C., FERRANNINI, L., MARCHIONNI, N., NAPPI, G., SCAPAGNINI, G. & TRABUCCHI, M. 2012. The potential protective effect of tramiprosate (homotaurine) against Alzheimer's disease: a review. *Aging Clin Exp Res,* 24**,** 580-7.

CARMONA, S., ZAHS, K., WU, E., DAKIN, K., BRAS, J. & GUERREIRO, R. 2018. The role of TREM2 in Alzheimer's disease and other neurodegenerative disorders. *Lancet Neurol,* 17**,** 721-730.

CARRILLO-JIMENEZ, A., DENIZ, O., NIKLISON-CHIROU, M. V., RUIZ, R., BEZERRA-SALOMAO, K., STRATOULIAS, V., AMOUROUX, R., YIP, P. K., VILALTA, A., CHERAY, M., SCOTT-EGERTON, A. M., RIVAS, E., TAYARA, K., GARCIA-DOMINGUEZ, I., GARCIA-REVILLA, J., FERNANDEZ-MARTIN, J. C., ESPINOSA-OLIVA, A. M., SHEN, X., ST GEORGE-HYSLOP, P., BROWN, G. C., HAJKOVA, P., JOSEPH, B., VENERO, J. L., BRANCO, M. R. & BURGUILLOS, M. A. 2019. TET2 Regulates the Neuroinflammatory Response in Microglia. *Cell Rep,* 29**,** 697-713.e8.

CARVALHO, K. M., WINTER, E. & ANTUNES, A. M. D. S. 2015. Analysis of Technological Developments in the Treatment of Alzheimer¡¯s Disease through Patent Documents. *Intelligent Information Management,* Vol.07No.05**,** 14.

CELARAIN, N., SANCHEZ-RUIZ DE GORDOA, J., ZELAYA, M. V., ROLDAN, M., LARUMBE, R., PULIDO, L., ECHAVARRI, C. & MENDIOROZ, M. 2016. TREM2 upregulation correlates with 5-hydroxymethycytosine enrichment in Alzheimer's disease hippocampus. *Clin Epigenetics,* 8**,** 37.

CHAI, K., LIANG, J., ZHANG, X., GU, H., CAO, P., YE, W., TANG, H. L., JINGJING, CHEN, S., WAN, F. & LIU, G. L. S., DAOJIANG 2021. ARHGDIB Plays a Novel Role in the Braak Stages of Alzheimer's Diseases via the Immune Response Mediated by Microglia. *Research Square,* Version 1.

CHAI, X., WU, S., MURRAY, T. K., KINLEY, R., CELLA, C. V., SIMS, H., BUCKNER, N., HANMER, J., DAVIES, P., O'NEILL, M. J., HUTTON, M. L. & CITRON, M. 2011. Passive immunization with anti-Tau antibodies in two transgenic models: reduction of Tau pathology and delay of disease progression. *J Biol Chem,* 286**,** 34457-67.

CHAKRABARTI, R., LEE, M. & HIGGS, H. N. 2021. Multiple roles for actin in secretory and endocytic pathways. *Current Biology,* 31**,** R603-R618.

CHAN, G., WHITE, C. C., WINN, P. A., CIMPEAN, M., REPLOGLE, J. M., GLICK, L. R., CUERDON, N. E., RYAN, K. J., JOHNSON, K. A., SCHNEIDER, J. A., BENNETT, D. A., CHIBNIK, L. B., SPERLING, R. A., BRADSHAW, E. M. & DE JAGER, P. L. 2015. CD33 modulates TREM2: convergence of Alzheimer loci. *Nature Neuroscience,* 18**,** 1556-1558.

CHAPMAN-SMITH, A. & CRONAN, J. E. 1999. Molecular biology of biotin attachment to proteins. *J Nutr,* 129**,** 477S-484S.

CHARTIER-HARLIN, M. C., CRAWFORD, F., HOULDEN, H., WARREN, A., HUGHES, D., FIDANI, L., GOATE, A., ROSSOR, M., ROQUES, P., HARDY, J. & ET AL. 1991. Early-onset Alzheimer's disease caused by mutations at codon 717 of the beta-amyloid precursor protein gene. *Nature,* 353**,** 844-6.

CHEIGNON, C., TOMAS, M., BONNEFONT-ROUSSELOT, D., FALLER, P., HUREAU, C. & COLLIN, F. 2018. Oxidative stress and the amyloid beta peptide in Alzheimer's disease. *Redox Biol,* 14**,** 450-464.

CHEN, B., BRINKMANN, K., CHEN, Z., PAK, C. W., LIAO, Y., SHI, S., HENRY, L., GRISHIN, N. V., BOGDAN, S. & ROSEN, M. K. 2014. The WAVE regulatory complex links diverse receptors to the actin cytoskeleton. *Cell,* 156**,** 195-207.

CHEN, B., CHOU, H.-T., BRAUTIGAM, C. A., XING, W., YANG, S., HENRY, L., DOOLITTLE, L. K., WALZ, T. & ROSEN, M. K. 2017a. Rac1 GTPase activates the WAVE regulatory complex through two distinct binding sites. *eLife,* 6**,** e29795.

CHEN, S., DONG, Z., CHENG, M., ZHAO, Y., WANG, M., SAI, N., WANG, X., LIU, H., HUANG, G. & ZHANG, X. 2017b. Homocysteine exaggerates microglia activation and neuroinflammation through microglia localized STAT3 overactivation following ischemic stroke. *Journal of Neuroinflammation,* 14**,** 187.

CHEN, S., FRAGOZA, R., KLEI, L., LIU, Y., WANG, J., ROEDER, K., DEVLIN, B. & YU, H. 2018. An interactome perturbation framework prioritizes damaging missense mutations for developmental disorders. *Nat Genet,* 50**,** 1032-1040.

CHIU, C. F., GHANEKAR, Y., FROST, L., DIAO, A., MORRISON, D., MCKENZIE, E. & LOWE, M. 2008. ZFPL1, a novel ring finger protein required for cis-Golgi integrity and efficient ER-to-Golgi transport. *Embo j,* 27**,** 934-47.

CHOI, H., LARSEN, B., LIN, Z. Y., BREITKREUTZ, A., MELLACHERUVU, D., FERMIN, D., QIN, Z. S., TYERS, M., GINGRAS, A. C. & NESVIZHSKII, A. I. 2011. SAINT: probabilistic scoring of affinity purification-mass spectrometry data. *Nat Methods,* 8**,** 70-3.

CHOJNOWSKI, A., ONG, P. F., WONG, E. S., LIM, J. S., MUTALIF, R. A., NAVASANKARI, R., DUTTA, B., YANG, H., LIOW, Y. Y., SZE, S. K., BOUDIER, T., WRIGHT, G. D., COLMAN, A., BURKE, B.,

STEWART, C. L. & DREESEN, O. 2015. Progerin reduces LAP2α-telomere association in Hutchinson-Gilford progeria. *eLife,* 4**,** e07759.
CIANCIULLI, A., PORRO, C., CALVELLO, R., TROTTA, T., LOFRUMENTO, D. D. & PANARO, M. A. 2020. Microglia Mediated Neuroinflammation: Focus on PI3K Modulation. *Biomolecules,* 10.
CICVARIC, A., YANG, J., BULAT, T., ZAMBON, A., DOMINGUEZ-RODRIGUEZ, M., KÜHN, R., SADOWICZ, M. G., SIWERT, A., EGEA, J., POLLAK, D. D., MOESLINGER, T. & MONJE, F. J. 2018. Enhanced synaptic plasticity and spatial memory in female but not male FLRT2-haplodeficient mice. *Scientific Reports,* 8**,** 3703.
CLAVAGUERA, F., LAVENIR, I., FALCON, B., FRANK, S., GOEDERT, M. & TOLNAY, M. 2013. "Prion-like" templated misfolding in tauopathies. *Brain Pathol,* 23**,** 342-9.
CLINE, E. N., BICCA, M. A., VIOLA, K. L. & KLEIN, W. L. 2018. The Amyloid-β Oligomer Hypothesis: Beginning of the Third Decade. *J Alzheimers Dis,* 64**,** S567-s610.
COBLEY, J. N., FIORELLO, M. L. & BAILEY, D. M. 2018. 13 reasons why the brain is susceptible to oxidative stress. *Redox Biol,* 15**,** 490-503.
COLIN, M., DUJARDIN, S., SCHRAEN-MASCHKE, S., MENO-TETANG, G., DUYCKAERTS, C., COURADE, J. P. & BUÉE, L. 2020. From the prion-like propagation hypothesis to therapeutic strategies of anti-tau immunotherapy. *Acta Neuropathol,* 139**,** 3-25.
COLLINS, F. S., BROOKS, L. D. & CHAKRAVARTI, A. 1998. A DNA polymorphism discovery resource for research on human genetic variation. *Genome Res,* 8**,** 1229-31.
COLLINS, F. S., GREEN, E. D., GUTTMACHER, A. E. & GUYER, M. S. 2003. A vision for the future of genomics research. *Nature,* 422**,** 835-47.
COLONNA, M. 2003. TREMs in the immune system and beyond. *Nat Rev Immunol,* 3**,** 445-53.
COMAN, H. & NEMES, B. 2017. New Therapeutic Targets in Alzheimer's Disease. *International Journal of Gerontology,* 11.
CONWAY, O. J., CARRASQUILLO, M. M., WANG, X., BREDENBERG, J. M., REDDY, J. S., STRICKLAND, S. L., YOUNKIN, C. S., BURGESS, J. D., ALLEN, M., LINCOLN, S. J., NGUYEN, T., MALPHRUS, K. G., SOTO, A. I., WALTON, R. L., BOEVE, B. F., PETERSEN, R. C., LUCAS, J. A., FERMAN, T. J., CHESHIRE, W. P., VAN GERPEN, J. A., UITTI, R. J., WSZOLEK, Z. K., ROSS, O. A., DICKSON, D. W., GRAFF-RADFORD, N. R. & ERTEKIN-TANER, N. 2018. ABI3 and PLCG2 missense variants as risk factors for neurodegenerative diseases in Caucasians and African Americans. *Mol Neurodegener,* 13**,** 53.
CORDER, E. H., SAUNDERS, A. M., RISCH, N. J., STRITTMATTER, W. J., SCHMECHEL, D. E., GASKELL, P. C., JR., RIMMLER, J. B., LOCKE, P. A., CONNEALLY, P. M., SCHMADER, K. E. & ET AL. 1994. Protective effect of apolipoprotein E type 2 allele for late onset Alzheimer disease. *Nat Genet,* 7**,** 180-4.
COSART, T., BEJA-PEREIRA, A., CHEN, S., NG, S. B., SHENDURE, J. & LUIKART, G. 2011. Exome-wide DNA capture and next generation sequencing in domestic and wild species. *BMC Genomics,* 12**,** 347.
COYAUD, E., MIS, M., LAURENT, E. M., DUNHAM, W. H., COUZENS, A. L., ROBITAILLE, M., GINGRAS, A. C., ANGERS, S. & RAUGHT, B. 2015. BioID-based Identification of Skp Cullin F-box (SCF)β-TrCP1/2 E3 Ligase Substrates. *Mol Cell Proteomics,* 14**,** 1781-95.
CULVER, J. A. & MARIAPPAN, M. 2020. Membrane Protein Biogenesis: PAT Complex Pats Membrane Proteins into Shape. *Current Biology,* 30**,** R1387-R1389.
CUNNINGHAM, C. L., MARTÍNEZ-CERDEÑO, V. & NOCTOR, S. C. 2013. Microglia regulate the number of neural precursor cells in the developing cerebral cortex. *J Neurosci,* 33**,** 4216-33.
D'SOUZA-SCHOREY, C. & CHAVRIER, P. 2006. ARF proteins: roles in membrane traffic and beyond. *Nature Reviews Molecular Cell Biology,* 7**,** 347-358.
DALMASSO, M. C., BRUSCO, L. I., OLIVAR, N., MUCHNIK, C., HANSES, C., MILZ, E., BECKER, J., HEILMANN-HEIMBACH, S., HOFFMANN, P., PRESTIA, F. A., GALEANO, P., AVALOS, M. S. S., MARTINEZ, L. E., CARULLA, M. E., AZURMENDI, P. J., LIBERCZUK, C., FEZZA, C., SAMPAÑO, M., FIERENS, M., JEMAR, G., SOLIS, P., MEDEL, N., LISSO, J., SEVILLANO, Z., BOSCO, P., BOSSÙ, P.,

SPALLETTA, G., GALIMBERTI, D., MANCUSO, M., NACMIAS, B., SORBI, S., MECOCCI, P., PILOTTO, A., CAFFARRA, P., PANZA, F., BULLIDO, M., CLARIMON, J., SÁNCHEZ-JUAN, P., COTO, E., SANCHEZ-GARCIA, F., GRAFF, C., INGELSSON, M., BELLENGUEZ, C., CASTAÑO, E. M., KAIRIYAMA, C., POLITIS, D. G., KOCHEN, S., SCARO, H., MAIER, W., JESSEN, F., MANGONE, C. A., LAMBERT, J. C., MORELLI, L. & RAMIREZ, A. 2019. Transethnic meta-analysis of rare coding variants in PLCG2, ABI3, and TREM2 supports their general contribution to Alzheimer's disease. *Transl Psychiatry,* 9**,** 55.

DARVESH, S. & HOPKINS, D. A. 2003. Differential distribution of butyrylcholinesterase and acetylcholinesterase in the human thalamus. *J Comp Neurol,* 463**,** 25-43.

DAVIES, P. & MALONEY, A. J. 1976. Selective loss of central cholinergic neurons in Alzheimer's disease. *Lancet,* 2**,** 1403.

DAVIS, D. G., SCHMITT, F. A., WEKSTEIN, D. R. & MARKESBERY, W. R. 1999. Alzheimer neuropathologic alterations in aged cognitively normal subjects. *J Neuropathol Exp Neurol,* 58**,** 376-88.

DAWS, M. R., LANIER, L. L., SEAMAN, W. E. & RYAN, J. C. 2001. Cloning and characterization of a novel mouse myeloid DAP12-associated receptor family. *Eur J Immunol,* 31**,** 783-91.

DAWS, M. R., SULLAM, P. M., NIEMI, E. C., CHEN, T. T., TCHAO, N. K. & SEAMAN, W. E. 2003. Pattern recognition by TREM-2: binding of anionic ligands. *J Immunol,* 171**,** 594-9.

DE LEEUW, C. A., MOOIJ, J. M., HESKES, T. & POSTHUMA, D. 2015. MAGMA: generalized gene-set analysis of GWAS data. *PLoS Comput Biol,* 11**,** e1004219.

DEANE, R., SAGARE, A., HAMM, K., PARISI, M., LANE, S., FINN, M. B., HOLTZMAN, D. M. & ZLOKOVIC, B. V. 2008. apoE isoform-specific disruption of amyloid beta peptide clearance from mouse brain. *J Clin Invest,* 118**,** 4002-13.

DEARDORFF, W. J., FEEN, E. & GROSSBERG, G. T. 2015. The Use of Cholinesterase Inhibitors Across All Stages of Alzheimer's Disease. *Drugs Aging,* 32**,** 537-47.

DECKER, M. W. & MCGAUGH, J. L. 1991. The role of interactions between the cholinergic system and other neuromodulatory systems in learning and memory. *Synapse,* 7**,** 151-68.

DECZKOWSKA, A., KEREN-SHAUL, H., WEINER, A., COLONNA, M., SCHWARTZ, M. & AMIT, I. 2018. Disease-Associated Microglia: A Universal Immune Sensor of Neurodegeneration. *Cell,* 173**,** 1073-1081.

DELLO RUSSO, C., CAPPOLI, N., COLETTA, I., MEZZOGORI, D., PACIELLO, F., POZZOLI, G., NAVARRA, P. & BATTAGLIA, A. 2018. The human microglial HMC3 cell line: where do we stand? A systematic literature review. *J Neuroinflammation,* 15**,** 259.

DELRIEU, J., OUSSET, P. J., CAILLAUD, C. & VELLAS, B. 2012. 'Clinical trials in Alzheimer's disease': immunotherapy approaches. *J Neurochem,* 120 Suppl 1**,** 186-93.

DICKSON, D. W., LEE, S. C., MATTIACE, L. A., YEN, S. H. & BROSNAN, C. 1993. Microglia and cytokines in neurological disease, with special reference to AIDS and Alzheimer's disease. *Glia,* 7**,** 75-83.

DINGAR, D., KALKAT, M., CHAN, P. K., SRIKUMAR, T., BAILEY, S. D., TU, W. B., COYAUD, E., PONZIELLI, R., KOLYAR, M., JURISICA, I., HUANG, A., LUPIEN, M., PENN, L. Z. & RAUGHT, B. 2015. BioID identifies novel c-MYC interacting partners in cultured cells and xenograft tumors. *J Proteomics,* 118**,** 95-111.

DIONNE, U., BOURGAULT, É., DUBÉ, A. K., BRADLEY, D., CHARTIER, F. J. M., DANDAGE, R., DIBYACHINTAN, S., DESPRÉS, P. C., GISH, G. D., PHAM, N. T. H., LÉTOURNEAU, M., LAMBERT, J.-P., DOUCET, N., BISSON, N. & LANDRY, C. R. 2021. Protein context shapes the specificity of SH3 domain-mediated interactions in vivo. *Nature Communications,* 12**,** 1597.

DOGGRELL, S. A. & EVANS, S. 2003. Treatment of dementia with neurotransmission modulation. *Expert Opin Investig Drugs,* 12**,** 1633-54.

DOODY, R. S., THOMAS, R. G., FARLOW, M., IWATSUBO, T., VELLAS, B., JOFFE, S., KIEBURTZ, K., RAMAN, R., SUN, X., AISEN, P. S., SIEMERS, E., LIU-SEIFERT, H. & MOHS, R. 2014. Phase 3 trials of solanezumab for mild-to-moderate Alzheimer's disease. *N Engl J Med,* 370**,** 311-21.

DOUVARAS, P., SUN, B., WANG, M., KRUGLIKOV, I., LALLOS, G., ZIMMER, M., TERRENOIRE, C., ZHANG, B., GANDY, S., SCHADT, E., FREYTES, D. O., NOGGLE, S. & FOSSATI, V. 2017. Directed Differentiation of Human Pluripotent Stem Cells to Microglia. *Stem Cell Reports,* 8**,** 1516-1524.

DREW, J., ARANCIBIA-CARCAMO, I. L., JOLIVET, R., LOPEZ-DOMENECH, G., ATTWELL, D. & KITTLER, J. T. 2020. Control of microglial dynamics by Arp2/3 and the autism and schizophrenia-associated protein Cyfip1. *bioRxiv***,** 2020.05.31.124941.

DRUBIN, D. G. & KIRSCHNER, M. W. 1986. Tau protein function in living cells. *J Cell Biol,* 103**,** 2739-46.

DUGGAN, J. M., BUECHLER, M. B., OLSON, R. M., HOHL, T. M. & HAMERMAN, J. A. 2017. BCAP inhibits proliferation and differentiation of myeloid progenitors in the steady state and during demand situations. *Blood,* 129**,** 1503-1513.

DUJARDIN, S., LÉCOLLE, K., CAILLIEREZ, R., BÉGARD, S., ZOMMER, N., LACHAUD, C., CARRIER, S., DUFOUR, N., AURÉGAN, G., WINDERICKX, J., HANTRAYE, P., DÉGLON, N., COLIN, M. & BUÉE, L. 2014. Neuron-to-neuron wild-type Tau protein transfer through a trans-synaptic mechanism: relevance to sporadic tauopathies. *Acta Neuropathol Commun,* 2**,** 14.

DUMANIS, S. B., CHAMBERLAIN, K. A., JIN SOHN, Y., JIN LEE, Y., GUÉNETTE, S. Y., SUZUKI, T., MATHEWS, P. M., PAK, D., REBECK, G. W., SUH, Y. H., PARK, H. S. & HOE, H. S. 2012. FE65 as a link between VLDLR and APP to regulate their trafficking and processing. *Mol Neurodegener,* 7**,** 9.

EDISON, P., ARCHER, H. A., GERHARD, A., HINZ, R., PAVESE, N., TURKHEIMER, F. E., HAMMERS, A., TAI, Y. F., FOX, N., KENNEDY, A., ROSSOR, M. & BROOKS, D. J. 2008. Microglia, amyloid, and cognition in Alzheimer's disease: An [11C](R)PK11195-PET and [11C]PIB-PET study. *Neurobiol Dis,* 32**,** 412-9.

EFTHYMIOU, A. G. & GOATE, A. M. 2017. Late onset Alzheimer's disease genetics implicates microglial pathways in disease risk. *Mol Neurodegener,* 12**,** 43.

EID, A., MHATRE, I. & RICHARDSON, J. R. 2019. Gene-environment interactions in Alzheimer's disease: A potential path to precision medicine. *Pharmacology & Therapeutics,* 199**,** 173-187.

ELROD, K. & BUCCAFUSCO, J. J. 1991. Correlation of the amnestic effects of nicotinic antagonists with inhibition of regional brain acetylcholine synthesis in rats. *J Pharmacol Exp Ther,* 258**,** 403-9.

ERTEKIN-TANER, N. 2010. Genetics of Alzheimer disease in the pre- and post-GWAS era. *Alzheimers Res Ther,* 2**,** 3.

FEDERSPIEL, J. D., GRECO, T. M., LUM, K. K. & CRISTEA, I. M. 2019. Hdac4 Interactions in Huntington's Disease Viewed Through the Prism of Multiomics. *Mol Cell Proteomics,* 18**,** S92-s113.

FERNÁNDEZ-CHACÓN, R., ACHIRILOAIE, M., JANZ, R., ALBANESI, J. P. & SÜDHOF, T. C. 2000. SCAMP1 Function in Endocytosis *. *Journal of Biological Chemistry,* 275**,** 12752-12756.

FERRARI, D., VILLALBA, M., CHIOZZI, P., FALZONI, S., RICCIARDI-CASTAGNOLI, P. & DI VIRGILIO, F. 1996. Mouse microglial cells express a plasma membrane pore gated by extracellular ATP. *J Immunol,* 156**,** 1531-9.

FIGUEROA-HALL, L. K., ANDERSON, M. B., DAS, S., STEVENS, C. W. & DAVIS, R. L. 2017. LPS-induced TLR4 neuroinflammatory signaling in CHME-5 microglial cells. *Neuroimmunology and Neuroinflammation,* 4**,** 219-231.

FONTAINE, S. N., ZHENG, D., SABBAGH, J. J., MARTIN, M. D., CHAPUT, D., DARLING, A., TROTTER, J. H., STOTHERT, A. R., NORDHUES, B. A., LUSSIER, A., BAKER, J., SHELTON, L., KAHN, M., BLAIR, L. J., STEVENS JR, S. M. & DICKEY, C. A. 2016. DnaJ/Hsc70 chaperone complexes control the extracellular release of neurodegenerative-associated proteins. *The EMBO Journal,* 35**,** 1537-1549.

FORABOSCO, P., RAMASAMY, A., TRABZUNI, D., WALKER, R., SMITH, C., BRAS, J., LEVINE, A. P., HARDY, J., POCOCK, J. M., GUERREIRO, R., WEALE, M. E. & RYTEN, M. 2013. Insights into

TREM2 biology by network analysis of human brain gene expression data. *Neurobiol Aging,* 34**,** 2699-714.

FORD, J. W. & MCVICAR, D. W. 2009. TREM and TREM-like receptors in inflammation and disease. *Curr Opin Immunol,* 21**,** 38-46.

FORD, M. G., PEARSE, B. M., HIGGINS, M. K., VALLIS, Y., OWEN, D. J., GIBSON, A., HOPKINS, C. R., EVANS, P. R. & MCMAHON, H. T. 2001. Simultaneous binding of PtdIns(4,5)P2 and clathrin by AP180 in the nucleation of clathrin lattices on membranes. *Science,* 291**,** 1051-5.

FORLENZA, O. V., DE PAULA, V. J., MACHADO-VIEIRA, R., DINIZ, B. S. & GATTAZ, W. F. 2012. Does lithium prevent Alzheimer's disease? *Drugs Aging,* 29**,** 335-42.

FOSTER, E. M., DANGLA-VALLS, A., LOVESTONE, S., RIBE, E. M. & BUCKLEY, N. J. 2019. Clusterin in Alzheimer's Disease: Mechanisms, Genetics, and Lessons From Other Pathologies. *Front Neurosci,* 13**,** 164.

FOX, N. C., FREEBOROUGH, P. A. & ROSSOR, M. N. 1996a. Visualisation and quantification of rates of atrophy in Alzheimer's disease. *Lancet,* 348**,** 94-7.

FOX, N. C., WARRINGTON, E. K., FREEBOROUGH, P. A., HARTIKAINEN, P., KENNEDY, A. M., STEVENS, J. M. & ROSSOR, M. N. 1996b. Presymptomatic hippocampal atrophy in Alzheimer's disease. A longitudinal MRI study. *Brain,* 119 (Pt 6)**,** 2001-7.

FRANCO-BOCANEGRA, D. K., MCAULEY, C., NICOLL, J. A. R. & BOCHE, D. 2019. Molecular Mechanisms of Microglial Motility: Changes in Ageing and Alzheimer's Disease. *Cells,* 8.

FURMAN, R., LEE, J. V. & AXELSEN, P. H. 2018. Analysis of eicosanoid oxidation products in Alzheimer brain by LC-MS with uniformly 13C-labeled internal standards. *Free Radic Biol Med,* 118**,** 108-118.

GALLARDO-VARA, E., RUIZ-LLORENTE, L., CASADO-VELA, J., RUIZ-RODRÍGUEZ, M. J., LÓPEZ-ANDRÉS, N., PATTNAIK, A. K., QUINTANILLA, M. & BERNABEU, C. 2019. Endoglin Protein Interactome Profiling Identifies TRIM21 and Galectin-3 as New Binding Partners. *Cells,* 8.

GANDAL, M. J., LEPPA, V., WON, H., PARIKSHAK, N. N. & GESCHWIND, D. H. 2016. The road to precision psychiatry: translating genetics into disease mechanisms. *Nat Neurosci,* 19**,** 1397-1407.

GAO, F., CHEN, D., HU, Q. & WANG, G. 2013. Rotenone directly induces BV2 cell activation via the p38 MAPK pathway. *PLoS One,* 8**,** e72046.

GARCIA-MESA, Y., JAY, T. R., CHECKLEY, M. A., LUTTGE, B., DOBROWOLSKI, C., VALADKHAN, S., LANDRETH, G. E., KARN, J. & ALVAREZ-CARBONELL, D. 2017. Immortalization of primary microglia: a new platform to study HIV regulation in the central nervous system. *J Neurovirol,* 23**,** 47-66.

GATZ, M., REYNOLDS, C. A., FRATIGLIONI, L., JOHANSSON, B., MORTIMER, J. A., BERG, S., FISKE, A. & PEDERSEN, N. L. 2006. Role of genes and environments for explaining Alzheimer disease. *Arch Gen Psychiatry,* 63**,** 168-74.

GENG, J., ZHAO, C., REN, J. & QU, X. 2010. Alzheimer's disease amyloid beta converting left-handed Z-DNA back to right-handed B-form. *Chem Commun (Camb),* 46**,** 7187-9.

GENTILE, A., D'ALESSANDRO, L., LAZZARI, L., MARTINOGLIO, B., BERTOTTI, A., MIRA, A., LANZETTI, L., COMOGLIO, P. M. & MEDICO, E. 2008. Met-driven invasive growth involves transcriptional regulation of Arhgap12. *Oncogene,* 27**,** 5590-5598.

GILLARDON, F., RIST, W., KUSSMAUL, L., VOGEL, J., BERG, M., DANZER, K., KRAUT, N. & HENGERER, B. 2007. Proteomic and functional alterations in brain mitochondria from Tg2576 mice occur before amyloid plaque deposition. *Proteomics,* 7**,** 605-616.

GINHOUX, F., GRETER, M., LEBOEUF, M., NANDI, S., SEE, P., GOKHAN, S., MEHLER, M. F., CONWAY, S. J., NG, L. G., STANLEY, E. R., SAMOKHVALOV, I. M. & MERAD, M. 2010. Fate mapping analysis reveals that adult microglia derive from primitive macrophages. *Science,* 330**,** 841-5.

GIOVANNONE, B., LEE, E., LAVIOLA, L., GIORGINO, F., CLEVELAND, K. A. & SMITH, R. J. 2003. Two novel proteins that are linked to insulin-like growth factor (IGF-I) receptors by the Grb10 adapter and modulate IGF-I signaling. *J Biol Chem,* 278**,** 31564-73.

GIULIAN, D. & BAKER, T. J. 1986. Characterization of ameboid microglia isolated from developing mammalian brain. *J Neurosci,* 6**,** 2163-78.

GLEBOV, K., WUNDERLICH, P., KARACA, I. & WALTER, J. 2016. Functional involvement of gamma-secretase in signaling of the triggering receptor expressed on myeloid cells-2 (TREM2). *J Neuroinflammation,* 13**,** 17.

GO, C. D., KNIGHT, J. D. R., RAJASEKHARAN, A., RATHOD, B., HESKETH, G. G., ABE, K. T., YOUN, J.-Y., SAMAVARCHI-TEHRANI, P., ZHANG, H., ZHU, L. Y., POPIEL, E., LAMBERT, J.-P., COYAUD, É., CHEUNG, S. W. T., RAJENDRAN, D., WONG, C. J., ANTONICKA, H., PELLETIER, L., PALAZZO, A. F., SHOUBRIDGE, E. A., RAUGHT, B. & GINGRAS, A.-C. 2021. A proximity-dependent biotinylation map of a human cell. *Nature,* 595**,** 120-124.

GOATE, A., CHARTIER-HARLIN, M. C., MULLAN, M., BROWN, J., CRAWFORD, F., FIDANI, L., GIUFFRA, L., HAYNES, A., IRVING, N., JAMES, L. & ET AL. 1991. Segregation of a missense mutation in the amyloid precursor protein gene with familial Alzheimer's disease. *Nature,* 349**,** 704-6.

GOEDERT, M., SPILLANTINI, M. G., JAKES, R., RUTHERFORD, D. & CROWTHER, R. A. 1989. Multiple isoforms of human microtubule-associated protein tau: sequences and localization in neurofibrillary tangles of Alzheimer's disease. *Neuron,* 3**,** 519-26.

GOEHLER, H., LALOWSKI, M., STELZL, U., WAELTER, S., STROEDICKE, M., WORM, U., DROEGE, A., LINDENBERG, K. S., KNOBLICH, M., HAENIG, C., HERBST, M., SUOPANKI, J., SCHERZINGER, E., ABRAHAM, C., BAUER, B., HASENBANK, R., FRITZSCHE, A., LUDEWIG, A. H., BÜSSOW, K., COLEMAN, S. H., GUTEKUNST, C. A., LANDWEHRMEYER, B. G., LEHRACH, H. & WANKER, E. E. 2004. A protein interaction network links GIT1, an enhancer of huntingtin aggregation, to Huntington's disease. *Mol Cell,* 15**,** 853-65.

GONG, C. X., SHAIKH, S., WANG, J. Z., ZAIDI, T., GRUNDKE-IQBAL, I. & IQBAL, K. 1995. Phosphatase activity toward abnormally phosphorylated tau: decrease in Alzheimer disease brain. *J Neurochem,* 65**,** 732-8.

GONG, C. X., SINGH, T. J., GRUNDKE-IQBAL, I. & IQBAL, K. 1993. Phosphoprotein phosphatase activities in Alzheimer disease brain. *J Neurochem,* 61**,** 921-7.

GONZÁLEZ, H., ELGUETA, D., MONTOYA, A. & PACHECO, R. 2014. Neuroimmune regulation of microglial activity involved in neuroinflammation and neurodegenerative diseases. *Journal of Neuroimmunology,* 274**,** 1-13.

GOOD, M. C., ZALATAN, J. G. & LIM, W. A. 2011. Scaffold proteins: hubs for controlling the flow of cellular information. *Science,* 332**,** 680-6.

GORDON, D. E., JANG, G. M., BOUHADDOU, M., XU, J., OBERNIER, K., WHITE, K. M., O'MEARA, M. J., REZELJ, V. V., GUO, J. Z., SWANEY, D. L., TUMMINO, T. A., HÜTTENHAIN, R., KAAKE, R. M., RICHARDS, A. L., TUTUNCUOGLU, B., FOUSSARD, H., BATRA, J., HAAS, K., MODAK, M., KIM, M., HAAS, P., POLACCO, B. J., BRABERG, H., FABIUS, J. M., ECKHARDT, M., SOUCHERAY, M., BENNETT, M. J., CAKIR, M., MCGREGOR, M. J., LI, Q., MEYER, B., ROESCH, F., VALLET, T., MAC KAIN, A., MIORIN, L., MORENO, E., NAING, Z. Z. C., ZHOU, Y., PENG, S., SHI, Y., ZHANG, Z., SHEN, W., KIRBY, I. T., MELNYK, J. E., CHORBA, J. S., LOU, K., DAI, S. A., BARRIO-HERNANDEZ, I., MEMON, D., HERNANDEZ-ARMENTA, C., LYU, J., MATHY, C. J. P., PERICA, T., PILLA, K. B., GANESAN, S. J., SALTZBERG, D. J., RAKESH, R., LIU, X., ROSENTHAL, S. B., CALVIELLO, L., VENKATARAMANAN, S., LIBOY-LUGO, J., LIN, Y., HUANG, X. P., LIU, Y., WANKOWICZ, S. A., BOHN, M., SAFARI, M., UGUR, F. S., KOH, C., SAVAR, N. S., TRAN, Q. D., SHENGJULER, D., FLETCHER, S. J., O'NEAL, M. C., CAI, Y., CHANG, J. C. J., BROADHURST, D. J., KLIPPSTEN, S., SHARP, P. P., WENZELL, N. A., KUZUOGLU-OZTURK, D., WANG, H. Y., TRENKER, R., YOUNG, J. M., CAVERO, D. A., HIATT, J., ROTH, T. L., RATHORE, U., SUBRAMANIAN, A., NOACK, J., HUBERT, M., STROUD, R. M., FRANKEL, A. D., ROSENBERG, O. S., VERBA, K. A., AGARD, D. A., OTT, M., EMERMAN, M., JURA, N., et al. 2020. A SARS-CoV-2 protein interaction map reveals targets for drug repurposing. *Nature,* 583**,** 459-468.

GOSSELIN, D., SKOLA, D., COUFAL, N. G., HOLTMAN, I. R., SCHLACHETZKI, J. C. M., SAJTI, E., JAEGER, B. N., O'CONNOR, C., FITZPATRICK, C., PASILLAS, M. P., PENA, M., ADAIR, A., GONDA, D. D.,

LEVY, M. L., RANSOHOFF, R. M., GAGE, F. H. & GLASS, C. K. 2017. An environment-dependent transcriptional network specifies human microglia identity. *Science,* 356.

GÖTZ, J., CHEN, F., VAN DORPE, J. & NITSCH, R. M. 2001. Formation of neurofibrillary tangles in P301l tau transgenic mice induced by Abeta 42 fibrils. *Science,* 293**,** 1491-5.

GOUVEIA, C., GIBBONS, E., DEHGHANI, N., EAPEN, J., GUERREIRO, R. & BRAS, J. 2022. Genome-wide association of polygenic risk extremes for Alzheimer's disease in the UK Biobank. *Sci Rep,* 12**,** 8404.

GRANT, M. K. O., SHAPIRO, S. L., ASHE, K. H., LIU, P. & ZAHS, K. R. 2019. A Cautionary Tale: Endogenous Biotinylated Proteins and Exogenously-Introduced Protein A Cause Antibody-Independent Artefacts in Western Blot Studies of Brain-Derived Proteins. *Biol Proced Online,* 21**,** 6.

GRICIUC, A., SERRANO-POZO, A., PARRADO, A. R., LESINSKI, A. N., ASSELIN, C. N., MULLIN, K., HOOLI, B., CHOI, S. H., HYMAN, B. T. & TANZI, R. E. 2013. Alzheimer's disease risk gene CD33 inhibits microglial uptake of amyloid beta. *Neuron,* 78**,** 631-43.

GRILL, J. D. & CUMMINGS, J. L. 2010. Current therapeutic targets for the treatment of Alzheimer's disease. *Expert review of neurotherapeutics,* 10**,** 711-728.

GUARGUAGLINI, G., DUNCAN, P. I., STIERHOF, Y. D., HOLMSTRÖM, T., DUENSING, S. & NIGG, E. A. 2005. The forkhead-associated domain protein Cep170 interacts with Polo-like kinase 1 and serves as a marker for mature centrioles. *Mol Biol Cell,* 16**,** 1095-107.

GUERREIRO, R., WOJTAS, A., BRAS, J., CARRASQUILLO, M., ROGAEVA, E., MAJOUNIE, E., CRUCHAGA, C., SASSI, C., KAUWE, J. S., YOUNKIN, S., HAZRATI, L., COLLINGE, J., POCOCK, J., LASHLEY, T., WILLIAMS, J., LAMBERT, J. C., AMOUYEL, P., GOATE, A., RADEMAKERS, R., MORGAN, K., POWELL, J., ST GEORGE-HYSLOP, P., SINGLETON, A. & HARDY, J. 2013. TREM2 variants in Alzheimer's disease. *N Engl J Med,* 368**,** 117-27.

GUO, M. H., HIRSCHHORN, J. N. & DAUBER, A. 2018. Insights and Implications of Genome-Wide Association Studies of Height. *J Clin Endocrinol Metab,* 103**,** 3155-3168.

HAENSELER, W., SANSOM, S. N., BUCHRIESER, J., NEWEY, S. E., MOORE, C. S., NICHOLLS, F. J., CHINTAWAR, S., SCHNELL, C., ANTEL, J. P., ALLEN, N. D., CADER, M. Z., WADE-MARTINS, R., JAMES, W. S. & COWLEY, S. A. 2017. A Highly Efficient Human Pluripotent Stem Cell Microglia Model Displays a Neuronal-Co-culture-Specific Expression Profile and Inflammatory Response. *Stem Cell Reports,* 8**,** 1727-1742.

HALL-ROBERTS, H., AGARWAL, D., OBST, J., SMITH, T. B., MONZÓN-SANDOVAL, J., DI DANIEL, E., WEBBER, C., JAMES, W. S., MEAD, E., DAVIS, J. B. & COWLEY, S. A. 2020. TREM2 Alzheimer's variant R47H causes similar transcriptional dysregulation to knockout, yet only subtle functional phenotypes in human iPSC-derived macrophages. *Alzheimer's Research & Therapy,* 12**,** 151.

HAMMER, M. F., ISHII, A., JOHNSTONE, L., TCHOURBANOV, A., LAU, B., SPRISSLER, R., HALLMARK, B., ZHANG, M., ZHOU, J., WATKINS, J. & HIROSE, S. 2017. Rare variants of small effect size in neuronal excitability genes influence clinical outcome in Japanese cases of SCN1A truncation-positive Dravet syndrome. *PLoS One,* 12**,** e0180485.

HAMOSH, A., SCOTT, A. F., AMBERGER, J. S., BOCCHINI, C. A. & MCKUSICK, V. A. 2005. Online Mendelian Inheritance in Man (OMIM), a knowledgebase of human genes and genetic disorders. *Nucleic Acids Res,* 33**,** D514-7.

HAMPEL, H., MESULAM, M.-M., CUELLO, A. C., FARLOW, M. R., GIACOBINI, E., GROSSBERG, G. T., KHACHATURIAN, A. S., VERGALLO, A., CAVEDO, E., SNYDER, P. J. & KHACHATURIAN, Z. S. 2018. The cholinergic system in the pathophysiology and treatment of Alzheimer's disease. *Brain,* 141**,** 1917-1933.

HAN, J., WANG, M., REN, M. & LOU, H. 2017. Contributions of triggering-receptor-expressed-on-myeloid-cells-2 to neurological diseases. *Int J Neurosci,* 127**,** 368-375.

HARDY, J. & ALLSOP, D. 1991. Amyloid deposition as the central event in the aetiology of Alzheimer's disease. *Trends Pharmacol Sci,* 12**,** 383-8.

HARDY, J. A. & HIGGINS, G. A. 1992. Alzheimer's disease: the amyloid cascade hypothesis. *Science,* 256**,** 184-5.

HAROLD, D., ABRAHAM, R., HOLLINGWORTH, P., SIMS, R., GERRISH, A., HAMSHERE, M. L., PAHWA, J. S., MOSKVINA, V., DOWZELL, K., WILLIAMS, A., JONES, N., THOMAS, C., STRETTON, A., MORGAN, A. R., LOVESTONE, S., POWELL, J., PROITSI, P., LUPTON, M. K., BRAYNE, C., RUBINSZTEIN, D. C., GILL, M., LAWLOR, B., LYNCH, A., MORGAN, K., BROWN, K. S., PASSMORE, P. A., CRAIG, D., MCGUINNESS, B., TODD, S., HOLMES, C., MANN, D., SMITH, A. D., LOVE, S., KEHOE, P. G., HARDY, J., MEAD, S., FOX, N., ROSSOR, M., COLLINGE, J., MAIER, W., JESSEN, F., SCHÜRMANN, B., HEUN, R., VAN DEN BUSSCHE, H., HEUSER, I., KORNHUBER, J., WILTFANG, J., DICHGANS, M., FRÖLICH, L., HAMPEL, H., HÜLL, M., RUJESCU, D., GOATE, A. M., KAUWE, J. S., CRUCHAGA, C., NOWOTNY, P., MORRIS, J. C., MAYO, K., SLEEGERS, K., BETTENS, K., ENGELBORGHS, S., DE DEYN, P. P., VAN BROECKHOVEN, C., LIVINGSTON, G., BASS, N. J., GURLING, H., MCQUILLIN, A., GWILLIAM, R., DELOUKAS, P., AL-CHALABI, A., SHAW, C. E., TSOLAKI, M., SINGLETON, A. B., GUERREIRO, R., MÜHLEISEN, T. W., NÖTHEN, M. M., MOEBUS, S., JÖCKEL, K. H., KLOPP, N., WICHMANN, H. E., CARRASQUILLO, M. M., PANKRATZ, V. S., YOUNKIN, S. G., HOLMANS, P. A., O'DONOVAN, M., OWEN, M. J. & WILLIAMS, J. 2009. Genome-wide association study identifies variants at CLU and PICALM associated with Alzheimer's disease. *Nat Genet,* 41**,** 1088-93.

HARTLEY, D., BLUMENTHAL, T., CARRILLO, M., DIPAOLO, G., ESRALEW, L., GARDINER, K., GRANHOLM, A. C., IQBAL, K., KRAMS, M., LEMERE, C., LOTT, I., MOBLEY, W., NESS, S., NIXON, R., POTTER, H., REEVES, R., SABBAGH, M., SILVERMAN, W., TYCKO, B., WHITTEN, M. & WISNIEWSKI, T. 2015. Down syndrome and Alzheimer's disease: Common pathways, common goals. *Alzheimers Dement,* 11**,** 700-9.

HASEGAWA, M., MORISHIMA-KAWASHIMA, M., TAKIO, K., SUZUKI, M., TITANI, K. & IHARA, Y. 1992. Protein sequence and mass spectrometric analyses of tau in the Alzheimer's disease brain. *J Biol Chem,* 267**,** 17047-54.

HE, Y., PAN, S., XU, M., HE, R., HUANG, W., SONG, P., HUANG, J., ZHANG, H. T. & HU, Y. 2017. Adeno-associated virus 9-mediated Cdk5 inhibitory peptide reverses pathologic changes and behavioral deficits in the Alzheimer's disease mouse model. *Faseb j,* 31**,** 3383-3392.

HEIDARI, A., YAZDANPANAH, N. & REZAEI, N. 2022. The role of Toll-like receptors and neuroinflammation in Parkinson's disease. *Journal of Neuroinflammation,* 19**,** 135.

HENN, A., LUND, S., HEDTJARN, M., SCHRATTENHOLZ, A., PORZGEN, P. & LEIST, M. 2009. The suitability of BV2 cells as alternative model system for primary microglia cultures or for animal experiments examining brain inflammation. *Altex,* 26**,** 83-94.

HENNE, W. M., BOUCROT, E., MEINECKE, M., EVERGREN, E., VALLIS, Y., MITTAL, R. & MCMAHON, H. T. 2010. FCHo Proteins Are Nucleators of Clathrin-Mediated Endocytosis. *Science,* 328**,** 1281-1284.

HERNÁNDEZ, F., GÓMEZ DE BARREDA, E., FUSTER-MATANZO, A., LUCAS, J. J. & AVILA, J. 2010. GSK3: a possible link between beta amyloid peptide and tau protein. *Exp Neurol,* 223**,** 322-5.

HICKEY, K. L., DICKSON, K., COGAN, J. Z., REPLOGLE, J. M., SCHOOF, M., D'ORAZIO, K. N., SINHA, N. K., HUSSMANN, J. A., JOST, M., FROST, A., GREEN, R., WEISSMAN, J. S. & KOSTOVA, K. K. 2020. GIGYF2 and 4EHP Inhibit Translation Initiation of Defective Messenger RNAs to Assist Ribosome-Associated Quality Control. *Molecular Cell,* 79**,** 950-962.e6.

HILLMER, E. J., ZHANG, H., LI, H. S. & WATOWICH, S. S. 2016. STAT3 signaling in immunity. *Cytokine & Growth Factor Reviews,* 31**,** 1-15.

HIPPIUS, H. & NEUNDÖRFER, G. 2003. The discovery of Alzheimer's disease. *Dialogues Clin Neurosci,* 5**,** 101-8.

HIRAO, N., SATO, S., GOTOH, T., MARUOKA, M., SUZUKI, J., MATSUDA, S., SHISHIDO, T. & TANI, K. 2006. NESH (Abi-3) is present in the Abi/WAVE complex but does notpromote c-Abl-mediated phosphorylation. *FEBS Letters,* 580**,** 6464-6470.

HITT, B., RIORDAN, S. M., KUKREJA, L., EIMER, W. A., RAJAPAKSHA, T. W. & VASSAR, R. 2012. β-Site amyloid precursor protein (APP)-cleaving enzyme 1 (BACE1)-deficient mice exhibit a close homolog of L1 (CHL1) loss-of-function phenotype involving axon guidance defects. *J Biol Chem,* 287**,** 38408-25.

HOE, H. S., MAGILL, L. A., GUENETTE, S., FU, Z., VICINI, S. & REBECK, G. W. 2006. FE65 interaction with the ApoE receptor ApoEr2. *J Biol Chem,* 281**,** 24521-30.

HOFFMANN, A., KANN, O., OHLEMEYER, C., HANISCH, U. K. & KETTENMANN, H. 2003. Elevation of basal intracellular calcium as a central element in the activation of brain macrophages (microglia): suppression of receptor-evoked calcium signaling and control of release function. *J Neurosci,* 23**,** 4410-9.

HONG, M., CHEN, D. C., KLEIN, P. S. & LEE, V. M. 1997. Lithium reduces tau phosphorylation by inhibition of glycogen synthase kinase-3. *J Biol Chem,* 272**,** 25326-32.

HORVATH, R. J., NUTILE-MCMENEMY, N., ALKAITIS, M. S. & DELEO, J. A. 2008. Differential migration, LPS-induced cytokine, chemokine, and NO expression in immortalized BV-2 and HAPI cell lines and primary microglial cultures. *J Neurochem,* 107**,** 557-69.

HSIEH, C. L., KOIKE, M., SPUSTA, S. C., NIEMI, E. C., YENARI, M., NAKAMURA, M. C. & SEAMAN, W. E. 2009. A role for TREM2 ligands in the phagocytosis of apoptotic neuronal cells by microglia. *J Neurochem,* 109**,** 1144-56.

HUANG, C., MA, R., SUN, S., WEI, G., FANG, Y., LIU, R. & LI, G. 2008. JAK2-STAT3 signaling pathway mediates thrombin-induced proinflammatory actions of microglia in vitro. *Journal of Neuroimmunology,* 204**,** 118-125.

HULSEN, T. 2022. DeepVenn -- a web application for the creation of area-proportional Venn diagrams using the deep learning framework Tensorflow.js. *Cornell University arxiv*.

HUMPHREYS, D. T., CARVER, J. A., EASTERBROOK-SMITH, S. B. & WILSON, M. R. 1999. Clusterin has chaperone-like activity similar to that of small heat shock proteins. *J Biol Chem,* 274**,** 6875-81.

HUTT, D. M., LOGUERCIO, S., CAMPOS, A. R. & BALCH, W. E. 2018. A Proteomic Variant Approach (ProVarA) for Personalized Medicine of Inherited and Somatic Disease. *J Mol Biol,* 430**,** 2951-2973.

HUTTLIN, E. L., BRUCKNER, R. J., NAVARRETE-PEREA, J., CANNON, J. R., BALTIER, K., GEBREAB, F., GYGI, M. P., THORNOCK, A., ZARRAGA, G., TAM, S., SZPYT, J., GASSAWAY, B. M., PANOV, A., PARZEN, H., FU, S., GOLBAZI, A., MAENPAA, E., STRICKER, K., GUHA THAKURTA, S., ZHANG, T., RAD, R., PAN, J., NUSINOW, D. P., PAULO, J. A., SCHWEPPE, D. K., VAITES, L. P., HARPER, J. W. & GYGI, S. P. 2021. Dual proteome-scale networks reveal cell-specific remodeling of the human interactome. *Cell,* 184**,** 3022-3040.e28.

IBANEZ, K. R., MCFARLAND, K. N., PHILLIPS, J., ALLEN, M., LESSARD, C. B., ZOBEL, L., DE LA CRUZ, E. G., SHAH, S., VO, Q., WANG, X., QUICKSALL, Z., RYU, D., FUNK, C., ERTEKIN-TANER, N., PROKOP, S., GOLDE, T. E. & CHAKRABARTY, P. 2022. Deletion of Abi3/Gngt2 influences age-progressive amyloid β and tau pathologies in distinctive ways. *Alzheimer's Research & Therapy,* 14**,** 104.

ICHIGOTANI, Y., YOKOZAKI, S., FUKUDA, Y., HAMAGUCHI, M. & MATSUDA, S. 2002. Forced expression of NESH suppresses motility and metastatic dissemination of malignant cells. *Cancer Res,* 62**,** 2215-9.

INGELSSON, M., FUKUMOTO, H., NEWELL, K. L., GROWDON, J. H., HEDLEY-WHYTE, E. T., FROSCH, M. P., ALBERT, M. S., HYMAN, B. T. & IRIZARRY, M. C. 2004. Early Abeta accumulation and progressive synaptic loss, gliosis, and tangle formation in AD brain. *Neurology,* 62**,** 925-31.

INNOCENTI, M. 2018. New insights into the formation and the function of lamellipodia and ruffles in mesenchymal cell migration. *Cell Adh Migr,* 12**,** 401-416.

INTERNATIONAL HUMAN GENOME SEQUENCING CONSORTIUM 2004. Finishing the euchromatic sequence of the human genome. *Nature,* 431**,** 931-45.

IQBAL, K., LIU, F. & GONG, C. X. 2016. Tau and neurodegenerative disease: the story so far. *Nat Rev Neurol,* 12**,** 15-27.

ITTNER, L. M. & GÖTZ, J. 2011. Amyloid-β and tau--a toxic pas de deux in Alzheimer's disease. *Nat Rev Neurosci,* 12**,** 65-72.

ITTNER, L. M., KE, Y. D., DELERUE, F., BI, M., GLADBACH, A., VAN EERSEL, J., WÖLFING, H., CHIENG, B. C., CHRISTIE, M. J., NAPIER, I. A., ECKERT, A., STAUFENBIEL, M., HARDEMAN, E. & GÖTZ, J. 2010. Dendritic function of tau mediates amyloid-beta toxicity in Alzheimer's disease mouse models. *Cell,* 142**,** 387-97.

IWATSUBO, T., SAIDO, T. C., MANN, D. M., LEE, V. M. & TROJANOWSKI, J. Q. 1996. Full-length amyloid-beta (1-42(43)) and amino-terminally modified and truncated amyloid-beta 42(43) deposit in diffuse plaques. *Am J Pathol,* 149**,** 1823-30.

JACK, C. R., JR., WISTE, H. J., LESNICK, T. G., WEIGAND, S. D., KNOPMAN, D. S., VEMURI, P., PANKRATZ, V. S., SENJEM, M. L., GUNTER, J. L., MIELKE, M. M., LOWE, V. J., BOEVE, B. F. & PETERSEN, R. C. 2013. Brain β-amyloid load approaches a plateau. *Neurology,* 80**,** 890-6.

JACKSON, M., MARKS, L., MAY, G. H. W. & WILSON, J. B. 2018. The genetic basis of disease. *Essays Biochem,* 62**,** 643-723.

JANABI, N., PEUDENIER, S., HÉRON, B., NG, K. H. & TARDIEU, M. 1995. Establishment of human microglial cell lines after transfection of primary cultures of embryonic microglial cells with the SV40 large T antigen. *Neurosci Lett,* 195**,** 105-8.

JANSEN, I. E., SAVAGE, J. E., WATANABE, K., BRYOIS, J., WILLIAMS, D. M., STEINBERG, S., SEALOCK, J., KARLSSON, I. K., HÄGG, S., ATHANASIU, L., VOYLE, N., PROITSI, P., WITOELAR, A., STRINGER, S., AARSLAND, D., ALMDAHL, I. S., ANDERSEN, F., BERGH, S., BETTELLA, F., BJORNSSON, S., BRÆKHUS, A., BRÅTHEN, G., DE LEEUW, C., DESIKAN, R. S., DJUROVIC, S., DUMITRESCU, L., FLADBY, T., HOHMAN, T. J., JONSSON, P. V., KIDDLE, S. J., RONGVE, A., SALTVEDT, I., SANDO, S. B., SELBÆK, G., SHOAI, M., SKENE, N. G., SNAEDAL, J., STORDAL, E., ULSTEIN, I. D., WANG, Y., WHITE, L. R., HARDY, J., HJERLING-LEFFLER, J., SULLIVAN, P. F., VAN DER FLIER, W. M., DOBSON, R., DAVIS, L. K., STEFANSSON, H., STEFANSSON, K., PEDERSEN, N. L., RIPKE, S., ANDREASSEN, O. A. & POSTHUMA, D. 2019. Genome-wide meta-analysis identifies new loci and functional pathways influencing Alzheimer's disease risk. *Nature Genetics,* 51**,** 404-413.

JANSEN, JOS C., TIMAL, S., VAN SCHERPENZEEL, M., MICHELAKAKIS, H., VICOGNE, D., ASHIKOV, A., MORAITOU, M., HOISCHEN, A., HUIJBEN, K., STEENBERGEN, G., VAN DEN BOOGERT, MARJOLEIN A. W., PORTA, F., CALVO, PIER L., MAVRIKOU, M., CENACCHI, G., VAN DEN BOGAART, G., SALOMON, J., HOLLEBOOM, ADRIAAN G., RODENBURG, RICHARD J., DRENTH, JOOST P. H., HUYNEN, MARTIJN A., WEVERS, RON A., MORAVA, E., FOULQUIER, F., VELTMAN, JORIS A. & LEFEBER, DIRK J. 2016. TMEM199 Deficiency Is a Disorder of Golgi Homeostasis Characterized by Elevated Aminotransferases, Alkaline Phosphatase, and Cholesterol and Abnormal Glycosylation. *The American Journal of Human Genetics,* 98**,** 322-330.

JAY, T. R., HIRSCH, A. M., BROIHIER, M. L., MILLER, C. M., NEILSON, L. E., RANSOHOFF, R. M., LAMB, B. T. & LANDRETH, G. E. 2017a. Disease Progression-Dependent Effects of TREM2 Deficiency in a Mouse Model of Alzheimer's Disease. *J Neurosci,* 37**,** 637-647.

JAY, T. R., MILLER, C. M., CHENG, P. J., GRAHAM, L. C., BEMILLER, S., BROIHIER, M. L., XU, G., MARGEVICIUS, D., KARLO, J. C., SOUSA, G. L., COTLEUR, A. C., BUTOVSKY, O., BEKRIS, L., STAUGAITIS, S. M., LEVERENZ, J. B., PIMPLIKAR, S. W., LANDRETH, G. E., HOWELL, G. R., RANSOHOFF, R. M. & LAMB, B. T. 2015. TREM2 deficiency eliminates TREM2+ inflammatory macrophages and ameliorates pathology in Alzheimer's disease mouse models. *J Exp Med,* 212**,** 287-95.

JAY, T. R., VON SAUCKEN, V. E. & LANDRETH, G. E. 2017b. TREM2 in Neurodegenerative Diseases. *Mol Neurodegener,* 12**,** 56.

JENDRESEN, C., ARSKOG, V., DAWS, M. R. & NILSSON, L. N. 2017. The Alzheimer's disease risk factors apolipoprotein E and TREM2 are linked in a receptor signaling pathway. *J Neuroinflammation,* 14**,** 59.

JENSEN, T. M. T., ALBERTSEN, L., BARTLING, C. R. O., HAUGAARD-KEDSTRÖM, L. M. & STRØMGAARD, K. 2018. Probing the Mint2 Protein-Protein Interaction Network Relevant to the Pathophysiology of Alzheimer's Disease. *Chembiochem*.

JIANG, T., TAN, L., ZHU, X. C., ZHANG, Q. Q., CAO, L., TAN, M. S., GU, L. Z., WANG, H. F., DING, Z. Z., ZHANG, Y. D. & YU, J. T. 2014. Upregulation of TREM2 ameliorates neuropathology and rescues spatial cognitive impairment in a transgenic mouse model of Alzheimer's disease. *Neuropsychopharmacology,* 39**,** 2949-62.

JOHNSON, J. K., HEAD, E., KIM, R., STARR, A. & COTMAN, C. W. 1999. Clinical and pathological evidence for a frontal variant of Alzheimer disease. *Arch Neurol,* 56**,** 1233-9.

JOLLY, S., LANG, V., KOELZER, V. H., SALA FRIGERIO, C., MAGNO, L., SALINAS, P. C., WHITING, P. & PALOMER, E. 2019. Single-Cell Quantification of mRNA Expression in The Human Brain. *Scientific Reports,* 9**,** 12353.

JONES, L., HOLMANS, P. A., HAMSHERE, M. L., HAROLD, D., MOSKVINA, V., IVANOV, D., POCKLINGTON, A., ABRAHAM, R., HOLLINGWORTH, P., SIMS, R., GERRISH, A., PAHWA, J. S., JONES, N., STRETTON, A., MORGAN, A. R., LOVESTONE, S., POWELL, J., PROITSI, P., LUPTON, M. K., BRAYNE, C., RUBINSZTEIN, D. C., GILL, M., LAWLOR, B., LYNCH, A., MORGAN, K., BROWN, K. S., PASSMORE, P. A., CRAIG, D., MCGUINNESS, B., TODD, S., HOLMES, C., MANN, D., SMITH, A. D., LOVE, S., KEHOE, P. G., MEAD, S., FOX, N., ROSSOR, M., COLLINGE, J., MAIER, W., JESSEN, F., SCHÜRMANN, B., HEUN, R., KÖLSCH, H., VAN DEN BUSSCHE, H., HEUSER, I., PETERS, O., KORNHUBER, J., WILTFANG, J., DICHGANS, M., FRÖLICH, L., HAMPEL, H., HÜLL, M., RUJESCU, D., GOATE, A. M., KAUWE, J. S., CRUCHAGA, C., NOWOTNY, P., MORRIS, J. C., MAYO, K., LIVINGSTON, G., BASS, N. J., GURLING, H., MCQUILLIN, A., GWILLIAM, R., DELOUKAS, P., AL-CHALABI, A., SHAW, C. E., SINGLETON, A. B., GUERREIRO, R., MÜHLEISEN, T. W., NÖTHEN, M. M., MOEBUS, S., JÖCKEL, K. H., KLOPP, N., WICHMANN, H. E., RÜTHER, E., CARRASQUILLO, M. M., PANKRATZ, V. S., YOUNKIN, S. G., HARDY, J., O'DONOVAN, M. C., OWEN, M. J. & WILLIAMS, J. 2010. Genetic evidence implicates the immune system and cholesterol metabolism in the aetiology of Alzheimer's disease. *PLoS One,* 5**,** e13950.

JONSSON, T., STEFANSSON, H., STEINBERG, S., JONSDOTTIR, I., JONSSON, P. V., SNAEDAL, J., BJORNSSON, S., HUTTENLOCHER, J., LEVEY, A. I., LAH, J. J., RUJESCU, D., HAMPEL, H., GIEGLING, I., ANDREASSEN, O. A., ENGEDAL, K., ULSTEIN, I., DJUROVIC, S., IBRAHIM-VERBAAS, C., HOFMAN, A., IKRAM, M. A., VAN DUIJN, C. M., THORSTEINSDOTTIR, U., KONG, A. & STEFANSSON, K. 2013. Variant of TREM2 associated with the risk of Alzheimer's disease. *N Engl J Med,* 368**,** 107-16.

JUN, G. R., CHUNG, J., MEZ, J., BARBER, R., BEECHAM, G. W., BENNETT, D. A., BUXBAUM, J. D., BYRD, G. S., CARRASQUILLO, M. M., CRANE, P. K., CRUCHAGA, C., DE JAGER, P., ERTEKIN-TANER, N., EVANS, D., FALLIN, M. D., FOROUD, T. M., FRIEDLAND, R. P., GOATE, A. M., GRAFF-RADFORD, N. R., HENDRIE, H., HALL, K. S., HAMILTON-NELSON, K. L., INZELBERG, R., KAMBOH, M. I., KAUWE, J. S. K., KUKULL, W. A., KUNKLE, B. W., KUWANO, R., LARSON, E. B., LOGUE, M. W., MANLY, J. J., MARTIN, E. R., MONTINE, T. J., MUKHERJEE, S., NAJ, A., REIMAN, E. M., REITZ, C., SHERVA, R., ST GEORGE-HYSLOP, P. H., THORNTON, T., YOUNKIN, S. G., VARDARAJAN, B. N., WANG, L. S., WENDLUND, J. R., WINSLOW, A. R., HAINES, J., MAYEUX, R., PERICAK-VANCE, M. A., SCHELLENBERG, G., LUNETTA, K. L. & FARRER, L. A. 2017. Transethnic genome-wide scan identifies novel Alzheimer's disease loci. *Alzheimers Dement,* 13**,** 727-738.

KANYENDA, L. J., VERDILE, G., BOULOS, S., KRISHNASWAMY, S., TADDEI, K., MELONI, B. P., MASTAGLIA, F. L. & MARTINS, R. N. 2011. The Dynamics of CD147 in Alzheimer's Disease Development and Pathology. *Journal of Alzheimer's Disease,* 26**,** 593-605.

KARAHAN, H., SMITH, D. C., KIM, B., DABIN, L. C., AL-AMIN, M. M., WIJERATNE, H. R. S., PENNINGTON, T., VIANA DI PRISCO, G., MCCORD, B., LIN, P. B., LI, Y., PENG, J., OBLAK, A. L., CHU, S., ATWOOD, B. K. & KIM, J. 2021. Deletion of Abi3 gene locus exacerbates neuropathological features of Alzheimer's disease in a mouse model of Aβ amyloidosis. *Sci Adv,* 7**,** eabe3954.

KAWABATA GALBRAITH, K., FUJISHIMA, K., MIZUNO, H., LEE, S. J., UEMURA, T., SAKIMURA, K., MISHINA, M., WATANABE, N. & KENGAKU, M. 2018. MTSS1 Regulation of Actin-Nucleating Formin DAAM1 in Dendritic Filopodia Determines Final Dendritic Configuration of Purkinje Cells. *Cell Rep,* 24**,** 95-106.e9.

KAWABORI, M., KACIMI, R., KAUPPINEN, T., CALOSING, C., KIM, J. Y., HSIEH, C. L., NAKAMURA, M. C. & YENARI, M. A. 2015. Triggering receptor expressed on myeloid cells 2 (TREM2) deficiency attenuates phagocytic activities of microglia and exacerbates ischemic damage in experimental stroke. *J Neurosci,* 35**,** 3384-96.

KELLEHER, R. J., 3RD & SHEN, J. 2010. Genetics. Gamma-secretase and human disease. *Science,* 330**,** 1055-6.

KEREN-SHAUL, H., SPINRAD, A., WEINER, A., MATCOVITCH-NATAN, O., DVIR-SZTERNFELD, R., ULLAND, T. K., DAVID, E., BARUCH, K., LARA-ASTAISO, D., TOTH, B., ITZKOVITZ, S., COLONNA, M., SCHWARTZ, M. & AMIT, I. 2017. A Unique Microglia Type Associated with Restricting Development of Alzheimer's Disease. *Cell,* 169**,** 1276-1290.e17.

KHAN, M., YOUN, J. Y., GINGRAS, A. C., SUBRAMANIAM, R. & DESVEAUX, D. 2018. In planta proximity dependent biotin identification (BioID). *Sci Rep,* 8**,** 9212.

KIIALAINEN, A., VECKMAN, V., SAHARINEN, J., PALONEVA, J., GENTILE, M., HAKOLA, P., HEMELSOET, D., RIDHA, B., KOPRA, O., JULKUNEN, I. & PELTONEN, L. 2007. Transcript profiles of dendritic cells of PLOSL patients link demyelinating CNS disorders with abnormalities in pathways of actin bundling and immune response. *J Mol Med (Berl),* 85**,** 971-83.

KIKUCHI, M., SEKIYA, M., HARA, N., MIYASHITA, A., KUWANO, R., IKEUCHI, T., IIJIMA, K. M. & NAKAYA, A. 2020. Disruption of a RAC1-centred network is associated with Alzheimer's disease pathology and causes age-dependent neurodegeneration. *Human Molecular Genetics,* 29**,** 817-833.

KIM, D. I., BIRENDRA, K. C., ZHU, W., MOTAMEDCHABOKI, K., DOYE, V. & ROUX, K. J. 2014. Probing nuclear pore complex architecture with proximity-dependent biotinylation. *Proc Natl Acad Sci U S A,* 111**,** E2453-61.

KIM, D. I., JENSEN, S. C., NOBLE, K. A., KC, B., ROUX, K. H., MOTAMEDCHABOKI, K. & ROUX, K. J. 2016. An improved smaller biotin ligase for BioID proximity labeling. *Mol Biol Cell,* 27**,** 1188-96.

KIM, K. S., MARCOGLIESE, P. C., YANG, J., CALLAGHAN, S. M., RESENDE, V., ABDEL-MESSIH, E., MARRAS, C., VISANJI, N. P., HUANG, J., SCHLOSSMACHER, M. G., TRINKLE-MULCAHY, L., SLACK, R. S., LANG, A. E. & PARK, D. S. 2018. Regulation of myeloid cell phagocytosis by LRRK2 via WAVE2 complex stabilization is altered in Parkinson's disease. *Proc Natl Acad Sci U S A,* 115**,** E5164-e5173.

KLEIN, R. J., ZEISS, C., CHEW, E. Y., TSAI, J. Y., SACKLER, R. S., HAYNES, C., HENNING, A. K., SANGIOVANNI, J. P., MANE, S. M., MAYNE, S. T., BRACKEN, M. B., FERRIS, F. L., OTT, J., BARNSTABLE, C. & HOH, J. 2005. Complement factor H polymorphism in age-related macular degeneration. *Science,* 308**,** 385-9.

KLEINBERGER, G., YAMANISHI, Y., SUÁREZ-CALVET, M., CZIRR, E., LOHMANN, E., CUYVERS, E., STRUYFS, H., PETTKUS, N., WENNINGER-WEINZIERL, A., MAZAHERI, F., TAHIROVIC, S., LLEÓ, A., ALCOLEA, D., FORTEA, J., WILLEM, M., LAMMICH, S., MOLINUEVO, J. L., SÁNCHEZ-VALLE, R., ANTONELL, A., RAMIREZ, A., HENEKA, M. T., SLEEGERS, K., VAN DER ZEE, J., MARTIN, J. J., ENGELBORGHS, S., DEMIRTAS-TATLIDEDE, A., ZETTERBERG, H., VAN BROECKHOVEN, C., GURVIT, H., WYSS-CORAY, T., HARDY, J., COLONNA, M. & HAASS, C. 2014. TREM2 mutations implicated in neurodegeneration impair cell surface transport and phagocytosis. *Sci Transl Med,* 6**,** 243ra86.

KLESNEY-TAIT, J., TURNBULL, I. R. & COLONNA, M. 2006. The TREM receptor family and signal integration. *Nat Immunol,* 7**,** 1266-73.

KONISHI, H. & KIYAMA, H. 2018. Microglial TREM2/DAP12 Signaling: A Double-Edged Sword in Neural Diseases. *Front Cell Neurosci,* 12**,** 206.

KOSIK, K. S., ORECCHIO, L. D., BAKALIS, S. & NEVE, R. L. 1989. Developmentally regulated expression of specific tau sequences. *Neuron,* 2**,** 1389-97.

KRAUTHAMMER, M., KAUFMANN, C. A., GILLIAM, T. C. & RZHETSKY, A. 2004. Molecular triangulation: bridging linkage and molecular-network information for identifying candidate genes in Alzheimer's disease. *Proc Natl Acad Sci U S A,* 101**,** 15148-53.

KUHN, P. H., WANG, H., DISLICH, B., COLOMBO, A., ZEITSCHEL, U., ELLWART, J. W., KREMMER, E., ROSSNER, S. & LICHTENTHALER, S. F. 2010. ADAM10 is the physiologically relevant, constitutive alpha-secretase of the amyloid precursor protein in primary neurons. *Embo j,* 29**,** 3020-32.

KULMINSKI, A. M., LOIKO, E., LOIKA, Y. & CULMINSKAYA, I. 2022. Pleiotropic predisposition to Alzheimer's disease and educational attainment: insights from the summary statistics analysis. *Geroscience,* 44**,** 265-280.

KURISU, S. & TAKENAWA, T. 2009. The WASP and WAVE family proteins. *Genome Biol,* 10**,** 226.

KUROCHKINA, N. & GUHA, U. 2013. SH3 domains: modules of protein-protein interactions. *Biophys Rev,* 5**,** 29-39.

KWAK, C., FINAN, G. M., PARK, Y. R., MUN, J. Y., RHEE, H.-W. & KIM, T.-W. 2023. Spatial Proteomics Reveals Novel TREM2 Interactors in ER-Mitochondria Interface in Microglia. *bioRxiv***,** 2023.03.21.533722.

KWON, K. & BECKETT, D. 2000. Function of a conserved sequence motif in biotin holoenzyme synthetases. *Protein Sci,* 9**,** 1530-9.

KWON, K., STREAKER, E. D., RUPARELIA, S. & BECKETT, D. 2000. Multiple disordered loops function in corepressor-induced dimerization of the biotin repressor. *J Mol Biol,* 304**,** 821-33.

LADU, M. J., FALDUTO, M. T., MANELLI, A. M., REARDON, C. A., GETZ, G. S. & FRAIL, D. E. 1994. Isoform-specific binding of apolipoprotein E to beta-amyloid. *J Biol Chem,* 269**,** 23403-6.

LAMBERT, J. C., HEATH, S., EVEN, G., CAMPION, D., SLEEGERS, K., HILTUNEN, M., COMBARROS, O., ZELENIKA, D., BULLIDO, M. J., TAVERNIER, B., LETENNEUR, L., BETTENS, K., BERR, C., PASQUIER, F., FIEVET, N., BARBERGER-GATEAU, P., ENGELBORGHS, S., DE DEYN, P., MATEO, I., FRANCK, A., HELISALMI, S., PORCELLINI, E., HANON, O., DE PANCORBO, M. M., LENDON, C., DUFOUIL, C., JAILLARD, C., LEVEILLARD, T., ALVAREZ, V., BOSCO, P., MANCUSO, M., PANZA, F., NACMIAS, B., BOSSU, P., PICCARDI, P., ANNONI, G., SERIPA, D., GALIMBERTI, D., HANNEQUIN, D., LICASTRO, F., SOININEN, H., RITCHIE, K., BLANCHE, H., DARTIGUES, J. F., TZOURIO, C., GUT, I., VAN BROECKHOVEN, C., ALPEROVITCH, A., LATHROP, M. & AMOUYEL, P. 2009. Genome-wide association study identifies variants at CLU and CR1 associated with Alzheimer's disease. *Nat Genet,* 41**,** 1094-9.

LAMBERT, J. C., IBRAHIM-VERBAAS, C. A., HAROLD, D., NAJ, A. C., SIMS, R., BELLENGUEZ, C., DESTAFANO, A. L., BIS, J. C., BEECHAM, G. W., GRENIER-BOLEY, B., RUSSO, G., THORTON-WELLS, T. A., JONES, N., SMITH, A. V., CHOURAKI, V., THOMAS, C., IKRAM, M. A., ZELENIKA, D., VARDARAJAN, B. N., KAMATANI, Y., LIN, C. F., GERRISH, A., SCHMIDT, H., KUNKLE, B., DUNSTAN, M. L., RUIZ, A., BIHOREAU, M. T., CHOI, S. H., REITZ, C., PASQUIER, F., CRUCHAGA, C., CRAIG, D., AMIN, N., BERR, C., LOPEZ, O. L., DE JAGER, P. L., DERAMECOURT, V., JOHNSTON, J. A., EVANS, D., LOVESTONE, S., LETENNEUR, L., MORÓN, F. J., RUBINSZTEIN, D. C., EIRIKSDOTTIR, G., SLEEGERS, K., GOATE, A. M., FIÉVET, N., HUENTELMAN, M. W., GILL, M., BROWN, K., KAMBOH, M. I., KELLER, L., BARBERGER-GATEAU, P., MCGUINESS, B., LARSON, E. B., GREEN, R., MYERS, A. J., DUFOUIL, C., TODD, S., WALLON, D., LOVE, S., ROGAEVA, E., GALLACHER, J., ST GEORGE-HYSLOP, P., CLARIMON, J., LLEO, A., BAYER, A., TSUANG, D. W., YU, L., TSOLAKI, M., BOSSÙ, P., SPALLETTA, G., PROITSI, P., COLLINGE, J., SORBI, S., SANCHEZ-GARCIA, F., FOX, N. C., HARDY, J., DENIZ NARANJO, M. C., BOSCO, P.,

CLARKE, R., BRAYNE, C., GALIMBERTI, D., MANCUSO, M., MATTHEWS, F., MOEBUS, S., MECOCCI, P., DEL ZOMPO, M., MAIER, W., HAMPEL, H., PILOTTO, A., BULLIDO, M., PANZA, F., CAFFARRA, P., NACMIAS, B., GILBERT, J. R., MAYHAUS, M., LANNEFELT, L., HAKONARSON, H., PICHLER, S., et al. 2013. Meta-analysis of 74,046 individuals identifies 11 new susceptibility loci for Alzheimer's disease. *Nat Genet,* 45**,** 1452-8.

LANE, R. M., POTKIN, S. G. & ENZ, A. 2006. Targeting acetylcholinesterase and butyrylcholinesterase in dementia. *Int J Neuropsychopharmacol,* 9**,** 101-24.

LANIER, L. L., CORLISS, B. C., WU, J., LEONG, C. & PHILLIPS, J. H. 1998. Immunoreceptor DAP12 bearing a tyrosine-based activation motif is involved in activating NK cells. *Nature,* 391**,** 703-7.

LARSSON, S. C., TRAYLOR, M., MALIK, R., DICHGANS, M., BURGESS, S. & MARKUS, H. S. 2017. Modifiable pathways in Alzheimer's disease: Mendelian randomisation analysis. *BMJ,* 359**,** j5375.

LASSER, R., SCHELTENS, P., DUBOIS, B., NIKOLCHEVA, T., RETOUT, S., VOLZ, D., CSOBOTH, C. & BOADA, M. 2016. Poster Number: NR 31 - Efficacy, Safety and Biomarker Data from SCarlet RoAD—a Global Phase 3 Study of Gantenerumab in Patients with Prodromal AD. *The American Journal of Geriatric Psychiatry,* 24**,** S161-S162.

LATINI, F. R., HEMERLY, J. P., FREITAS, B. C., OLER, G., RIGGINS, G. J. & CERUTTI, J. M. 2011. ABI3 ectopic expression reduces in vitro and in vivo cell growth properties while inducing senescence. *BMC Cancer,* 11**,** 11.

LAU, C. G., TAKEUCHI, K., RODENAS-RUANO, A., TAKAYASU, Y., MURPHY, J., BENNETT, M. V. & ZUKIN, R. S. 2009. Regulation of NMDA receptor Ca2+ signalling and synaptic plasticity. *Biochem Soc Trans,* 37**,** 1369-74.

LAU, K. F., MCLOUGHLIN, D. M., STANDEN, C. & MILLER, C. C. 2000. X11 alpha and x11 beta interact with presenilin-1 via their PDZ domains. *Mol Cell Neurosci,* 16**,** 557-65.

LEBOIS, E. P., THORN, C., EDGERTON, J. R., POPIOLEK, M. & XI, S. 2018. Muscarinic receptor subtype distribution in the central nervous system and relevance to aging and Alzheimer's disease. *Neuropharmacology,* 136**,** 362-373.

LEE, J. H., LAU, K. F., PERKINTON, M. S., STANDEN, C. L., ROGELJ, B., FALINSKA, A., MCLOUGHLIN, D. M. & MILLER, C. C. 2004. The neuronal adaptor protein X11beta reduces amyloid beta-protein levels and amyloid plaque formation in the brains of transgenic mice. *J Biol Chem,* 279**,** 49099-104.

LEE, J. H., LAU, K. F., PERKINTON, M. S., STANDEN, C. L., SHEMILT, S. J., MERCKEN, L., COOPER, J. D., MCLOUGHLIN, D. M. & MILLER, C. C. 2003. The neuronal adaptor protein X11alpha reduces Abeta levels in the brains of Alzheimer's APPswe Tg2576 transgenic mice. *J Biol Chem,* 278**,** 47025-9.

LEISHMAN, E., MACKIE, K. & BRADSHAW, H. B. 2019. Elevated Levels of Arachidonic Acid-Derived Lipids Including Prostaglandins and Endocannabinoids Are Present Throughout ABHD12 Knockout Brains: Novel Insights Into the Neurodegenerative Phenotype. *Front Mol Neurosci,* 12**,** 142.

LENZ, K. M. & NELSON, L. H. 2018. Microglia and Beyond: Innate Immune Cells As Regulators of Brain Development and Behavioral Function. *Front Immunol,* 9**,** 698.

LEVY-LAHAD, E., WASCO, W., POORKAJ, P., ROMANO, D. M., OSHIMA, J., PETTINGELL, W. H., YU, C. E., JONDRO, P. D., SCHMIDT, S. D., WANG, K. & ET AL. 1995. Candidate gene for the chromosome 1 familial Alzheimer's disease locus. *Science,* 269**,** 973-7.

LEWIS, F., SCHAFFER, S. K., SUSSEX, J., O'NEILL, P. & COCKCROFT, L. 2014. The Trajectory of Dementia in the UK - Making a Difference. https://www.ohe.org/publications/trajectory-dementia-uk-making-difference#: Office of Health Economics Consulting.

LEWIS, J., DICKSON, D. W., LIN, W. L., CHISHOLM, L., CORRAL, A., JONES, G., YEN, S. H., SAHARA, N., SKIPPER, L., YAGER, D., ECKMAN, C., HARDY, J., HUTTON, M. & MCGOWAN, E. 2001.

Enhanced neurofibrillary degeneration in transgenic mice expressing mutant tau and APP. *Science,* 293**,** 1487-91.

LI, J., SHINODA, Y., OGAWA, S., IKEGAYA, S., LI, S., MATSUYAMA, Y., SATO, K. & YAMAGISHI, S. 2021. Expression of FLRT2 in Postnatal Central Nervous System Development and After Spinal Cord Injury. *Frontiers in Molecular Neuroscience,* 14.

LI, R.-Y., QIN, Q., YANG, H.-C., WANG, Y.-Y., MI, Y.-X., YIN, Y.-S., WANG, M., YU, C.-J. & TANG, Y. 2022. TREM2 in the pathogenesis of AD: a lipid metabolism regulator and potential metabolic therapeutic target. *Molecular Neurodegeneration,* 17**,** 40.

LIAO, F., YOON, H. & KIM, J. 2017. Apolipoprotein E metabolism and functions in brain and its role in Alzheimer's disease. *Curr Opin Lipidol,* 28**,** 60-67.

LIAO, F., ZHANG, T. J., JIANG, H., LEFTON, K. B., ROBINSON, G. O., VASSAR, R., SULLIVAN, P. M. & HOLTZMAN, D. M. 2015. Murine versus human apolipoprotein E4: differential facilitation of and co-localization in cerebral amyloid angiopathy and amyloid plaques in APP transgenic mouse models. *Acta Neuropathol Commun,* 3**,** 70.

LICASTRO, F., CARBONE, I., IANNI, M. & PORCELLINI, E. 2011. Gene Signature in Alzheimer's Disease and Environmental Factors: The Virus Chronicle. *Journal of Alzheimer's Disease,* 27**,** 809-817.

LIN, J., LIU, J., WANG, Y., ZHU, J., ZHOU, K., SMITH, N. & ZHAN, X. 2005. Differential regulation of cortactin and N-WASP-mediated actin polymerization by missing in metastasis (MIM) protein. *Oncogene,* 24**,** 2059-66.

LIN, W. L., LEWIS, J., YEN, S. H., HUTTON, M. & DICKSON, D. W. 2003. Ultrastructural neuronal pathology in transgenic mice expressing mutant (P301L) human tau. *J Neurocytol,* 32**,** 1091-105.

LINDERS, P. T., HORST, C. V., BEEST, M. T. & VAN DEN BOGAART, G. 2019. Stx5-Mediated ER-Golgi Transport in Mammals and Yeast. *Cells,* 8.

LINNARTZ-GERLACH, B., BODEA, L. G., KLAUS, C., GINOLHAC, A., HALDER, R., SINKKONEN, L., WALTER, J., COLONNA, M. & NEUMANN, H. 2019. TREM2 triggers microglial density and age-related neuronal loss. *Glia,* 67**,** 539-550.

LIU, B., ARCHER, C. T., BURDINE, L., GILLETTE, T. G. & KODADEK, T. 2007. Label transfer chemistry for the characterization of protein-protein interactions. *J Am Chem Soc,* 129**,** 12348-9.

LIU, C.-C., KANEKIYO, T., XU, H. & BU, G. 2013. Apolipoprotein E and Alzheimer disease: risk, mechanisms and therapy. *Nature Reviews Neurology,* 9**,** 106-118.

LIU, H., SADYGOV, R. G. & YATES, J. R. 2004. A Model for Random Sampling and Estimation of Relative Protein Abundance in Shotgun Proteomics. *Analytical Chemistry,* 76**,** 4193-4201.

LIU, J., LI, M., LUO, X. J. & SU, B. 2018. Systems-level analysis of risk genes reveals the modular nature of schizophrenia. *Schizophr Res,* 201**,** 261-269.

LIU, S., LIU, Y., HAO, W., WOLF, L., KILIAAN, A. J., PENKE, B., RÜBE, C. E., WALTER, J., HENEKA, M. T., HARTMANN, T., MENGER, M. D. & FASSBENDER, K. 2012. TLR2 is a primary receptor for Alzheimer's amyloid β peptide to trigger neuroinflammatory activation. *J Immunol,* 188**,** 1098-107.

LIU, Z. P., WANG, Y., ZHANG, X. S. & CHEN, L. 2010. Identifying dysfunctional crosstalk of pathways in various regions of Alzheimer's disease brains. *BMC Syst Biol,* 4 Suppl 2**,** S11.

LLOYD, A. F., DAVIES, C. L., HOLLOWAY, R. K., LABRAK, Y., IRELAND, G., CARRADORI, D., DILLENBURG, A., BORGER, E., SOONG, D., RICHARDSON, J. C., KUHLMANN, T., WILLIAMS, A., POLLARD, J. W., DES RIEUX, A., PRILLER, J. & MIRON, V. E. 2019. Central nervous system regeneration is driven by microglia necroptosis and repopulation. *Nature Neuroscience,* 22**,** 1046-1052.

LO, M. T., KAUPPI, K., FAN, C. C., SANYAL, N., REAS, E. T., SUNDAR, V. S., LEE, W. C., DESIKAN, R. S., MCEVOY, L. K. & CHEN, C. H. 2019. Identification of genetic heterogeneity of Alzheimer's disease across age. *Neurobiol Aging,* 84**,** 243.e1-243.e9.

LOGUE, M. W., SCHU, M., VARDARAJAN, B. N., BUROS, J., GREEN, R. C., GO, R. C., GRIFFITH, P., OBISESAN, T. O., SHATZ, R., BORENSTEIN, A., CUPPLES, L. A., LUNETTA, K. L., FALLIN, M. D.,

BALDWIN, C. T. & FARRER, L. A. 2011. A comprehensive genetic association study of Alzheimer disease in African Americans. *Arch Neurol,* 68**,** 1569-79.

LORD, J., LU, A. J. & CRUCHAGA, C. 2014. Identification of rare variants in Alzheimer's disease. *Front Genet,* 5**,** 369.

LUCIN, K. M., O'BRIEN, C. E., BIERI, G., CZIRR, E., MOSHER, K. I., ABBEY, R. J., MASTROENI, D. F., ROGERS, J., SPENCER, B., MASLIAH, E. & WYSS-CORAY, T. 2013. Microglial beclin 1 regulates retromer trafficking and phagocytosis and is impaired in Alzheimer's disease. *Neuron,* 79**,** 873-86.

LUCK, K., KIM, D. K., LAMBOURNE, L., SPIROHN, K., BEGG, B. E., BIAN, W., BRIGNALL, R., CAFARELLI, T., CAMPOS-LABORIE, F. J., CHARLOTEAUX, B., CHOI, D., COTÉ, A. G., DALEY, M., DEIMLING, S., DESBULEUX, A., DRICOT, A., GEBBIA, M., HARDY, M. F., KISHORE, N., KNAPP, J. J., KOVÁCS, I. A., LEMMENS, I., MEE, M. W., MELLOR, J. C., POLLIS, C., PONS, C., RICHARDSON, A. D., SCHLABACH, S., TEEKING, B., YADAV, A., BABOR, M., BALCHA, D., BASHA, O., BOWMAN-COLIN, C., CHIN, S. F., CHOI, S. G., COLABELLA, C., COPPIN, G., D'AMATA, C., DE RIDDER, D., DE ROUCK, S., DURAN-FRIGOLA, M., ENNAJDAOUI, H., GOEBELS, F., GOEHRING, L., GOPAL, A., HADDAD, G., HATCHI, E., HELMY, M., JACOB, Y., KASSA, Y., LANDINI, S., LI, R., VAN LIESHOUT, N., MACWILLIAMS, A., MARKEY, D., PAULSON, J. N., RANGARAJAN, S., RASLA, J., RAYHAN, A., ROLLAND, T., SAN-MIGUEL, A., SHEN, Y., SHEYKHKARIMLI, D., SHEYNKMAN, G. M., SIMONOVSKY, E., TAŞAN, M., TEJEDA, A., TROPEPE, V., TWIZERE, J. C., WANG, Y., WEATHERITT, R. J., WEILE, J., XIA, Y., YANG, X., YEGER-LOTEM, E., ZHONG, Q., ALOY, P., BADER, G. D., DE LAS RIVAS, J., GAUDET, S., HAO, T., RAK, J., TAVERNIER, J., HILL, D. E., VIDAL, M., ROTH, F. P. & CALDERWOOD, M. A. 2020. A reference map of the human binary protein interactome. *Nature,* 580**,** 402-408.

LVOVS, D., FAVOROVA, O. O. & FAVOROV, A. V. 2012. A Polygenic Approach to the Study of Polygenic Diseases. *Acta Naturae,* 4**,** 59-71.

MA, K., THOMASON, L. A. & MCLAURIN, J. 2012. scyllo-Inositol, preclinical, and clinical data for Alzheimer's disease. *Adv Pharmacol,* 64**,** 177-212.

MACDONALD, A., BRIGGS, K., POPPE, M., HIGGINS, A., VELAYUDHAN, L. & LOVESTONE, S. 2008. A feasibility and tolerability study of lithium in Alzheimer's disease. *Int J Geriatr Psychiatry,* 23**,** 704-11.

MADEIRA, F., PARK, Y. M., LEE, J., BUSO, N., GUR, T., MADHUSOODANAN, N., BASUTKAR, P., TIVEY, A. R. N., POTTER, S. C., FINN, R. D. & LOPEZ, R. 2019. The EMBL-EBI search and sequence analysis tools APIs in 2019. *Nucleic Acids Res,* 47**,** W636-w641.

MAGNO, L., LESSARD, C. B., MARTINS, M., LANG, V., CRUZ, P., ASI, Y., KATAN, M., BILSLAND, J., LASHLEY, T., CHAKRABARTY, P., GOLDE, T. E. & WHITING, P. J. 2019. Alzheimer's disease phospholipase C-gamma-2 (PLCG2) protective variant is a functional hypermorph. *Alzheimer's Research & Therapy,* 11**,** 16.

MARÍN-TEVA, J. L., DUSART, I., COLIN, C., GERVAIS, A., VAN ROOIJEN, N. & MALLAT, M. 2004. Microglia promote the death of developing Purkinje cells. *Neuron,* 41**,** 535-47.

MARIONI, R. E., HARRIS, S. E., ZHANG, Q., MCRAE, A. F., HAGENAARS, S. P., HILL, W. D., DAVIES, G., RITCHIE, C. W., GALE, C. R., STARR, J. M., GOATE, A. M., PORTEOUS, D. J., YANG, J., EVANS, K. L., DEARY, I. J., WRAY, N. R. & VISSCHER, P. M. 2018. GWAS on family history of Alzheimer's disease. *Transl Psychiatry,* 8**,** 99.

MARTIN-ESTEBANE, M. & GOMEZ-NICOLA, D. 2020. Targeting Microglial Population Dynamics in Alzheimer's Disease: Are We Ready for a Potential Impact on Immune Function? *Front Cell Neurosci,* 14**,** 149.

MARTINEZ, F. O. & GORDON, S. 2014. The M1 and M2 paradigm of macrophage activation: time for reassessment. *F1000Prime Rep,* 6**,** 13.

MARTISKAINEN, H., VISWANATHAN, J., NYKANEN, N. P., KURKI, M., HELISALMI, S., NATUNEN, T., SARAJARVI, T., KURKINEN, K. M., PURSIHEIMO, J. P., RAURAMAA, T., ALAFUZOFF, I., JAASKELAINEN, J. E., LEINONEN, V., SOININEN, H., HAAPASALO, A., HUTTUNEN, H. J. &

HILTUNEN, M. 2015. Transcriptomics and mechanistic elucidation of Alzheimer's disease risk genes in the brain and in vitro models. *Neurobiol Aging,* 36**,** 1221.e15-28.

MASLIAH, E., MALLORY, M., HANSEN, L., ALFORD, M., ALBRIGHT, T., DETERESA, R., TERRY, R., BAUDIER, J. & SAITOH, T. 1991. Patterns of aberrant sprouting in Alzheimer's disease. *Neuron,* 6**,** 729-39.

MASTRODONATO, V., MORELLI, E. & VACCARI, T. 2018. How to use a multipurpose SNARE: The emerging role of Snap29 in cellular health. *Cell Stress,* 2**,** 72-81.

MATHIS, C. A., LOPRESTI, B. J. & KLUNK, W. E. 2007. Impact of amyloid imaging on drug development in Alzheimer's disease. *Nucl Med Biol,* 34**,** 809-22.

MATSUDA, S., IRIYAMA, C., YOKOZAKI, S., ICHIGOTANI, Y., SHIRAFUJI, N., YAMAKI, K., HAYAKAWA, T. & HAMAGUCHI, M. 2001. Cloning and sequencing of a novel human gene that encodes a putative target protein of Nesh-SH3. *J Hum Genet,* 46**,** 483-6.

MATSUI, T., JIANG, P., NAKANO, S., SAKAMAKI, Y., YAMAMOTO, H. & MIZUSHIMA, N. 2018. Autophagosomal YKT6 is required for fusion with lysosomes independently of syntaxin 17. *Journal of Cell Biology,* 217**,** 2633-2645.

MATTSON, M. P., CHENG, B., DAVIS, D., BRYANT, K., LIEBERBURG, I. & RYDEL, R. E. 1992. beta-Amyloid peptides destabilize calcium homeostasis and render human cortical neurons vulnerable to excitotoxicity. *J Neurosci,* 12**,** 376-89.

MAWUENYEGA, K. G., SIGURDSON, W., OVOD, V., MUNSELL, L., KASTEN, T., MORRIS, J. C., YARASHESKI, K. E. & BATEMAN, R. J. 2010. Decreased clearance of CNS beta-amyloid in Alzheimer's disease. *Science,* 330**,** 1774.

MAY, D. G., SCOTT, K. L., CAMPOS, A. R. & ROUX, K. J. 2020. Comparative Application of BioID and TurboID for Protein-Proximity Biotinylation. *Cells,* 9**,** 1070.

MAZAHERI, F., SNAIDERO, N., KLEINBERGER, G., MADORE, C., DARIA, A., WERNER, G., KRASEMANN, S., CAPELL, A., TRUMBACH, D., WURST, W., BRUNNER, B., BULTMANN, S., TAHIROVIC, S., KERSCHENSTEINER, M., MISGELD, T., BUTOVSKY, O. & HAASS, C. 2017. TREM2 deficiency impairs chemotaxis and microglial responses to neuronal injury. *EMBO Rep,* 18**,** 1186-1198.

MCCARTHY, M. I., ABECASIS, G. R., CARDON, L. R., GOLDSTEIN, D. B., LITTLE, J., IOANNIDIS, J. P. & HIRSCHHORN, J. N. 2008. Genome-wide association studies for complex traits: consensus, uncertainty and challenges. *Nat Rev Genet,* 9**,** 356-69.

MCCARTHY, S., DAS, S., KRETZSCHMAR, W., DELANEAU, O., WOOD, A. R., TEUMER, A., KANG, H. M., FUCHSBERGER, C., DANECEK, P., SHARP, K., LUO, Y., SIDORE, C., KWONG, A., TIMPSON, N., KOSKINEN, S., VRIEZE, S., SCOTT, L. J., ZHANG, H., MAHAJAN, A., VELDINK, J., PETERS, U., PATO, C., VAN DUIJN, C. M., GILLIES, C. E., GANDIN, I., MEZZAVILLA, M., GILLY, A., COCCA, M., TRAGLIA, M., ANGIUS, A., BARRETT, J. C., BOOMSMA, D., BRANHAM, K., BREEN, G., BRUMMETT, C. M., BUSONERO, F., CAMPBELL, H., CHAN, A., CHEN, S., CHEW, E., COLLINS, F. S., CORBIN, L. J., SMITH, G. D., DEDOUSSIS, G., DORR, M., FARMAKI, A. E., FERRUCCI, L., FORER, L., FRASER, R. M., GABRIEL, S., LEVY, S., GROOP, L., HARRISON, T., HATTERSLEY, A., HOLMEN, O. L., HVEEM, K., KRETZLER, M., LEE, J. C., MCGUE, M., MEITINGER, T., MELZER, D., MIN, J. L., MOHLKE, K. L., VINCENT, J. B., NAUCK, M., NICKERSON, D., PALOTIE, A., PATO, M., PIRASTU, N., MCINNIS, M., RICHARDS, J. B., SALA, C., SALOMAA, V., SCHLESSINGER, D., SCHOENHERR, S., SLAGBOOM, P. E., SMALL, K., SPECTOR, T., STAMBOLIAN, D., TUKE, M., TUOMILEHTO, J., VAN DEN BERG, L. H., VAN RHEENEN, W., VOLKER, U., WIJMENGA, C., TONIOLO, D., ZEGGINI, E., GASPARINI, P., SAMPSON, M. G., WILSON, J. F., FRAYLING, T., DE BAKKER, P. I., SWERTZ, M. A., MCCARROLL, S., KOOPERBERG, C., DEKKER, A., ALTSHULER, D., WILLER, C., IACONO, W., RIPATTI, S., et al. 2016. A reference panel of 64,976 haplotypes for genotype imputation. *Nat Genet,* 48**,** 1279-83.

MCKHANN, G. M., KNOPMAN, D. S., CHERTKOW, H., HYMAN, B. T., JACK, C. R., JR., KAWAS, C. H., KLUNK, W. E., KOROSHETZ, W. J., MANLY, J. J., MAYEUX, R., MOHS, R. C., MORRIS, J. C., ROSSOR, M. N., SCHELTENS, P., CARRILLO, M. C., THIES, B., WEINTRAUB, S. & PHELPS, C. H. 2011. The diagnosis of dementia due to Alzheimer's disease: recommendations from the

National Institute on Aging-Alzheimer's Association workgroups on diagnostic guidelines for Alzheimer's disease. *Alzheimers Dement,* 7**,** 263-9.

MCNALLY, K. E. & CULLEN, P. J. 2018. Endosomal Retrieval of Cargo: Retromer Is Not Alone. *Trends in Cell Biology,* 28**,** 807-822.

MELIEF, J., SNEEBOER, M. A., LITJENS, M., ORMEL, P. R., PALMEN, S. J., HUITINGA, I., KAHN, R. S., HOL, E. M. & DE WITTE, L. D. 2016. Characterizing primary human microglia: A comparative study with myeloid subsets and culture models. *Glia,* 64**,** 1857-68.

MENTING, K. W. & CLAASSEN, J. A. 2014. β-secretase inhibitor; a promising novel therapeutic drug in Alzheimer's disease. *Front Aging Neurosci,* 6**,** 165.

MERAZ-RÍOS, M. A., TORAL-RIOS, D., FRANCO-BOCANEGRA, D., VILLEDA-HERNÁNDEZ, J. & CAMPOS-PEÑA, V. 2013. Inflammatory process in Alzheimer's Disease. *Front Integr Neurosci,* 7**,** 59.

MERTENS, J., PAQUOLA, A. C. M., KU, M., HATCH, E., BÖHNKE, L., LADJEVARDI, S., MCGRATH, S., CAMPBELL, B., LEE, H., HERDY, J. R., GONÇALVES, J. T., TODA, T., KIM, Y., WINKLER, J., YAO, J., HETZER, M. W. & GAGE, F. H. 2015. Directly Reprogrammed Human Neurons Retain Aging-Associated Transcriptomic Signatures and Reveal Age-Related Nucleocytoplasmic Defects. *Cell Stem Cell,* 17**,** 705-718.

MIYASHITA, A., KOIKE, A., JUN, G., WANG, L. S., TAKAHASHI, S., MATSUBARA, E., KAWARABAYASHI, T., SHOJI, M., TOMITA, N., ARAI, H., ASADA, T., HARIGAYA, Y., IKEDA, M., AMARI, M., HANYU, H., HIGUCHI, S., IKEUCHI, T., NISHIZAWA, M., SUGA, M., KAWASE, Y., AKATSU, H., KOSAKA, K., YAMAMOTO, T., IMAGAWA, M., HAMAGUCHI, T., YAMADA, M., MORIHARA, T., TAKEDA, M., TAKAO, T., NAKATA, K., FUJISAWA, Y., SASAKI, K., WATANABE, K., NAKASHIMA, K., URAKAMI, K., OOYA, T., TAKAHASHI, M., YUZURIHA, T., SERIKAWA, K., YOSHIMOTO, S., NAKAGAWA, R., KIM, J. W., KI, C. S., WON, H. H., NA, D. L., SEO, S. W., MOOK-JUNG, I., ST GEORGE-HYSLOP, P., MAYEUX, R., HAINES, J. L., PERICAK-VANCE, M. A., YOSHIDA, M., NISHIDA, N., TOKUNAGA, K., YAMAMOTO, K., TSUJI, S., KANAZAWA, I., IHARA, Y., SCHELLENBERG, G. D., FARRER, L. A. & KUWANO, R. 2013. SORL1 is genetically associated with late-onset Alzheimer's disease in Japanese, Koreans and Caucasians. *PLoS One,* 8**,** e58618.

MIYAZAKI, K., MATSUDA, S., ICHIGOTANI, Y., TAKENOUCHI, Y., HAYASHI, K., FUKUDA, Y., NIMURA, Y. & HAMAGUCHI, M. 2000. Isolation and characterization of a novel human gene (NESH) which encodes a putative signaling molecule similar to e3B1 protein. *Biochim Biophys Acta,* 1493**,** 237-41.

MIZUTANI, K., MIYATA, M., SHIOTANI, H., KAMEYAMA, T. & TAKAI, Y. 2022. Nectin-2 in general and in the brain. *Molecular and Cellular Biochemistry,* 477**,** 167-180.

MORAES, L., ZANCHIN, N. I. T. & CERUTTI, J. M. 2017. ABI3, a component of the WAVE2 complex, is potentially regulated by PI3K/AKT pathway. *Oncotarget,* 8**,** 67769-67781.

MORETH, J., MAVOUNGOU, C. & SCHINDOWSKI, K. 2013. Passive anti-amyloid immunotherapy in Alzheimer's disease: What are the most promising targets? *Immun Ageing,* 10**,** 18.

MORITA, M., LER, L. W., FABIAN, M. R., SIDDIQUI, N., MULLIN, M., HENDERSON, V. C., ALAIN, T., FONSECA, B. D., KARASHCHUK, G., BENNETT, C. F., KABUTA, T., HIGASHI, S., LARSSON, O., TOPISIROVIC, I., SMITH, R. J., GINGRAS, A. C. & SONENBERG, N. 2012. A novel 4EHP-GIGYF2 translational repressor complex is essential for mammalian development. *Mol Cell Biol,* 32**,** 3585-93.

MORRIS, G. & BERK, M. 2016. The Putative Use of Lithium in Alzheimer's Disease. *Curr Alzheimer Res,* 13**,** 853-61.

MORRIS, G. P., CLARK, I. A. & VISSEL, B. 2014. Inconsistencies and controversies surrounding the amyloid hypothesis of Alzheimer's disease. *Acta Neuropathol Commun,* 2**,** 135.

MOSSER, D. M. & EDWARDS, J. P. 2008. Exploring the full spectrum of macrophage activation. *Nat Rev Immunol,* 8**,** 958-69.

MUELLER, H. T., BORG, J. P., MARGOLIS, B. & TURNER, R. S. 2000. Modulation of amyloid precursor protein metabolism by X11alpha /Mint-1. A deletion analysis of protein-protein interaction domains. *J Biol Chem,* 275**,** 39302-6.

MUFFAT, J., LI, Y., YUAN, B., MITALIPOVA, M., OMER, A., CORCORAN, S., BAKIASI, G., TSAI, L. H., AUBOURG, P., RANSOHOFF, R. M. & JAENISCH, R. 2016. Efficient derivation of microglia-like cells from human pluripotent stem cells. *Nat Med,* 22**,** 1358-1367.

MÜLLER, U. C., DELLER, T. & KORTE, M. 2017. Not just amyloid: physiological functions of the amyloid precursor protein family. *Nat Rev Neurosci,* 18**,** 281-298.

MUNGARRO-MENCHACA, X., FERRERA, P., MORÁN, J. & ARIAS, C. 2002. beta-Amyloid peptide induces ultrastructural changes in synaptosomes and potentiates mitochondrial dysfunction in the presence of ryanodine. *J Neurosci Res,* 68**,** 89-96.

MURRAY, P. J., ALLEN, J. E., BISWAS, S. K., FISHER, E. A., GILROY, D. W., GOERDT, S., GORDON, S., HAMILTON, J. A., IVASHKIV, L. B., LAWRENCE, T., LOCATI, M., MANTOVANI, A., MARTINEZ, F. O., MEGE, J. L., MOSSER, D. M., NATOLI, G., SAEIJ, J. P., SCHULTZE, J. L., SHIREY, K. A., SICA, A., SUTTLES, J., UDALOVA, I., VAN GINDERACHTER, J. A., VOGEL, S. N. & WYNN, T. A. 2014. Macrophage activation and polarization: nomenclature and experimental guidelines. *Immunity,* 41**,** 14-20.

NAGAI, A., NAKAGAWA, E., HATORI, K., CHOI, H. B., MCLARNON, J. G., LEE, M. A. & KIM, S. U. 2001. Generation and characterization of immortalized human microglial cell lines: expression of cytokines and chemokines. *Neurobiol Dis,* 8**,** 1057-68.

NAJ, A. C., BEECHAM, G. W., MARTIN, E. R., GALLINS, P. J., POWELL, E. H., KONIDARI, I., WHITEHEAD, P. L., CAI, G., HAROUTUNIAN, V., SCOTT, W. K., VANCE, J. M., SLIFER, M. A., GWIRTSMAN, H. E., GILBERT, J. R., HAINES, J. L., BUXBAUM, J. D. & PERICAK-VANCE, M. A. 2010. Dementia revealed: novel chromosome 6 locus for late-onset Alzheimer disease provides genetic evidence for folate-pathway abnormalities. *PLoS Genet,* 6**,** e1001130.

NAJ, A. C. & SCHELLENBERG, G. D. 2017. Genomic variants, genes, and pathways of Alzheimer's disease: An overview. *Am J Med Genet B Neuropsychiatr Genet,* 174**,** 5-26.

NAPOLI, I., MERCALDO, V., BOYL, P. P., ELEUTERI, B., ZALFA, F., DE RUBEIS, S., DI MARINO, D., MOHR, E., MASSIMI, M., FALCONI, M., WITKE, W., COSTA-MATTIOLI, M., SONENBERG, N., ACHSEL, T. & BAGNI, C. 2008. The fragile X syndrome protein represses activity-dependent translation through CYFIP1, a new 4E-BP. *Cell,* 134**,** 1042-54.

NAZARIAN, A., YASHIN, A. I. & KULMINSKI, A. M. 2019. Genome-wide analysis of genetic predisposition to Alzheimer's disease and related sex disparities. *Alzheimers Res Ther,* 11**,** 5.

NCT00021723 2002. Randomized Safety, Tolerability and Pilot Efficacy of AN-1792 in Alzheimer's Disease. https://ClinicalTrials.gov/show/NCT00021723.

NCT02579252 2019. 24 Months Safety and Efficacy Study of AADvac1 in Patients With Mild Alzheimer's Disease. https://ClinicalTrials.gov/show/NCT02579252.

NCT03887455 2019. A Placebo-Controlled, Double-Blind, Parallel-Group, 18-Month Study With an Open-Label Extension Phase to Confirm Safety and Efficacy of BAN2401 in Subjects With Early Alzheimer's Disease. https://clinicaltrials.gov/ct2/show/study/NCT03887455.

NEUMANN, H. & TAKAHASHI, K. 2007. Essential role of the microglial triggering receptor expressed on myeloid cells-2 (TREM2) for central nervous tissue immune homeostasis. *J Neuroimmunol,* 184**,** 92-9.

NEWHOUSE, P. A., POTTER, A., CORWIN, J. & LENOX, R. 1994. Age-related effects of the nicotinic antagonist mecamylamine on cognition and behavior. *Neuropsychopharmacology,* 10**,** 93-107.

NGUYEN, H. N., BYERS, B., CORD, B., SHCHEGLOVITOV, A., BYRNE, J., GUJAR, P., KEE, K., SCHÜLE, B., DOLMETSCH, R. E., LANGSTON, W., PALMER, T. D. & PERA, R. R. 2011. LRRK2 mutant iPSC-derived DA neurons demonstrate increased susceptibility to oxidative stress. *Cell Stem Cell,* 8**,** 267-80.

NICKERSON, D. A., TAYLOR, S. L., WEISS, K. M., CLARK, A. G., HUTCHINSON, R. G., STENGÅRD, J., SALOMAA, V., VARTIAINEN, E., BOERWINKLE, E. & SING, C. F. 1998. DNA sequence diversity in a 9.7-kb region of the human lipoprotein lipase gene. *Nat Genet,* 19**,** 233-40.

NIE, Q., DU, X.-G. & GENG, M.-Y. 2011. Small molecule inhibitors of amyloid β peptide aggregation as a potential therapeutic strategy for Alzheimer's disease. *Acta Pharmacologica Sinica,* 32**,** 545-551.

NIIKURA, T., TAJIMA, H. & KITA, Y. 2006. Neuronal cell death in Alzheimer's disease and a neuroprotective factor, humanin. *Curr Neuropharmacol,* 4**,** 139-47.

NILSSON, L., NORDBERG, A., HARDY, J., WESTER, P. & WINBLAD, B. 1986. Physostigmine restores 3H-acetylcholine efflux from Alzheimer brain slices to normal level. *J Neural Transm,* 67**,** 275-85.

NIMMERJAHN, A., KIRCHHOFF, F. & HELMCHEN, F. 2005. Resting microglial cells are highly dynamic surveillants of brain parenchyma in vivo. *Science,* 308**,** 1314-8.

NOLZ, J. C., GOMEZ, T. S., ZHU, P., LI, S., MEDEIROS, R. B., SHIMIZU, Y., BURKHARDT, J. K., FREEDMAN, B. D. & BILLADEAU, D. D. 2006. The WAVE2 complex regulates actin cytoskeletal reorganization and CRAC-mediated calcium entry during T cell activation. *Curr Biol,* 16**,** 24-34.

NOVAK, P., KOVACECH, B., KATINA, S., SCHMIDT, R., SCHELTENS, P., KONTSEKOVA, E., ROPELE, S., FIALOVA, L., KRAMBERGER, M., PAULENKA-IVANOVOVA, N., SMISEK, M., HANES, J., STEVENS, E., KOVAC, A., SUTOVSKY, S., PARRAK, V., KOSON, P., PRCINA, M., GALBA, J., CENTE, M., HROMADKA, T., FILIPCIK, P., PIESTANSKY, J., SAMCOVA, M., PRENN-GOLOGRANC, C., SIVAK, R., FROELICH, L., FRESSER, M., RAKUSA, M., HARRISON, J., HORT, J., OTTO, M., TOSUN, D., ONDRUS, M., WINBLAD, B., NOVAK, M. & ZILKA, N. 2021. ADAMANT: a placebo-controlled randomized phase 2 study of AADvac1, an active immunotherapy against pathological tau in Alzheimer's disease. *Nature Aging,* 1**,** 521-534.

NOVAK, P., ZILKA, N., ZILKOVA, M., KOVACECH, B., SKRABANA, R., ONDRUS, M., FIALOVA, L., KONTSEKOVA, E., OTTO, M. & NOVAK, M. 2019. AADvac1, an Active Immunotherapy for Alzheimer's Disease and Non Alzheimer Tauopathies: An Overview of Preclinical and Clinical Development. *J Prev Alzheimers Dis,* 6**,** 63-69.

ODDO, S., BILLINGS, L., KESSLAK, J. P., CRIBBS, D. H. & LAFERLA, F. M. 2004. Abeta immunotherapy leads to clearance of early, but not late, hyperphosphorylated tau aggregates via the proteasome. *Neuron,* 43**,** 321-32.

OLCESE, L., CAMBIAGGI, A., SEMENZATO, G., BOTTINO, C., MORETTA, A. & VIVIER, E. 1997. Human killer cell activatory receptors for MHC class I molecules are included in a multimeric complex expressed by natural killer cells. *J Immunol,* 158**,** 5083-6.

OLD, W. M., MEYER-ARENDT, K., AVELINE-WOLF, L., PIERCE, K. G., MENDOZA, A., SEVINSKY, J. R., RESING, K. A. & AHN, N. G. 2005. Comparison of Label-free Methods for Quantifying Human Proteins by Shotgun Proteomics*S. *Molecular & Cellular Proteomics,* 4**,** 1487-1502.

OLIVE, C., IBANEZ, L., FARIAS, F. H. G., WANG, F., BUDDE, J. P., NORTON, J. B., GENTSCH, J., MORRIS, J. C., LI, Z., DUBE, U., DEL-AGUILA, J., BERGMANN, K., BRADLEY, J., BENITEZ, B. A., HARARI, O., FAGAN, A., ANCES, B., CRUCHAGA, C. & FERNANDEZ, M. V. 2020. Examination of the Effect of Rare Variants in TREM2, ABI3, and PLCG2 in LOAD Through Multiple Phenotypes. *J Alzheimers Dis,* 77**,** 1469-1482.

OLMOS-ALONSO, A., SCHETTERS, S. T., SRI, S., ASKEW, K., MANCUSO, R., VARGAS-CABALLERO, M., HOLSCHER, C., PERRY, V. H. & GOMEZ-NICOLA, D. 2016. Pharmacological targeting of CSF1R inhibits microglial proliferation and prevents the progression of Alzheimer's-like pathology. *Brain,* 139**,** 891-907.

OLNEY, J. W., WOZNIAK, D. F. & FARBER, N. B. 1997. Excitotoxic neurodegeneration in Alzheimer disease. New hypothesis and new therapeutic strategies. *Arch Neurol,* 54**,** 1234-40.

OTERO, K., SHINOHARA, M., ZHAO, H., CELLA, M., GILFILLAN, S., COLUCCI, A., FACCIO, R., ROSS, F. P., TEITELBAUM, S. L., TAKAYANAGI, H. & COLONNA, M. 2012. TREM2 and beta-catenin regulate bone homeostasis by controlling the rate of osteoclastogenesis. *J Immunol,* 188**,** 2612-21.

OUGHTRED, R., RUST, J., CHANG, C., BREITKREUTZ, B. J., STARK, C., WILLEMS, A., BOUCHER, L., LEUNG, G., KOLAS, N., ZHANG, F., DOLMA, S., COULOMBE-HUNTINGTON, J., CHATR-ARYAMONTRI, A., DOLINSKI, K. & TYERS, M. 2021. The BioGRID database: A comprehensive biomedical resource of curated protein, genetic, and chemical interactions. *Protein Sci,* 30**,** 187-200.

PALONEVA, J., MANDELIN, J., KIIALAINEN, A., BOHLING, T., PRUDLO, J., HAKOLA, P., HALTIA, M., KONTTINEN, Y. T. & PELTONEN, L. 2003. DAP12/TREM2 deficiency results in impaired osteoclast differentiation and osteoporotic features. *J Exp Med,* 198**,** 669-75.

PALONEVA, J., MANNINEN, T., CHRISTMAN, G., HOVANES, K., MANDELIN, J., ADOLFSSON, R., BIANCHIN, M., BIRD, T., MIRANDA, R., SALMAGGI, A., TRANEBJAERG, L., KONTTINEN, Y. & PELTONEN, L. 2002. Mutations in two genes encoding different subunits of a receptor signaling complex result in an identical disease phenotype. *Am J Hum Genet,* 71**,** 656-62.

PANDYA, H., SHEN, M. J., ICHIKAWA, D. M., SEDLOCK, A. B., CHOI, Y., JOHNSON, K. R., KIM, G., BROWN, M. A., ELKAHLOUN, A. G., MARIC, D., SWEENEY, C. L., GOSSA, S., MALECH, H. L., MCGAVERN, D. B. & PARK, J. K. 2017. Differentiation of human and murine induced pluripotent stem cells to microglia-like cells. *Nat Neurosci,* 20**,** 753-759.

PAOLICELLI, R. C., BOLASCO, G., PAGANI, F., MAGGI, L., SCIANNI, M., PANZANELLI, P., GIUSTETTO, M., FERREIRA, T. A., GUIDUCCI, E., DUMAS, L., RAGOZZINO, D. & GROSS, C. T. 2011. Synaptic pruning by microglia is necessary for normal brain development. *Science,* 333**,** 1456-8.

PARADOWSKA-GORYCKA, A. & JURKOWSKA, M. 2013. Structure, expression pattern and biological activity of molecular complex TREM-2/DAP12. *Hum Immunol,* 74**,** 730-7.

PARK, J. S., JI, I. J., AN, H. J., KANG, M. J., KANG, S. W., KIM, D. H. & YOON, S. Y. 2015. Disease-Associated Mutations of TREM2 Alter the Processing of N-Linked Oligosaccharides in the Golgi Apparatus. *Traffic,* 16**,** 510-8.

PARK, J. S., JI, I. J., KIM, D. H., AN, H. J. & YOON, S. Y. 2016. The Alzheimer's Disease-Associated R47H Variant of TREM2 Has an Altered Glycosylation Pattern and Protein Stability. *Front Neurosci,* 10**,** 618.

PEDERSEN, J. T. & SIGURDSSON, E. M. 2015. Tau immunotherapy for Alzheimer's disease. *Trends Mol Med,* 21**,** 394-402.

PENG, Q., MALHOTRA, S., TORCHIA, J. A., KERR, W. G., COGGESHALL, K. M. & HUMPHREY, M. B. 2010. TREM2- and DAP12-dependent activation of PI3K requires DAP10 and is inhibited by SHIP1. *Sci Signal,* 3**,** ra38.

PENROD, N. M., COWPER-SAL-LARI, R. & MOORE, J. H. 2011. Systems genetics for drug target discovery. *Trends Pharmacol Sci,* 32**,** 623-30.

PÉREZ-BERCOFF, Å., HUDSON, C. M. & CONANT, G. C. 2013. A conserved mammalian protein interaction network. *PLoS One,* 8**,** e52581.

PERICAK-VANCE, M. A., BEBOUT, J. L., GASKELL, P. C., JR., YAMAOKA, L. H., HUNG, W. Y., ALBERTS, M. J., WALKER, A. P., BARTLETT, R. J., HAYNES, C. A., WELSH, K. A. & ET AL. 1991. Linkage studies in familial Alzheimer disease: evidence for chromosome 19 linkage. *Am J Hum Genet,* 48**,** 1034-50.

PERRY, E., WALKER, M., GRACE, J. & PERRY, R. 1999. Acetylcholine in mind: a neurotransmitter correlate of consciousness? *Trends Neurosci,* 22**,** 273-80.

PERRY, E. K., GIBSON, P. H., BLESSED, G., PERRY, R. H. & TOMLINSON, B. E. 1977. Neurotransmitter enzyme abnormalities in senile dementia. Choline acetyltransferase and glutamic acid decarboxylase activities in necropsy brain tissue. *J Neurol Sci,* 34**,** 247-65.

PICKETT, E. K., ROSE, J., MCCRORY, C., MCKENZIE, C.-A., KING, D., SMITH, C., GILLINGWATER, T. H., HENSTRIDGE, C. M. & SPIRES-JONES, T. L. 2018. Region-specific depletion of synaptic mitochondria in the brains of patients with Alzheimer's disease. *Acta Neuropathologica,* 136**,** 747-757.

PILLAI-KASTOORI, L., HEATON, S., SHIFLETT, S. D., ROBERTS, A. C., SOLACHE, A. & SCHUTZ-GESCHWENDER, A. R. 2020. Antibody validation for Western blot: By the user, for the user. *J Biol Chem,* 295**,** 926-939.

POLANCO, J. C., SCICLUNA, B. J., HILL, A. F. & GÖTZ, J. 2016. Extracellular Vesicles Isolated from the Brains of rTg4510 Mice Seed Tau Protein Aggregation in a Threshold-dependent Manner *. *Journal of Biological Chemistry,* 291**,** 12445-12466.

PORTA, S., SERRA, S. A., HUCH, M., VALVERDE, M. A., LLORENS, F., ESTIVILL, X., ARBONÉS, M. L. & MARTÍ, E. 2007. RCAN1 (DSCR1) increases neuronal susceptibility to oxidative stress: a potential pathogenic process in neurodegeneration. *Hum Mol Genet,* 16**,** 1039-50.

POURHAGHIGHI, R., ASH, P. E. A., PHANSE, S., GOEBELS, F., HU, L. Z. M., CHEN, S., ZHANG, Y., WIERBOWSKI, S. D., BOUDEAU, S., MOUTAOUFIK, M. T., MALTY, R. H., MALOLEPSZA, E., TSAFOU, K., NATHAN, A., CROMAR, G., GUO, H., ABDULLATIF, A. A., APICCO, D. J., BECKER, L. A., GITLER, A. D., PULST, S. M., YOUSSEF, A., HEKMAN, R., HAVUGIMANA, P. C., WHITE, C. A., BLUM, B. C., RATTI, A., BRYANT, C. D., PARKINSON, J., LAGE, K., BABU, M., YU, H., BADER, G. D., WOLOZIN, B. & EMILI, A. 2020. BraInMap Elucidates the Macromolecular Connectivity Landscape of Mammalian Brain. *Cell Syst,* 10**,** 333-350.e14.

PRADA, I., ONGANIA, G. N., BUONSANTI, C., PANINA-BORDIGNON, P. & MELDOLESI, J. 2006. Triggering receptor expressed in myeloid cells 2 (TREM2) trafficking in microglial cells: continuous shuttling to and from the plasma membrane regulated by cell stimulation. *Neuroscience,* 140**,** 1139-48.

PRASAD, A., MANIVANNAN, J., LOONG, D. T., CHUA, S. M., GHARIBANI, P. M. & ALL, A. H. 2016. A review of induced pluripotent stem cell, direct conversion by trans-differentiation, direct reprogramming and oligodendrocyte differentiation. *Regen Med,* 11**,** 181-91.

PRICE, B. R., SUDDUTH, T. L., WEEKMAN, E. M., JOHNSON, S., HAWTHORNE, D., WOOLUMS, A. & WILCOCK, D. M. 2020. Therapeutic Trem2 activation ameliorates amyloid-beta deposition and improves cognition in the 5XFAD model of amyloid deposition. *Journal of Neuroinflammation,* 17**,** 238.

PRIDE, M., SEUBERT, P., GRUNDMAN, M., HAGEN, M., ELDRIDGE, J. & BLACK, R. S. 2008. Progress in the active immunotherapeutic approach to Alzheimer's disease: clinical investigations into AN1792-associated meningoencephalitis. *Neurodegener Dis,* 5**,** 194-6.

PRINCE, M., KNAPP, M., GUERCHET, M., MCCRONE, P., PRINA, M., COMAS HERRERA, A., WITTENBERG, A., ADELAJA, R., HU, B., KING, B., REHILL, D. & SALIMKUMAR, D. 2014. *Dementia UK: update*.

PRINCE, M., WIMO, A., GUERCHET, M., ALI, G.-C., WU, Y.-T. & PRINA, M. 2015. *World Alzheimer Report 2015. The Global Impact of Dementia. An Analysis of Prevalence, Incidence, Cost and Trends*.

PRZANOWSKI, P., DABROWSKI, M., ELLERT-MIKLASZEWSKA, A., KLOSS, M., MIECZKOWSKI, J., KAZA, B., RONOWICZ, A., HU, F., PIOTROWSKI, A., KETTENMANN, H., KOMOROWSKI, J. & KAMINSKA, B. 2014. The signal transducers Stat1 and Stat3 and their novel target Jmjd3 drive the expression of inflammatory genes in microglia. *Journal of Molecular Medicine,* 92**,** 239-254.

PULST, S. M. 1999. Genetic linkage analysis. *Arch Neurol,* 56**,** 667-72.

QIAN, W., HE, X., CHAN, E., XU, H. & ZHANG, J. 2011. Measuring the evolutionary rate of protein-protein interaction. *Proc Natl Acad Sci U S A,* 108**,** 8725-30.

QIN, J. Y., ZHANG, L., CLIFT, K. L., HULUR, I., XIANG, A. P., REN, B.-Z. & LAHN, B. T. 2010. Systematic Comparison of Constitutive Promoters and the Doxycycline-Inducible Promoter. *PLOS ONE,* 5**,** e10611.

QIN, Q. & LI, Y. 2019. Herpesviral infections and antimicrobial protection for Alzheimer's disease: Implications for prevention and treatment. *Journal of Medical Virology,* 91**,** 1368-1377.

QIN, Y., ZHOU, Y., SHEN, Z., XU, B., CHEN, M., LI, Y., CHEN, M., BEHRENS, A., ZHOU, J., QI, X., MENG, W., WANG, Y. & GAO, F. 2019. WDR62 is involved in spindle assembly by interacting with CEP170 in spermatogenesis. *Development,* 146.

QIU, S., LAVALLÉE-ADAM, M. & CÔTÉ, M. 2021. Proximity Interactome Map of the Vac14-Fig4 Complex Using BioID. *J Proteome Res,* 20**,** 4959-4973.

R CORE TEAM. 2022. *R: A Language and Environment for Statistical Computing* [Online]. Vienna, Austria. Available: https://www.R-project.org/ [Accessed 2022].

RAGOZZINO, D., DI ANGELANTONIO, S., TRETTEL, F., BERTOLLINI, C., MAGGI, L., GROSS, C., CHARO, I. F., LIMATOLA, C. & EUSEBI, F. 2006. Chemokine fractalkine/CX3CL1 negatively modulates active glutamatergic synapses in rat hippocampal neurons. *J Neurosci,* 26**,** 10488-98.

RAMANAN, V. K., RISACHER, S. L., NHO, K., KIM, S., SWAMINATHAN, S., SHEN, L., FOROUD, T. M., HAKONARSON, H., HUENTELMAN, M. J., AISEN, P. S., PETERSEN, R. C., GREEN, R. C., JACK, C. R., KOEPPE, R. A., JAGUST, W. J., WEINER, M. W. & SAYKIN, A. J. 2014. APOE and BCHE as modulators of cerebral amyloid deposition: a florbetapir PET genome-wide association study. *Mol Psychiatry,* 19**,** 351-7.

RANGARAJU, S., DAMMER, E. B., RAZA, S. A., RATHAKRISHNAN, P., XIAO, H., GAO, T., DUONG, D. M., PENNINGTON, M. W., LAH, J. J., SEYFRIED, N. T. & LEVEY, A. I. 2018. Identification and therapeutic modulation of a pro-inflammatory subset of disease-associated-microglia in Alzheimer's disease. *Mol Neurodegener,* 13**,** 24.

RANSOHOFF, R. M. 2016. A polarizing question: do M1 and M2 microglia exist? *Nat Neurosci,* 19**,** 987-91.

RAULIN, A.-C., DOSS, S. V., TROTTIER, Z. A., IKEZU, T. C., BU, G. & LIU, C.-C. 2022. ApoE in Alzheimer's disease: pathophysiology and therapeutic strategies. *Molecular Neurodegeneration,* 17**,** 72.

REDDY, A. & KAELIN, W. G., JR. 2002. Using cancer genetics to guide the selection of anticancer drug targets. *Curr Opin Pharmacol,* 2**,** 366-73.

REDDY, P. H. & BEAL, M. F. 2008. Amyloid beta, mitochondrial dysfunction and synaptic damage: implications for cognitive decline in aging and Alzheimer's disease. *Trends Mol Med,* 14**,** 45-53.

RENAUD-GABARDOS, E., HANTELYS, F., MORFOISSE, F., CHAUFOUR, X., GARMY-SUSINI, B. & PRATS, A. C. 2015. Internal ribosome entry site-based vectors for combined gene therapy. *World J Exp Med,* 5**,** 11-20.

RENTZ, D. M., LOCASCIO, J. J., BECKER, J. A., MORAN, E. K., ENG, E., BUCKNER, R. L., SPERLING, R. A. & JOHNSON, K. A. 2010. Cognition, reserve, and amyloid deposition in normal aging. *Ann Neurol,* 67**,** 353-64.

RIGHI, M., MORI, L., DE LIBERO, G., SIRONI, M., BIONDI, A., MANTOVANI, A., DONINI, S. D. & RICCIARDI-CASTAGNOLI, P. 1989. Monokine production by microglial cell clones. *Eur J Immunol,* 19**,** 1443-8.

ROBERSON, E. D., SCEARCE-LEVIE, K., PALOP, J. J., YAN, F., CHENG, I. H., WU, T., GERSTEIN, H., YU, G. Q. & MUCKE, L. 2007. Reducing endogenous tau ameliorates amyloid beta-induced deficits in an Alzheimer's disease mouse model. *Science,* 316**,** 750-4.

ROBINSON, S. R., BISHOP, G. M., LEE, H. G. & MÜNCH, G. 2004. Lessons from the AN 1792 Alzheimer vaccine: lest we forget. *Neurobiol Aging,* 25**,** 609-15.

ROGAEV, E. I., SHERRINGTON, R., ROGAEVA, E. A., LEVESQUE, G., IKEDA, M., LIANG, Y., CHI, H., LIN, C., HOLMAN, K., TSUDA, T. & ET AL. 1995. Familial Alzheimer's disease in kindreds with missense mutations in a gene on chromosome 1 related to the Alzheimer's disease type 3 gene. *Nature,* 376**,** 775-8.

ROLLAND, T., TAŞAN, M., CHARLOTEAUX, B., PEVZNER, S. J., ZHONG, Q., SAHNI, N., YI, S., LEMMENS, I., FONTANILLO, C., MOSCA, R., KAMBUROV, A., GHIASSIAN, S. D., YANG, X., GHAMSARI, L., BALCHA, D., BEGG, B. E., BRAUN, P., BREHME, M., BROLY, M. P., CARVUNIS, A. R., CONVERY-ZUPAN, D., COROMINAS, R., COULOMBE-HUNTINGTON, J., DANN, E., DREZE, M., DRICOT, A., FAN, C., FRANZOSA, E., GEBREAB, F., GUTIERREZ, B. J., HARDY, M. F., JIN, M., KANG, S.,

KIROS, R., LIN, G. N., LUCK, K., MACWILLIAMS, A., MENCHE, J., MURRAY, R. R., PALAGI, A., POULIN, M. M., RAMBOUT, X., RASLA, J., REICHERT, P., ROMERO, V., RUYSSINCK, E., SAHALIE, J. M., SCHOLZ, A., SHAH, A. A., SHARMA, A., SHEN, Y., SPIROHN, K., TAM, S., TEJEDA, A. O., TRIGG, S. A., TWIZERE, J. C., VEGA, K., WALSH, J., CUSICK, M. E., XIA, Y., BARABÁSI, A. L., IAKOUCHEVA, L. M., ALOY, P., DE LAS RIVAS, J., TAVERNIER, J., CALDERWOOD, M. A., HILL, D. E., HAO, T., ROTH, F. P. & VIDAL, M. 2014. A proteome-scale map of the human interactome network. *Cell,* 159**,** 1212-1226.

ROTTNER, K., STRADAL, T. E. B. & CHEN, B. 2021. WAVE regulatory complex. *Current Biology,* 31**,** R512-R517.

ROUX, K. J., KIM, D. I., RAIDA, M. & BURKE, B. 2012. A promiscuous biotin ligase fusion protein identifies proximal and interacting proteins in mammalian cells. *J Cell Biol,* 196**,** 801-10.

RUAL, J. F., VENKATESAN, K., HAO, T., HIROZANE-KISHIKAWA, T., DRICOT, A., LI, N., BERRIZ, G. F., GIBBONS, F. D., DREZE, M., AYIVI-GUEDEHOUSSOU, N., KLITGORD, N., SIMON, C., BOXEM, M., MILSTEIN, S., ROSENBERG, J., GOLDBERG, D. S., ZHANG, L. V., WONG, S. L., FRANKLIN, G., LI, S., ALBALA, J. S., LIM, J., FRAUGHTON, C., LLAMOSAS, E., CEVIK, S., BEX, C., LAMESCH, P., SIKORSKI, R. S., VANDENHAUTE, J., ZOGHBI, H. Y., SMOLYAR, A., BOSAK, S., SEQUERRA, R., DOUCETTE-STAMM, L., CUSICK, M. E., HILL, D. E., ROTH, F. P. & VIDAL, M. 2005. Towards a proteome-scale map of the human protein-protein interaction network. *Nature,* 437**,** 1173-8.

RYLETT, R. J., BALL, M. J. & COLHOUN, E. H. 1983. Evidence for high affinity choline transport in synaptosomes prepared from hippocampus and neocortex of patients with Alzheimer's disease. *Brain Res,* 289**,** 169-75.

SAARIKANGAS, J., MATTILA, P. K., VARJOSALO, M., BOVELLAN, M., HAKANEN, J., CALZADA-WACK, J., TOST, M., JENNEN, L., RATHKOLB, B., HANS, W., HORSCH, M., HYVÖNEN, M. E., PERÄLÄ, N., FUCHS, H., GAILUS-DURNER, V., ESPOSITO, I., WOLF, E., DE ANGELIS, M. H., FRILANDER, M. J., SAVILAHTI, H., SARIOLA, H., SAINIO, K., LEHTONEN, S., TAIPALE, J., SALMINEN, M. & LAPPALAINEN, P. 2011. Missing-in-metastasis MIM/MTSS1 promotes actin assembly at intercellular junctions and is required for integrity of kidney epithelia. *J Cell Sci,* 124**,** 1245-55.

SAMAVARCHI-TEHRANI, P., SAMSON, R. & GINGRAS, A. C. 2020. Proximity dependent biotinylation: key enzymes and adaptation to proteomics approaches. *Mol Cell Proteomics*.

SAMBAMURTI, K., REFOLO, L. M., SHIOI, J., PAPPOLLA, M. A. & ROBAKIS, N. K. 1992. The Alzheimer's amyloid precursor is cleaved intracellularly in the trans-Golgi network or in a post-Golgi compartment. *Ann N Y Acad Sci,* 674**,** 118-28.

SANABRIA-CASTRO, A., ALVARADO-ECHEVERRÍA, I. & MONGE-BONILLA, C. 2017. Molecular Pathogenesis of Alzheimer's Disease: An Update. *Ann Neurosci,* 24**,** 46-54.

SANGER, F., NICKLEN, S. & COULSON, A. R. 1977. DNA sequencing with chain-terminating inhibitors. *Proc Natl Acad Sci U S A,* 74**,** 5463-7.

SANO, Y., SYUZO-TAKABATAKE, A., NAKAYA, T., SAITO, Y., TOMITA, S., ITOHARA, S. & SUZUKI, T. 2006. Enhanced amyloidogenic metabolism of the amyloid beta-protein precursor in the X11L-deficient mouse brain. *J Biol Chem,* 281**,** 37853-60.

SATOH, J. I., KINO, Y., YANAIZU, M., TOSAKI, Y., SAKAI, K., ISHIDA, T. & SAITO, Y. 2017. Microglia express ABI3 in the brains of Alzheimer's disease and Nasu-Hakola disease. *Intractable Rare Dis Res,* 6**,** 262-268.

SAUNDERS, A. M., SCHMADER, K., BREITNER, J. C., BENSON, M. D., BROWN, W. T., GOLDFARB, L., GOLDGABER, D., MANWARING, M. G., SZYMANSKI, M. H., MCCOWN, N. & ET AL. 1993a. Apolipoprotein E epsilon 4 allele distributions in late-onset Alzheimer's disease and in other amyloid-forming diseases. *Lancet,* 342**,** 710-1.

SAUNDERS, A. M., STRITTMATTER, W. J., SCHMECHEL, D., GEORGE-HYSLOP, P. H., PERICAK-VANCE, M. A., JOO, S. H., ROSI, B. L., GUSELLA, J. F., CRAPPER-MACLACHLAN, D. R., ALBERTS, M. J. &

ET AL. 1993b. Association of apolipoprotein E allele epsilon 4 with late-onset familial and sporadic Alzheimer's disease. *Neurology,* 43**,** 1467-72.

SAVORY, J., GHRIBI, O. & HERMAN, M. M. 2002. Is amyloid beta-peptide neurotoxic or neuroprotective and what is its role in the binding of metal ions? *Neurobiol Aging,* 23**,** 1089-92.

SAZONOVS, A. & BARRETT, J. C. 2018. Rare-Variant Studies to Complement Genome-Wide Association Studies. *Annu Rev Genomics Hum Genet,* 19**,** 97-112.

SCAHILL, R. I., SCHOTT, J. M., STEVENS, J. M., ROSSOR, M. N. & FOX, N. C. 2002. Mapping the evolution of regional atrophy in Alzheimer's disease: unbiased analysis of fluid-registered serial MRI. *Proc Natl Acad Sci U S A,* 99**,** 4703-7.

SCHAPANSKY, J., GRINBERG, Y. Y., OSIECKI, D. M., FREEMAN, E. A., WALKER, S. G., KARRAN, E., GOPALAKRISHNAN, S. M. & TALANIAN, R. V. 2021. MEK1/2 activity modulates TREM2 cell surface recruitment. *Journal of Biological Chemistry,* 296.

SCHEIBEL, A. B. & TOMIYASU, U. 1978. Dendritic sprouting in Alzheimer's presenile dementia. *Exp Neurol,* 60**,** 1-8.

SCHEUNER, D., ECKMAN, C., JENSEN, M., SONG, X., CITRON, M., SUZUKI, N., BIRD, T. D., HARDY, J., HUTTON, M., KUKULL, W., LARSON, E., LEVY-LAHAD, E., VIITANEN, M., PESKIND, E., POORKAJ, P., SCHELLENBERG, G., TANZI, R., WASCO, W., LANNFELT, L., SELKOE, D. & YOUNKIN, S. 1996. Secreted amyloid beta-protein similar to that in the senile plaques of Alzheimer's disease is increased in vivo by the presenilin 1 and 2 and APP mutations linked to familial Alzheimer's disease. *Nat Med,* 2**,** 864-70.

SCHINDELIN, J., ARGANDA-CARRERAS, I., FRISE, E., KAYNIG, V., LONGAIR, M., PIETZSCH, T., PREIBISCH, S., RUEDEN, C., SAALFELD, S., SCHMID, B., TINEVEZ, J.-Y., WHITE, D. J., HARTENSTEIN, V., ELICEIRI, K., TOMANCAK, P. & CARDONA, A. 2012. Fiji: an open-source platform for biological-image analysis. *Nature Methods,* 9**,** 676-682.

SCHLEPCKOW, K., KLEINBERGER, G., FUKUMORI, A., FEEDERLE, R., LICHTENTHALER, S. F., STEINER, H. & HAASS, C. 2017. An Alzheimer-associated TREM2 variant occurs at the ADAM cleavage site and affects shedding and phagocytic function. *EMBO Mol Med,* 9**,** 1356-1365.

SCHMID, C. D., SAUTKULIS, L. N., DANIELSON, P. E., COOPER, J., HASEL, K. W., HILBUSH, B. S., SUTCLIFFE, J. G. & CARSON, M. J. 2002. Heterogeneous expression of the triggering receptor expressed on myeloid cells-2 on adult murine microglia. *J Neurochem,* 83**,** 1309-20.

SCHUSTER, S. C. 2008. Next-generation sequencing transforms today's biology. *Nat Methods,* 5**,** 16-8.

SCHWARTZENTRUBER, J., COOPER, S., LIU, J. Z., BARRIO-HERNANDEZ, I., BELLO, E., KUMASAKA, N., YOUNG, A. M. H., FRANKLIN, R. J. M., JOHNSON, T., ESTRADA, K., GAFFNEY, D. J., BELTRAO, P. & BASSETT, A. 2021. Genome-wide meta-analysis, fine-mapping and integrative prioritization implicate new Alzheimer's disease risk genes. *Nat Genet,* 53**,** 392-402.

SEAMAN, M. N. 2012a. The retromer complex - endosomal protein recycling and beyond. *J Cell Sci,* 125**,** 4693-702.

SEAMAN, M. N. J. 2012b. The retromer complex – endosomal protein recycling and beyond. *Journal of Cell Science,* 125**,** 4693-4702.

SEKINO, S., KASHIWAGI, Y., KANAZAWA, H., TAKADA, K., BABA, T., SATO, S., INOUE, H., KOJIMA, M. & TANI, K. 2015. The NESH/Abi-3-based WAVE2 complex is functionally distinct from the Abi-1-based WAVE2 complex. *Cell Commun Signal,* 13**,** 41.

SELKOE, D. J. 1991. The molecular pathology of Alzheimer's disease. *Neuron,* 6**,** 487-98.

SELKOE, D. J. 2011. Resolving controversies on the path to Alzheimer's therapeutics. *Nat Med,* 17**,** 1060-5.

SELKOE, D. J. & HARDY, J. 2016. The amyloid hypothesis of Alzheimer's disease at 25 years. *EMBO Mol Med,* 8**,** 595-608.

SEPULVEDA, F. J., PARODI, J., PEOPLES, R. W., OPAZO, C. & AGUAYO, L. G. 2010. Synaptotoxicity of Alzheimer beta amyloid can be explained by its membrane perforating property. *PLoS One,* 5**,** e11820.

SESSA, G., PODINI, P., MARIANI, M., MERONI, A., SPREAFICO, R., SINIGAGLIA, F., COLONNA, M., PANINA, P. & MELDOLESI, J. 2004. Distribution and signaling of TREM2/DAP12, the receptor system mutated in human polycystic lipomembraneous osteodysplasia with sclerosing leukoencephalopathy dementia. *Eur J Neurosci,* 20**,** 2617-28.

SEYFRIED, N. T., DAMMER, E. B., SWARUP, V., NANDAKUMAR, D., DUONG, D. M., YIN, L., DENG, Q., NGUYEN, T., HALES, C. M., WINGO, T., GLASS, J., GEARING, M., THAMBISETTY, M., TRONCOSO, J. C., GESCHWIND, D. H., LAH, J. J. & LEVEY, A. I. 2017. A Multi-network Approach Identifies Protein-Specific Co-expression in Asymptomatic and Symptomatic Alzheimer's Disease. *Cell Syst,* 4**,** 60-72.e4.

SHARAN, R., SUTHRAM, S., KELLEY, R. M., KUHN, T., MCCUINE, S., UETZ, P., SITTLER, T., KARP, R. M. & IDEKER, T. 2005. Conserved patterns of protein interaction in multiple species. *Proc Natl Acad Sci U S A,* 102**,** 1974-9.

SHARMA, P., SRIVASTAVA, P., SETH, A., TRIPATHI, P. N., BANERJEE, A. G. & SHRIVASTAVA, S. K. 2019. Comprehensive review of mechanisms of pathogenesis involved in Alzheimer's disease and potential therapeutic strategies. *Prog Neurobiol,* 174**,** 53-89.

SHEN, L. & JIA, J. 2016. An Overview of Genome-Wide Association Studies in Alzheimer's Disease. *Neurosci Bull,* 32**,** 183-90.

SHERRINGTON, R., ROGAEV, E. I., LIANG, Y., ROGAEVA, E. A., LEVESQUE, G., IKEDA, M., CHI, H., LIN, C., LI, G., HOLMAN, K., TSUDA, T., MAR, L., FONCIN, J. F., BRUNI, A. C., MONTESI, M. P., SORBI, S., RAINERO, I., PINESSI, L., NEE, L., CHUMAKOV, I., POLLEN, D., BROOKES, A., SANSEAU, P., POLINSKY, R. J., WASCO, W., DA SILVA, H. A., HAINES, J. L., PERKICAK-VANCE, M. A., TANZI, R. E., ROSES, A. D., FRASER, P. E., ROMMENS, J. M. & ST GEORGE-HYSLOP, P. H. 1995. Cloning of a gene bearing missense mutations in early-onset familial Alzheimer's disease. *Nature,* 375**,** 754-60.

SHI, Y. & HOLTZMAN, D. M. 2018. Interplay between innate immunity and Alzheimer disease: APOE and TREM2 in the spotlight. *Nat Rev Immunol,* 18**,** 759-772.

SHINOTSUKA, C., WAGURI, S., WAKASUGI, M., UCHIYAMA, Y. & NAKAYAMA, K. 2002. Dominant-negative mutant of BIG2, an ARF–guanine nucleotide exchange factor, specifically affects membrane trafficking from the trans-Golgi network through inhibiting membrane association of AP-1 and GGA coat proteins. *Biochemical and Biophysical Research Communications,* 294**,** 254-260.

SHIROTANI, K., HATTA, D., WAKITA, N., WATANABE, K. & IWATA, N. 2022. The role of TREM2 N-glycans in trafficking to the cell surface and signal transduction of TREM2. *The Journal of Biochemistry,* 172**,** 347-353.

SHUKLA, V., SEO, J., BINUKUMAR, B. K., AMIN, N. D., REDDY, P., GRANT, P., KUNTZ, S., KESAVAPANY, S., STEINER, J., MISHRA, S. K., TSAI, L. H. & PANT, H. C. 2017. TFP5, a Peptide Inhibitor of Aberrant and Hyperactive Cdk5/p25, Attenuates Pathological Phenotypes and Restores Synaptic Function in CK-p25Tg Mice. *J Alzheimers Dis,* 56**,** 335-349.

SIMONAZZI, E., JONES, R. E., CHEN, F., RANSON, A., STEVENSON-HOARE, J., ESCOTT-PRICE, V., SENGPIEL, F., MORGAN, B. P. & TAYLOR, P. R. 2021. Abi3 regulates microglial ramification and dynamic tissue surveillance <em>in vivo</em&gt. *bioRxiv***,** 2021.03.19.436147.

SIMONETTI, B. & CULLEN, P. J. 2019. Actin-dependent endosomal receptor recycling. *Current Opinion in Cell Biology,* 56**,** 22-33.

SIMS, R., HILL, M. & WILLIAMS, J. 2020. The multiplex model of the genetics of Alzheimer's disease. *Nat Neurosci,* 23**,** 311-322.

SIMS, R., VAN DER LEE, S. J., NAJ, A. C., BELLENGUEZ, C., BADARINARAYAN, N., JAKOBSDOTTIR, J., KUNKLE, B. W., BOLAND, A., RAYBOULD, R., BIS, J. C., MARTIN, E. R., GRENIER-BOLEY, B., HEILMANN-HEIMBACH, S., CHOURAKI, V., KUZMA, A. B., SLEEGERS, K., VRONSKAYA, M., RUIZ, A., GRAHAM, R. R., OLASO, R., HOFFMANN, P., GROVE, M. L., VARDARAJAN, B. N., HILTUNEN, M., NÖTHEN, M. M., WHITE, C. C., HAMILTON-NELSON, K. L., EPELBAUM, J., MAIER, W., CHOI, S. H., BEECHAM, G. W., DULARY, C., HERMS, S., SMITH, A. V., FUNK, C. C.,

DERBOIS, C., FORSTNER, A. J., AHMAD, S., LI, H., BACQ, D., HAROLD, D., SATIZABAL, C. L., VALLADARES, O., SQUASSINA, A., THOMAS, R., BRODY, J. A., QU, L., SÁNCHEZ-JUAN, P., MORGAN, T., WOLTERS, F. J., ZHAO, Y., GARCIA, F. S., DENNING, N., FORNAGE, M., MALAMON, J., NARANJO, M. C. D., MAJOUNIE, E., MOSLEY, T. H., DOMBROSKI, B., WALLON, D., LUPTON, M. K., DUPUIS, J., WHITEHEAD, P., FRATIGLIONI, L., MEDWAY, C., JIAN, X., MUKHERJEE, S., KELLER, L., BROWN, K., LIN, H., CANTWELL, L. B., PANZA, F., MCGUINNESS, B., MORENO-GRAU, S., BURGESS, J. D., SOLFRIZZI, V., PROITSI, P., ADAMS, H. H., ALLEN, M., SERIPA, D., PASTOR, P., CUPPLES, L. A., PRICE, N. D., HANNEQUIN, D., FRANK-GARCÍA, A., LEVY, D., CHAKRABARTY, P., CAFFARRA, P., GIEGLING, I., BEISER, A. S., GIEDRAITIS, V., HAMPEL, H., GARCIA, M. E., WANG, X., LANNFELT, L., MECOCCI, P., EIRIKSDOTTIR, G., CRANE, P. K., PASQUIER, F., BOCCARDI, V., et al. 2017. Rare coding variants in PLCG2, ABI3, and TREM2 implicate microglial-mediated innate immunity in Alzheimer's disease. *Nat Genet,* 49**,** 1373-1384.

SINGLA, A., FEDOSEIENKO, A., GIRIDHARAN, S. S. P., OVERLEE, B. L., LOPEZ, A., JIA, D., SONG, J., HUFF-HARDY, K., WEISMAN, L., BURSTEIN, E. & BILLADEAU, D. D. 2019. Endosomal PI(3)P regulation by the COMMD/CCDC22/CCDC93 (CCC) complex controls membrane protein recycling. *Nat Commun,* 10**,** 4271.

SIRKIS, D. W., APARICIO, R. E. & SCHEKMAN, R. 2017. Neurodegeneration-associated mutant TREM2 proteins abortively cycle between the ER and ER-Golgi intermediate compartment. *Mol Biol Cell,* 28**,** 2723-2733.

SLATKIN, M. 2008. Linkage disequilibrium--understanding the evolutionary past and mapping the medical future. *Nat Rev Genet,* 9**,** 477-85.

SLATKO, B. E., GARDNER, A. F. & AUSUBEL, F. M. 2018. Overview of Next-Generation Sequencing Technologies. *Curr Protoc Mol Biol,* 122**,** e59.

SMITH-GARVIN, J. E., KORETZKY, G. A. & JORDAN, M. S. 2009. T cell activation. *Annu Rev Immunol,* 27**,** 591-619.

SOKOLINA, K., KITTANAKOM, S., SNIDER, J., KOTLYAR, M., MAURICE, P., GANDÍA, J., BENLEULMI-CHAACHOUA, A., TADAGAKI, K., OISHI, A., WONG, V., MALTY, R. H., DEINEKO, V., AOKI, H., AMIN, S., YAO, Z., MORATÓ, X., OTASEK, D., KOBAYASHI, H., MENENDEZ, J., AUERBACH, D., ANGERS, S., PRŽULJ, N., BOUVIER, M., BABU, M., CIRUELA, F., JOCKERS, R., JURISICA, I. & STAGLJAR, I. 2017. Systematic protein-protein interaction mapping for clinically relevant human GPCRs. *Mol Syst Biol,* 13**,** 918.

SRINIVASA RAO, V., SRINIVAS, K., KUMAR, G. N. & SUJIN, G. N. 2013. Protein interaction network for Alzheimer's disease using computational approach. *Bioinformation,* 9**,** 968-72.

ST GEORGE-HYSLOP, P. H., TANZI, R. E., POLINSKY, R. J., HAINES, J. L., NEE, L., WATKINS, P. C., MYERS, R. H., FELDMAN, R. G., POLLEN, D., DRACHMAN, D. & ET AL. 1987. The genetic defect causing familial Alzheimer's disease maps on chromosome 21. *Science,* 235**,** 885-90.

STADLER, C., REXHEPAJ, E., SINGAN, V. R., MURPHY, R. F., PEPPERKOK, R., UHLÉN, M., SIMPSON, J. C. & LUNDBERG, E. 2013. Immunofluorescence and fluorescent-protein tagging show high correlation for protein localization in mammalian cells. *Nat Methods,* 10**,** 315-23.

STANSLEY, B., POST, J. & HENSLEY, K. 2012. A comparative review of cell culture systems for the study of microglial biology in Alzheimer's disease. *J Neuroinflammation,* 9**,** 115.

STAROKADOMSKYY, P., GLUCK, N., LI, H., CHEN, B., WALLIS, M., MAINE, G. N., MAO, X., ZAIDI, I. W., HEIN, M. Y., MCDONALD, F. J., LENZNER, S., ZECHA, A., ROPERS, H. H., KUSS, A. W., MCGAUGHRAN, J., GECZ, J. & BURSTEIN, E. 2013. CCDC22 deficiency in humans blunts activation of proinflammatory NF-κB signaling. *J Clin Invest,* 123**,** 2244-56.

STEEGMAIER, M., KLUMPERMAN, J., FOLETTI, D. L., YOO, J. S. & SCHELLER, R. H. 1999. Vesicle-associated membrane protein 4 is implicated in trans-Golgi network vesicle trafficking. *Mol Biol Cell,* 10**,** 1957-72.

STELLBERGER, T., HÄUSER, R., BAIKER, A., POTHINENI, V. R., HAAS, J. & UETZ, P. 2010. Improving the yeast two-hybrid system with permutated fusions proteins: the Varicella Zoster Virus interactome. *Proteome Sci,* 8**,** 8.

STENSON, P. D., MORT, M., BALL, E. V., SHAW, K., PHILLIPS, A. & COOPER, D. N. 2014. The Human Gene Mutation Database: building a comprehensive mutation repository for clinical and molecular genetics, diagnostic testing and personalized genomic medicine. *Hum Genet,* 133**,** 1-9.

STOTHARD, P. 2000. The sequence manipulation suite: JavaScript programs for analyzing and formatting protein and DNA sequences. *Biotechniques,* 28**,** 1102, 1104.

STRITTMATTER, W. J., SAUNDERS, A. M., SCHMECHEL, D., PERICAK-VANCE, M., ENGHILD, J., SALVESEN, G. S. & ROSES, A. D. 1993. Apolipoprotein E: high-avidity binding to beta-amyloid and increased frequency of type 4 allele in late-onset familial Alzheimer disease. *Proc Natl Acad Sci U S A,* 90**,** 1977-81.

SU, F., BAI, F., ZHOU, H. & ZHANG, Z. 2016. Reprint of: Microglial toll-like receptors and Alzheimer's disease. *Brain, Behavior, and Immunity,* 55**,** 166-178.

SUZUKI, N., CHEUNG, T. T., CAI, X. D., ODAKA, A., OTVOS, L., JR., ECKMAN, C., GOLDE, T. E. & YOUNKIN, S. G. 1994. An increased percentage of long amyloid beta protein secreted by familial amyloid beta protein precursor (beta APP717) mutants. *Science,* 264**,** 1336-40.

SWISTOWSKI, A., ZHANG, Q., ORCHOLSKI, M. E., CRIPPEN, D., VITELLI, C., KURAKIN, A. & BREDESEN, D. E. 2009. Novel mediators of amyloid precursor protein signaling. *J Neurosci,* 29**,** 15703-12.

SZKLARCZYK, D., GABLE, A. L., NASTOU, K. C., LYON, D., KIRSCH, R., PYYSALO, S., DONCHEVA, N. T., LEGEAY, M., FANG, T., BORK, P., JENSEN, L. J. & VON MERING, C. 2021. The STRING database in 2021: customizable protein-protein networks, and functional characterization of user-uploaded gene/measurement sets. *Nucleic Acids Res,* 49**,** D605-d612.

TAI, L. M., BILOUSOVA, T., JUNGBAUER, L., ROESKE, S. K., YOUMANS, K. L., YU, C., POON, W. W., CORNWELL, L. B., MILLER, C. A., VINTERS, H. V., VAN ELDIK, L. J., FARDO, D. W., ESTUS, S., BU, G., GYLYS, K. H. & LADU, M. J. 2013. Levels of Soluble Apolipoprotein E/Amyloid-β (Aβ) Complex Are Reduced and Oligomeric Aβ Increased with APOE4 and Alzheimer Disease in a Transgenic Mouse Model and Human Samples*, [S]♦. *Journal of Biological Chemistry,* 288**,** 5914-5926.

TAKAHASHI, K., ROCHFORD, C. D. & NEUMANN, H. 2005. Clearance of apoptotic neurons without inflammation by microglial triggering receptor expressed on myeloid cells-2. *J Exp Med,* 201**,** 647-57.

TAKENAWA, T. & SUETSUGU, S. 2007. The WASP-WAVE protein network: connecting the membrane to the cytoskeleton. *Nat Rev Mol Cell Biol,* 8**,** 37-48.

TAM, V., PATEL, N., TURCOTTE, M., BOSSÉ, Y., PARÉ, G. & MEYRE, D. 2019. Benefits and limitations of genome-wide association studies. *Nat Rev Genet,* 20**,** 467-484.

TEO, G., LIU, G., ZHANG, J., NESVIZHSKII, A. I., GINGRAS, A. C. & CHOI, H. 2014. SAINTexpress: improvements and additional features in Significance Analysis of INTeractome software. *J Proteomics,* 100**,** 37-43.

TERRY, A. V., JR. & BUCCAFUSCO, J. J. 2003. The cholinergic hypothesis of age and Alzheimer's disease-related cognitive deficits: recent challenges and their implications for novel drug development. *J Pharmacol Exp Ther,* 306**,** 821-7.

TERRY, A. V., JR., BUCCAFUSCO, J. J. & JACKSON, W. J. 1993. Scopolamine reversal of nicotine enhanced delayed matching-to-sample performance in monkeys. *Pharmacol Biochem Behav,* 45**,** 925-9.

TERWEL, D., DEWACHTER, I. & VAN LEUVEN, F. 2002. Axonal transport, tau protein, and neurodegeneration in Alzheimer's disease. *Neuromolecular Med,* 2**,** 151-65.

THE INTERNATIONAL HAPMAP CONSORTIUM 2005. A haplotype map of the human genome. *Nature,* 437**,** 1299-320.

TIMMERMAN, R., BURM, S. M. & BAJRAMOVIC, J. J. 2018. An Overview of in vitro Methods to Study Microglia. *Front Cell Neurosci,* 12**,** 242.

TREMBLAY, M., LECOURS, C., SAMSON, L., SÁNCHEZ-ZAFRA, V. & SIERRA, A. 2015. From the Cajal alumni Achúcarro and Río-Hortega to the rediscovery of never-resting microglia. *Front Neuroanat,* 9**,** 45.

TROMMSDORFF, M., BORG, J. P., MARGOLIS, B. & HERZ, J. 1998. Interaction of cytosolic adaptor proteins with neuronal apolipoprotein E receptors and the amyloid precursor protein. *J Biol Chem,* 273**,** 33556-60.

TROUTMAN, T. D., HU, W., FULENCHEK, S., YAMAZAKI, T., KUROSAKI, T., BAZAN, J. F. & PASARE, C. 2012. Role for B-cell adapter for PI3K (BCAP) as a signaling adapter linking Toll-like receptors (TLRs) to serine/threonine kinases PI3K/Akt. *Proc Natl Acad Sci U S A,* 109**,** 273-8.

TURNBULL, I. R. & COLONNA, M. 2007. Activating and inhibitory functions of DAP12. *Nat Rev Immunol,* 7**,** 155-61.

TURNBULL, I. R., GILFILLAN, S., CELLA, M., AOSHI, T., MILLER, M., PICCIO, L., HERNANDEZ, M. & COLONNA, M. 2006. Cutting edge: TREM-2 attenuates macrophage activation. *J Immunol,* 177**,** 3520-4.

TURNER, A. K., SHAW, B. C., SIMPSON, J. F. & ESTUS, S. 2022. Identification and Quantitation of Novel ABI3 Isoforms Relative to Alzheimer’s Disease Genetics and Neuropathology. *Genes,* 13**,** 1607.

TURNER, M. & BILLADEAU, D. D. 2002. VAV proteins as signal integrators for multi-subunit immune-recognition receptors. *Nat Rev Immunol,* 2**,** 476-86.

UEZU, A., KANAK, D. J., BRADSHAW, T. W., SODERBLOM, E. J., CATAVERO, C. M., BURETTE, A. C., WEINBERG, R. J. & SODERLING, S. H. 2016. Identification of an elaborate complex mediating postsynaptic inhibition. *Science,* 353**,** 1123-9.

VAN DYCK, C. H., SWANSON, C. J., AISEN, P., BATEMAN, R. J., CHEN, C., GEE, M., KANEKIYO, M., LI, D., REYDERMAN, L., COHEN, S., FROELICH, L., KATAYAMA, S., SABBAGH, M., VELLAS, B., WATSON, D., DHADDA, S., IRIZARRY, M., KRAMER, L. D. & IWATSUBO, T. 2022. Lecanemab in Early Alzheimer's Disease. *New England Journal of Medicine,* 388**,** 9-21.

VENKATESAN, K., RUAL, J.-F., VAZQUEZ, A., STELZL, U., LEMMENS, I., HIROZANE-KISHIKAWA, T., HAO, T., ZENKNER, M., XIN, X., GOH, K.-I., YILDIRIM, M. A., SIMONIS, N., HEINZMANN, K., GEBREAB, F., SAHALIE, J. M., CEVIK, S., SIMON, C., SMET, A.-S. D., DANN, E., SMOLYAR, A., VINAYAGAM, A., YU, H., SZETO, D., BORICK, H., DRICOT, A., KLITGORD, N., MURRAY, R. R., LIN, C., LALOWSKI, M., TIMM, J., RAU, K., BOONE, C., BRAUN, P., CUSICK, M. E., ROTH, F. P., HILL, D. E., TAVERNIER, J., WANKER, E. E., BARABÁSI, A.-L. & VIDAL, M. 2008. An empirical framework for binary interactome mapping. *Nature Methods,* 6**,** 83-90.

VERDIER, Y. & PENKE, B. 2004. Binding sites of amyloid beta-peptide in cell plasma membrane and implications for Alzheimer's disease. *Curr Protein Pept Sci,* 5**,** 19-31.

VINCENT, C., SIDDIQUI, T. A. & SCHLICHTER, L. C. 2012. Podosomes in migrating microglia: components and matrix degradation. *J Neuroinflammation,* 9**,** 190.

VITIELLO, B., MARTIN, A., HILL, J., MACK, C., MOLCHAN, S., MARTINEZ, R., MURPHY, D. L. & SUNDERLAND, T. 1997. Cognitive and behavioral effects of cholinergic, dopaminergic, and serotonergic blockade in humans. *Neuropsychopharmacology,* 16**,** 15-24.

VITNER, E. B., SALOMON, R., FARFEL-BECKER, T., MESHCHERIAKOVA, A., ALI, M., KLEIN, A. D., PLATT, F. M., COX, T. M. & FUTERMAN, A. H. 2014. RIPK3 as a potential therapeutic target for Gaucher's disease. *Nature Medicine,* 20**,** 204-208.

VLASSENKO, A. G., MINTUN, M. A., XIONG, C., SHELINE, Y. I., GOATE, A. M., BENZINGER, T. L. & MORRIS, J. C. 2011. Amyloid-beta plaque growth in cognitively normal adults: longitudinal [11C]Pittsburgh compound B data. *Ann Neurol,* 70**,** 857-61.

WANG, C., SAAR, V., LEUNG, K. L., CHEN, L. & WONG, G. 2018. Human amyloid β peptide and tau co-expression impairs behavior and causes specific gene expression changes in Caenorhabditis elegans. *Neurobiology of Disease,* 109**,** 88-101.

WANG, H., LO, M. T., ROSENTHAL, S. B., MAKOWSKI, C., ANDREASSEN, O. A., SALEM, R. M., MCEVOY, L. K., FIECAS, M. & CHEN, C. H. 2021. Similar Genetic Architecture of Alzheimer's Disease and Differential APOE Effect Between Sexes. *Front Aging Neurosci,* 13**,** 674318.

WANG, Q., WALSH, D. M., ROWAN, M. J., SELKOE, D. J. & ANWYL, R. 2004. Block of long-term potentiation by naturally secreted and synthetic amyloid beta-peptide in hippocampal slices is mediated via activation of the kinases c-Jun N-terminal kinase, cyclin-dependent kinase 5, and p38 mitogen-activated protein kinase as well as metabotropic glutamate receptor type 5. *J Neurosci,* 24**,** 3370-8.

WANG, S., CHU, C. H., STEWART, T., GINGHINA, C., WANG, Y., NIE, H., GUO, M., WILSON, B., HONG, J. S. & ZHANG, J. 2015a. α-Synuclein, a chemoattractant, directs microglial migration via H2O2-dependent Lyn phosphorylation. *Proc Natl Acad Sci U S A,* 112**,** E1926-35.

WANG, Y., CELLA, M., MALLINSON, K., ULRICH, JASON D., YOUNG, KATHERINE L., ROBINETTE, MICHELLE L., GILFILLAN, S., KRISHNAN, GOKUL M., SUDHAKAR, S., ZINSELMEYER, BERND H., HOLTZMAN, DAVID M., CIRRITO, JOHN R. & COLONNA, M. 2015b. TREM2 Lipid Sensing Sustains the Microglial Response in an Alzheimer's Disease Model. *Cell,* 160**,** 1061-1071.

WANG, Y., ULLAND, T. K., ULRICH, J. D., SONG, W., TZAFERIS, J. A., HOLE, J. T., YUAN, P., MAHAN, T. E., SHI, Y., GILFILLAN, S., CELLA, M., GRUTZENDLER, J., DEMATTOS, R. B., CIRRITO, J. R., HOLTZMAN, D. M. & COLONNA, M. 2016. TREM2-mediated early microglial response limits diffusion and toxicity of amyloid plaques. *J Exp Med,* 213**,** 667-75.

WASINGER, V. C., CORDWELL, S. J., CERPA-POLJAK, A., YAN, J. X., GOOLEY, A. A., WILKINS, M. R., DUNCAN, M. W., HARRIS, R., WILLIAMS, K. L. & HUMPHERY-SMITH, I. 1995. Progress with gene-product mapping of the Mollicutes: Mycoplasma genitalium. *Electrophoresis,* 16**,** 1090-4.

WATERHOUSE, A. M., PROCTER, J. B., MARTIN, D. M., CLAMP, M. & BARTON, G. J. 2009. Jalview Version 2--a multiple sequence alignment editor and analysis workbench. *Bioinformatics,* 25**,** 1189-91.

WEAVER, A. M., KARGINOV, A. V., KINLEY, A. W., WEED, S. A., LI, Y., PARSONS, J. T. & COOPER, J. A. 2001. Cortactin promotes and stabilizes Arp2/3-induced actin filament network formation. *Current Biology,* 11**,** 370-374.

WEILL, U., KRIEGER, G., AVIHOU, Z., MILO, R., SCHULDINER, M. & DAVIDI, D. 2019. Assessment of GFP Tag Position on Protein Localization and Growth Fitness in Yeast. *J Mol Biol,* 431**,** 636-641.

WEINER, H. L. & FRENKEL, D. 2006. Immunology and immunotherapy of Alzheimer's disease. *Nat Rev Immunol,* 6**,** 404-16.

WEINGARTEN, M. D., LOCKWOOD, A. H., HWO, S. Y. & KIRSCHNER, M. W. 1975. A protein factor essential for microtubule assembly. *Proc Natl Acad Sci U S A,* 72**,** 1858-62.

WELLER, R. O., SUBASH, M., PRESTON, S. D., MAZANTI, I. & CARARE, R. O. 2008. Perivascular drainage of amyloid-beta peptides from the brain and its failure in cerebral amyloid angiopathy and Alzheimer's disease. *Brain Pathol,* 18**,** 253-66.

WENDT, S., MARICOS, M., VANA, N., MEYER, N., GUNEYKAYA, D., SEMTNER, M. & KETTENMANN, H. 2017. Changes in phagocytosis and potassium channel activity in microglia of 5xFAD mice indicate alterations in purinergic signaling in a mouse model of Alzheimer's disease. *Neurobiol Aging,* 58**,** 41-53.

WEST, A. G. & FRASER, P. 2005. Remote control of gene transcription. *Hum Mol Genet,* 14 Spec No 1**,** R101-11.

WHITEHOUSE, P. J., PRICE, D. L., STRUBLE, R. G., CLARK, A. W., COYLE, J. T. & DELON, M. R. 1982. Alzheimer's disease and senile dementia: loss of neurons in the basal forebrain. *Science,* 215**,** 1237-9.

WIATRAK, B., PIASNY, J., KUŹNIARSKI, A. & GĄSIOROWSKI, K. 2021. Interactions of Amyloid-β with Membrane Proteins. *Int J Mol Sci,* 22.

WINGO, T. S., LAH, J. J., LEVEY, A. I. & CUTLER, D. J. 2012. Autosomal recessive causes likely in early-onset Alzheimer disease. *Arch Neurol,* 69**,** 59-64.

WOLLERT, T. & HURLEY, J. H. 2010. Molecular mechanism of multivesicular body biogenesis by ESCRT complexes. *Nature,* 464**,** 864-9.

WORLD HEALTH ORGANISATION 2018. Projections of mortality and causes of death, 2016 to 2060. https://www.who.int/healthinfo/global_burden_disease/projections/en/: World Heath Organisation.

WORLD HEALTH ORGANISATION 2019. Dementia Fact Sheet. https://www.who.int/news-room/fact-sheets/detail/dementia: World Heath Organisation.

WU, D., LI, Y., REN, Q., PEI, S., WANG, L., YANG, L., CHONG, Y., SUN, S., HAO, J. & FENG, F. 2021. TANC1 methylation as a novel biomarker for the diagnosis of patients with anti-tuberculosis drug-induced liver injury. *Sci Rep,* 11**,** 17423.

WU, Y., DISSING-OLESEN, L., MACVICAR, B. A. & STEVENS, B. 2015. Microglia: Dynamic Mediators of Synapse Development and Plasticity. *Trends Immunol,* 36**,** 605-613.

WUNDERLICH, P., GLEBOV, K., KEMMERLING, N., TIEN, N. T., NEUMANN, H. & WALTER, J. 2013. Sequential proteolytic processing of the triggering receptor expressed on myeloid cells-2 (TREM2) protein by ectodomain shedding and γ-secretase-dependent intramembranous cleavage. *J Biol Chem,* 288**,** 33027-36.

XIE, F., YE, L., TA, M., ZHANG, L. & JIANG, W. G. 2011. MTSS1: a multifunctional protein and its role in cancer invasion and metastasis. *Front Biosci (Schol Ed),* 3**,** 621-31.

XU, W., TAN, L. & YU, J. T. 2015. The Role of PICALM in Alzheimer's Disease. *Mol Neurobiol,* 52**,** 399-413.

XU, Y. J., AU, N. P. B. & MA, C. H. E. 2022. Functional and Phenotypic Diversity of Microglia: Implication for Microglia-Based Therapies for Alzheimer's Disease. *Front Aging Neurosci,* 14**,** 896852.

YANG, J., ZHAO, Y., ZHANG, L., FAN, H., QI, C., ZHANG, K., LIU, X., FEI, L., CHEN, S., WANG, M., KUANG, F., WANG, Y. & WU, S. 2018. RIPK3/MLKL-Mediated Neuronal Necroptosis Modulates the M1/M2 Polarization of Microglia/Macrophages in the Ischemic Cortex. *Cereb Cortex,* 28**,** 2622-2635.

YE, S., DHILLON, S., KE, X., COLLINS, A. R. & DAY, I. N. 2001. An efficient procedure for genotyping single nucleotide polymorphisms. *Nucleic Acids Res,* 29**,** E88-8.

YEH, F. L., WANG, Y., TOM, I., GONZALEZ, L. C. & SHENG, M. 2016. TREM2 Binds to Apolipoproteins, Including APOE and CLU/APOJ, and Thereby Facilitates Uptake of Amyloid-Beta by Microglia. *Neuron,* 91**,** 328-40.

YIANNOPOULOU, K. G. & PAPAGEORGIOU, S. G. 2013. Current and future treatments for Alzheimer's disease. *Ther Adv Neurol Disord,* 6**,** 19-33.

YIN, J., LIU, X., HE, Q., ZHOU, L., YUAN, Z. & ZHAO, S. 2016. Vps35-dependent recycling of Trem2 regulates microglial function. *Traffic,* 17**,** 1286-1296.

YOON, S. S. & JO, S. A. 2012. Mechanisms of Amyloid-β Peptide Clearance: Potential Therapeutic Targets for Alzheimer's Disease. *Biomol Ther (Seoul),* 20**,** 245-55.

YU, H., TARDIVO, L., TAM, S., WEINER, E., GEBREAB, F., FAN, C., SVRZIKAPA, N., HIROZANE-KISHIKAWA, T., RIETMAN, E., YANG, X., SAHALIE, J., SALEHI-ASHTIANI, K., HAO, T., CUSICK, M. E., HILL, D. E., ROTH, F. P., BRAUN, P. & VIDAL, M. 2011. Next-generation sequencing to generate interactome datasets. *Nat Methods,* 8**,** 478-80.

ZEC, R. F. & BURKETT, N. R. 2008. Non-pharmacological and pharmacological treatment of the cognitive and behavioral symptoms of Alzheimer disease. *NeuroRehabilitation,* 23**,** 425-38.

ZEMPEL, H., THIES, E., MANDELKOW, E. & MANDELKOW, E. M. 2010. Abeta oligomers cause localized Ca(2+) elevation, missorting of endogenous Tau into dendrites, Tau phosphorylation, and destruction of microtubules and spines. *J Neurosci,* 30**,** 11938-50.

ZHANG, W., DUAN, N., ZHANG, Q., SONG, T., LI, Z., CHEN, X. & WANG, K. 2018. The intracellular NADH level regulates atrophic nonunion pathogenesis through the CtBP2-p300-Runx2 transcriptional complex. *Int J Biol Sci,* 14**,** 2023-2036.

ZHANG, W., YANG, S.-L., YANG, M., HERRLINGER, S., SHAO, Q., COLLAR, J. L., FIERRO, E., SHI, Y., LIU, A., LU, H., HERRING, B. E., GUO, M.-L., BUCH, S., ZHAO, Z., XU, J., LU, Z. & CHEN, J.-F. 2019a. Modeling microcephaly with cerebral organoids reveals a WDR62–CEP170–KIF2A pathway promoting cilium disassembly in neural progenitors. *Nature Communications,* 10**,** 2612.

ZHANG, X., LI, Y., XU, H. & ZHANG, Y. W. 2014a. The γ-secretase complex: from structure to function. *Front Cell Neurosci,* 8**,** 427.

ZHANG, Y., CHEN, K., SLOAN, S. A., BENNETT, M. L., SCHOLZE, A. R., O'KEEFFE, S., PHATNANI, H. P., GUARNIERI, P., CANEDA, C., RUDERISCH, N., DENG, S., LIDDELOW, S. A., ZHANG, C., DANEMAN, R., MANIATIS, T., BARRES, B. A. & WU, J. Q. 2014b. An RNA-sequencing transcriptome and splicing database of glia, neurons, and vascular cells of the cerebral cortex. *J Neurosci,* 34**,** 11929-47.

ZHANG, Y., KANG, H. R. & HAN, K. 2019b. Differential cell-type-expression of CYFIP1 and CYFIP2 in the adult mouse hippocampus. *Anim Cells Syst (Seoul),* 23**,** 380-383.

ZHAO, L. N., LONG, H., MU, Y. & CHEW, L. Y. 2012. The toxicity of amyloid β oligomers. *Int J Mol Sci,* 13**,** 7303-27.

ZHAO, X., GUAN, Y., LIU, F., YAN, S., WANG, Y., HU, M., LI, Y., LI, R. & ZHANG, C. X. 2022. SNARE Proteins Mediate α-Synuclein Secretion via Multiple Vesicular Pathways. *Molecular Neurobiology,* 59**,** 405-419.

ZHAO, Y., BHATTACHARJEE, S., JONES, B. M., DUA, P., ALEXANDROV, P. N., HILL, J. M. & LUKIW, W. J. 2013. Regulation of TREM2 expression by an NF-small ka, CyrillicB-sensitive miRNA-34a. *Neuroreport,* 24**,** 318-23.

ZHENG, H., JIA, L., LIU, C. C., RONG, Z., ZHONG, L., YANG, L., CHEN, X. F., FRYER, J. D., WANG, X., ZHANG, Y. W., XU, H. & BU, G. 2017. TREM2 Promotes Microglial Survival by Activating Wnt/beta-Catenin Pathway. *J Neurosci,* 37**,** 1772-1784.

ZHI, Y., ZHOU, X., YU, J., YUAN, L., ZHANG, H., NG, D. C. H., XU, Z. & XU, D. 2021. Pathophysiological Significance of WDR62 and JNK Signaling in Human Diseases. *Frontiers in Cell and Developmental Biology,* 9.

ZHONG, L., ZHANG, Z. L., LI, X., LIAO, C., MOU, P., WANG, T., WANG, Z., WANG, Z., WEI, M., XU, H., BU, G. & CHEN, X. F. 2017. TREM2/DAP12 Complex Regulates Inflammatory Responses in Microglia via the JNK Signaling Pathway. *Front Aging Neurosci,* 9**,** 204.

ZHONG, Q., PEVZNER, S. J., HAO, T., WANG, Y., MOSCA, R., MENCHE, J., TAIPALE, M., TAŞAN, M., FAN, C., YANG, X., HALEY, P., MURRAY, R. R., MER, F., GEBREAB, F., TAM, S., MACWILLIAMS, A., DRICOT, A., REICHERT, P., SANTHANAM, B., GHAMSARI, L., CALDERWOOD, M. A., ROLLAND, T., CHARLOTEAUX, B., LINDQUIST, S., BARABÁSI, A. L., HILL, D. E., ALOY, P., CUSICK, M. E., XIA, Y., ROTH, F. P. & VIDAL, M. 2016. An inter-species protein-protein interaction network across vast evolutionary distance. *Mol Syst Biol,* 12**,** 865.

ZHOU, J. Y., SCHEPMOES, A. A., ZHANG, X., MOORE, R. J., MONROE, M. E., LEE, J. H., CAMP, D. G., SMITH, R. D. & QIAN, W. J. 2010. Improved LC-MS/MS spectral counting statistics by recovering low-scoring spectra matched to confidently identified peptide sequences. *J Proteome Res,* 9**,** 5698-704.

ZHOU, T., HUANG, Z., SUN, X., ZHU, X., ZHOU, L., LI, M., CHENG, B., LIU, X. & HE, C. 2017. Microglia Polarization with M1/M2 Phenotype Changes in rd1 Mouse Model of Retinal Degeneration. *Front Neuroanat,* 11**,** 77.

ZHOU, Y., ZHOU, B., PACHE, L., CHANG, M., KHODABAKHSHI, A. H., TANASEICHUK, O., BENNER, C. & CHANDA, S. K. 2019. Metascape provides a biologist-oriented resource for the analysis of systems-level datasets. *Nat Commun,* 10**,** 1523.

ZHU, X. C., YU, J. T., JIANG, T., WANG, P., CAO, L. & TAN, L. 2015. CR1 in Alzheimer's disease. *Mol Neurobiol,* 51**,** 753-65.

References

ZHU, Z., LIN, Y., LI, X., DRIVER, J. A. & LIANG, L. 2019. Shared genetic architecture between metabolic traits and Alzheimer's disease: a large-scale genome-wide cross-trait analysis. *Hum Genet,* 138**,** 271-285.

Appendix 1

HA-BirA* Sequence:

TACCCATACGATGTTCCAGATTACGCTGGATCCAAGGACAACACCGTGCCCCTGAAGCTGATCGCCCTGCTGGCCAACGGCG
AGTTCCACTCTGGCGAGCAGCTGGGAGAGACCCTGGGAATGAGCAGAGCCGCCATCAACAAGCACATCCAGACACTGAGAGA
CTGGGGAGTGGACGTGTTCACCGTGCCTGGCAAGGGCTACAGCCTGCCTGAGCCTATCCAGCTGCTGAACGCCAAGCAGATC
CTGGGACAGCTGGATGGCGGAAGCGTGGCCGTGCTGCCTGTGATCGACTCCACCAATCAGTACCTGCTGGACAGAATCGGA
GAGCTGAAGTCCGGCGACGCCTGCATCGCCGAGTACCAGCAGGCTGGCAGAGGAGGCAGAGGACGGAAGTGGTTCAGCCC
ATTCGGAGCCAACCTGTACCTGTCCATGTTCTGGAGACTGGAGCAGGGACCTGCTGCTGCCATCGGACTGAGTCTGGTGATC
GGAATCGTGATGGCCGAGGTGCTGAGAAAGCTGGGAGCCGACAAGGTGAGAGTGAAGTGGCCTAATGACCTGTACCTCCAG
GACCGCAAGCTGGCTGGCATCCTGGTGGAGCTGACAGGCAAGACAGGCGATGCCGCTCAGATCGTGATCGGAGCCGGAATC
AACATGGCCATGAGAAGAGTGGAGGAGAGCGTGGTGAACCAGGGCTGGATCACCCTGCAGGAGGCTGGCATCAACCTGGAC
CGGAACACCCTGGCCGCCATGCTGATCAGAGAGCTGAGAGCCGCTCTGGAGCTGTTCGAGCAGGAGGGACTGGCTCCTTAC
CTGAGCAGATGGGAGAAGCTGGACAACTTCATCAACAGACCTGTGAAGCTGATCATCGGCGACAAGGAAATCTTCGGCATCTC
CAGAGGAATCGACAAGCAGGGAGCTCTGCTGCTGGAGCAGGACGGAATCATCAAGCCCTGGATGGGCGGAGAAATCTCCCT
GAGAAGCGCAGAGAAG

HA-BirA*-Abi3 Sequence:

TACCCATACGATGTTCCAGATTACGCTGGATCCAAGGACAACACCGTGCCCCTGAAGCTGATCGCCCTGCTGGCCAACGGCG
AGTTCCACTCTGGCGAGCAGCTGGGAGAGACCCTGGGAATGAGCAGAGCCGCCATCAACAAGCACATCCAGACACTGAGAGA
CTGGGGAGTGGACGTGTTCACCGTGCCTGGCAAGGGCTACAGCCTGCCTGAGCCTATCCAGCTGCTGAACGCCAAGCAGATC
CTGGGACAGCTGGATGGCGGAAGCGTGGCCGTGCTGCCTGTGATCGACTCCACCAATCAGTACCTGCTGGACAGAATCGGA
GAGCTGAAGTCCGGCGACGCCTGCATCGCCGAGTACCAGCAGGCTGGCAGAGGAGGCAGAGGACGGAAGTGGTTCAGCCC

ATTCGGAGCCAACCTGTACCTGTCCATGTTCTGGAGACTGGAGCAGGGACCTGCTGCTGCCATCGGACTGAGTCTGGTGATC
GGAATCGTGATGGCCGAGGTGCTGAGAAAGCTGGGAGCCGACAAGGTGAGAGTGAAGTGGCCTAATGACCTGTACCTCCAG
GACCGCAAGCTGGCTGGCATCCTGGTGGAGCTGACAGGCAAGACAGGCGATGCCGCTCAGATCGTGATCGGAGCCGGAATC
AACATGGCCATGAGAAGAGTGGAGGAGAGCGTGGTGAACCAGGGCTGGATCACCCTGCAGGAGGCTGGCATCAACCTGGAC
CGGAACACCCTGGCCGCCATGCTGATCAGAGAGCTGAGAGCCGCTCTGGAGCTGTTCGAGCAGGAGGGACTGGCTCCTTAC
CTGAGCAGATGGGAGAAGCTGGACAACTTCATCAACAGACCTGTGAAGCTGATCATCGGCGACAAGGAAATCTTCGGCATCTC
CAGAGGAATCGACAAGCAGGGAGCTCTGCTGCTGGAGCAGGACGGAATCATCAAGCCCTGGATGGGCGGAGAAATCTCCCT
GAGAAGCGCAGAGAAGGGTGCTGGCGCCGGAGCAGGGGCGGGTGCCATGGCGGAGCTGCAGCAGTTACAGCAGCTGCAGG
AGTTTGATATCCCCACGGGCCGGGAGGCTCTGCGGGGCAACCACAGCGCCCTGCTACGGGTGGCCAACTACTGCGAGGATA
ACTACTTGCAGGCCACAGACAAGCGGAAGGCGCTGGAAGAGACGATGGCTTTCACCACCCAGGCCCTAGCCAGTGTGGCCTA
CCAAGTGGGTAACCTGGCCGGGCATACTCTTCGAATGCTGGATCTACAGGGTGCTGCCCTGCGGCAGGTAGAAGCCAAGATG
AGCACACTGGGCCAGATGGTAAACATGCATATGGAGAAGGTAGCTAGAAGGGAGATCGGCACTTTGGCCACTGTTGTGCGGC
TGCCCTCTAACCAGAAAGTCATCCCTCCTGAGAGCCTGCCTTCCCTCACTCCCTACCACAGAAAACCCCTCAACTTTGCCTGCT
TGGATGACATTGGCCACGGAGTCAAGGACTTGAGCACGCAGCTGTCACGGACCGGGACCCTGTCTCGCAAGAGCATAAAGGC
GCCTGCTACACCTGTTTCCGCCACGCTGGGGAGACCACCCCGGATCCCTGAGCCGGTGCAGCTCCCAGCCGTGCCAGACGG
CAAGCTCTCCGCTGCCTCCTCTGCCTCTTCCTTGGCCTCGGCAGGCAGTGCGGAAGGTGCCAGTGGGATCCCCCAGTCCAAG
GGACAGGTAGCGCCTGCAACCCCGCCTCCTCCACCTGTAGCACCTGTAACCCCGCCTCCTCCACCGTTGTCTGCCGAGGTCT
TCTTGCCGCCCCCTCCGCTGGAGGTGTCCCAGCCCCCTCTGGAAGCAGAGTTGCCCCTGCCTCCTCCCCCAGCTCTAGAGGG
GGATGAACTGGGGCTGCTGCCTCCGCCCCCACCAGGTTTTGGACCAGATGAGCCCAGCTGGGTCCCTGCTAGCTACTTGGAG
AAAGTGGTGACCCTGTACCCATACACCCGGCAAAAGGACAATGAGCTCTCCTTCTCTGAAGGCACCGTCATCTGTGTCACTCG
CCGCTACTCGGATGGCTGGTGTGAGGGTGTCAGTTCAGAGGGCACTGGATTCTTCCCAGGGAACTATGTGGAGCCCAGCTGC
TGA

Supplementary table 1.1 Known ABI3 interactors. *Known interactions of human ABI3 downloaded from the National Center for Biotechnology Information (NCBI) database. Interactors are supported by experimental evidence including two-hybrid and affinity capture methods. Descriptions have been extracted from the corresponding NCBI entry for each protein. Human equivalent orthologues of mouse protein interactors identified by mass spectrometry of BioID samples which are considered to be high-confidence interactors after SAINTexpress analysis are highlighted in red. Sources of the interaction data: Biological General Repository for Interaction Databases (BioGRID), Human Protein Reference Database (HPRD).*

Interactor	Description	Source	Experimental Evidence	Cell/Tissue Type	Publication
ABI2	Regulator of actin cytoskeleton dynamics underlying cell motility and adhesion. Functions as a component of the WAVE complex, which activates actin nucleating machinery Arp2/3 to drive lamellipodia formation.	BioGRID	Two-hybrid	Yeast	Luck et al. (2020)
ABI3	This gene encodes a member of an adaptor protein family. Members of this family encode proteins containing a homeobox homology domain, proline rich region and Src-homology 3 (SH3) domain and are components of the Abi/WAVE complex which regulates actin polymerization. The encoded protein inhibits ectopic metastasis of tumour cells as well as cell migration.	BioGRID	Two-hybrid	Yeast	Luck et al. (2020) Rolland et al. (2014)
ABI3BP	Binds to ABI3, function unknown.	HPRD, BioGRID	Two-hybrid	Yeast, human placenta cDNA	Matsuda et al. (2001)
ACTN3	This gene encodes a member of the alpha-actin binding protein gene family. The encoded protein is primarily expressed in	BioGRID	Two-hybrid	Yeast	Rolland et al. (2014)

	skeletal muscle and functions as a structural component of sarcomeric Z line. This protein is involved in crosslinking actin containing thin filaments.				
AGTR1	Angiotensin II is a potent vasopressor hormone and a primary regulator of aldosterone secretion. It is an important effector controlling blood pressure and volume in the cardiovascular system. It acts through at least two types of receptors. This gene encodes the type 1 receptor which is thought to mediate the major cardiovascular effects of angiotensin II. This gene may play a role in the generation of reperfusion arrhythmias following restoration of blood flow to ischemic or infarcted myocardium.	BioGRID	Two-hybrid	Yeast	Sokolina et al. (2017)
ARHGAP9	This gene encodes a member of the Rho-GAP family of GTPase activating proteins. The protein has substantial GAP activity towards several Rho-family GTPases in vitro, converting them to an inactive GDP-bound state. It is implicated in regulating adhesion of hematopoietic cells to the extracellular matrix.	BioGRID	Two-hybrid	Yeast	Luck et al. (2020) Luck et al. (2020)
ARMC7	Protein coding gene, unknown function	BioGRID	Two-hybrid	Yeast	Rolland et al. (2014)
BAIAP2L2	The protein encoded by this gene binds phosphoinositides and promotes the formation of planar or curved membrane structures. The encoded protein is found in RAB13-positive vesicles and at intercellular contacts with the plasma membrane.	BioGRID	Two-hybrid	Yeast	Luck et al. (2020)

BFSP2	More than 99% of the vertebrate ocular lens is comprised of terminally differentiated lens fibre cells. Two lens-specific intermediate filament-like proteins, the protein product of this gene (phakinin), and filensin, are expressed only after fibre cell differentiation has begun. Both proteins are found in a structurally unique cytoskeletal element that is referred to as the beaded filament (BF).	BioGRID	Two-hybrid	Yeast	Luck et al. (2020)
BIL1	*Saccharomyces cerevisiae* protein	BioGRID	Two-hybrid	Yeast	Zhong et al. (2016)
BLOC1S5	This gene encodes a component of BLOC-1 (biogenesis of lysosome-related organelles complex 1). Components of this complex are involved in the biogenesis of organelles such as melanosomes and platelet-dense granules.	BioGRID	Two-hybrid	Yeast	Luck et al. (2020)
CENPQ	CENPQ is a subunit of a CENPH (MIM 605607)-CENPI (MIM 300065)-associated centromeric complex that targets CENPA (MIM 117139) to centromeres and is required for proper kinetochore function and mitotic progression.	BioGRID	Two-hybrid	Yeast	Luck et al. (2020)
CEP170P1	This locus appears to be a transcribed pseudogene similar to centrosomal protein 170kDa (CEP170).	BioGRID	Two-hybrid	Yeast	Rual et al. (2005)
CEP44	Centriole-enriched microtubule-binding protein involved in centriole biogenesis. In collaboration with CEP295 and POC1B, is required for the centriole-to-centrosome conversion by ensuring the formation of bona fide centriole wall. Functions as a	HPRD, BioGRID	Two-hybrid	Yeast	Luck et al. (2020) Rolland et al. (2014)

	linker component that maintains centrosome cohesion. Associates with CROCC and regulates its stability and localization to the centrosome.				Rual et al. (2005)
CTBP2	This gene produces alternative transcripts encoding two distinct proteins. One protein is a transcriptional repressor, while the other isoform is a major component of specialized synapses known as synaptic ribbons. Both proteins contain a NAD+ binding domain similar to NAD+-dependent 2-hydroxyacid dehydrogenases.	BioGRID	Affinity capture-MS	Human primary osteoblasts	Zhang et al. (2018)
CYFIP2	Involved in T-cell adhesion and p53/TP53-dependent induction of apoptosis. Does not bind RNA. As component of the WAVE1 complex, required for BDNF-NTRK2 endocytic trafficking and signalling from early endosomes.	HPRD	Affinity capture-Western; Reconstituted complex	Human umbilical vein endothelial cells	Hirao et al. (2006)
DESI1	Protease which deconjugates SUMO1, SUMO2 and SUMO3 from some substrate proteins. Has isopeptidase but not SUMO-processing activity. Desumoylates ZBTB46. Collaborates with UBQLN4 in the export of ubiquitinated proteins from the nucleus to the cytoplasm.	BioGRID	Two-hybrid	Yeast	Luck et al. (2020)
DTNB	This gene encodes dystrobrevin beta, a component of the dystrophin-associated protein complex (DPC). The DPC consists of dystrophin and several integral and peripheral membrane proteins, including dystroglycans, sarcoglycans, syntrophins and dystrobrevin alpha and beta. The DPC localizes to the	BioGRID	Two-hybrid	Yeast	Rolland et al. (2014)

	sarcolemma and its disruption is associated with various forms of muscular dystrophy. Dystrobrevin beta is thought to interact with syntrophin and the DP71 short form of dystrophin.				
DTNBP1	This gene encodes a protein that may play a role in organelle biogenesis associated with melanosomes, platelet dense granules, and lysosomes. A similar protein in mouse is a component of a protein complex termed biogenesis of lysosome-related organelles complex 1 (BLOC-1), and binds to alpha- and beta-dystrobrevins, which are components of the dystrophin-associated protein complex (DPC).	HPRD, BioGRID	Two-hybrid	Yeast	Rual et al. (2005)
EIF3H	Component of the eukaryotic translation initiation factor 3 (eIF-3) complex, which is required for several steps in the initiation of protein synthesis. The eIF-3 complex specifically targets and initiates translation of a subset of mRNAs involved in cell proliferation, including cell cycling, differentiation and apoptosis, and uses different modes of RNA stem-loop binding to exert either translational activation or repression.	HPRD, BioGRID	Two-hybrid	Yeast	Luck et al. (2020) Rolland et al. (2014) (Rual et al., 2005) Venkatesan et al. (2008)
EIF3M	This gene encodes a protein that is part of the eukaryotic translation initiation factor 3 complete (eIF-3) required for protein synthesis. Elevated levels of the encoded protein are present in cancer cell lines. Inactivation of the encoded protein has been	BioGRID	Two-hybrid	Yeast	Luck et al. (2020)

	shown to interfere with translation of herpes virus mRNAs by preventing the association of mRNAs with the ribosomes.				
EMILIN1	This gene encodes an extracellular matrix glycoprotein that is characterized by an N-terminal microfibril interface domain, a coiled-coiled alpha-helical domain, a collagenous domain and a C-terminal globular C1q domain. The encoded protein associates with elastic fibres at the interface between elastin and microfibrils and may play a role in the development of elastic tissues including large blood vessels, dermis, heart, and lung.	BioGRID	Two-hybrid	Yeast	Luck et al. (2020)
ENAH	This gene encodes a member of the enabled/ vasodilator-stimulated phosphoprotein. Members of this gene family are involved in actin-based motility. This protein is involved in regulating the assembly of actin filaments and modulates cell adhesion and motility.	HPRD, BioGRID	Affinity Capture-Western; Reconstituted Complex	Human umbilical vein endothelial cells	Hirao et al. (2006)
ENG	This gene encodes a homodimeric transmembrane protein which is a major glycoprotein of the vascular endothelium. This protein is a component of the transforming growth factor beta receptor complex and binds to the beta1 and beta3 peptides with high affinity.	BioGRID	Affinity Capture-MS	Human umbilical vein endothelial cells; Chinese hamster ovary cells	Gallardo-Vara et al. (2019)
EVL	Ena/VASP proteins are actin-associated proteins involved in a range of processes dependent on cytoskeleton remodelling and cell polarity such as axon guidance and lamellipodial and	BioGRID	Two-hybrid; Affinity capture-Western	Yeast; HEK 293T	Chen et al. (2018) Luck et al.

	filopodial dynamics in migrating cells. EVL enhances actin nucleation and polymerization.				(2020) Rolland et al. (2014)
FAM124B	Part of CHD7/CHD8 complex which organises chromatin.	BioGRID	Two-hybrid	Yeast	Luck et al. (2020)
FARSA	Aminoacyl-tRNA synthetases are a class of enzymes that charge tRNAs with their cognate amino acids. This gene encodes a product which is similar to the catalytic subunit of prokaryotic and Saccharomyces cerevisiae phenylalanyl-tRNA synthetases (PheRS).	BioGRID	Two-hybrid	Yeast	Rolland et al. (2014)
FBF1	Keratin-binding protein required for epithelial cell polarization. Involved in apical junction complex (AJC) assembly via its interaction with PARD3. Required for ciliogenesis.	BioGRID	Two-hybrid	Yeast	Rolland et al. (2014)
GNG13	Heterotrimeric G proteins, which consist of alpha, beta, and gamma subunits, function as signal transducers for the 7-transmembrane-helix G protein-coupled receptors. GNG13 is a gamma subunit that is expressed in taste, retinal, and neuronal tissues and plays a key role in taste transduction.	BioGRID	Two-hybrid	Yeast	Luck et al. (2020)
GOLM1	The Golgi complex plays a key role in the sorting and modification of proteins exported from the endoplasmic reticulum. The protein encoded by this gene is a type II Golgi transmembrane protein. It processes proteins synthesized in the	BioGRID	Two-hybrid	Yeast	Luck et al. (2020)

	rough endoplasmic reticulum and assists in the transport of protein cargo through the Golgi apparatus.				
GRB2	The protein encoded by this gene binds the epidermal growth factor receptor and contains one SH2 domain and two SH3 domains. Its two SH3 domains direct complex formation with proline-rich regions of other proteins, and its SH2 domain binds tyrosine phosphorylated sequences.	BioGRID	Two-hybrid	Yeast	Rolland et al. (2014)
HOMER1	This gene encodes a member of the homer family of dendritic proteins. Members of this family regulate group 1 metabotropic glutamate receptor function.	HPRD, BioGRID	Two-hybrid	Yeast	Luck et al. (2020) Rual et al. (2005)
HOMER2	This gene encodes a member of the homer family of dendritic proteins. Members of this family regulate group 1 metabotropic glutamate receptor function. The encoded protein is a postsynaptic density scaffolding protein.	BioGRID	Two-hybrid	Yeast	Luck et al. (2020)
HOMER3	This gene encodes a member of the HOMER family of postsynaptic density scaffolding proteins that share a similar domain structure consisting of an N-terminal Enabled/vasodilator-stimulated phosphoprotein homology 1 domain which mediates protein-protein interactions, and a carboxy-terminal coiled-coil domain and two leucine zipper motifs that are involved in self-oligomerization. The encoded protein binds numerous other proteins including group I metabotropic glutamate receptors,	BioGRID	Two-hybrid	Yeast	Luck et al. (2020) Venkatesan et al. (2008)

	inositol 1,4,5-trisphosphate receptors and amyloid precursor proteins and has been implicated in diverse biological functions such as neuronal signalling, T-cell activation and trafficking of amyloid beta peptides.				
IFT20	This gene encodes an intraflagellar transport protein important for intracellular transport. The encoded protein forms part of a complex involved in trafficking of proteins from the Golgi body, including recycling of immune signalling components.	BioGRID	Two-hybrid	Yeast	Luck et al. (2020)
IHO1	Required for DNA double-strand breaks (DSBs) formation in unsynapsed regions during meiotic recombination. Probably acts by forming a complex with MEI4 and REC114, which activates DSBs formation in unsynapsed regions, an essential step to ensure completion of synapsis.	BioGRID	Two-hybrid	Yeast	Luck et al. (2020)
KANK2	This gene encodes a member of the KN motif and ankyrin repeat domains (KANK) family of proteins, which play a role in cytoskeletal formation by regulating actin polymerization. The encoded protein functions in the sequestration of steroid receptor coactivators and possibly other proteins.	BioGRID	Two-hybrid	Yeast	Luck et al. (2020) Rolland et al. (2014)
KIAA0408	Uncharacterised protein, function unknown.	HPRD, BioGRID	Two-hybrid	Yeast	Luck et al. (2020) Rual et al. (2005)

KIFC3	This gene encodes a member of the kinesin-14 family of microtubule motors. Members of this family play a role in the formation, maintenance and remodelling of the bipolar mitotic spindle. The protein encoded by this gene has cytoplasmic functions in the interphase cells. It may also be involved in the final stages of cytokinesis.	BioGRID	Two-hybrid	Yeast	Luck et al. (2020)
KLC3	This gene encodes a member of the kinesin light chain gene family. Kinesins are molecular motors involved in the transport of cargo along microtubules and are composed of two kinesin heavy chain (KHC) and two kinesin light chain (KLC) molecules. KLCs are thought to typically be involved in binding cargo and regulating kinesin activity.	BioGRID	Two-hybrid	Yeast	Rolland et al. (2014)
KLC4	Kinesin is a microtubule-associated force-producing protein that may play a role in organelle transport. The light chain may function in coupling of cargo to the heavy chain or in the modulation of its ATPase activity.	BioGRID	Two-hybrid	Yeast	Rolland et al. (2014)
KRT13	The protein encoded by this gene is a member of the keratin gene family. The keratins are intermediate filament proteins responsible for the structural integrity of epithelial cells and are subdivided into cytokeratins and hair keratins. Most of the type I cytokeratins consist of acidic proteins which are arranged in pairs of heterotypic keratin chains. This type I cytokeratin is paired with	BioGRID	Two-hybrid	Yeast	Rolland et al. (2014)

	keratin 4 and expressed in the suprabasal layers of non-cornified stratified epithelia.				
KRT14	This gene encodes a member of the keratin family, the most diverse group of intermediate filaments. This gene product, a type I keratin, is usually found as a heterotetramer with two keratin 5 molecules, a type II keratin. Together they form the cytoskeleton of epithelial cells.	BioGRID	Two-hybrid	Yeast	Luck et al. (2020)
KRT15	The protein encoded by this gene is a member of the keratin gene family. The keratins are intermediate filament proteins responsible for the structural integrity of epithelial cells and are subdivided into cytokeratins and hair keratins.	HPR, BioGRID	Two-hybrid	Yeast	Rual et al. (2005)
KRT24	This gene encodes a member of the type I (acidic) keratin family, which belongs to the superfamily of intermediate filament (IF) proteins. Keratins are heteropolymeric structural proteins which form the intermediate filament. These filaments, along with actin microfilaments and microtubules, compose the cytoskeleton of epithelial cells.	BioGRID	Two-hybrid	Yeast	Luck et al. (2020)
KRT28	This gene encodes a member of the type I (acidic) keratin family, which belongs to the superfamily of intermediate filament (IF) proteins. Keratins are heteropolymeric structural proteins which form the intermediate filament. These filaments, along with actin microfilaments and microtubules, compose the cytoskeleton of epithelial cells.	BioGRID	Two-hybrid	Yeast	Luck et al. (2020)

KRT31	The protein encoded by this gene is a member of the keratin gene family. As a type I hair keratin, it is an acidic protein which heterodimerizes with type II keratins to form hair and nails.	BioGRID	Two-hybrid	Yeast	Luck et al. (2020)
KRT35	The protein encoded by this gene is a member of the keratin gene family. This type I hair keratin is an acidic protein which heterodimerizes with type II keratins to form hair and nails.	BioGRID	Two-hybrid	Yeast	Luck et al. (2020)
KRT36	The protein encoded by this gene is a member of the keratin gene family. This type I hair keratin is an acidic protein which heterodimerizes with type II keratins to form hair and nails.	BioGRID	Two-hybrid	Yeast	Luck et al. (2020)
KRT38	The protein encoded by this gene is a member of the keratin gene family. As a type I hair keratin, it is an acidic protein which heterodimerizes with type II keratins to form hair and nails.	BioGRID	Two-hybrid	Yeast	Luck et al. (2020)
MAGEA12	This gene is closely related to several other genes clustered on chromosome X. These genes may be overexpressed in tumours.	BioGRID	Two-hybrid	Yeast	Rolland et al. (2014)
MED29	MED29 is a subunit of the Mediator complex, a multiprotein coactivator of RNA transcription that interacts with DNA-bound transcriptional activators, RNA polymerase II (see MIM 180660), and general initiation factors.	BioGRID	Two-hybrid	Yeast	Luck et al. (2020)
MIS18A	Required for recruitment of CENPA to centromeres and normal chromosome segregation during mitosis.	BioGRID	Two-hybrid	Yeast	Luck et al. (2020)
MRFAP1	This gene encodes an intracellular protein that interacts with members of the MORF4/MRG (mortality factor on chromosome	BioGRID	Two-hybrid	Yeast	Luck et al. (2020)

	4/MORF4 related gene) family and the tumour suppressor Rb (retinoblastoma protein.) The protein may play a role in senescence, cell growth and immortalization.				
MRFAP1L1	Protein coding gene, function unknown.	BioGRID	Two-hybrid	Yeast	Rolland et al. (2014)
NCK2	This gene encodes a member of the NCK family of adaptor proteins. The protein contains three SH3 domains and one SH2 domain. The protein has no known catalytic function but has been shown to bind and recruit various proteins involved in the regulation of receptor protein tyrosine kinases. It is through these regulatory activities that this protein is believed to be involved in cytoskeletal reorganization.	BioGRID	Two-hybrid	Yeast	Luck et al. (2020) Rolland et al. (2014)
NDEL1	This gene encodes a coiled-coil protein that plays a role in multiple processes including cytoskeletal organization, cell signalling and neuron migration, outgrowth, and maintenance.	BioGRID	Two-hybrid	Yeast	Luck et al. (2020)
NHSL2	Involved in cell differentiation, exact function unknown.	BioGRID	Two-hybrid	Yeast	Luck et al. (2020)
NUP58	This gene encodes a member of the nucleoporin family that shares 87% sequence identity with rat nucleoporin p58. The protein is localized to the nuclear rim and is a component of the nuclear pore complex (NPC). All molecules entering or leaving	BioGRID	Two-hybrid	Yeast	Luck et al. (2020) Rolland et al.

	the nucleus either diffuse through or are actively transported by the NPC.				(2014) Yu et al. (2011)
OIP5	The protein encoded by this gene localizes to centromeres, where it is essential for recruitment of CENP-A through the mediator Holliday junction recognition protein.	BioGRID	Two-hybrid	Yeast	Luck et al. (2020)
PAK1	This gene encodes a family member of serine/threonine p21-activating kinases, known as PAK proteins. These proteins are critical effectors that link Rho GTPases to cytoskeleton reorganization and nuclear signalling, and they serve as targets for the small GTP binding proteins Cdc42 and Rac. This specific family member regulates cell motility and morphology.	HPRD, BioGRID	Reconstituted complex	Mouse fibroblasts	Ichigotani et al. (2002)
PAK2	The p21 activated kinases (PAK) are critical effectors that link Rho GTPases to cytoskeleton reorganization and nuclear signalling. The PAK proteins are a family of serine/threonine kinases that serve as targets for the small GTP binding proteins, CDC42 and RAC1, and have been implicated in a wide range of biological activities. The protein encoded by this gene is activated by proteolytic cleavage during caspase-mediated apoptosis and may play a role in regulating the apoptotic events in the dying cell.	HPRD, BioGRID	Reconstituted complex	Mouse fibroblasts	Ichigotani et al. (2002)
PRP39	*Saccharomyces cerevisiae* protein	BioGRID	Two-hybrid	Yeast	Zhong et al. (2016)

PSMA1	The proteasome is a multicatalytic proteinase complex with a highly ordered ring-shaped 20S core structure. Proteasomes are distributed throughout eukaryotic cells at a high concentration and cleave peptides in an ATP/ubiquitin-dependent process in a non-lysosomal pathway. An essential function of a modified proteasome, the immunoproteasome, is the processing of class I MHC peptides. This gene encodes a member of the peptidase T1A family, which is a 20S core alpha subunit.	BioGRID	Two-hybrid	Yeast	Rolland et al. (2014)
RUFY3	This gene encodes a RPIP8, UNC-14, and NESCA domain-containing protein that is required for maintenance of neuronal polarity. In addition, it has been implicated in mediation of gastric cancer cell migration and invasion via interaction with P21-activated kinase-1, which promotes its expression. The encoded protein localizes to F-actin-enriched invadopodia to induce formation of protrusions, thereby facilitating cell migration.	BioGRID	Two-hybrid	Yeast	Luck et al. (2020)
RUNX1T1	This gene encodes a member of the myeloid translocation gene family which interact with DNA-bound transcription factors and recruit a range of corepressors to facilitate transcriptional repression.	HPRD, BioGRID	Two-hybrid	Yeast	Luck et al. (2020) Rolland et al. (2014) Rual et al. (2005)
SH3BP1	This gene encodes a member of the Rho GTPase activating protein (RhoGAP) family. The encoded protein regulates Rac	BioGRID	Two-hybrid	Yeast	Luck et al. (2020)

	signalling and plays a role in cytoskeletal dynamics, cell motility and epithelial junction formation. This protein's association with the exocyst complex, which tethers secretory vesicles to the plasma membrane, has been demonstrated to be important in cell motility. In a distinct complex, this protein has been shown to regulate epithelial junction formation and morphogenesis. By interacting with the Plexin-D1 cell surface receptor, this protein mediates changes in the cytoskeleton in response to semaphorin binding. This protein may promote metastasis in human liver cancer cells and tissues.				
SMARCD1	The protein encoded by this gene is a member of the SWI/SNF family of proteins, whose members display helicase and ATPase activities, and which are thought to regulate transcription of certain genes by altering the chromatin structure around those genes. The encoded protein is part of the large ATP-dependent chromatin remodelling complex SNF/SWI and has sequence similarity to the yeast Swp73 protein.	BioGRID	Two-hybrid	Yeast	Luck et al. (2020)
SNAP23	Specificity of vesicular transport is regulated, in part, by the interaction of a vesicle-associated membrane protein termed synaptobrevin/VAMP with a target compartment membrane protein termed syntaxin. These proteins, together with SNAP25 (synaptosome-associated protein of 25 kDa), form a complex which serves as a binding site for the general membrane fusion	HPRD, BioGRID	Two-hybrid	Yeast	Rual et al. (2005)

	machinery. Synaptobrevin/VAMP and syntaxin are believed to be involved in vesicular transport in most, if not all cells, while SNAP25 is present almost exclusively in the brain, suggesting that a ubiquitously expressed homolog of SNAP25 exists to facilitate transport vesicle/target membrane fusion in other tissues. The protein encoded by this gene is structurally and functionally similar to SNAP25 and binds tightly to multiple syntaxins and synaptobrevins/VAMPs. It is an essential component of the high affinity receptor for the general membrane fusion machinery and is an important regulator of transport vesicle docking and fusion.				
SOS1	This gene encodes a protein that is a guanine nucleotide exchange factor for RAS proteins, membrane proteins that bind guanine nucleotides and participate in signal transduction pathways. GTP binding activates and GTP hydrolysis inactivates RAS proteins. The product of this gene may regulate RAS proteins by facilitating the exchange of GTP for GDP.	HPRD	Two-hybrid	Yeast	Ichigotani et al. (2002)
STX1A	This gene encodes a member of the syntaxin superfamily. Syntaxins are nervous system-specific proteins implicated in the docking of synaptic vesicles with the presynaptic plasma membrane. Syntaxins bind synaptotagmin in a calcium-dependent fashion and interact with voltage dependent calcium and potassium channels via the C-terminal H3 domain. This gene	BioGRID	Two-hybrid	Yeast	Luck et al. (2020)

	product is a key molecule in ion channel regulation and synaptic exocytosis.				
STX2	The product of this gene belongs to the syntaxin/epimorphin family of proteins. The syntaxins are a large protein family implicated in the targeting and fusion of intracellular transport vesicles. The product of this gene regulates epithelial-mesenchymal interactions and epithelial cell morphogenesis and activation.	BioGRID	Two-hybrid	Yeast	Luck et al. (2020)
SUFU	The Hedgehog signalling pathway plays an important role in early human development. The pathway is a signalling cascade that plays a role in pattern formation and cellular proliferation during development. This gene encodes a negative regulator of the hedgehog signalling pathway.	BioGRID	Two-hybrid	Yeast	Luck et al. (2020)
TAE1	*Saccharomyces cerevisiae* protein	BioGRID	Two-hybrid	Yeast	Zhong et al. (2016)
TMEM147	Component of a ribosome-associated endoplasmic reticulum (ER) translocon complex involved in multi-pass membrane protein transport into the ER membrane and biogenesis.	HPRD, BioGRID	Two-hybrid	Yeast	Rual et al. (2005)
TRAF4	This gene encodes a member of the TNF receptor associated factor (TRAF) family. TRAF proteins are associated with, and mediate signal transduction from members of the TNF receptor superfamily. The encoded protein has been shown to interact with neurotrophin receptor, p75 (NTR/NTSR1), and negatively	BioGRID	Two-hybrid	Yeast	Luck et al. (2020)

	regulate NTR induced cell death and NF-kappa B activation. This protein has been found to bind to p47phox, a cytosolic regulatory factor included in a multi-protein complex known as NAD(P)H oxidase. This protein thus, is thought to be involved in the oxidative activation of MAPK8/JNK.				
TXN2	This nuclear gene encodes a mitochondrial member of the thioredoxin family, a group of small multifunctional redox-active proteins. The encoded protein may play important roles in the regulation of the mitochondrial membrane potential and in protection against oxidant-induced apoptosis.	BioGRID	Two-hybrid	Yeast	Luck et al. (2020)
VARS2	This gene encodes a mitochondrial aminoacyl-tRNA synthetase, which catalyses the attachment of valine to tRNA(Val) for mitochondrial translation.	BioGRID	Two-hybrid	Yeast	Luck et al. (2020)
VASP	Vasodilator-stimulated phosphoprotein (VASP) is a member of the Ena-VASP protein family. VASP is associated with filamentous actin formation and likely plays a widespread role in cell adhesion and motility. VASP may also be involved in the intracellular signalling pathways that regulate integrin-extracellular matrix interactions. VASP is regulated by the cyclic nucleotide-dependent kinases PKA and PKG.	BioGRID	Two-hybrid	Yeast	Luck et al. (2020) Rolland et al. (2014)
WAS	The Wiskott-Aldrich syndrome (WAS) family of proteins share similar domain structure and are involved in transduction of signals from receptors on the cell surface to the actin	BioGRID	Two-hybrid	Yeast	Rolland et al. (2014)

	cytoskeleton. Recent studies have demonstrated that these proteins, directly or indirectly, associate with the small GTPase, Cdc42, known to regulate formation of actin filaments, and the cytoskeletal organizing complex, Arp2/3. The WAS gene product is a cytoplasmic protein, expressed exclusively in hematopoietic cells.				Yu et al. (2011)
WASF1	The protein encoded by this gene, a member of the Wiskott-Aldrich syndrome protein (WASP)-family, plays a critical role downstream of Rac, a Rho-family small GTPase, in regulating the actin cytoskeleton required for membrane ruffling. It has been shown to associate with an actin nucleation core Arp2/3 complex while enhancing actin polymerization in vitro.	BioGRID	Two-hybrid	Yeast	Luck et al. (2020)
WASF2	This gene encodes a member of the Wiskott-Aldrich syndrome protein family. The gene product is a protein that forms a multiprotein complex that links receptor kinases and actin. Binding to actin occurs through a C-terminal verprolin homology domain in all family members. The multiprotein complex serves to transduce signals that involve changes in cell shape, motility, or function.	HPRD, BioGRID	Affinity Capture-Western; Reconstituted Complex	Human umbilical vein endothelial cells	Hirao et al. (2006)

Supplementary table 1.2 Known Abi3 interactors. *Known interactions of mouse Abi3 downloaded from the National Center for Biotechnology Information (NCBI) database. Interactors are supported by experimental evidence including co-fractionation and affinity capture methods. Descriptions have been extracted from the corresponding NCBI entry for each protein. Interactors identified by mass spectrometry of BioID samples which are considered to be high-confidence interactors after SAINTexpress analysis are highlighted in red. Sources of the interaction data: Biological General Repository for Interaction Databases (BioGRID), Human Protein Reference Database (HPRD).*

Interactor	Description	Source	Experimental Evidence	Cell/Tissue Type	Publication
Actn3	This gene encodes a member of the alpha-actin binding protein gene family. The encoded protein is primarily expressed in skeletal muscle and functions as a structural component of sarcomeric Z line. This protein is involved in crosslinking actin containing thin filaments.	BioGRID	Co-fractionation	Adult CD1 mouse whole brain lysate	Pourhaghighi et al. (2020)
Eif3h	Component of the eukaryotic translation initiation factor 3 (eIF-3) complex, which is required for several steps in the initiation of protein synthesis. The eIF-3 complex stimulates mRNA recruitment to the 43S PIC and scanning of the mRNA for AUG recognition, is required for disassembly and recycling of post-termination ribosomal complexes and subsequently prevents premature joining of the 40S and 60S ribosomal subunits prior to initiation, specifically targets and initiates translation of a subset of mRNAs involved in cell proliferation, including cell cycling, differentiation and apoptosis, and uses different modes of RNA	BioGRID	Co-fractionation	Adult CD1 mouse whole brain lysate	Pourhaghighi et al. (2020)

	stem-loop binding to exert either translational activation or repression.				
Hdac4	Responsible for the deacetylation of lysine residues on the N-terminal part of the core histones (H2A, H2B, H3 and H4). Histone deacetylation gives a tag for epigenetic repression and plays an important role in transcriptional regulation, cell cycle progression and developmental events. Histone deacetylases act via the formation of large multiprotein complexes. Involved in muscle maturation via its interaction with the myocyte enhancer factors such as MEF2A, MEF2C and MEF2D. Deacetylates HSPA1A and HSPA1A at 'Lys-77' leading to their preferential binding to co-chaperone STUB1.	BioGRID	Affinity Capture-MS	HttQ20 mouse striatum lysates (at 10 months but not 2 months of age)	Federspiel et al. (2019)
Kank2	Involved in transcription regulation by sequestering in the cytoplasm nuclear receptor coactivators such as NCOA1, NCOA2 and NCOA3. Involved in regulation of caspase-independent apoptosis by sequestering the proapoptotic factor AIFM1 in mitochondria. Pro-apoptotic stimuli can induce its proteasomal degradation allowing the translocation of AIFM1 to the nucleus to induce apoptosis. Involved in the negative control of vitamin D receptor signalling pathway. Involved in actin stress fibres formation through its interaction with ARHGDIA and the regulation of the Rho signalling pathway. May thereby play a role in cell adhesion and migration, regulating for instance podocytes	BioGRID	Co-fractionation	Adult CD1 mouse whole brain lysate	Pourhaghighi et al. (2020)

	migration during development of the kidney. Through the Rho signalling pathway may also regulate cell proliferation.				

Supplementary table 1.3 Mass spectrometry data for Abi3-associated proteins. *Peptide sequences of high-confidence interactors of Abi3 as determined by SAINTexpress. Peptide sequences identified by mass spectrometry are presented with each interactor with peptide count and percentage coverage values generated from each biological replicate.*

Protein	Peptide Sequences		MS Data
Cep170	AESEVPIVK	MQQQEQKEQAQWTPTKFPSK	Abi3 R1
	ALHPAAAGVAAAASTEFENAESEADFSIHFNR	MQSTGSAMPASSSFK	Coverage:
	ALLHSGSSSSK	NALGHIDK	72%
	AQSTEKHQEQAATSSTHHR	NALGHIDKCR	Peptide
	ASPGTQDLPGIQTGMMAPENK	NQATSASSEKDNDDDQSDKGTYTIELENPNSEEVEAR	Count: 101
	ASVASEVSTTSSTSKPPTGR	NWDDIENK	
	ATLEEHLR	NWDDIENKLR	Abi3 R2
	ATLEEHLRR	PQPAEHPDHLTITR	Coverage:
	CREESSKQESQLLEK	QDTELQEK	63%
	CSTSSPSKDVTK	QDTELQEKEAQVYQSEKHDADR	Peptide
	DKDRNWDDIENK	QESQLLEK	Count: 90
	DLGSLNGTFVNDVR	QGSFTIDKPSSNIPIELIPHINK	
	DNSISPESDVDTASTISLVTGETER	QGSFTIDKPSSNIPIELIPHINKQNSSVPTALALTSASR	Abi3 R3
	DTEAVMAFLEAK	QHAVINYDASMDEHLVK	Coverage:
	DWALNSAAVVMEER	QKSEEPSVSLPFLQTALLR	58%
	DWTAHREEIAR	QLQVINAMIDPDGTLEALNNMGFPNAILPSPPK	Peptide
	EAQVYQSEK	QNSSVPTALALTSASR	Count: 76

	EAQVYQSEKHDADR EDNNKTDEGPDTPSYNR EESSKQESQLLEK EEVGDLHGEMHK EFQQPSQIAESTIHEIPTK EINDVAGEIDSVTSSGTAPSTTVSTAATTPGSAIDTR EKSETEKETSLVK EPSYFEIPTK EPSYFEIPTKEFQQPSQIAESTIHEIPTK EQAQWTPTKFPSK ERSDSLDTDSSMDTTLILK FGYDTNLFTVVR FNPDGEEEDVTVHE FPTDYASTSEDEFGSNR FTIQLQLSQK FVQSSGR GEMRVPEEALK GGHGVPHGK GLIKDWALNSAAVVMEER GTDSKVEAAAEVQPR GTPLYGQPSWWGDAEEDEQR	QSIDKTAGK RATLEEHLR RFPTDYASTSEDEFGSNR RTLPQLPNEEK SDSEATISR SDSLDTDSSMDTTLILK SDVPVYLK SDVPVYLKR SEEPSVSLPFLQTALLR SEIGEKQDTELQEK SEIGEKQDTELQEKEAQVYQSEK SETEKETSLVK SFTSLYKDR SIKSDVPVYLKR SKTSPVASGSTSK SMSSTHGSPSVNSR SQEAGASGCSTEAK SSESELPK SSGSLGHRPSQEMDVMLK SSPVNNHSSPSQTPALCPPETR STSCTTSLASQGER	Abi3 R4 Coverage: 63% Peptide Count: 82 Abi3 R5 Coverage: 52% Peptide Count: 66

	HQEQAATSSTHHR	SVDKQHAVINYDASMDEHLVK	
	HVEGQSAAASEEALFPFCR	SVDSRPQPAEHPDHLTITR	
	IDLLAQPR	TAEAVIR	
	IKEQEDYIR	TDEGPDTPSYNR	
	IKEQEDYIRDWTAHR	TLPQLPNEEK	
	ILFKDKDR	TLPQLPNEEKLLESSR	
	IPEQTYITLK	TPLTSADEHNIHSK	
	IRQPSIDLTDDDQTSSVPHSAISDIMSSDQETYSCK	TSPVASGSTSK	
	ISQDLALIAR	TSSMEISSILQELK	
	KAEEIPK	TSSMEISSILQELKR	
	KASPGTQDLPGIQTGMMAPENK	TWSRDEVMGDNLLLSSVFQFSR	
	KFVQSSGR	VADWLAQNNPPQMVWER	
	KIPPLVHSK	VADWLAQNNPPQMVWERTEEDSK	
	KPLSTPGFHNSEEAISSSGSK	VEAAAEVQPR	
	KPLSTPGFHNSEEAISSSGSKR	VFDESLNFR	
	KSFTSLYK	VFDESLNFRK	
	KSFTSLYKDR	VFGVDDNQDYNRPIINEK	
	LGEASDSELADADK	VIQNESK	
	LGEASDSELADADKASVASEVSTTSSTSKPPTGR	VIQNESKR	
	LGSLSAR	VKSMSSTHGSPSVNSR	
	LKGNKHDDGTQSDSENAGAHR	VPEEALK	

	LMELSATVENETDTGDAGVSLR LRAESEVPIVK LREDNNKTDEGPDTPSYNR LRTSPALK LVPSDKLSPR	VPEEALKHEK VSGHSTSKGDR VTIRDHVTK WVSQWASLAANHTR	
Wasf2	DDGKEALK DVVGNDVATILSR EEEVSLQGINTR FYTNPSYFFDLWK GSVLAGPK GSVLAGPKR KDNPNRGNVNPR MGQEFVESK MKMGQEFVESK MLQDTKDIMK MLQDTKDIMKEK NSLPVPVLETYNSCDAPPPLNNLSPYR	NSLPVPVLETYNSCDAPPPLNNLSPYRDDGK NSLPVPVLETYNSCDAPPPLNNLSPYRDDGKEALK QLGSLSK QTLPSDTSELECR SDLLSAIR SSLPAVSDAR TNITLANVIR TRKEEWEK TSMVSPSHPPPAPPLSSPPGPK VNSLAER VTQLDPKEEEVSLQGINTR YAEDIFGEICTQASAFASR	Abi3 R1 Coverage: 37% Peptide Count: 19 Abi3 R2 Coverage: 37% Peptide Count: 16 Abi3 R3 Coverage: 36% Peptide Count: 16

			Abi3 R4 Coverage: 33% Peptide Count: 14 Abi3 R5 Coverage: 34% Peptide Count: 14
Cyfip1	ALNLAYSSIYGSYR AVGPSSTQLYMVR DFVSEAYLITLGK DKQPNAQPQYLHGSK EANHNVSAPYGR EASMMEYVLYSLDLYNDSAHYALTK EFFLELTMGR EGDLLTK FALVEVIAMIK	MADPQSIQESQNLSMFLANHNK MESVFNHAIR MYLTPSEK NAFVTGIAR NFVGPPHFQVICR NVIQSVLQAIR QPNAQPQYLHGSK SGDGESTPVEHVR SLELAIGR	Abi3 R1 Coverage: 35% Peptide Count: 38 Abi3 R2 Coverage: 11%

	FAVLDFCYHLLK FINMFAVLDELKNMK FISELAR FQILNDEIITILDK HTVYAALQDFSQVTLR HVQLLGR KDFVSEAYLITLGK KFQILNDEIITILDK KNVIQSVLQAIR LGTPQQIAIAR LLGYQGIAVVMEELLK LMNFMYFQR LVHPTDK LVHPTDKYSNKDCPDNAEEYER	SSLEGPTILDIEK TFLDDPIWR TMLESLIADK TVCDWETGHEPFNDPALR TVCFQNLR TVEVLEPEVTK VMAGSLLLDKR VSAAMYK WTCASSSSSPQYNICEQMIQIR YAPLHLVPLIER YLTLDSFDAMFR YNYTTEEK YSNKDCPDNAEEYER YSNSEVVTGSGR	Peptide Count: 12 Abi3 R3 Coverage: 19% Peptide Count: 21 Abi3 R4 Coverage: 12% Peptide Count: 13 Abi3 R5 Coverage: 2% Peptide Count: 2
Ccdc22	AAQEQELESLR DCPGDEDRVR	QENAGLLGR QLIEHLR	Abi3 R1

	DLLLFLAER FTFHLEPQVQAAQVADVPATSQR HRVPLLAEYR ILEIVGNIR ILIHSLR ILSDTKELQK LAEIQELHHSVR LPSDASEDADQPAGDSAIFLR LQGSALQQPFHSSR	QLVSELETLPK QSELSVAEQEQALR QSWGPLGAPTQVR TLGINLVQVETECR TVELLPDGAANLAK VINPDVGSGLSHLLPPAMSAR VPLLAEYR YLAALHENCSQLIQTIEDTGTIMR	Coverage: 33% Peptide Count: 17 Abi3 R2 Coverage: 6% Peptide Count: 4 Abi3 R3 Coverage: 11% Peptide Count: 5 Abi3 R4 Coverage: 4% Peptide Count: 2

			Abi3 R5 Coverage: 3% Peptide Count: 2
Mtss1	DWAKPGPYDQPLVNTLQR EPDSNGGGPTTTGGPPAGAEEAQRPR GDIQPQLDSALQDVNDKYLLLEETEK GLQLDVQR GTIGAGPIPIK KSSVCSSLNSVNSSDSR LSSVSSHDSGFISQDAFQSK NSDISQSYR PGPYDQPLVNTLQR RGTIGAGPIPIK	RGTIGAGPIPIKTPVIPVK RPASTAGLPTTLGPAMVTPGVATIR RTPSTKPSVR SSNLAQQAPVR SSVCSSLNSVNSSDSR TPSTKPSVR TPVIPVK TTVVAAAAFLDAFQK VANQLDKDHAK	Abi3 R1 Coverage: 16% Peptide Count: 8 Abi3 R2 Coverage: 15% Peptide Count: 8 Abi3 R3 Coverage: 18%

			Peptide Count: 11 Abi3 R4 Coverage: 11% Peptide Count: 5 Abi3 R5 Coverage: 14% Peptide Count: 8
Tanc1	ADAALISK ADNEPSCSPAAQELLTR ANFQEIISALPFVK AVVQYLVEEGAEIDQTDKNGR DKGTTQVQGGTAEHRPR DLLIKEPQLQSMLSLR DSGIIATITSSSENDDRSGSSLEWNR	LVCLLIK LVEEGNVMYK MSSSTSSLTSSSSVSDGFK NGHALLAFMFSR NQHLEGTGPFTAGTGCGHFGDR NTAVVVTLLR NTELAENR	Abi3 R1 Coverage: 35% Peptide Count: 43 Abi3 R2

	EAGGDFGSETPALSSSGDSPVNSLSTTEDTYR ETVAQSGLVMQPTK FAPYKPQEILLKPLLFEVPSITTDSVFVGR FMTQSAFDR FQQQSNPPNR GAALSSLDKEGLSALSWACLK GCDVNLSDK GHSDILQYLLNCEWSAGPPQPGTLR GKVEICELLLER GQCALVHSALR GTTQVQGGTAEHRPR GVLEPLTSLR HPASLSSSGSSGSPSSSIK IPEEEYIILIDGLNEAEFHKPDYGDTLSSFITK LCPNNQEIKR LGASQSLQLQR LLAHASVAVDMAPPNQGGPVSCSDVR LLILGGANVNYR LSLDDFPDNKDIHSDLHAYVQHR LTLDLFQR LVALSCHGSR	QFLAALADLQEAVK QGHWQVVR QSLLTQSR RADNCSPVAEEETTGSAESVLPK SCVQDPVAAFK SESGTAYPLPSK SGSSLEWNR SHLTSAKPK SPCETISSPSSTLESK SQPPPSVPSPYIR SSDPTQDLPGTPLLSPSSSTSALSVTR SYEAFYAR TGVSSSHLQALWIGYSTEGLSAALASLR TNDFGLAEEFASK TPAGPGTADSQRPR VHSSQDILSNISLNGK VPGDPVMIPFGEGSKPSEPSATEAK VSAAPAVSR VSLYLNLSR VSSHLVLR VVPVSLSELYLLQCNMK	Coverage: 14% Peptide Count: 19 Abi3 R3 Coverage: 14% Peptide Count: 19 Abi3 R4 Coverage: 11% Peptide Count: 15 Abi3 R5 Coverage: 2% Peptide Count: 3

Pik3ap1	APDLSSGNVSLK DEELPTLLHFAAK HGHYPNTIAEK HTDLEITVPIR IVPYNTETLDK LGIVNVDEAVLHFK	LGNFYVSSESIR LVPDASFSAQDLWVFR NLTALLLTCPGALQAYSVANK QLITLQEQVK SLLSVSSGMEGDNEDNEIPEITR VSTEAEFSPEDSPSIR	Abi3 R1 Coverage: 19% Peptide Count: 11 Abi3 R2 Coverage: 9% Peptide Count: 5 Abi3 R3 Coverage: 5% Peptide Count: 3 Abi3 R4 Coverage: 3%

			Peptide Count: 2 Abi3 R5 Coverage: 3% Peptide Count: 2
Gigyf2	AAETQTLNFGPEWLR AAKLEQER ADPSLLGFSVNASSER AEQVEKAEEENRSENSLSAK ALQQQQQQQQQK ALSSGGSITSPPLSPALPK AYLGDTSEAK AYLGDTSEAKEFAK DVGRPNFEESGPTSVGR	EVESPYEVHDYTR IFREEQNGEDEDGGWR LQQQQQQQQLAQMK MSDQNIIPSVTR NSNMGFWDDAVK QQQQQQQQQQQHQQSNR RKQEELLR SESENWR	Abi3 R1 Coverage: 14% Peptide Count: 14 Abi3 R2 Coverage: 3% Peptide Count: 3 Abi3 R3

			Coverage: 3% Peptide Count: 3 Abi3 R4 Coverage: 3% Peptide Count: 3 Abi3 R5 Coverage: 0% Peptide Count: 0
Ripk3	DKVDAAVSEVK DLKPSNILLDPELHAK GTTPGPVFTETPGPHPQR KLEFVGK QAQDTSVGPATPAR	TWNHDVAVK GGFGVVFR LWPTGASAVPLVSR LADFGLSTFQGGSQSGSGSGSGSGSR	Abi3 R1 Coverage: 15% Peptide Count: 6

			Abi3 R2 Coverage: 8% Peptide Count: 3 Abi3 R3 Coverage: 8% Peptide Count: 2 Abi3 R4 Coverage: 5% Peptide Count: 2 Abi3 R5 Coverage: 0 Peptide Count: 0

Appendix 2

HA-BirA*-Abi3S212F Sequence (g.624C<T):

TACCCATACGATGTTCCAGATTACGCTGGATCCAAGGACAACACCGTGCCCCTGAAGCTGATCGCCCTGCTGGCCAACGGCG
AGTTCCACTCTGGCGAGCAGCTGGGAGAGACCCTGGGAATGAGCAGAGCCGCCATCAACAAGCACATCCAGACACTGAGAGA
CTGGGGAGTGGACGTGTTCACCGTGCCTGGCAAGGGCTACAGCCTGCCTGAGCCTATCCAGCTGCTGAACGCCAAGCAGATC
CTGGGACAGCTGGATGGCGGAAGCGTGGCCGTGCTGCCTGTGATCGACTCCACCAATCAGTACCTGCTGGACAGAATCGGA
GAGCTGAAGTCCGGCGACGCCTGCATCGCCGAGTACCAGCAGGCTGGCAGAGGAGGCAGAGGACGGAAGTGGTTCAGCCC
ATTCGGAGCCAACCTGTACCTGTCCATGTTCTGGAGACTGGAGCAGGGACCTGCTGCTGCCATCGGACTGAGTCTGGTGATC
GGAATCGTGATGGCCGAGGTGCTGAGAAAGCTGGGAGCCGACAAGGTGAGAGTGAAGTGGCCTAATGACCTGTACCTCCAG
GACCGCAAGCTGGCTGGCATCCTGGTGGAGCTGACAGGCAAGACAGGCGATGCCGCTCAGATCGTGATCGGAGCCGGAATC
AACATGGCCATGAGAAGAGTGGAGGAGAGCGTGGTGAACCAGGGCTGGATCACCCTGCAGGAGGCTGGCATCAACCTGGAC
CGGAACACCCTGGCCGCCATGCTGATCAGAGAGCTGAGAGCCGCTCTGGAGCTGTTCGAGCAGGAGGGACTGGCTCCTTAC
CTGAGCAGATGGGAGAAGCTGGACAACTTCATCAACAGACCTGTGAAGCTGATCATCGGCGACAAGGAAATCTTCGGCATCTC
CAGAGGAATCGACAAGCAGGGAGCTCTGCTGCTGGAGCAGGACGGAATCATCAAGCCCTGGATGGGCGGAGAAATCTCCCT
GAGAAGCGCAGAGAAGGGTGCTGGCGCCGGAGCAGGGGCGGGTGCCATGGCGGAGCTGCAGCAGTTACAGCAGCTGCAGG
AGTTTGATATCCCCACGGGCCGGGAGGCTCTGCGGGGCAACCACAGCGCCCTGCTACGGGTGGCCAACTACTGCGAGGATA
ACTACTTGCAGGCCACAGACAAGCGGAAGGCGCTGGAAGAGACGATGGCTTTCACCACCCAGGCCCTAGCCAGTGTGGCCTA
CCAAGTGGGTAACCTGGCCGGGCATACTCTTCGAATGCTGGATCTACAGGGTGCTGCCCTGCGGCAGGTAGAAGCCAAGATG
AGCACACTGGGCCAGATGGTAAACATGCATATGGAGAAGGTAGCTAGAAGGGAGATCGGCACTTTGGCCACTGTTGTGCGGC
TGCCCTCTAACCAGAAAGTCATCCCTCCTGAGAGCCTGCCTTCCCTCACTCCCTACCACAGAAAACCCCTCAACTTTGCCTGCT
TGGATGACATTGGCCACGGAGTCAAGGACTTGAGCACGCAGCTGTCACGGACCGGGACCCTGTCTCGCAAGAGCATAAAGGC

GCCTGCTACACCTGTTTCCGCCACGCTGGGGAGACCACCCCGGATCCCTGAGCCGGTGCAGCTCCCAGCCGTGCCAGACGG
CAAGCTCTCCGCTGC**T**TCCTCTGCCTCTTCCTTGGCCTCGGCAGGCAGTGCGGAAGGTGCCAGTGGGATCCCCCAGTCCAAG
GGACAGGTAGCGCCTGCAACCCCGCCTCCTCCACCTGTAGCACCTGTAACCCCGCCTCCTCCACCGTTGTCTGCCGAGGTCT
TCTTGCCGCCCCCTCCGCTGGAGGTGTCCCAGCCCCCTCTGGAAGCAGAGTTGCCCCTGCCTCCTCCCCCAGCTCTAGAGGG
GGATGAACTGGGGCTGCTGCCTCCGCCCCCACCAGGTTTTGGACCAGATGAGCCCAGCTGGGTCCCTGCTAGCTACTTGGAG
AAAGTGGTGACCCTGTACCCATACACCCGGCAAAAGGACAATGAGCTCTCCTTCTCTGAAGGCACCGTCATCTGTGTCACTCG
CCGCTACTCGGATGGCTGGTGTGAGGGTGTCAGTTCAGAGGGCACTGGATTCTTCCCAGGGAACTATGTGGAGCCCAGCTGC
TGA

Supplementary table 2.1 **Mass spectrometry data for Abi3-S212F-associated proteins.** *Peptide sequences of high-confidence interactors of Abi3-S212F as determined by SAINTexpress. Peptide sequences identified by mass spectrometry are presented with each interactor with peptide count and percentage coverage values generated from each biological replicate.*

Protein	Peptides		MS Data
Abi3	AELQQLQQLQEFDIPTGR ALEETMAFTTQALASVAYQVGNLAGHTLR APATPVSATLGR APATPVSATLGRPPR DLSTQLSR DNELSFSEGTVICVTR EALRGNHSALLR EIGTLATVVR EIGTLATVVRLPSNQK GNHSALLR IPEPVQLPAVPDGK KALEETMAFTTQALASVAYQVGNLAGHTLR KPLNFACLDDIGHGVK KPLNFACLDDIGHGVKDLSTQLSR	MLDLQGAALR MSTLGQMVNMHMEK PLNFACLDDIGHGVK QKDNELSFSEGTVICVTR REIGTLATVVR RYSDGWCEGVSSEGTGFFPGNYVEPSC SIKAPATPVSATLGRPPR VANYCEDNYLQATDK VANYCEDNYLQATDKR VANYCEDNYLQATDKRK VIPPESLPSLTPYHR VVTLYPYTR YSDGWCEGVSSEGTGFFPGNYVEPSC	Abi3-S212F R1 Coverage: 64% Peptide Count 25 Abi3-S212F R2 Coverage: 60% Peptide Count 23 Abi3-S212F R3

			Coverage: 59% Peptide Count: 22 Abi3-S212F R4 Coverage: 61% Peptide Count 26 Abi3-S212F R5 Coverage: 57% Peptide Count: 21
Cep170	AESEVPIVK ALHPAAAGVAAAASTEFENAESEADFSIHFNR ALLHSGSSSSK ASPGTQDLPGIQTGMMAPENK	LRAESEVPIVK LREDNNKTDEGPDTPSYNR MQQQEQKEQAQWTPTK MQQQEQKEQAQWTPTKFPSK	Abi3-S212F R1 Coverage: 58%

	ASVASEVSTTSSTSKPPTGR ATLEEHLR CREESSKQESQLLEK CSTSSPSKDVTK DDCELMLQSR DEVMGDNLLLSSVFQFSR DKDRNWDDIENK DLGSLNGTFVNDVR DLGSLNGTFVNDVRIPEQTYITLK DTEAVMAFLEAK DTPSSHTAGAGHASFTIEFDDSTPGK DWALNSAAVVMEER DWTAHREEIAR EAQVYQSEK EAQVYQSEKHDADR EAQVYQSEKHDADRGLSK EDNNKTDEGPDTPSYNR EESSKQESQLLEK EEVGDLHGEMHK EFQQPSQIAESTIHEIPTK EINDVAGEIDSVTSSGTAPSTTVSTAATTPGSAIDTR	MQSTGSAMPASSSFK NALGHIDK NALGHIDKCR NQATSASSEKDNDDDQSDKGTYTIELENPNSEE VEAR NWDDIENK NWDDIENKLR PQPAEHPDHLTITR QDTELQEK QDTELQEKEAQVYQSEK QESQLLEK QGSFTIDKPSSNIPIELIPHINK QHAVINYDASMDEHLVK QKSEEPSVSLPFLQTALLR QLQVINAMIDPDGTLEALNNMGFPNAILPSPPK QNSSVPTALALTSASR RATLEEHLR RATLEEHLRR RFPTDYASTSEDEFGSNR RTLPQLPNEEK RWVSQWASLAANHTR	Peptide Count 86 Abi3-S212F R2 Coverage: 68% Peptide Count: 97 Abi3-S212F R3 Coverage: 61% Peptide Count: 84 Abi3-S212F R4 Coverage: 60%

	EKSETEKETSLVK EMIFVGR EMIFVGRDDCELMLQSR EPSYFEIPTK EPSYFEIPTKEFQQPSQIAESTIHEIPTK EQAQWTPTK EQAQWTPTKFPSK ERSDSLDTDSSMDTTLILK FGYDTNLFTVVR FNPDGEEEDVTVHE FPTDYASTSEDEFGSNR FTIQLQLSQK GEMRVPEEALK GLIKDWALNSAAVVMEER GTDSKVEAAAEVQPR GTPLYGQPSWWGDAEEDEQR HVEGQSAAASEEALFPFCR IDLLAQPR IKEQEDYIR IKEQEDYIRDWTAHR ILFKDKDR	SDSEATISR SDSLDTDSSMDTTLILK SDVPVYLK SDVPVYLKR SEEPSVSLPFLQTALLR SEIGEKQDTELQEK SETEKETSLVK SFTSLYK SFTSLYKDR SIKSDVPVYLKR SKTSPVASGSTSK SMSSTHGSPSVNSR SSESELPK SSGSLGHRPSQEMDVMLK SSPVNNHSSPSQTPALCPPETR STSCTTSLASQGER SVDKQHAVINYDASMDEHLVK SVDSRPQPAEHPDHLTITR TAEAVIR TDEGPDTPSYNR TLPQLPNEEK	Peptide Count: 80 Abi3-S212F R5 Coverage: 54% Peptide Count: 71

	IPEQTYITLK IRQPSIDLTDDDQTSSVPHSAISDIMSSDQETYSCK ISQDLALIAR KAEEIPK KASPGTQDLPGIQTGMMAPENK KFVQSSGR KIPPLVHSK KPLSTPGFHNSEEAISSSGSK KPLSTPGFHNSEEAISSSGSKR KSFTSLYK KSFTSLYKDR LGEASDSELADADK LGEASDSELADADKASVASEVSTTSSTSKPPTGR LKGNKHDDGTQSDSENAGAHR LMELSATVENETDTGDAGVSLR	TLPQLPNEEKLLESSR TPLTSADEHNIHSK TSSMEISSILQELK TSSMEISSILQELKR TWSRDEVMGDNLLLSSVFQFSR VADWLAQNNPPQMVWER VADWLAQNNPPQMVWERTEEDSK VEAAAEVQPR VFDESLNFR VFDESLNFRK VFGVDDNQDYNRPIINEK VKSMSSTHGSPSVNSR VPEEALK VPEEALKHEK VTIRDHVTK WVSQWASLAANHTR	
Wasf2	DVVGNDVATILSR EEEVSLQGINTR FYTNPSYFFDLWK GSVLAGPK GSVLAGPKR	QTLPSDTSELECR RDVVGNDVATILSR SDLLSAIR SSLPAVSDAR TNITLANVIR	Abi3-S212F R1 Coverage: 32%

	MGQEFVESK MKMGQEFVESK MLQDTKDIMK NSLPVPVLETYNSCDAPPPLNNLSPYR NSLPVPVLETYNSCDAPPPLNNLSPYRDDGK NSLPVPVLETYNSCDAPPPLNNLSPYRDDGKEALK QLGSLSK	TRKEEWEK TSMVSPSHPPPAPPLSSPPGPK VNSLAER VTQLDPK VTQLDPKEEEVSLQGINTR YAEDIFGEICTQASAFASR	Peptide Count: 17 Abi3-S212F R2 Coverage: 42% Peptide Count: 20 Abi3-S212F R3 Coverage: 28% Peptide Count: 12 Abi3-S212F R4 Coverage: 37%

			Peptide Count: 16 Abi3-S212F R5 Coverage: 36% Peptide Count: 17
Tanc1	ADAALISK ADGESTAFLCEPR ADNEPSCSPAAQELLTR AEPSAGDGPVPYPQSSGSLIMPR ALELKPK ANFQEIISALPFVK AVVQYLVEEGAEIDQTDKNGR DKGTTQVQGGTAEHRPR DLLIKEPQLQSMLSLR DSGIIATITSSSENDDR DWLFHQIEENLR ETVAQSGLVMQPTK	LGASQSLQLQR LGNAAWAMATSKPDILIILLQK LLAHASVAVDMAPPNQGGPVSCSDVR LLILGGANVNYR LTLDLFQR LVALSCHGSR LVCLLIK LVEEGNVMYK NEQKIPEEEYIILIDGLNEAEFHKPDYGDTLSSFITK NGHALLAFMFSR NLQEGLQSK	Abi3-S212F R1 Coverage: 13% Peptide Count: 19 Abi3-S212F R2 Coverage: 35% Peptide Count: 43

	FAPYKPQEILLKPLLFEVPSITTDSVFVGR FMTQSAFDR FQQQSNPPNR GAALSSLDKEGLSALSWACLK GAVVVGSVGFGK GKVEICELLLER GQCALVHSALR GTTQVQGGTAEHRPR GVLEPLTSLR GVPHLYPEGVSK GVPPLFCAAR HPASLSSSGSSGSPSSSIK IPEEEYIILIDGLNEAEFHKPDYGDTLSSFITK KEAGGDFGSETPALSSSGDSPVNSLSTTEDTYR KTGVSSSHLQALWIGYSTEGLSAALASLR LCPNNQEIKR	NTAVVVTLLR QFLAALADLQEAVK QQTMELGHHILK RADNCSPVAEEETTGSAESVLPK SCVQDPVAAFK SESGTAYPLPSK SGSSLEWNR SHQLAAYR SPCETISSPSSTLESK TNDFGLAEEFASK TPAGPGTADSQRPR TPLMVASCEGHLSTVEFLLSK VPGDPVMIPFGEGSKPSEPSATEAK VSAAPAVSR VSLYLNLSR VSSHLVLR VVPVSLSELYLLQCNMK	Abi3-S212F R3 Coverage: 26% Peptide Count: 32 Abi3-S212F R4 Coverage: 21% Peptide Count: 31 Abi3-S212F R5 Coverage: 21% Peptide Count: 29

Cyfip1	ALNLAYSSIYGSYR AVGPSSTQLYMVR DFVSEAYLITLGK DKQPNAQPQYLHGSK EANHNVSAPYGR EASMMEYVLYSLDLYNDSAHYALTK EFFLELTMGR EGDLLTK FALVEVIAMIK FAVLDFCYHLLK FINMFAVLDELK FISELAR FQILNDEIITILDK GLQVLMGR GPLPSNGVMHVDECVEFHR HEYGSPGILEFFHHQLK HTVYAALQDFSQVTLR HVQLLGR IQFPIEMSMPWILTDHILETK KDFVSEAYLITLGK KFQILNDEIITILDK	MESVFNHAIR MYLTPSEK NAFVTGIAR NFVGPPHFQVICR NVIQSVLQAIR NVIQSVLQAIRK QLQVVPLFGDMQIELAR QPNAQPQYLHGSK RFAVLDFCYHLLK RIQFPIEMSMPWILTDHILETK RKDFVSEAYLITLGK SGDGESTPVEHVR SLELAIGR SLLQGTILQYVK SSLEGPTILDIEK TFLDDPIWR TMLESLIADK TVCDWETGHEPFNDPALR TVCFQNLR TVEVLEPEVTK TVLPFSQEFQR	Abi3-S212F R1 Coverage: 16% Peptide Count: 18 Abi3-S212F R2 Coverage: 24% Peptide Count 28 Abi3-S212F R3 Coverage: 45% Peptide Count: 51

	KTVCDWETGHEPFNDPALR LADQIFAYYK LCCGLSMFEVILTR LGTPQQIAIAR LLGYQGIAVVMEELLK LMNFMYFQR LVHPTDK LVHPTDKYSNK	VMAGSLLLDKR WTCASSSSSPQYNICEQMIQIR YAPLHLVPLIER YLTLDSFDAMFR YNYTTEEK YSNKDCPDNAEEYER YSNSEVVTGSGR	Abi3-S212F R4 Coverage: 20% Peptide Count: 23 Abi3-S212F R5 Coverage: 21 Peptide Count: 22
Ruvbl2	AAGVVLEMIR ALESDMAPVLIMATNR ARDYDAMGSQTK AVLIAGQPGTGK DKVQAGDVITIDK EVVHTVSLHEIDVINSR EYQDAFLFNELK EYQDAFLFNELKGETMDTS FVQCPDGELQKR	IGLETSLR IRCEEEDVEMSEDAYTVLTR KGTEVQVDDIKR LLIVSTSPYSEK LLIVSTSPYSEKDTK QASQGMVGQLAAR TEALTQAFR TQGFLALFSGDTGEIK TQGFLALFSGDTGEIKSEVR	Abi3-S212F R1 Coverage: 33% Peptide Count: 14 Abi3-S212F R2

	GLGLDDALEPR GTEVQVDDIK GTEVQVDDIKR GTSYQSPHGIPIDLLDR IGAHSHIR	TTEMETIYDLGTK VQAGDVITIDK VYSLFLDESR YAIQLITAASLVCR	Coverage: 56% Peptide Count: 24 Abi3-S212F R3 Coverage: 44% Peptide Count: 17 Abi3-S212F R4 Coverage: 46% Peptide Count: 18 Abi3-S212F R5

			Coverage: 40% Peptide Count: 15
Mtss1	DWAKPGPYDQPLVNTLQR ECSALGGLFQTIISDMK EPDSNGGGPTTTGGPPAGAEEAQRPR ESPQGEDMLNAIR GDIQPQLDSALQDVNDK GDIQPQLDSALQDVNDKYLLLEETEK GLQLDVQR GSYPVWEDFINK GTIGAGPIPIK KALIEER KSSVCSSLNSVNSSDSR KVANQLDKDHAK LPSSSEQVILDLK LSSVSSHDSGFISQDAFQSK MEAVIEK NSDISQSYR	PSIPEEHR QAIPESEAEDQERDPPSATVSPGPIPESDPADLSPR REPDSNGGGPTTTGGPPAGAEEAQRPR RGTIGAGPIPIK RGTIGAGPIPIKTPVIPVK RPASTAGLPTTLGPAMVTPGVATIR RTPSTKPSVR SMTVSAATRPGEEMAACEELTLALSR SSNLAQQAPVR TPSTKPSVR TPVIPVK TTVVAAAAFLDAFQK VANQLDKDHAK VTSVHLPDYAHYYTIGPGMFPSSQIPSWK YLLLEETEK	Abi3-S212F R1 Coverage: 27% Peptide Count: 15 Abi3-S212F R2 Coverage: 43% Peptide Count: 24 Abi3-S212F R3 Coverage: 30%

			Peptide Count: 16 Abi3-S212F R4 Coverage: 28% Peptide Count: 13 Abi3-S212F R5 Coverage: 34 Peptide Count: 20
Usp15	AAYVLFYQR AEGGAADLDTQR DDIYVFEININR FSYVTPR IFAVDENLSSIMER IGNILDLCTALSALSGVPADK ISPSSLSNNYNNINNR	LKDCIELFTTK LYNLLLLR MIVTDIYNHR MSTETEETDGHLR NEDGTWPR NNTEDKLYNLLLLR QDTFSGTGFFPLDR	Abi3-S212F R1 Coverage: 11% Peptide Count: 9

	ISVTFDPFCYLTLPLPMKK KGDTWYLVDSR KLDLWSLPPVLVVHLK LFTFQFNNLGNNDINYIK LFTFQFNNLGNNDINYIKDDTSHIR	RNDSIIVDIFHGLFK SDIATLLK SFLALDWDPDLK SLEVYLVR VEVYLTELK	Abi3-S212F R2 Coverage: 14% Peptide Count: 13 Abi3-S212F R3 Coverage: 17% Peptide Count: 14 Abi3-S212F R4 Coverage: 13% Peptide Count: 11

			Abi3-S212F R5 Coverage: 13 Peptide Count: 12
Arhgap12	DANQNFGSNYNSGQTLNLSLDLTHNNGK DQVFGSNLANLCQR ELPEPLFTFNHFNDFVNAIK HSTIVLDSNDKDSPTTTK KNWLSSWAVLQGSSLLFTK LCIEHVEEHGLDVDGIYR LDLNDSKWEDIHVITGALK LFGHFPGPEFLDIEK	MTYQSIAIVFGPTLLKPER QLPKPNQDTMQILFR RLQEPIVLTK SEWELPK TQGSSTSWFGSNQSKPEFTVDLK TSFSQEQSCDSAGEGSER VSGNLAVIQK YGLLNVTK	Abi3-S212F R1 Coverage: 7% Peptide Count: 4 Abi3-S212F R2 Coverage: 22% Peptide Count: 11 Abi3-S212F R3

			Coverage:16 % Peptide Count: 8 Abi3-S212F R4 Coverage: 9% Peptide Count: 5 Abi3-S212F R5 Coverage: 16% Peptide Count: 9
Evi2b	ASVVSLMTWKPSK KPVLNDQNWAGR	LFESSEHINDTSNLK SPFADGETPEMCMDNIR	Abi3-S212F R1 Coverage: 7%

			Peptide Count: 2 Abi3-S212F R2 Coverage: 13% Peptide Count: 4 Abi3-S212F R3 Coverage: 13% Peptide Count: 4 Abi3-S212F R4 Coverage: 13%

			Peptide Count: 4 Abi3-S212F R5 Coverage: 13% Peptide Count: 4
Mtmr1	DPHFVLDVPLGVISR HAFPLSNGQVLFAFNYK IGAQSHGDNSCGIEIVCK	LTIFDAR NVERDPHFVLDVPLGVISR VLLAGAVR	Abi3-S212F R1 Coverage: 5% Peptide Count: 3 Abi3-S212F R2 Coverage: 5% Peptide Count: 3

			Abi3-S212F R3 Coverage: 7% Peptide Count: 4 Abi3-S212F R4 Coverage: 5% Peptide Count: 3 Abi3-S212F R5 Coverage: 5% Peptide Count: 3
Pik3ap1	APDLSSGNVSLK DEELPTLLHFAAK	LGNFYVSSESIR NLTALLLTCPGALQAYSVANK	Abi3-S212F R1

	FQQENLKR HTDLEITVPIR LGIVNVDEAVLHFK	QFIDEYVETVDMLK QLITLQEQVK VSTEAEFSPEDSPSIR	Coverage: 5% Peptide Count: 3 Abi3-S212F R2 Coverage: 11% Peptide Count: 7 Abi3-S212F R3 Coverage: 11% Peptide Count: 6 Abi3-S212F R4

			Coverage: 12% Peptide Count: 7 Abi3-S212F R5 Coverage: 13% Peptide Count: 8
Abl2	AGKPTASDDTSKPFPR LLSEHQVTSSGDKDRPR LPLLPSK MEQPEGCPPK STQASSGSPALPR	TVSTSSQPEENVDR VGEAPGLQQPQPR VLGYNQNGEWSEVR VYVTAESR	Abi3-S212F R1 Coverage: 3% Peptide Count: 2 Abi3-S212F R2 Coverage: 4%

			Peptide Count: 4 Abi3-S212F R3 Coverage: 3% Peptide Count: 3 Abi3-S212F R4 Coverage: 3% Peptide Count: 3 Abi3-S212F R5 Coverage: 5% Peptide Count: 5

Cbl	ADAAEFWR ALVIAHNNIEMAK APVPASTSVLGTASK ASSYQQGGGATANPVATAPSPQLSSEIER EFVSISSPAHVAT EGFYLFPDGR GIFPSGLFQGDTFR GTEPIVVDPFDPR HSLPFSLPSQMEPR ICAENDKDVK KASSYQQGGGATANPVATAPSPQLSSEIER LDLLQQR	LFQPWSSLLR LGSTFSLDTSMTMNSSPVAGPESEHPK LSLIFSHMLAEIK METLGENEYFR MYEENSQPR NQNPDLTGLCEPTPQDHIK NSPPYILDILPDTYQHLR QALHEVHPISSGLEAMALK RPLEATQSSR RPLPCTPGDCPSR SSGAGGGGSGGSGAGGLIGLMK VPVATPNPGDPWNGR	Abi3-S212F R1 Coverage: 7% Peptide Count: 6 Abi3-S212F R2 Coverage: 31% Peptide Count: 20 Abi3-S212F R3 Coverage: 16 Peptide Count: 10 Abi3-S212F R4

			Coverage: 13 Peptide Count: 8 Abi3-S212F R5 Coverage: 16% Peptide Count: 10
Eif4g2	ASSLISLLK DLGVFIPAPMAQGR EDITQEFPGK ENPLLPEEEEQR FIGELGK FLLQDTVELR GLSFLFPLLK GLSFLFPLLKLEK GVILLIVDK KAFLDNGPK KPPPSKEELLK	LEVDIPLVK LQDEFENR LQDREWLTELFQQSK LTEAVVTDYLNSGNANDAVSGVR NVDVYDKR QLLLSFKPVMQK SLMDQYFAR SQGLSQLYHNQSQGLLSQLQGQSK SYLAQFAAR TAGNSEFLGK TQTPPLGQTPQLGLK	Abi3-S212F R1 Coverage: 8% Peptide Count: 8 Abi3-S212F R2 Coverage: 22% Peptide Count: 16

	LAEDAPNFDGPAAEGQPGQK LDLIHESILHK	VIILSLDR	Abi3-S212F R3 Coverage: 17% Peptide Count: 13 Abi3-S212F R4 Coverage: 13% Peptide Count: 9 Abi3-S212F R5 Coverage: 19% Peptide Count: 14

Glmn	AVEELQSIIK AVEELQSIIKR	GLELLETSLLR SFLAVPQGLVK	Abi3-S212F R1 Coverage: 4% Peptide Count: 3 Abi3-S212F R2 Coverage: 4% Peptide Count: 2 Abi3-S212F R3 Coverage: 4% Peptide Count: 2

			Abi3-S212F R4 Coverage: 4% Peptide Count: 2 Abi3-S212F R5 Coverage: 4% Peptide Count: 2
Dbt	AASLGLLQFPILNASVDENCQNITYK AQIMNVSWSADHR ASHNIGIAMDTELGLIVPNVK DRTEPVTGFQK DRTFPTPIAKPPVFTGK EDILSFLEK ILKEDILSFLEK IPHFGYCDEIDLTQLVK LGSSGQLGTTDLTGGTFTLSNIGSIGGTYAK	LSEVVGSGK LSFMPFFLK PVILPPEVAIGALGAIK QTGAILPPSPK RLAMENNIK SEITPPPPQPK SVFEIAMELNR SYLENPAFMLLDLK TFPTPIAKPPVFTGK	Abi3-S212F R1 Coverage: 13% Peptide Count: 4 Abi3-S212F R2

	LREELKPVALAR LSDIGEGIR	TLATPAVR VIDGATMSR	Coverage: 16% Peptide Count: 6 Abi3-S212F R3 Coverage: 44% Peptide Count: 17 Abi-S212F R4 Coverage: 45% Peptide Count: 16 Abi3-S212F R5

			Coverage: 40% Peptide Count: 13
Stat3	AILSTKPPGTFLLR EGGVTFTWVEK ESHATLVFHNLLGEIDQQYSR GLSIEQLTTLAEK	LLGPGVNYSGCQITWAK LLQTAATAAQQGGQANHPTAAVVTEK TGVQFTTK TQIQSVEPYTK	Abi3-S212F R1 Coverage: 0% Peptide Count: 0 Abi3-S212F R2 Coverage: 7% Peptide Count: 3 Abi3-S212 R3 Coverage: 9%

			Peptide Count: 4 Abi3-S212F R4 Coverage: 13% Peptide Count: 6 Abi3-S212F R5 Coverage: 13% Peptide Count: 6
Arfgap1	AEDSSDRPLEGHSYQNSSGDNSQNSNIDQSFWETFGSAEPPK AFEDWLNDDLGSYQGAQENR ASELGHSLNENVLKPAQEK ASGQPQSAAASGDKAFEDWLNDDLGSYQGAQENR DKVATLAEGK	EFLETQDDYEPSWSLQDK FREFLETQDDYEPSWSLQDK GLGVHLSFVR IFDDVSSGVSQLASK NSNSDGWESWEGASGEGR SPSSDSWTCADASTGR	Abi3-S212F R1 Coverage: 9% Peptide Count: 2

	DVTTFFSGK EDDFLNNAMSSLYSGWSSFTTGASK	VATLAEGK	Abi3-S212F R2 Coverage: 41% Peptide Count: 10 Abi3-S212F R3 Coverage: 41% Peptide Count: 10 Abi3-S212F R4 Coverage: 36% Peptide Count: 9

			Abi3-S212F R5 Coverage: 32% Peptide Count: 8
Wdr62	AGTGYMSSDGTNVLSGQK HHFETLTDAPTEELFHGSLGDIK ISETEDYFFNPR KPPTPTSVLTTGR LAAAPEDTVQNR LQTAFQEALDLYR	LSISTQFLSR NYNLEQTLDDHSSSITAIK SISLIDFYSGECVAK SPEAQPVGQGGNQPK VTSTVPLVGR	Abi3-S212F R1 Coverage: 0% Peptide Count: 0 Abi3-S212F R2 Coverage: 6% Peptide Count: 6 Abi3-S212F R3

			Coverage: 3% Peptide Count: 3 Abi3-S212F R4 Coverage: 3% Peptide Count: 4 Abi3-S212F R5 Coverage: 3% Peptide Count: 4
Ripk3	DLKPSNILLDPELHAK GGFGVVFR GTTPGPVFTETPGPHPQR KLEFVGK	LWPTGASAVPLVSR QAQDTSVGPATPAR TNEVYNLVK TSSDPVAGTPQIPHTLPFR	Abi3-S212F R1 Coverage: 0%

			Peptide Count: 0 Abi3-S212F R2 Coverage: 11% Peptide Count: 4 Abi3-S212F R3 Coverage: 11% Peptide Count: 4 Abi3-S212F R4 Coverage: 5%

			Peptide Count: 2 Abi3-S212F R5 Coverage: 9% Peptide Count: 4

Appendix 3

Trem2-BirA*-HA Sequence:

ATGGGACCTCTCCACCAGTTTCTCCTGCTGCTGATCACAGCCCTGTCCCAAGCCCTCAACACCACGGTGCTGCAGGGCATG
GCCGGCCAGTCCTTGAGGGTGTCATGTACTTATGACGCCTTGAAGCACTGGGGGAGACGCAAGGCCTGGTGTCGGCAGCT
GGGTGAGGAGGGCCCATGCCAGCGTGTGGTGAGCACACACGGTGTGTGGCTGCTGGCCTTCCTGAAGAAGCGGAATGGGA
GCACAGTCATCGCAGATGACACCCTTGCTGGAACCGTCACCATCACTCTGAAGAACCTCCAAGCCGGTGACGCGGGCCTCT
ACCAGTGTCAGAGTCTCCGAGGCCGAGAGGCTGAGGTCCTGCAGAAAGTACTGGTGGAGGTGCTGGAGGACCCTCTAGAT
GACCAAGATGCTGGAGATCTCTGGGTCCCCGAGGAGTCATCGAGTTTCGAGGGTGCCCAAGTGGAACACAGCACCTCCAG
GAATCAAGAGACCTCCTTCCCACCCACCTCCATTCTTCTCCTCCTGGCCTGCGTTCTCCTGAGCAAGTTTCTTGCAGCCAGC
ATCCTCTGGGCTGTGGCCAGGGGCAGGCAGAAGCCGGGAACACCTGTGGTCAGAGGGCTGGACTGTGGCCAAGATGCTG
GGCACCAACTTCAGATCCTCACTGGACCCGGAGGTACG**GGTGCTGGCGCCGGAGCAGGGGCGGGTGCC**AAGGACAACAC
CGTGCCCCTGAAGCTGATCGCCCTGCTGGCCAACGGCGAGTTCCACTCTGGCGAGCAGCTGGGAGAGACCCTGGGAATGA
GCAGAGCCGCCATCAACAAGCACATCCAGACACTGAGAGACTGGGGAGTGGACGTGTTCACCGTGCCTGGCAAGGGCTAC
AGCCTGCCTGAGCCTATCCAGCTGCTGAACGCCAAGCAGATCCTGGGACAGCTGGATGGCGGAAGCGTGGCCGTGCTGCC
TGTGATCGACTCCACCAATCAGTACCTGCTGGACAGAATCGGAGAGCTGAAGTCCGGCGACGCCTGCATCGCCGAGTACC
AGCAGGCTGGCAGAGGAGGCAGAGGACGGAAGTGGTTCAGCCCATTCGGAGCCAACCTGTACCTGTCCATGTTCTGGAGA
CTGGAGCAGGGACCTGCTGCTGCCATCGGACTGAGTCTGGTGATCGGAATCGTGATGGCCGAGGTGCTGAGAAAGCTGGG
AGCCGACAAGGTGAGAGTGAAGTGGCCTAATGACCTGTACCTCCAGGACCGCAAGCTGGCTGGCATCCTGGTGGAGCTGA
CAGGCAAGACAGGCGATGCCGCTCAGATCGTGATCGGAGCCGGAATCAACATGGCCATGAGAAGAGTGGAGGAGAGCGT
GGTGAACCAGGGCTGGATCACCCTGCAGGAGGCTGGCATCAACCTGGACCGGAACACCCTGGCCGCCATGCTGATCAGAG
AGCTGAGAGCCGCTCTGGAGCTGTTCGAGCAGGAGGGACTGGCTCCTTACCTGAGCAGATGGGAGAAGCTGGACAACTTC

ATCAACAGACCTGTGAAGCTGATCATCGGCGACAAGGAAATCTTCGGCATCTCCAGAGGAATCGACAAGCAGGGAGCTCT
GCTGCTGGAGCAGGACGGAATCATCAAGCCCTGGATGGGCGGAGAAATCTCCCTGAGAAGCGCAGAGAAGGGATCCTACC
CATACGATGTTCCAGATTACGCTTAG

Supplementary table 3.1 Protein interactors of human TREM2. *Known interactions of human TREM2 downloaded from the National Center for Biotechnology Information (NCBI) database. Interactors are supported by experimental evidence including two-hybrid and affinity capture methods. Descriptions have been extracted from the corresponding NCBI or GeneCards entry for each protein. Sources of the interaction data: Biological General Repository for Interaction Databases (BioGRID), Human Protein Reference Database (HPRD).*

Interactor	Description	Source	Experimental Evidence	Cell/Tissue Type	Publication
TYROBP	This gene encodes a transmembrane signalling polypeptide which contains an immunoreceptor tyrosine-based activation motif (ITAM) in its cytoplasmic domain. The encoded protein may associate with the killer-cell inhibitory receptor (KIR) family of membrane glycoproteins and may act as an activating signal transduction element. This protein may bind zeta-chain (TCR) associated protein kinase 70kDa (ZAP-70) and spleen tyrosine kinase (SYK) and play a role in signal transduction, bone modelling, brain myelination, and inflammation.	HPRD	Affinity Capture	Monocyte-derived dendritic cells	Paloneva et al. (2002) Bouchon et al. (2001)
APOA1	This gene encodes apolipoprotein A-I, which is the major protein component of high-density lipoprotein (HDL) in plasma. The encoded preproprotein is proteolytically processed to generate the mature protein, which promotes cholesterol efflux from tissues to the liver for excretion and is a cofactor for lecithin cholesterolacyltransferase (LCAT), an enzyme responsible for the formation of most plasma cholesteryl esters.	BioGRID	Protein Microarray	Trem2-Fc fusion protein	Yeh et al. (2016)

APOA2	This gene encodes apolipoprotein (apo-) A-II, which is the second most abundant protein of the high-density lipoprotein particles. The protein is found in plasma as a monomer, homodimer, or heterodimer with apolipoprotein D.	BioGRID	Protein Microarray	Trem2-Fc fusion protein	Yeh et al. (2016)
APOB	This gene product is the main apolipoprotein of chylomicrons and low-density lipoproteins (LDL) and is the ligand for the LDL receptor. It occurs in plasma as two main isoforms, apoB-48 and apoB-100: the former is synthesized exclusively in the gut and the latter in the liver.	BioGRID	Protein Microarray	Trem2-Fc fusion protein	Yeh et al. (2016)
APOE	The protein encoded by this gene is a major apoprotein of the chylomicron. It binds to a specific liver and peripheral cell receptor and is essential for the normal catabolism of triglyceride-rich lipoprotein constituents. This gene maps to chromosome 19 in a cluster with the related apolipoprotein C1 and C2 genes.	BioGRID	Protein Microarray	Trem2-Fc fusion protein	Yeh et al. (2016)
ATP6V0A2	The protein encoded by this gene is a subunit of the vacuolar ATPase (v-ATPase), an heteromultimeric enzyme that is present in intracellular vesicles and in the plasma membrane of specialized cells, and which is essential for the acidification of diverse cellular components. V-ATPase is comprised of a membrane peripheral V(1) domain for ATP hydrolysis, and an integral membrane V(0) domain for proton translocation. The subunit encoded by this gene is a component of the V(0) domain.	BioGRID	Affinity Capture-MS	HEK293T HCT116	Huttlin et al. (2021)

CLU	The protein encoded by this gene is a secreted chaperone that can under some stress conditions also be found in the cell cytosol. It has been suggested to be involved in several basic biological events such as cell death, tumour progression, and neurodegenerative disorders.	BioGRID	Protein Microarray	Trem2-Fc fusion protein	Yeh et al. (2016)
GH1	The protein encoded by this gene is a member of the somatotropin/prolactin family of hormones which play an important role in growth control. The gene, along with four other related genes, is located at the growth hormone locus on chromosome 17 where they are interspersed in the same transcriptional orientation; an arrangement which is thought to have evolved by a series of gene duplications.	BioGRID	Protein Microarray	Trem2-Fc fusion protein	Yeh et al. (2016)
NRN1L	The protein encoded by this gene is extracellular and enhances both neurite growth and neuronal survival. The encoded protein is found both as a GPI anchored membrane-bound form and as a secreted form. This activity-related ligand functions as a homodimer or heterodimer.	BioGRID	Protein Microarray	Trem2-Fc fusion protein	Yeh et al. (2016)
NUCB2	This gene encodes a protein with a suggested role in calcium level maintenance, eating regulation in the hypothalamus, and release of tumour necrosis factor from vascular endothelial cells. This protein binds calcium and has EF-folding domains.	BioGRID	Affinity Capture-MS	HEK293T HCT116	Huttlin et al. (2021)

SCGB2A2	Protein Coding gene. Diseases associated with SCGB2A2 include Breast Cancer and Mammary Analogue Secretory Carcinoma.	BioGRID	Protein Microarray	Trem2-Fc fusion protein	Yeh et al. (2016)
UNC5B	This gene encodes a member of the netrin family of receptors. This particular protein mediates the repulsive effect of netrin-1 and is a vascular netrin receptor. This encoded protein is also in a group of proteins called dependence receptors (DpRs) which are involved in pro- and anti-apoptotic processes. Many DpRs are involved in embryogenesis and in cancer progression.	BioGRID	Protein Microarray	Trem2-Fc fusion protein	Yeh et al. (2016)

Supplementary table 3.2 Mass spectrometry data for Trem2-associated proteins. *Peptide sequences of high-confidence interactors of Trem2 as determined by SAINTexpress. Peptide sequences identified by mass spectrometry are presented with each interactor with peptide count and percentage coverage values generated from each biological replicate.*

Protein	Peptide Sequences		MS Data
Abhd12	GWGDSVGTPSER	KRTEPVTLEHER	Trem2 R1
	KLYNIAAPSR	VQFIPFHSDLGYR	Coverage: 10%
	VPYFIDLK	SGDNPVYIWGHSLGTGVATNLVR	Peptide Count: 4
	LIFLNFVR	GMTYDALHVFDWIK	
	ETPPDALILESPFTNIR		Trem2 R2
			Coverage: 4%
			Peptide Count: 2
			Trem2 R3
			Coverage: 13%
			Peptide Count: 4
			Trem2 R4
			Coverage: 12%
			Peptide Count: 4
			Trem2 R5
			Coverage: 29%

			Peptide Count: 9
Arfgap2	SSGLESSEAR	ACFDCGAK	Trem2 R1
	STELDSNWSWLQLR	LGMGLVSR	Coverage: 24%
	QLGSAALTR	FACHSASLTVR	Peptide Count: 12
	DNPFSLGETFGSR	AGEVFIHK	
	LREQQAADAK	YKDNPFSLGETFGSR	Trem2 R2
	SQLDLFDDVGTFASGPPK	LQQLSGSSAISSSDLFGNMDGAHGGGTVSLGNVLPTADIAQFK	Coverage: 7%
	LAYQELQIDR	SLGVHLSFIR	Peptide Count: 3
	AISSDMFFGR	QAEESMVASMR	
	EVDSEYEAR	MAVLANGVMNSLQDR	Trem2 R3
	KLQNLEGK	TEIQTIFKR	Coverage: 14%
			Peptide Count: 7
			Trem2 R4
			Coverage: 22%
			Peptide Count: 7
			Trem2 R5
			Coverage: 31%
			Peptide Count: 12
Atp2b1	QVVAVTGDGTNDGPALK	YGDLLPADGILIQGNDLK	Trem2 R1
	EANHDGDFGITLTELR	GGQVIQIPVADITVGDIAQVK	Coverage: 4%
	LAVQIGK	VYTFNSVR	Peptide Count: 4

	MVTGDNINTAR NEKGEIEQER TSPNEGLSGNPADLER	EASDIILTDDNFTSIVK GIIDSTVSEQR	 Trem2 R2 Coverage: 2% Peptide Count: 2 Trem2 R3 Coverage: 3% Peptide Count: 2 Trem2 R4 Coverage: 8% Peptide Count: 7 Trem2 R5 Coverage: 5% Peptide Count: 4
Bsg	SGEYSCIFLPEPVGR SEHSSEGELAK ETISLR SEINVEGPPR VLQEDTLPDLHTK	YIVDADDR RKPDQTLDEDDPGAAPLK YVVVSTPEK KSEHSSEGELAK	Trem2 R1 Coverage: 16% Peptide Count: 6 Trem2 R2 Coverage: 7% Peptide Count: 3

			Trem2 R3 Coverage: 21% Peptide Count: 8 Trem2 R4 Coverage: 19% Peptide Count: 6 Trem2 R5 Coverage: 11% Peptide Count: 4
Ccdc47	ELLESNFTLVGDDGTNK QDLLNVLAR RQDLLNVLAR RLEEAALR IMNEEDPEKQR VTMNDEDMDTYVFAVGTR TLLFTFNVPGSGNTYPK	ELLESNFTLVGDDGTNKEATSTGK LAQAWFNSHR MMRPVSDQVQIK LNQENEHIYNLWCSGR VCCEGMLIQLR IMQEEGQPLKLPDTK	Trem2 R1 Coverage: 6% Peptide Count: 3 Trem2 R2 Coverage: 4% Peptide Count: 2 Trem2 R3 Coverage: 9% Peptide Count: 11

			Trem2 R4 Coverage: 22% Peptide Count: 9 Trem2 R5 Coverage: 25% Peptide Count: 10
Cpd	GFVLDATDGR	DLDTDFTSNASQPETK	Trem2 R1
	TSDDEVFR	ESLITLIEK	Coverage: 4%
	TTGLYSK	IFGLPR	Peptide Count: 6
	AGDYWR	GHSTSTDDTSDPTSKEFEALIK	
	NPVVTQLVDR	PLWVLR	Trem2 R2
	IVIVPSLNPDGR	SLLSMLVEVHK	Coverage: 2%
	AVIVLNEGIK	EFEALIK	Peptide Count: 2
	QHHDEYEDEIR	AYPFVLSANLHGGSLVVNYPYDDNEQGVATYSK	
	NFGTDPEVTDLVR	LFSIGSSVEGRPLWVLR	Trem2 R3
	QVLVYLAR	LFSIGSSVEGR	Coverage: 14%
	LRQHHDEYEDEIR	LLVPGTYK	Peptide Count: 15
	LTAGLGPPPTAAAGLDAAGPLLPGRPQVK	LVGNMHGDETVSR	
	YIGNMHGNEVVGR	ELYVMEISDNPGVHEPGEPEFK	Trem2 R4
	SPDDAVFQQIALSYSK	ALIDWIR	Coverage: 16%
	SQEGDSISVVGR		Peptide Count: 19

			Trem2 R5 Coverage: 14% Peptide Count: 15
Emd	SSLGLSYYPTSSTSSVSSSSSSPSSWLTR QPGTSLVDADTFHHQVR QAPAAALGQDR QYNIPHGPIVGSTR KEDALLYQSK DDIFSSLEEEGKDRER LIYGQDSAYQSIAHYRPISNVSR PGGLLLGDEAPNFEANTTIGR LPFPIIDDKGR VVDSLQLTGTKPVATPVDWK	LPFPIIDDK IDVSVEAASGGK ADGSTQVIDTK DYNDDYYEESYLTTK LLPPNSSSSSFSYQFSDLDSAAVDSDMYDLPK KIFEYETQR KLYEKK DDIFSSLEEEGKDR IFEYETQR TYGEPESVGMSK	Trem2 R1 Coverage: 46% Peptide Count: 7 Trem2 R2 Coverage: 22% Peptide Count: 4 Trem2 R3 Coverage: 53% Peptide Count: 9 Trem2 R4 Coverage: 61% Peptide Count: 10 Trem2 R5 Coverage: 57% Peptide Count: 9

Esyt1	ALTLGALTLPLAR	VLQAGVLDNWYPLQGGQGQVHLR	Trem2 R1
	VGTQTFCSR	VELGEKPLR	Coverage: 9%
	IHVLEAQDLIAK	TVSQSSAPVWEESASFLIR	Peptide Count: 7
	GANPHLQTFTFTR	FEWDLPLDGTLR	
	ILYLDYSEIR	DLPDPYVSVLLLPDKNR	Trem2 R2
	MEHSPEEGASPEPSGQPPATDSTR	AQDLPLKK	Coverage: 4%
	ATYSTNSPVWEEAFR	KPHAESLELQVR	Peptide Count: 5
	ERELLGK	LTPRPTAAELEEVLQVNSLIQTQK	
	FLGGLVK		Trem2 R3
	LLAETVAPAVR		Coverage: 8%
	KLDVSVK		Peptide Count: 8
			Trem2 R4
			Coverage: 18%
			Peptide Count: 16
			Trem2 R5
			Coverage: 10%
			Peptide Count: 7
Esyt2	ALALLEDEEQAVR	VIKENLSPK	Trem2 R1
	VDVGQQPLR	VYTENVDKR	Coverage: 5%
	VGNQIFQSK	TLDVAVK	Peptide Count: 4

	FQLSNSGPNSTLK	SSSSLLASPSHIAAK	
	NSGGFLSK	SSAGGEGPEAGPGR	Trem2 R2
	NLIAFSEDGSDPYVR	TSEPVWEENFTFFIHNPR	Coverage: 3%
	QLENGTTLGQSPLGQIQLTIR	EPTPSIASDISLPIATQELR	Peptide Count: 2
	IPLSQLLTSDNMTINQR	IHFIEAQDLQGK	
	ITVPLVSEVQIAQLR	GWTQWYDLTEDGTRPQVIT	Trem2 R3
	VLVVLASEELAK	KINSNPNPLVQMSVGHK	Coverage: 14%
			Peptide Count: 10
			Trem2 R4
			Coverage: 24%
			Peptide Count: 14
			Trem2 R5
			Coverage: 7%
			Peptide Count: 4
Fcho2	ERPGLIEFEECDPASAVEGIKPR	LSEQNPAASYYNVDVLK	Trem2 R1
	ATIEEAYSR	ITGDVTISFPSGIIK	Coverage: 4%
	TKEEVAGTLEAVQAIQNITQALQK	VFTSNPSPAVLCFR	Peptide Count: 2
	ELADFVR	EIHLQIGQVHEEFINNMANTTIESLIQK	
	SKPSSLPTEK	TFALPGIIK	Trem2 R2
	SASNYSQLGTFAPMWDVFK	FQDIEETHLIHIK	Coverage: 4%
	LSGINEIPRPFSPPVTSNTSPPPTAPLAR		Peptide Count: 2

			Trem2 R3 Coverage: 4% Peptide Count: 2 Trem2 R4 Coverage: 20% Peptide Count: 9 Trem2 R5 Coverage: 11% Peptide Count: 6
Flrt2	QHLSLVNLEPR LDISNNQLR AALAQLLK VLHLQENNIQTISR NSLSHPPPDLPGTHLIR NHLSSVPVGLPVDLQELR LIVDGNLLTNK ICLVPLDAFNYR	LEELHLDDNSISTVGVEDGAFR LLFLSK GIAEGTFSHLTK LKEFSIVR LYLQDNQINHIPLTAFANLR YCNSSVPDLEHCHT LLFISK GFMCQGPEQVR	Trem2 R1 Coverage: 9% Peptide Count: 5 Trem2 R2 Coverage: 17% Peptide Count: 9 Trem2 R3 Coverage: 14% Peptide Count: 8

			Trem2 R4 Coverage: 27% Peptide Count: 13 Trem2 R5 Coverage: 23% Peptide Count: 12
Golga5	EGSSLQNQALQTLQER	TSKQELETELER	Trem2 R1
	TVGDATHPTEHASAPR	MEVDRQNLAEAVTLAER	Coverage: 38%
	LEQQVHSASSGPNSGSAINMSGVDSGEGTR	AEDLLNR	Peptide Count: 25
	EMQKEEIQK	LQEADQVLSSR	
	QNLAEAVTLAER	TLSNSSQSELESR	Trem2 R2
	SELQDMEAQQVSEAESAR	LHQLTETLIQK	Coverage: 24%
	ANYISSAADNIR	LGIFLR	Peptide Count: 15
	KAASSIDQFSIR	NVPVLFNDTETNLAGMYGK	
	SKETQEELNK	TEALEALR	Trem2 R3
	KKVDELQQQVK	SQELSNLR	Coverage: 32%
	LHEADATLKR	DSQLAVLK	Peptide Count: 19
	AQVDDLTEAVAAK	ENTSNIFYSK	
	QELETELER	APVSPSSPSGVSSVNTSVTTTK	Trem2 R4
	VDQGAATALR	GRAPVSPSSPSGVSSVNTSVTTTK	Coverage: 42%
	EQLQDLQDQIAK	QTMLESLSTEK	Peptide Count: 26

	PSSQFVR	NEVQSLNQEMASLLQR	
	NTDYPELQQQNTDSNYQTGQK	AEDLLNRVDQGAATALR	Trem2 R5
	ATILAGTANVK	ASLESAKQELVDYK	Coverage: 48%
	SWFADLAGR	LMGQMHQLR	Peptide Count: 30
	LENQLLR	NSLVFQLER	
	AASSIDQFSIR	YMEEDLHR	
	QMQSEFAAR		
Gosr1	AAGTSNYWEDLRK	ANFTAIR	Trem2 R1
	LIEETISIAMATK	QLENELDLK	Coverage: 24%
	YSSDTTPLLNGSSQDR	MFETMAIEIEQLLAR	Peptide Count: 5
	KDIESYK	MAEYTHSAGVPSLNAALMHTLQR	
	LCTSYSHSGSR		Trem2 R2
			Coverage: 12%
			Peptide Count: 3
			Trem2 R3
			Coverage: 18%
			Peptide Count: 4
			Trem2 R4
			Coverage: 15%
			Peptide Count: 3

			Trem2 R5 Coverage: 43% Peptide Count: 8
H2-K1	GYQQYAYDGCDYIALNEDLK AYLEGTCVEWLR TWTAADMAALITK YMEVGYVDDTEFVR AKGNEQSFR AHVTHHSRPEDK GGSHTIQVISGCEVGSDGR WMEQEGPEYWER HKWEQAGEAER GNEQSFR	YMEVGYVDDTEFVRFDSDAENPR YFVTAVSRPGLGEPR WASVVVPLGK PGLGEPR WEQAGEAER FDSDAENPR YFVTAVSR FDSDAENPRYEPR EQYYTCHVYHQGLPEPLTLR ARWMEQEGPEYWER	Trem2 R1 Coverage: 42% Peptide Count: 13 Trem2 R2 Coverage: 28% Peptide Count: 9 Trem2 R3 Coverage: 46% Peptide Count: 15 Trem2 R4 Coverage: 46% Peptide Count: 16 Trem2 R5 Coverage: 39% Peptide Count: 10
Igf2r	SEGGSGGNWYAMENSR	PLNPVPGCDR	Trem2 R1

	TYSIGVCTAAAGLGQEGCK	HDLNPLIK	Coverage: 20%
	LSSDVCSAHDGSK	VSLCNNK	Peptide Count: 41
	DGQENGHITTK	EKEDLLCGAINGK	
	LTYYDGMIQLSYR	DGPQWTDGVTVLQYVDGDLCPDKIR	Trem2 R2
	YSDNWEAVTR	PAYGCEAETQIEDIK	Coverage: 11%
	FTCSDNQVNSR	YFFINVCHR	Peptide Count: 22
	KVGTSDMTK	YSDGDLTLIYSGGDECSSGFQR	
	KPWTAVDTSAYGK	TTQKPVFLK	Trem2 R3
	IQTSITFLCGK	EYTFFINVCGDTK	Coverage: 21%
	VPVDGPPIDIGR	ADKEVPCYAFDDK	Peptide Count: 37
	SATGQVQVLGLVHTQK	ATLITFLCDR	
	LGKDGQENGHITTK	VRDGPQWTDGVTVLQYVDGDLCPDK	Trem2 R4
	SSGVSYK	VSKEEETDENETEWLMEEIQVPAPR	Coverage: 25%
	SVGDSLLR	YENHEGSLAETVSISNLGVAK	Peptide Count: 41
	LTFENGLLK	STTIYFYCDR	
	TLGTPEFVTATDCVHYFEWR	TASSVIELTCAK	Trem2 R5
	ETSDCSYMFEWR	VAGLLSQK	Coverage: 28%
	YDLSVLAR	TGATEHYLINVCK	Peptide Count: 48
	GNQAFDVGRPK	DYLQSESCSLSSEQHDITIDLSPLAQYGGSPYVSDGR	
	HSESEQNWEAVDGSQAESEK	YYVQDGDLDVVFTSSSK	
	FICNDDIYPGAPK	LEVIDETVIVTYSK	
	GCEVTFEWK	LASMQLDYR	
	SFSLGEIYFK	GAEVESSQPLRNPQR	

	EAAVCQEK	SDGCFYEFEWHTAAACVLSK	
	LFSASGDMR	NCPEDAAVCAVDK	
	VCPAGTAACLLK	SNTHDDCQVTNPSTGHLFDLSSLSGR	
	YASACQMK	TYSIGVCTAAAGLGQEGCKDGGVCLLSGNK	
	VYKGPLDCSER	LNGGYLVDDSDPDTSLFINVCR	
	YEVEWITEYACHR	GEPVFTGEVDCTYFFTWDTK	
	GTAFIIR	NCPEDAAVCAVDKNGSK	
	LSYKDQVLQLVYENGSPCPSLSDLR	MSAIIFTCDESEDIGRPQVFSEDR	
	AEALSSLHGDDQDSEDEVLTVPEVK	SVSSTIFFHCDPLVK	
	SYDECVLEGR	SLQLSAEGFLTLTYK	
	FLHQDIDSTR	DIDSLRDPSTQLR	
	LVLTYVK		
Itgb1	LLVFSTDAGFHFAGDGK	TLVLSNLSYSATK	Trem2 R1
	SAVTTVVNPK	SEADAEKNLEEK	Coverage: 11%
	GCQPSDIENPR	SVSLYYTGEK	Peptide Count: 8
	GEFFNELVGQQR	ITSDFR	
	IGFGSFVEK	TVMPYISTTPAK	Trem2 R2
	DNTNEIYSGK	NVLSLTDRGEFFNELVGQQR	Coverage: 3%
	FCECDNFNCDR	LRPEDITQIQPQQLLLK	Peptide Count: 2
	SLGTDLMNEMR	EKLPQPVQVDPVTHCK	
	ETLEEVFEK	FQGPTCETCQTCLGVCAEHK	Trem2 R3
	FGYVDFESAEDLEK	LPDGVTINYK	Coverage: 9%
	GIAYIEFK	KGCQPSDIENPR	Peptide Count: 7

			Trem2 R4 Coverage: 20% Peptide Count: 14 Trem2 R5 Coverage: 8% Peptide Count: 6
Itgb2	VTYDSFCSNGASSIGK VMASECIQEQSFVIR SSQELER SIANPEFDQR LGAILTPNDGR YNSQVCGGSDR LSESNIQPIFAVTK LVECSGR SNEFDYPSVGQLAHK GDCDGVQINNPVTFQVK LGGDLLQALNEITESGR VFLDHSTLPDTLK TVLPFVNTHPEK GCPADDIMDPR	SAVGELSDDSSNVVQLIK LTEIIPK LTDNSNQFQTEVGK STTGCLNAR SRGDCDGVQINNPVTFQVK DSEGCWITYTLQQK IGFGSFVDK GVMECGICR NIYNIHVEDSLECVK SQWNNDNPLFK IGFGSFVDKTVLPFVNTHPEK LLVFATDDGFHFAGDGK KLGGDLLQALNEITESGR	Trem2 R1 Coverage: 23% Peptide Count: 14 Trem2 R2 Coverage: 15% Peptide Count: 9 Trem2 R3 Coverage: 22% Peptide Count: 13 Trem2 R4 Coverage: 30% Peptide Count: 18

			Trem2 R5 Coverage: 24% Peptide Count: 13
Lgals3	VAVNDAHLLQYNHR GNDVAFHFNPR IQVLVEADHFK IVLDFR RGNDVAFHFNPR	VIVCNTK QDNNWGKEER RVIVCNTK QSAFPFESGKPFK	Trem2 R1 Coverage: 19% Peptide Count: 6 Trem2 R2 Coverage: 19% Peptide Count: 6 Trem2 R3 Coverage: 28% Peptide Count: 8 Trem2 R4 Coverage: 16% Peptide Count: 5 Trem2 R5 Coverage: 21% Peptide Count: 5

Lilrb4	FNIPSMTTSYAGIYK	NEPQVWSKPSNSLDLMISETK	Trem2 R1
	ETQDVTYAQLCIR	SVNPWDTQVPLETR	Coverage: 21%
	PSNSLDLMISETK	DQSSTPTEDGLETYQK	Peptide Count: 6
	FILIQEGK	DTACKETQDVTYAQLCIR	
			Trem2 R2
			Coverage: 7%
			Peptide Count: 2
			Trem2 R3
			Coverage: 18%
			Peptide Count: 5
			Trem2 R4
			Coverage: 20%
			Peptide Count: 6
			Trem2 R5
			Coverage: 22%
			Peptide Count: 5
Niban2	DILQAVK	TDMDQIITSK	Trem2 R1
	FDVSSTSVFK	EQMDNAVYTFETLLHQELGK	Coverage: 4%
	HEIEGTGPPQAQLLWR	EALLQITIPFLLKK	Peptide Count: 3

	VEGPAFTDAIR	FILVENTYEEVVLQTVMK	
	KYDYDSSSVR	FYEDQYGVSLFNSMR	Trem2 R2
	GPTKEELCK	EVTDMNLNVINEGGIDK	Coverage: 5%
	NHVQPYIPSILEALMVPTSQGFTEVR	AVINSAGYK	Peptide Count: 4
	FQELIFEDFAR	IIFSGNLFQYQEDNKK	
	LSQLAYHPLK		Trem2 R3
			Coverage: 5%
			Peptide Count: 2
			Trem2 R4
			Coverage: 23%
			Peptide Count: 13
			Trem2 R5
			Coverage: 7%
			Peptide Count: 4
Pdxdc1	YEHANDDDTSLK	HACHLSQR	Trem2 R1
	EEFKQEVEGTAGLLYVDDPNWPGIGVVR	LQESLK	Coverage: 40%
	GEDVDQLITCIQSK	LPLLLVANAGTAAVGHTDK	Peptide Count: 26
	SFNLTAGSLESTEYTYVHK	YENGCAYFHEEER	
	KLNELESDLTFK	ERHSCDALNR	Trem2 R2
	ILVEDELSSPVVVFR	LIKDDVER	Coverage: 23%
	LNELESDLTFK	GIQEAQVQLQK	Peptide Count: 17

	IADPTLAEMGK	QEVEGTAGLLYVDDPNWPGIGVVR	
	KGIQEAQVQLQK	QLVPQCGLTVIDLEVDGTCVR	Trem2 R3
	LLENMTEVVR	LLEEGVLR	Coverage: 38%
	ILSDTTLWLR	IKHACHLSQR	Peptide Count: 28
	FSPLMTAEGLGTR	IHTGLLKK	
	HDDPALTLVAGLTSNKPADK	IHTGLLK	Trem2 R4
	HSCDALNR	QTEALQNQAQHQEDDHSQVEELER	Coverage: 56%
	LPGQKPFKR	IQNIGEQGHMALLGHSLGAYISTLDKEK	Peptide Count: 35
	VQGTGVTPPPTPLGTR	VEQLSSGLEHDNLEAHSPEQPPR	
	QRLPGQKPFK	LLENMTEVVRK	Trem2 R5
	KPVIYLSAAAR	GSDAVSETSSVSHIEDLEK	Coverage: 51%
	FFQELPASDSAFK	LPLLLVANAGTAAVGHTDKIGR	Peptide Count: 35
	LPVLTCTLQLR	LPGQKPFK	
	YEHANDDDTSLKSDPEGEK	YEDFVVDGFNVLYNKKPVIYLSAAAR	
	YEDFVVDGFNVLYNK	GSDAVSETSSVSHIEDLEKVEQLSSGLEHDNLEAHSPEQPPR	
	GRLPLLLVANAGTAAVGHTDK	GRLPLLLVANAGTAAVGHTDKIGR	
	AVPVSNIAPAAVGR	HDDPALTLVAGLTSNKPADKLR	
	LQESLKK		
Pgrmc2	LSTLGSGGESGGDGSPGGAGATAAR	AAGDGDVK	Trem2 R1
	GLCSGPGAGEESPAATLPR	EKYDYVGR	Coverage: 64%
	DALRDEYDDLSDLNAVQMESVR	GLATFCLDKDALR	Peptide Count: 16
	RGLCSGPGAGEESPAATLPR	YDYVGR	
	DEYDDLSDLNAVQMESVR	DFSLEQLR	Trem2 R2

	LLKPGEEPSEYTDEEDTK ILLAVNGK GLATFCLDKDALRDEYDDLSDLNAVQMESVR EWEMQFK QYDGAR	RDFSLEQLR LLKPGEEPSEYTDEEDTKDHSK ILLAVNGKVFDVTK GLATFCLDK	Coverage: 46% Peptide Count: 7 Trem2 R3 Coverage: 47% Peptide Count: 9 Trem2 R4 Coverage: 62% Peptide Count: 12 Trem2 R5 Coverage: 59% Peptide Count: 14
Plpp3	NGGSPALNNNPR STTQNPYVAALYK MQSYKYDK GFYCNDESIKYPLK	TSLSLPAPAIR EILSPVDIIDR AIVPESKNGGSPALNNNPR	Trem2 R1 Coverage: 19% Peptide Count: 5 Trem2 R2 Coverage: 11% Peptide Count: 3 Trem2 R3

			Coverage: 12% Peptide Count: 3 Trem2 R4 Coverage: 10% Peptide Count: 2 Trem2 R5 Coverage: 7% Peptide Count: 2
Rab32	AGEGLGQQGASATAAPETR LQLWDIAGQER DNINIDEATR VLVIGELGVGK FLVENMLANQQSFPSEEIDLDR	ATIGVDFALK VHLPNGSPIPAVLLANK EALGAFVVFDISR SSTFDAVLK	Trem2 R1 Coverage: 18% Peptide Count: 3 Trem2 R2 Coverage: 13% Peptide Count: 12 Trem2 R3 Coverage: 28% Peptide Count: 4 Trem2 R4

			Coverage: 36% Peptide Count: 6 Trem2 R5 Coverage: 40% Peptide Count: 7
Rab6a	SAGGDFGNPLRK SAGGDFGNPLR GSDVIIMLVGNK VAAALPGMESTQDR QVSIEEGER	SLIPSYIR IQIWDTAGQER LVFLGEQSVGK TDLADKR DSTVAVVVYDITNVNSFQQTTK	Trem2 R1 Coverage: 32% Peptide Count: 7 Trem2 R2 Coverage: 16% Peptide Count: 3 Trem2 R3 Coverage: 20% Peptide Count: 4 Trem2 R4 Coverage: 41% Peptide Count: 7 Trem2 R5

			Coverage: 27% Peptide Count: 4
Sirpa	VVLNSMDVNSK LLIYSFAGEYVPR AQPAPKPEPSFSEYASVQVQR VPRPEDTLTYADLDMVHLSR VICEVAHITLDR GSSEPDTEIQSGGGTEVYVLAKPSPPEVSGPADR EDVVFTCQVK PSPPEVSGPADR	GSSEPDTEIQSGGGTEVYVLAK NNMDFSIR ISNVTPADAGIYYCVK SHGFSPR HDQQPAITR DGQELHPLETTVNPSGK APEPNNHTEYASIETGK GIANLSNFIR	Trem2 R1 Coverage: 31% Peptide Count: 13 Trem2 R2 Coverage: 14% Peptide Count: 6 Trem2 R3 Coverage: 29% Peptide Count: 11 Trem2 R4 Coverage: 30% Peptide Count: 10 Trem2 R5 Coverage: 21% Peptide Count: 7
Slc38a1	SLMGEEDAFSAWYVDGR LGEQVFGTTGK	SLTNSHLEK YVTFNSK	Trem2 R1 Coverage: 16%

	ETGCMVYEK RSLTNSHLEK SSLFELAK	NELPSAIK VQSDLLHK SLTNSHLEKR	Peptide Count: 9 Trem2 R2 Coverage: 9% Peptide Count: 6 Trem2 R3 Coverage: 14% Peptide Count: 8 Trem2 R4 Coverage: 11% Peptide Count: 5 Trem2 R5 Coverage: 9% Peptide Count: 5
Slc38a2	TANEGGSLLYEQLGHK SHYADVDPENQNFLLESNLGK SSVTHLLCPTK	YELPLVIK FNISPDEDSSSYSSNSDFNYSYPTK EFSWLR	Trem2 R1 Coverage: 16% Peptide Count: 5 Trem2 R2 Coverage: 10%

			Peptide Count: 3 Trem2 R3 Coverage: 13% Peptide Count: 4 Trem2 R4 Coverage: 16% Peptide Count: 5 Trem2 R5 Coverage: 16% Peptide Count: 5
Slc3a2	EALSSWLQDGVDGFQFR QINPTLGSQEDFKDLLQSAK GQNEDPGSLLTQFR IGDLQAFVGR VAEDETEAGVK SHLEYLSTLK DAGGIAGLK LLLSTDSAR IKVAEDETEAGVK LGASNLPAGISLPASAK	TESLVTR NLSEDR VAGSPGWVR QPMNAADGAAAGEK MKEALSSWLQDGVDGFQFR HWDQNER NQKDEINETDLK SQDTEVDMKDVELNELEPEKQPMNAADGAAAGEK DVELNELEPEKQPMNAADGAAAGEK GLVLGPIHK	Trem2 R1 Coverage: 45% Peptide Count: 23 Trem2 R2 Coverage: 29% Peptide Count: 15 Trem2 R3 Coverage: 43%

	YLVVLNFR	VKGLVLGPIHK	Peptide Count: 18
	FTGLSKEELLK	DEINETDLK	
	SQDTEVDMK	DVELNELEPEK	Trem2 R4
	SLLHGDFHALSSSPDLFSYIR	LGASNLPAGISLPASAKLLLSTDSAR	Coverage: 44%
			Peptide Count: 21
			Trem2 R5
			Coverage: 37%
			Peptide Count: 14
Slc6a8	VAESGPGLAFIAYPR	RSPVIEFWENK	Trem2 R1
	SAENGIYSVSGDEK	KGPLIVSGPDGAPAKGDGPAGLGAPGGR	Coverage: 11%
	GDGPAGLGAPGGR	SPVIEFWENK	Peptide Count: 8
	GPLIVSGPDGAPAKGDGPAGLGAPGGR	AGSINVWNICPLFK	
	GPLIVSGPDGAPAK	KGPLIVSGPDGAPAK	Trem2 R2
	KSAENGIYSVSGDEK		Coverage: 10%
			Peptide Count: 5
			Trem2 R3
			Coverage: 13%
			Peptide Count: 6
			Trem2 R4
			Coverage: 11%

			Peptide Count: 7 Trem2 R5 Coverage: 8% Peptide Count: 4
Slc7a5	AVATPAAAAAEEER DMGQGDASNLQQK RAVATPAAAAAEEER VQDAFAAAK	LFFVGSR RGDGADPEGEGVTLQR GDGADPEGEGVTLQR KPELERPIK	Trem2 R1 Coverage: 12% Peptide Count: 6 Trem2 R2 Coverage: 6% Peptide Count: 2 Trem2 R3 Coverage: 4% Peptide Count: 2 Trem2 R4 Coverage: 13% Peptide Count: 8 Trem2 R5 Coverage: 7%

			Peptide Count: 4
Snap29	LQDAELDSVPKEPSSTVNTEVYPK	VDKLDVNIK	Trem2 R1
	IDSNLDELSVGLGHLK	DLPDGPDAPIDR	Coverage: 41%
	LKEAINTSK	RLQDAELDSVPKEPSSTVNTEVYPK	Peptide Count: 9
	EPSSTVNTEVYPK	RAEATAASTSR	
	SVFGGFINYFK	LQDAELDSVPK	Trem2 R2
	IGVASSEELVR	MVDKMDQDLK	Coverage: 14%
	SLSLMYESEK	SKPVEPPPEQNGSIVSQPNSR	Peptide Count: 3
	LKEAINTSKDQENK	DIALGMQTEIEEQDDILDR	
	SYNPFDDDVEEEDTRPAPWK	DQENKYQASHPNLR	Trem2 R3
	YQASHPNLR		Coverage: 38%
			Peptide Count: 7
			Trem2 R4
			Coverage: 57%
			Peptide Count: 14
			Trem2 R5
			Coverage: 60%
			Peptide Count: 13
Stam	AVYDFEAAEDNELTFK	NLKEQGVTFPAIGSQAAEQAK	Trem2 R1
	VMEALSLYTK	AGEIITVLDDSDPNWWK	Coverage: 18%
	DFASEVSNVLNK	QQSAPVSTLYPSTSNLLTNHQHEGR	Peptide Count: 7

	PLFATNPFDQDVEK	EQGVTFPAIGSQAAEQAK	
	GETHQGVGLFPSNFVTADLTAEPEMIK	AIELSLK	Trem2 R2
	HSELSELNVK	KHSELSELNVK	Coverage: 4%
	IFHLEVCSR	DPGTVATKKEEEDLAK	Peptide Count: 2
			Trem2 R3
			Coverage: 14%
			Peptide Count: 5
			Trem2 R4
			Coverage: 26%
			Peptide Count: 11
			Trem2 R5
			Coverage: 30%
			Peptide Count: 12
Stx4	LGSPDDEFFQK	QALNEISAR	Trem2 R1
	VALVVHSGAAR	QGLQNLR	Coverage: 16%
	TQHGVLSQQFVELINK	QQVTILATPLPEESMK	Peptide Count: 4
	HSEIQQLER	ITNAGMVSDEELEQMLDSGQSEVFVSNILK	
	AIEPQKEEADENYNSVNTR		Trem2 R2
			Coverage: 10%
			Peptide Count: 2

			Trem2 R3 Coverage: 22% Peptide Count: 5 Trem2 R4 Coverage: 22% Peptide Count: 5 Trem2 R5 Coverage: 28% Peptide Count: 5
Stx5	QIAQLQDFVR TSQQLQLIDEQDSYIQSR APVSALPLAPNNLGGGPIILGAESR EQEETIQR HLQTHSNTIVVSLQSK QIAQLQDFVR	SVLEVR IDENVLGAQLDVEAAHSEILK AVEIEELTYIIK QNGIQTSKPALHAAR LASMSNDFK	Trem2 R1 Coverage: 22% Peptide Count: 5 Trem2 R2 Coverage: 10% Peptide Count: 2 Trem2 R3 Coverage: 27% Peptide Count: 6

			Trem2 R4 Coverage: 26% Peptide Count: 6 Trem2 R5 Coverage: 35% Peptide Count: 8
Tfrc	LNSIEFADTIK SAFSNLFGGEPLSYTR LAETEETDKSETMETEDVPTSSR LAADEEENADNNMK ILNIFGVIK VPQLNQMVR VEYHFLSPYVSPR TAAEVAGQLIIK AFTYINLDK LDTYEALTQK	QLSQNTYTPR LYWADLK LVHANFGTK VVLGTSNFK AGEITFAEK VSASPLLYTLMGK SSVGTGLLLK DMGLSLQWLYSAR EAGSQKDESLAYYIENQFHEFK LAQVFSDMISK	Trem2 R1 Coverage: 10% Peptide Count: 5 Trem2 R2 Coverage: 13% Peptide Count: 8 Trem2 R3 Coverage: 15% Peptide Count: 10 Trem2 R4 Coverage: 25% Peptide Count: 16

			Trem2 R5 Coverage: 14% Peptide Count: 8
Tgoln1	ISPDTETSKTDK ISPDTETSK VDLDKPTSK IIAFALEGK NEKDDLYK	DADSGDSQNPPNQPSK IIAFALEGKR KIIAFALEGK PLSPVNPK TAATDHSLGDSR	Trem2 R1 Coverage: 8% Peptide Count: 4 Trem2 R2 Coverage: 5% Peptide Count: 2 Trem2 R3 Coverage: 12% Peptide Count: 6 Trem2 R4 Coverage: 17% Peptide Count: 6 Trem2 R5 Coverage: 15% Peptide Count: 6

Tmem199	ASSLLAGER	ALGPGGELEREQLPR	Trem2 R1
	NVTCQDAQCGGTLSDLGK	AQLEAALGKK	Coverage: 38%
	LYLHELLEGSDIYFPEIVKPPR	LRAQLEAALGKK	Peptide Count: 7
	NPELVAR	LYLHELLEGSDIYFPEIVKPPRNPELVAR	
	ALGPGGELER	AMEGELGEL	Trem2 R2
	AQLEAALGK	HAGSDNATGPR	Coverage: 37%
			Peptide Count: 7
			Trem2 R3
			Coverage: 28%
			Peptide Count: 5
			Trem2 R4
			Coverage: 37%
			Peptide Count: 7
			Trem2 R5
			Coverage: 50%
			Peptide Count: 11
Trem2	NLQAGDAGLYQCQSLR	QKPGTPVVR	Trem2 R1
	FLAASILWAVAR	VLVEVLEDPLDDQDAGDLWVPEESSSFEGAQVEHSTSR	Coverage: 24%
	QLGEEGPCQR	VVSTHGVWLLAFLKK	Peptide Count: 5
	EAEVLQK	VVSTHGVWLLAFLK	

	VSCTYDALK		Trem2 R2 Coverage: 25% Peptide Count: 5 Trem2 R3 Coverage: 19% Peptide Count: 4 Trem2 R4 Coverage: 36% Peptide Count: 5 Trem2 R5 Coverage: 43% Peptide Count: 7
Ube2j1	GEGAIGSLDYTPEER TALLAIIGFMPTK GPPDSDFDGGVYHGR RPSTSPDVLQGQPPR DVLLPLK	IVLPPEYPMKPPSIILLTANGR TALLAIIGFMPTKGEGAIGSLDYTPEER SQDFCCEGCGSAMK EAAELKDPTDHYHAQPLEDNLFEWHFTVR	Trem2 R1 Coverage: 27% Peptide Count: 6 Trem2 R2 Coverage: 12% Peptide Count: 3

			Trem2 R3 Coverage: 12% Peptide Count: 3 Trem2 R4 Coverage: 27% Peptide Count: 7 Trem2 R5 Coverage: 41% Peptide Count: 9
Vamp3	LQQTQNQVDEVVDIMR STGVPSGSSAATGSNR RLQQTQNQVDEVVDIMR ADALQAGASQFETSAAK	LSELDDRADALQAGASQFETSAAK LSELDDR STGVPSGSSAATGSNRR	Trem2 R1 Coverage: 55% Peptide Count: 6 Trem2 R2 Coverage: 39% Peptide Count: 4 Trem2 R3 Coverage: 40% Peptide Count: 5

			Trem2 R4 Coverage: 55% Peptide Count: 6 Trem2 R5 Coverage: 55% Peptide Count: 5
Vapa	KVAHSDKPGSTSAVSFR KLMEECKR ASASGAMAK HEQILVLDPPSDLK EAKPDELMDSK HLRDEGLR FKGPFTDVVTTNLK QDGPLPKPHSVSLNDTETR	VAHSDKPGSTSAVSFR GPFTDVVTTNLK PHSVSLNDTETR VKTTAPR FMVQTIFAPPNISDMEAVWK AVPLNASK CVFEMPNENDKLNDMEPSK YCVRPNSGIIDPGSIVTVSVMLQPFDYDPNEK	Trem2 R1 Coverage: 40% Peptide Count: 10 Trem2 R2 Coverage: 16% Peptide Count: 4 Trem2 R3 Coverage: 55% Peptide Count: 13 Trem2 R4 Coverage: 30% Peptide Count: 8

			Trem2 R5 Coverage: 62% Peptide Count: 12
Ykt6	SDSLAGVVIADSEYPSR IDWPVGSPATIQYTGLDDHLSK AAYDVSSFSFFQR GEKLDDLVSK VAFTLLEK EADPMSK VLDEFSK ASVKEQEYLCHVYVR SEVLGTQSK SSVQEFMTFTSQLIVER	LDDLVSK MKLYSLSVLYK EQEYLCHVYVR QVDRIDWPVGSPATIQYTGLDDHLSK LYSLSVLYK LYSLSVLYKGDPK VQAELDETK LDDLVSKSEVLGTQSK GEKLDDLVSKSEVLGTQSK	Trem2 R1 Coverage: 63% Peptide Count: 11 Trem2 R2 Coverage: 57% Peptide Count: 10 Trem2 R3 Coverage: 74% Peptide Count: 17 Trem2 R4 Coverage: 69% Peptide Count: 17 Trem2 R5 Coverage: 62% Peptide Count: 11
Zfpl1	LCNTPLASR	DDDRTAGIHGDCDDDKYR	Trem2 R1

	LATVNWAR VNVCEHCLVANHAK LVCYDLFHWACINER VTNLFCFEHR KRPLTLLQR	RPALGWLAQLLR TAGIHGDCDDDKYR AAADSDPNLDPLMNPHIR NTAPAGYQCPSCNGPIFPPANLAGPVASALR	Coverage: 21% Peptide Count: 6 Trem2 R2 Coverage: 7% Peptide Count: 2 Trem2 R3 Coverage: 13% Peptide Count: 3 Trem2 R4 Coverage: 29% Peptide Count: 7 Trem2 R5 Coverage: 44% Peptide Count: 10
Bcap29	ASDALLK YSSTNVVEK IFSFSVWGK ENLKTELK	ENLKTELKK LLKEHSELQNR KASDALLK	Trem2 R1 Coverage: 7% Peptide Count: 2 Trem2 R2

			Coverage: 8% Peptide Count: 2 Trem2 R3 Coverage: 8% Peptide Count: 3 Trem2 R4 Coverage: 8% Peptide Count: 2 Trem2 R5 Coverage: 10% Peptide Count: 4
Copb1	KPITDDDVDR TNNVSEHEDTDKYR YVALVQEK YEAAGTLVTLSSAPTAIK LIVLDR NAVLAIYTIYR	VLSTPDLEVR EAGELKPEEEITVGPVQK LVEKPSPLTLAPHDFANIK VTVNTNMTDLNDYLQHILK EAADPLASK VLQDLVMDILR	Trem2 R1 Coverage: 5% Peptide Count: 4 Trem2 R2 Coverage: 4% Peptide Count: 4 Trem2 R3

			Coverage: 5% Peptide Count: 4 Trem2 R4 Coverage: 9% Peptide Count: 6 Trem2 R5 Coverage: 6% Peptide Count: 4
Gorasp2	EASVTPSNLWGGQGLLGVSIR ADASSLTVDVTSPASK LYVYNTDTDNCR DNDTLKDLLK EVIITPNSAWGGEGSLGCGIGYGYLHR LNKDNDTLKDLLK VPTTVEDR VQENSPGHR ANVEKPVK FCSFDGANENVWHVLEVESNSPAALAGLR	IPTRPFEEGK IPTRPFEEGKK ISLPGQMTGTPITPLK LNKDNDTLK MLIYSSK VSDCTPAVEKPVSDADASEPS PHSDYIIGADTVMNESEDLFSLIETHEAK PHSDYIIGADTVMNESEDLFSLIETHEAKPLK ADASSLTVDVTSPASKVPTTVEDR	Trem2 R1 Coverage: 39% Peptide Count: 15 Trem2 R2 Coverage: 16% Peptide Count: 7 Trem2 R3 Coverage: 42% Peptide Count: 15 Trem2 R4

			Coverage: 42% Peptide Count: 14 Trem2 R5 Coverage: 45% Peptide Count: 17
Larp7	ESAVDSSSSGVCK VSAQGPQFVTGVIVK AIEFLNNPPEEAPR TQQASQHIR DKVEASSLPEAR IVSGEPLPGR IKKEESVQAK SSSVVELDLEGTR TASEGSEAETPEAPK GFAFVEFETK NVTHSWIER QVDFWFGDANLHK	METENQKTMEESTK IVSGEPLPGRK VKQVLADIAK TASEGSEAETPEAPKQPAK DLEFCSTEEEKETDR DGVGQAASEVSK LESEMETDCKAPTAGSGQECSTQEK QVDFWFGDANLHKDK QVLADIAK FKTPEDAQAVMNAQTEIR APTAGSGQECSTQEK	Trem2 R1 Coverage: 11% Peptide Count: 5 Trem2 R2 Coverage: 10% Peptide Count: 5 Trem2 R3 Coverage: 18% Peptide Count: 8 Trem2 R4 Coverage: 36% Peptide Count: 17 Trem2 R5

			Coverage: 34% Peptide Count: 17
Mindy1	IQQPELDFYCVK MEQPQTENPAPSK NNHFSTMTK ATSAETVESENHEALSGPEK	SEGLQLNFQQNVDDAMTVLPK LSYNQLVEK LATGLDVNVR	Trem2 R1 Coverage: 12% Peptide Count: 4 Trem2 R2 Coverage: 16% Peptide Count: 5 Trem2 R3 Coverage: 11% Peptide Count: 4 Trem2 R4 Coverage: 18% Peptide Count: 6 Trem2 R5 Coverage: 18% Peptide Count: 6
Nectin2	ITWISSLGGEAK ARPETNADLR	YSLVPVGR DTQEPGIQAGTVTIISR	Trem2 R1 Coverage: 4%

	VIAQPENHAEAQEVTIGPQSVAVAR AEQVILVR	VLPEVR VEHESFEEPILLPVTLSVR	Peptide Count: 2 Trem2 R2 Coverage: 8% Peptide Count: 3 Trem2 R3 Coverage: 6% Peptide Count: 2 Trem2 R4 Coverage: 8% Peptide Count: 2 Trem2 R5 Coverage: 9% Peptide Count: 3
Pdia3	DLLTAYYDVDYEK VDCTANTNTCNK GFPTIYFSPANK LAPEYEAAATR LNFAVASR YGVSGYPTLK	EATNPPIIQEEKPK DGEEAGAYDGPR DASVVGFFR LKGIVPLAK KTFSHELSDFGLESTTGEVPVVAIR MDATANDVPSPYEVK	Trem2 R1 Coverage: 16% Peptide Count: 7 Trem2 R2 Coverage: 7%

	FISDKDASVVGFFR SEPIPESNEGPVK TADGIVSHLKK	FAHTNIESLVK ALEQFLQEYFDGNLKR	Peptide Count: 3 Trem2 R3 Coverage: 28% Peptide Count: 12 Trem2 R4 Coverage: 16% Peptide Count: 5 Trem2 R5 Coverage: 5% Peptide Count: 2
Ptgir	GFTQAIAPDSR SVHGDLQAPLSR EMGDLLAFR	CLALSHPYLYAQLDGPR DPPAPTSLQAK HHGSFVPTSR	Trem2 R1 Coverage: 12% Peptide Count: 4 Trem2 R2 Coverage: 6% Peptide Count: 2 Trem2 R3 Coverage: 5%

			Peptide Count: 2 Trem2 R4 Coverage: 7% Peptide Count: 2 Trem2 R5 Coverage: 8% Peptide Count: 3
Stam2	VLEALDLYNK SMKEEGVTFPSAGSQTVAAAAK ALYPPAESQLNNK PLFTANPFEQDVEK SEPEPVYIDEGK HGELITVLDDSDANWWQGENHR GTGLFPSNFVTTDLSTEVETATVDK LVNEAPVYSVYSK DPQFSLISATIK ALYDFEAVEDNELTFK NKEDEDIAK	SEPEPVYIDEGKMDR AIELSLQEQK ALQILQSIDPK HSELSELNVK LNVIDDDVEEIKK VNHKVPHVALQALTLLGACVANCGK VPHVALQALTLLGACVANCGK ATNEYNTTEDWSLIMDICDR KHSELSELNVK VLEALDLYNKLVNEAPVYSVYSK KSEPEPVYIDEGKMDR	Trem2 R1 Coverage: 36% Peptide Count: 14 Trem2 R2 Coverage: 20% Peptide Count: 8 Trem2 R3 Coverage: 29% Peptide Count: 11 Trem2 R4 Coverage: 48%

			Peptide Count: 19 Trem2 R5 Coverage: 45% Peptide Count: 18
Vamp4	SESLSDNATAFSNR LDELQDKSESLSDNATAFSNR HVQNQVDEVIDVMQENITK HLNDDDVTGSVK GERLDELQDKSESLSDNATAFSNR	NLLEDDSDEEEDFFLR LDELQDK GERLDELQDK RHLNDDDVTGSVK	Trem2 R1 Coverage: 39% Peptide Count: 5 Trem2 R2 Coverage: 18% Peptide Count: 2 Trem2 R3 Coverage: 50% Peptide Count: 8 Trem2 R4 Coverage: 40% Peptide Count: 7 Trem2 R5 Coverage: 40%

			Peptide Count: 8
Arf6	ILMLGLDAAGK DAIILIFANK FNVWDVGGQDK TTILYK	LGQSVTTIPTVGFNVETVTYK LKLGQSVTTIPTVGFNVETVTYK HYYTGTQGLIFVVDCADRDR	Trem2 R1 Coverage: 18% Peptide Count: 3 Trem2 R2 Coverage: 27% Peptide Count: 4 Trem2 R3 Coverage: 23% Peptide Count: 4 Trem2 R4 Coverage: 37% Peptide Count: 5 Trem2 R5 Coverage: 37% Peptide Count: 5
Lmna	SVGGSGGGSFGDNLVTR ITESEEVVSR SNEDQSMGNWQIR	IRIDSLSAQLSQLQK LQEKEDLQELNDR VAVEEVDEEGKFVR	Trem2 R1 Coverage: 24% Peptide Count: 14

	SGAQASSTPLSPTR	EGDLLAAQAR	
	LADALQELR	NSNLVGAAHEELQQSR	Trem2 R2
	SSFSQHAR	LQLELSK	Coverage: 11%
	SLETENAGLR	MQQQLDEYQELLDIK	Peptide Count: 6
	LRDLEDSLAR	IDSLSAQLSQLQK	
	EAALSTALSEK	TALINSTGEEVAMR	Trem2 R3
	AAYEAELGDAR	AAGGAGAQVGGSISSGSSASSVTVTR	Coverage: 18%
	LSPSPTSQR	LKDLEALLNSK	Peptide Count: 11
	TLEGELHDLR	AQHEDQVEQYKK	
	LQTLKEELDFQK	LLEGEEER	Trem2 R4
			Coverage: 21%
			Peptide Count: 11
			Trem2 R5
			Coverage: 28%
			Peptide Count: 14
Osbpl8	VVLPTFILEPR	GEAVGSITQPLPSSYLIIR	Trem2 R1
	SLIWTLLK	GIDLGDIQSSIESIK	Coverage: 2%
	TGYSAILEFK	ANNLHSGDNFQLNDSEIER	Peptide Count: 2
	DLPQPSLSPASLHSQGFER	LFHPLEQSIWAVK	
	LKPFLGSSDYVNQISGK	GKEDISQNKDDSSLSMSK	Trem2 R2
			Coverage: 2%
			Peptide Count: 2

			Trem2 R3 Coverage: 10% Peptide Count: 6 Trem2 R4 Coverage: 12% Peptide Count: 7 Trem2 R5 Coverage: 8% Peptide Count: 5
Rasal3	TPGKTEPEAAGSNQVHNVR AGPGQLFWAER ESLATLSELDLGAER VGSASSENSMQAALGNLK LVAQEYLQDTLGQVVR SAGPAGATVGR TEPEAAGSNQVHNVR FHFEALPPAR CPTPELPK TQDSLEPLPTILR LVCASLFLR	EALLFR HTPLISK ATVPGVR YKELAEFLTFHYAR ISTQVQSSFFSGEKPGFLAPR SELGAYTPR YQTTGTHRPVGK WFPVLGAPAGAVLR SFQGAGSWASR AQALVTDLGTAELAR LLCPAILAPSLFGLAPEHPAPGPAR	Trem2 R1 Coverage: 23% Peptide Count: 22 Trem2 R2 Coverage: 19% Peptide Count: 18 Trem2 R3 Coverage: 9% Peptide Count: 7

	APAAGLER	HKNVAPLEPKPNPK	
	ALSHQEPMVNSQPAPR	QFQPSQDNVER	Trem2 R4
	GSEALGPR	LTEMECSQDQLR	Coverage: 25%
	LCGALEPALSAQAK	DSLQSLQLLSK	Peptide Count: 22
	TLTLIAK	ALSLLVESLSTQVQALK	
	DGPPSALGSR	ASASLPR	Trem2 R5
	NVAPLEPKPNPK		Coverage: 20%
			Peptide Count: 16
Scamp1	EMQNLSQHGR	SDFDSNPFADPDLNNPFKDPSVTQVTR	Trem2 R1
	QEELER	TVQTAAANAASTAATSAAQNAFK	Coverage: 23%
	NVPPGLDEYNPFSDSR	EHALAQAELLK	Peptide Count: 7
	TTGASFEK	AQQEFATGVMSNK	
	RQEELER	EREMQNLSQHGR	Trem2 R2
	EHALAQAELLKR		Coverage: 0%
			Peptide Count: 0
			Trem2 R3
			Coverage: 30%
			Peptide Count: 7
			Trem2 R4
			Coverage: 31%
			Peptide Count: 8

			Trem2 R5 Coverage: 30% Peptide Count: 7
Slc30a1	ESALILLQTVPK	IIATAHIK	Trem2 R1
	APTVSISCLELSENLEK	TKAEGSLPAVVIEIK	Coverage: 16%
	APDQEETNTLVANTSNSNGLK	TIKDVFHNHGIHATTIQPEFASVGSK	Peptide Count: 6
	AGQLNMR	CEDPASYMQVAK	
	ADQAEPEKLR	DAEKAPTVSISCLELSENLEK	Trem2 R2
	AGVEAGAPPGR	APDQEETNTLVANTSNSNGLKADQAEPEKLR	Coverage: 0%
	SDDPVDVQVNGNLIQESDNLEAEDNR	SSVLPCELACR	Peptide Count: 0
	LRSDDPVDVQVNGNLIQESDNLEAEDNR	ELRDVDGVEEVHELHVWQLAGSR	
	AGVEAGAPPGRAPDQEETNTLVANTSNSNGLK	DVFHNHGIHATTIQPEFASVGSK	Trem2 R3
	AEGSLPAVVIEIK		Coverage: 23% Peptide Count: 8
			Trem2 R4 Coverage: 32% Peptide Count: 15
			Trem2 R5 Coverage: 35% Peptide Count: 14

Tjap1	QAISLSLVEDGSER	LLQQENEELR	Trem2 R1
	VIEFSEDKIR	TPPPAAVVQR	Coverage: 24%
	LQNSYTASQR	QSLLPDKEGTEEASGPSHVDGR	Peptide Count: 10
	LDCNLAVQLLK	LSPYPTPSPPHPLYPGR	
	LEQEESLTDAER	MKLLQQENEELR	Trem2 R2
	VLEKPESLLLNSAQSGSAGR	YRLDCNLAVQLLK	Coverage: 9%
	RLQNSYTASQR	SSVPSSPASAQGSPHHQPSPAPSALSAPASSASSEEDLLASWQR	Peptide Count: 5
	SGQEVASPSPSPSSSLSPGAVVPTSVIAR	TNQELEDKLHALIK	
	NTINKLEELNER	ELEIGQDCLELELGQSR	Trem2 R3
	TLDWEIVELTNK	ELRLEIPVSR	Coverage: 25%
	LEIPVSR	GLVLPAEPDSGFPQDEEEEMLNLPVSPEEER	Peptide Count: 11
	LEEINER	KTLDWEIVELTNK	
	NSPLPNCTYATR	LADLPCELQDMVR	Trem2 R4
			Coverage: 0%
			Peptide Count: 0
			Trem2 R5
			Coverage: 58%
			Peptide Count: 21
Arfgef2	VSLENGEAPR	EIIEHGIELFNK	Trem2 R1
	MENQVLQEAR	DLYVNPNHQATLGQER	Coverage: 8%
	LDSTQVGEFLGDSTR	DAFLVFR	Peptide Count: 12
	VLQEYTSDDMNVAPGDR	DLPEEYLSSIYDEIEGKK	

	LGAAAPPK HLDVDLDR SGHELGMTPLQELSLR ALMEAVSHAK VGCNPNEDVAIFAVDSLR ILADKEVK LDGNAIVDFVR TCYNIYLASK LIAYGHITGNAPDSGAPGK VVSTSLDCLQK SYGHTFAK	LLASLLIK IVETICNCFQGPQTDEGVQLQIIK IVEISYYNMNR SGTNCLENLVISNGEK FSLLTASSSITEMK FLEKGELANFR ALLTAVTSPHIEIHEGTILQTVR LPDQEMGDGK GHSLAGEEFMGLGLGNLVSGGVDKR GLECLVSILK	Trem2 R2 Coverage: 0% Peptide Count: 0 Trem2 R3 Coverage: 4% Peptide Count: 4 Trem2 R4 Coverage: 8% Peptide Count: 12 Trem2 R5 Coverage: 16% Peptide Count: 22
Ebag9	QTDVEEWTSWDEDAPTSVK EPLNFGVPDGSTGFSSR KREPLNFGVPDGSTGFSSR REPLNFGVPDGSTGFSSR VCTCLATVFSFLK	VCTCLATVFSFLKR AITQFR IEGGNGNVATQQNSLEQLEPDYFK IEGGNGNVATQQNSLEQLEPDYFKDMTPTIR KLSGDQITLPTTVDYSSVPK	Trem2 R1 Coverage: 18% Peptide Count: 3 Trem2 R2 Coverage: 0% Peptide Count: 0

			Trem2 R3 Coverage: 51% Peptide Count: 10 Trem2 R4 Coverage: 32% Peptide Count: 4 Trem2 R5 Coverage: 31% Peptide Count: 4
Metap1	SAQFEHTLLVTDTGCEILTR VCETDGCSSEAK LLSSEDIEGMR NCYPSPLNYYNFPK HAQANGFSVVR NGYHGDLNETFFVGDVDEGAR SCCTSVNEVICHGIPDR LVQTTYECLMQAIDAVKPGVR EVLDIAAGMIK	AGVTTEEIDHAVHLACIAR LGIQGSYFCSQECFK NGYHGDLNETFFVGDVDEGARK RPLQEGDIVNVDITLYR SGHVFTIEPMICEGGWQDETWPDGWTAVTR ELGNIIQK LFHTAPNVPHYAK KLVQTTYECLMQAIDAVKPGVR	Trem2 R1 Coverage: 11% Peptide Count: 3 Trem2 R2 Coverage: 0% Peptide Count: 0 Trem2 R3 Coverage: 18% Peptide Count: 5

			Trem2 R4 Coverage: 42% Peptide Count: 10 Trem2 R5 Coverage: 59% Peptide Count: 16
Vps45	ENVEYLIQELR HVTVVGELSR LVSAVVEYGGK MNVVFAVK VTEFDAVR IVLGGTTIHNTK LKENLYPYLGPSTLR EYELFEFR AFVENYPQFK	LVMLYALHYER HSSNSLPGLIVDLR EVYLFER LESIADMK NLLEVSEVEQELACQNDHSSALQNVK RTEVPPLLLILDR SFLEEVLASGLHSR TTQGLTALLLSLK TTQGLTALLLSLKK	Trem2 R1 Coverage: 21% Peptide Count: 11 Trem2 R2 Coverage: 9% Peptide Count: 5 Trem2 R3 Coverage: 0% Peptide Count: 0 Trem2 R4 Coverage: 25% Peptide Count: 12

			Trem2 R5 Coverage: 18% Peptide Count: 9
Arfgef1	VSAWEEVQQR AFNSNNEQR MENQALQEAK LFLEGFR LIAYGHLTGR IVEISYYNMGR DAYVQALAR KEDAENLAAAQR VDTQDQGMYR SGTNCLENVVILNGEK DQAPDEFVGLGLVGGNVDWK	FLTSQQLFK FTLLTVSSGITEMK DAFLVFR LDGNAIVDFVR LLDCLLESHR QQAPLVSVSTVSEEVSK FLEKGELANFR ATLTQMLNVIFAR GSQELGMSNVQELSLR GLECLVSILK	Trem2 R1 Coverage: 6% Peptide Count: 10 Trem2 R2 Coverage: 2% Peptide Count: 3 Trem2 R3 Coverage: 0% Peptide Count: 0 Trem2 R4 Coverage: 6% Peptide Count: 9 Trem2 R5 Coverage: 7% Peptide Count: 11
Cd86	DMGSYDCFIQK	LHNVQIK	Trem2 R1

	LVLYEHYLGTEK LDSVNAK	LVLYEHYLGTEKLDSVNAK LHNVQIKDMGSYDCFIQK	Coverage: 12% Peptide Count: 4 Trem2 R2 Coverage: 0% Peptide Count: 0 Trem2 R3 Coverage: 12% Peptide Count: 6 Trem2 R4 Coverage: 10% Peptide Count: 4 Trem2 R5 Coverage: 10% Peptide Count: 3
Gcc1	LLQLDLENK AYAADQVEGFELQTK VLQEQIAETK LLQEER AQEQSDHALMLR	LQELQQEAAR LLQVAAR FLTLPDSLGR ALAVLAEKDLELEQLR	Trem2 R1 Coverage: 7% Peptide Count: 5 Trem2 R2

			Coverage: 4% Peptide Count: 3 Trem2 R3 Coverage: 0% Peptide Count: 0 Trem2 R4 Coverage: 6% Peptide Count: 4 Trem2 R5 Coverage: 8% Peptide Count: 5
Hmox2	GTLGGSNCPFQTTVAVLR AENTQFVK LPSTGEGTQFYLFEHVDNAQQFK YFFGENWEEQVK IHYVGQNEPELLVAHAYTR MADLSELLK MNALDLNLK NKDHPAFAPLYFPTELHR YMGDLSGGQVLKK	AENTQFVKDFLK DHPAFAPLYFPTELHR LATTALYFTYSALEEEMDR IVEEANKAFEYNMQIFSELDQAGSMLAR IVEEANK YMGDLSGGQVLK SSEVETSEGVDESEKNSMAPEKENHTK ETLEDGLPVHDGK ERIVEEANK	Trem2 R1 Coverage: 25% Peptide Count: 5 Trem2 R2 Coverage: 0% Peptide Count: 0 Trem2 R3

	ALKLPSTGEGTQFYLFEHVDNAQQFK AFEYNMQIFSELDQAGSMLAR	AALIKDMK	Coverage: 8% Peptide Count: 3 Trem2 R4 Coverage: 49% Peptide Count: 11 Trem2 R5 Coverage: 67% Peptide Count: 18
Snx3	GDDGIFDDNFIEER VVVPPLPGK YSDFEWLR	TNLPIFK VAGHPLAQNER FTTYEIR	Trem2 R1 Coverage: 23% Peptide Count: 4 Trem2 R2 Coverage: 30% Peptide Count: 5 Trem2 R3 Coverage: 35% Peptide Count: 6 Trem2 R4

		Coverage: 0% Peptide Count: 0 Trem2 R5 Coverage: 25% Peptide Count: 4

Supplementary table 3.3. *All enriched terms for Trem2 putative interactors.*

Enriched term	-log10(p)	Enriched term	-log10(p)	Enriched term	-log10(p)	Enriched term	-log10(p)	Enriched term	-log10(p)
Membrane trafficking	19.56	Localization within membrane	9.38	Regulation of i-kappab kinase/nf-kappab signalling	2.49	Ferroptosis	3.33	Cellular response to lipoprotein particle stimulus	4.06
Vesicle-mediated transport	19.01	Protein localization to membrane	4.91	Negative regulation of T cell activation	2.44	Monoatomic cation transport	3.32	Cell adhesion mediated by integrin	3.96
Intra-Golgi and retrograde Golgi-to-ER traffic	16.51	Protein localization to plasma membrane	2.92	Negative regulation of leukocyte cell-cell adhesion	2.28	Carboxylic acid transport	3.23	Neuroinflammatory response	3.75
Clathrin-mediated endocytosis	10.25	Protein localization to cell periphery	2.62	Negative regulation of immune system process	2.22	Organic acid transport	3.22	PID ARF6 TRAFFICKING PATHWAY	3.69
Cargo recognition for clathrin-mediated endocytosis	9.86	Regulation of immune effector process	8.84	Negative regulation of lymphocyte activation	2.15	Sodium ion transport	3.06	Viral myocarditis	3.43
Retrograde transport at the Trans-Golgi-Network	8.80	Positive regulation of leukocyte activation	7.77	Positive regulation of leukocyte differentiation	2.03	Regulation of neurotransmitter transport	2.80	Integrin cell surface interactions	2.99

Membrane organization	16.64	Positive regulation of cell activation	7.59	Positive regulation of hemopoiesis	2.03	Organic anion transport	2.72	Cell activation	2.87
Endomembrane system organization	15.40	Regulation of leukocyte activation	6.89	Organelle localization	8.56	Regulation of transmembrane transport	2.50	Integrin-mediated signalling pathway	2.86
Vesicle organization	13.38	Positive regulation of immune effector process	6.68	Establishment of organelle localization	4.47	Modulation of chemical synaptic transmission	2.25	Phagocytosis	2.23
Golgi vesicle transport	14.50	Regulation of production of molecular mediator of immune response	6.51	Vesicle targeting	3.35	Regulation of trans-synaptic signalling	2.25	Gastrulation	2.15
Endosomal transport	9.79	Regulation of cell activation	6.50	Exocytic process	3.25	Circulatory system process	2.24	Cell-substrate adhesion	2.04
Intra-Golgi traffic	9.09	Immunoregulatory interactions between a Lymphoid and a non-Lymphoid cell	6.15	Establishment of vesicle localization	2.14	Import across plasma membrane	2.16	Inflammatory response	2.02

Retrograde transport, endosome to Golgi	7.15	Positive regulation of cell-cell adhesion	6.10	Vesicle localization	2.05	Female pregnancy	2.12	Intracellular protein transport	6.22
Endoplasmic reticulum to Golgi vesicle-mediated transport	6.33	Positive regulation of leukocyte mediated immunity	5.88	Movement in host	7.43	Response to inorganic substance	2.08	Signalling by MET	4.46
Intra-Golgi vesicle-mediated transport	5.94	Adaptive Immune System	5.83	Biological process involved in interaction with host	7.05	Positive regulation of protein localization to membrane	6.86	Protein localization to organelle	4.28
Cytosolic transport	5.83	Positive regulation of cell adhesion	5.77	Haemostasis	6.74	Positive regulation of protein localization to plasma membrane	6.55	Vegfa-vegfr2 signalling	2.48
COPI-mediated anterograde transport	5.42	Regulation of leukocyte mediated immunity	5.75	Viral life cycle	6.72	Positive regulation of protein localization to cell periphery	6.27	EGF/EGFR signalling pathway	2.20
ER to Golgi Anterograde Transport	4.53	Regulation of cell-cell adhesion	5.70	Biological process involved in symbiotic interaction	6.67	Positive regulation of protein localization	5.86	Vacuolar transport	2.15

Transport to the Golgi and subsequent modification	4.15	Regulation of leukocyte cell-cell adhesion	5.57	Viral entry into host cell	6.66	Regulation of protein localization to membrane	5.45	Signalling by Receptor Tyrosine Kinases	2.13
Asparagine N-linked glycosylation	4.12	Positive regulation of leukocyte cell-cell adhesion	5.48	Entry into host	6.61	Regulation of vesicle-mediated transport	5.43	Trans-Golgi Network Vesicle Budding	6.15
Golgi-to-ER retrograde transport	2.44	Regulation of T cell proliferation	5.37	Basigin interactions	6.49	Regulation of protein localization to plasma membrane	5.33	Golgi Associated Vesicle Biogenesis	5.05
SNARE interactions in vesicular transport	11.97	Positive regulation of production of molecular mediator of immune response	4.80	Cell surface interactions at the vascular wall	6.10	Regulation of protein localization to cell periphery	4.88	Golgi organization	5.97
Membrane docking	10.48	Regulation of lymphocyte proliferation	4.71	Viral process	5.76	Negative regulation of endocytosis	4.55	Regulation of tumour necrosis factor superfamily cytokine production	5.27
Membrane fusion	9.87	Regulation of mononuclear cell proliferation	4.67	Hormone transport	2.73	Regulation of secretion by cell	4.27	Regulation of tumour necrosis factor production	4.15

Organelle localization by membrane tethering	9.18	Positive regulation of alpha-beta t cell activation	4.64	Alanine transport	7.10	Regulation of endocytosis	4.22	Negative regulation of cytokine production involved in inflammatory response	3.93
Vesicle fusion	6.91	Positive regulation of t cell activation	4.61	Amino acid transport across the plasma membrane	5.99	Regulation of secretion	3.98	Regulation of type ii interferon production	3.77
Export from cell	6.87	Regulation of t cell activation	4.56	Proline transport	5.71	Pid ecadherin stabilization pathway	3.93	Regulation of cytokine production involved in immune response	3.74
Organelle membrane fusion	6.86	Regulation of leukocyte proliferation	4.43	Regulation of amino acid transport	5.48	Negative regulation of transport	3.88	Response to bacterium	3.66
Organelle fusion	6.27	Regulation of lymphocyte mediated immunity	4.14	Neutral amino acid transport	5.15	Regulation of protein transport	3.70	Cellular response to biotic stimulus	3.52

Exocytosis	5.91	Regulation of adaptive immune response based on somatic recombination of immune receptors built from immunoglobulin superfamily domains	4.09	Regulation of amino acid import across plasma membrane	5.02	Negative regulation of cellular component organization	3.59	Positive regulation of cell development	3.25
SNARE complex assembly	5.59	Positive regulation of T cell proliferation	3.98	Regulation of amino acid transmembrane transport	5.02	Regulation of establishment of protein localization	3.58	Negative regulation of tumour necrosis factor production	3.10
Secretion by cell	5.32	Positive regulation of lymphocyte activation	3.95	L-alpha-amino acid transmembrane transport	4.93	Positive regulation of secretion by cell	3.25	Negative regulation of tumour necrosis factor superfamily cytokine production	3.07

Vesicle docking	4.85	Regulation of adaptive immune response	3.94	Carboxylic acid transmembrane transport	4.76	Positive regulation of protein transport	3.11	Regulation of cytokine production involved in inflammatory response	3.05
Secretion	4.54	Positive regulation of b cell mediated immunity	3.89	Neurotransmitter transport	4.74	Positive regulation of secretion	3.07	Response to lipopolysaccharide	2.96
ER-Phagosome pathway	4.24	Positive regulation of immunoglobulin mediated immune response	3.89	Organic acid transmembrane transport	4.74	Positive regulation of exocytosis	3.07	Response to molecule of bacterial origin	2.84
Antigen processing-Cross presentation	3.98	Regulation of alpha-beta T cell activation	3.82	L-amino acid transport	4.62	Positive regulation of establishment of protein localization	3.02	Cellular response to cytokine stimulus	2.83
Post-Golgi vesicle-mediated transport	2.86	Regulation of T cell receptor signalling pathway	3.80	SLC-mediated transmembrane transport	4.62	Positive regulation of cell migration	2.69	Cellular response to lipid	2.82
Cellular response to type II interferon	2.73	Regulation of lymphocyte activation	3.78	Positive regulation of amino acid transport	4.58	Regulation of synapse organization	2.65	Regulation of chemokine production	2.81

Class I MHC mediated antigen processing & presentation	2.72	T cell modulation in pancreatic cancer	3.78	Regulation of organic acid transport	4.44	Regulation of synapse structure or activity	2.62	Regulation of phagocytosis	2.77
Response to type II interferon	2.48	Positive regulation of adaptive immune response based on somatic recombination of immune receptors built from immunoglobulin superfamily domains	3.71	Transport of small molecules	4.34	Positive regulation of cell motility	2.60	Cellular response to molecule of bacterial origin	2.73
RHOG GTPase cycle	11.14	Positive regulation of lymphocyte mediated immunity	3.66	Vascular transport	4.31	Regulation of protein-containing complex assembly	2.56	Regulation of interleukin-1 beta production	2.65
RHO GTPase cycle	10.50	Positive regulation of adaptive immune response	3.63	Transport across blood-brain barrier	4.31	Positive regulation of locomotion	2.55	Negative regulation of cell population proliferation	2.64

RAC3 GTPase cycle	8.64	Positive regulation of immunoglobulin production	3.59	Amino acid transmembrane transport	4.22	Regulation of metal ion transport	2.52	Regulation of peptidyl-tyrosine phosphorylation	2.56
Signalling by Rho GTPases	8.12	Positive regulation of lymphocyte proliferation	3.44	Regulation of amine transport	4.09	Positive regulation of protein secretion	2.32	Osteoclast differentiation	2.48
Signalling by Rho GTPases, Miro GTPases and RHOBTB3	8.00	Positive regulation of mononuclear cell proliferation	3.41	Amino acid import across plasma membrane	4.06	Positive regulation of cellular component biogenesis	2.20	Regulation of interleukin-1 production	2.45
RAC2 GTPase cycle	7.24	Regulation of B cell mediated immunity	3.37	Metal ion transport	3.95	Neutrophil degranulation	6.80	Positive regulation of cytokine production	2.23
RHOA GTPase cycle	5.92	Regulation of immunoglobulin mediated immune response	3.37	Transport of inorganic cations/anions and amino acids/oligopeptides	3.93	Endocytosis	6.42	Regulation of interleukin-6 production	2.09
RAC1 GTPase cycle	5.34	Regulation of antigen receptor-mediated signalling pathway	3.31	Import into cell	3.92	Receptor-mediated endocytosis	5.64	Negative regulation of MAPK cascade	2.05

RHOD GTPase cycle	5.12	Positive regulation of immune response	3.23	Regulation of neurotransmitter levels	3.90	Receptor internalization	4.60	Membrane invagination	5.18
CDC42 GTPase cycle	3.33	Positive regulation of leukocyte proliferation	3.22	Positive regulation of amine transport	3.86	Phagosome	4.55	Negative regulation of protein localization	2.79
RHOC GTPase cycle	3.16	Regulation of immunoglobulin production	3.13	Amino acid transport	3.81	Cell adhesion molecules	4.49	Regulation of intracellular transport	2.13
Endocytosis	10.84	Negative regulation of immune response	2.91	Positive regulation of organic acid transport	3.69	Response to lipoprotein particle	4.17	Insertion of tail-anchored proteins into the endoplasmic reticulum membrane	4.75
Endosome organization	5.64	Regulation of t cell mediated immunity	2.81	Positive regulation of transmembrane transport	3.66	Cellular response to low-density lipoprotein particle stimulus	4.17	Vesicle budding from membrane	3.11
Vesicle-mediated transport to the plasma membrane	4.93	Negative regulation of cell activation	2.72	Vascular process in circulatory system	3.41	Heterotypic cell-cell adhesion	4.10	Protein localization	2.18

Endocytic recycling	3.15	Negative regulation of immune effector process	2.52						

Supplementary table 3.4 Variants of NECTIN2 associated with AD. *The variant and paper identifying the variant was extracted from the EBI GWAS Catalog.*

Mapped Gene	Risk Variants		Papers
NECTIN2	rs11673139	MAF 0.06629	Gouveia et al. (2022)
	rs56394238	MAF 0.3642	Marioni et al. (2018)
	rs111371860	MAF 0.04113	Jansen et al. (2019)
	rs77241309	MAF 0.03654	Schwartzentruber et al. (2021)
	rs406456	MAF 0.2456	Ramanan et al. (2014)
	rs143459034	MAF 0.01498	Zhu et al. (2019)
	rs4802240	MAF 0.269	Nazarian et al. (2019)
	rs2927468	MAF 0.4277	Wang et al. (2021)
	rs2972558	MAF 0.4129	Lo et al. (2019)
	rs73050293	MAF 0.04692	Jun et al. (2017)
	rs375972689	MAF 0.02955	Naj et al. (2010)
	rs8112526	MAF 0.1084	Logue et al. (2011)
	rs11669338	MAF 0.06629	Miyashita et al. (2013)
	rs150639620	MAF 0.03694	Abraham et al. (2008)
	rs41290120	MAF 0.01258	Beecham et al. (2014)
	rs283810	MAF 0.1775	
	rs12974942	MAF 0.3458	
	rs12978931	MAF 0.262	
	rs41289512	MAF 0.007788	
	rs138607350	MAF 0.003395	

	rs79701229 MAF 0.003195 rs183427010 MAF 0.001997 rs419010 MAF 0.4461 rs6859 MAF 0.3664 rs11665676 MAF 0.03514 rs41290100 MAF 0.008986 rs41290108 MAF 0.007388 rs11666329 MAF 0.3478 rs4803764 MAF 0.1859 rs3112440 MAF 0.1552 rs283813 MAF 0.1761 rs146275714 MAF 0.005192 rs148601586 MAF 0.003994 rs4803760 MAF 0.1847 rs11668738 MAF 0.2776 rs112262807 MAF 0.2887 rs1466435 MAF 0.0593 rs10412413 MAF 0.2554 rs78986976 MAF 0.02296 rs10407439 MAF 0.3846 rs55840414 MAF 0.04233 rs547509922 MAF 0.000599 rs28399664 MAF 0.004393	

	rs393584 MAF 0.4601 rs412776 MAF 0.1516 rs3852860 MAF 0.4752 rs365653 MAF 0.1747 rs2972562 MAF 0.223 rs117310449 MAF 0.003794 rs6857 MAF 0.1104 rs406315 MAF 0.1955 rs58826447 MAF 0.2528 rs1871047 MAF 0.2734 rs440277 MAF 0.2161 rs283815 MAF 0.3037 rs10405693 MAF 0.2416 rs10402271 MAF 0.2332 rs10426423 MAF 0.2724 rs144261139 MAF 0.008786 rs283811 MAF 0.278 rs519113 MAF 0.2668	